UNIVERSIDADE NOVA DE LISBOA

Faculdade de Ciências e Tecnologia

Depº de Ciências e Engenharia do Ambiente

Monitoring Chlorophyll-*a* with remote sensing techniques in the Tagus Estuary

Akli Ait Benali

Dissertação apresentada na Faculdade de Ciências e Tecnologia da Universidade Nova de Lisboa para obtenção do grau de Mestre em Gestão e Sistemas Ambientais

Orientador : Doutora Maria Júlia Fonseca Seixas
Co-Orientador : Doutor João Gomes Ferreira

Lisboa
2008

Acknowledgments

This work has been one big and rocky road with lots of signs and complications. Many have a been part of it, and I dedicate my work to you all. First, my family, the ones who have suffered the most from the lack of patience, humour and lots of nerves. This road has been possible because of you and remember, every step was taken aiming at making you proud. Thank you. Second, to my girlfriend Liandra. I know that this thesis as been my primary lover for the last year, but you were always a fantastic "part time" lover ;) Thanks for the patience and confort you have provided, and forgive me for the lack of the same. I love you with all my heart.

I would like to thank my scientific advisors, Drª Júlia Seixas and Drº João Gomes Ferreira, for the support, advises and expert knowledge. Also, thanks to Ricardo Pacheco and Bruno Urmal for the technical expertises in informatics, namely in the help provided using the Linux environment. It was a smooth shock thanks to you both. Special thanks for the NASA Ocean Color Group which provided extremely valuable technical assistance in ocean color issues and SeaDas handling. You were fantastic and without you this work would have been far more difficult and probably not ready on time. Many thanks to Vânia Bento for the help with the EcoWin2000 initial model handling.

Thanks to Nuno Grosso, Joana Monjardino and Mario Sanches for the last call urgent help. Particularly the former, for the brief and helpful insights on remote sensing of atmosphere. Special thanks to João Pedro Nunes and Nuno Carvalhais for the interesting and very helpful scientific coffee breaks. I didn't know that coffees had so much to teach, thank you very much. Particularly Carvalhais, thanks for some of your MatLab functions and knowledge provided during the CARBERIAN project. It made a huge difference.

A last acknowledgement for the "fight budies" (companheiros de luta kirikirikirki) which have been many along this big path. Especially the ones who have put their faith on me. You know who you are. Thanks to you all, I hope that you (we) succeed. Final thanks for the everyday "buddy", Mr. Marley, you have been a great inspiration…there is truly a natural mystic blowing in the air.

Resumo

Os estuários são ecossistemas de transição com elevada variabilidade espacial e temporal, sujeitos a elevadas pressões antropogénicas. Actualmente é um desafio monitorizar estes sistemas de uma forma robusta, frequente, sistemática e com precisão adequada. Com a implementação da Directiva Quadro Agua, os estados membros da UE são obrigados a monitorizar regularmente os parâmetros biológicos e físicos mais relevantes. A informação sobre um estuário é adquirida recorrendo a dados de campo, implementação de modelos e/ou através de detecção remota.

Avaliou-se a aplicabilidade e precisão de produtos de clorofila-a do sensor MODIS no estuário do Tejo comparando-os (2000-2002) com estimativas de um modelo ecológico, o EcoWin2000, previamente calibrado (1998 e 1999) e validado (2000). Propõe-se um quadro conceptual e metodológico para futura monitorização do estuário usando detecção remota.

Numa primeira etapa, os algoritmos típicos para águas tipo 1 foram avaliados e os algoritmos tipo 2 foram calibrados em 2000. Os algoritmos GSM e Clark tiveram as melhores performances, com erros na ordem dos 1.1 μg chl-a l^{-1} (ou 20%) e correlações de 0.4-0.5. Na calibração o rácio R678/R551 apresentou uma correlação razoável (r = 0.83) e com baixos erros (~1μg chl-a l^{-1}). A sua avaliação em 2002 evidenciou correlações baixas e negativas com erros na ordem dos 2μg chl-a l^{-1}. Em concordância com a avaliação preliminar, em 2002, o algoritmo GSM apresentou a melhor correlação (r~0.50) com erros á volta de 0.8μg chl-a l^{-1}. A fiabilidade da aplicação dos produtos de detecção remota é superior na primavera e verão, e espacialmente, nas secções médias mais largas.

Os produtos de detecção remota, apesar de necessitarem de um desenvolvimento extenso, são uma hipótese viável e com grandes vantagens na monitorização sistemática da clorofila-a no estuário do Tejo. Especificamente, é uma ferramenta com potencial para ajudar os estados membros a cumprir a Directiva Quadro Agua.

Abstract

Estuaries are transitional ecosystems with high temporal and spatial variability and suffer high anthropogenic pressures. At the present there is a major challenge to monitor these systems in a robust, frequent, systematic and accurate fashion. With the implementation of the Water Framework Directive (WFD), the EU Member States must monitor regularly the most relevant physical and biological parameters. Estuarine information is attained using in-situ samples, model analysis and/or remote sensing data.

This work assessed the applicability and accuracy of chlorophyll-a products from the MODIS sensor in the Tagus estuary, comparing them (2000-2002) with simulations of an ecological model, the EcoWin2000. The latter was previously calibrated (1998 & 1999) and validated (2000). It is proposed a conceptual and methodological framework for future monitoring of the estuary using remote sensing data.

In a first stage, in the year 2000, typical Case 1 algorithms were pre-assessed and Case 2 algorithms were regionally calibrated. The GSM and Clark algorithms had the best performances, with errors of approximately of 1.1 μg chl-a l^{-1} (or 20%) and correlations ranging 0.4-0.5. During calibration, the ratio R_{678}/R_{551} had a good correlation (r = 0.83) and low errors (~1μg chl-a l^{-1}). Its evaluation in 2002, showed low and sometimes negative correlations, with errors of about 2 μg chl-a l^{-1}. In agreement with the preliminary assessment, in 2002, the GSM algorithm had the best correlation (r~0.50) and errors of approximately 0.8μg chl-a l^{-1}. The reliability of remote sensing is higher in the Spring and Summer, and spatially, in the wider mid estuary sections.

Although remote sensing needs extensive further development, it was proven to be a reliable tool with several advantages for systematic chl-a monitoring in the Tagus estuary. Specifically, it is a tool with high to assist the EU Member States to accomplish the WFD objectives.

Acronyms

AOP	:	Apparent Optical Property
B2k	:	BarcaWin2000 ®
Chl-a	:	Clorophyll-a concentration
CDOM	:	Colored Dissolved Organic Matter
CO_2	:	Carbon dioxide
CSZS	:	Coastal Zone Color Scanner
DIN	:	Dissolved Inorganic Nitrogen
E2K	:	EcoWin2000 ®
EEA	:	European Environmental Agency
EU	:	European Union
FLH	:	Fluorescence Line Height
FW	:	Fresh Weight
GPP	:	Gross primary production
GSM	:	Garver-Siegel-Maritorena Algorithm
INAG	:	Instituto Nacional da Agua (Portuguese National Water Institute)
IOCCG	:	International Ocean-Color Coordinating Group
IOP	:	Inherent Optical Property
L1B	:	Level 1B
L2	:	Level 2 (products)
LAADS	:	Level 1 and Atmosphere Archive and Distribution System
MAE	:	Mean Absolute Error (%)
MODIS	:	MODerate resolution Imaging Spectroradiometer
MERIS	:	European MEdium Resolution Imaging Spectrometer
N	:	Nitrogen
NASA	:	National Aeronautics and Space Administration
NIR	:	Near Infrared
nLw	:	Normalized Water Leaving Radiance
NPP	:	Net Primary Production
OOP	:	Object Oriented Programming
SeaDas	:	SeaWifs Data Analysis System
SPM	:	Suspended Particulate Matter
STD	:	Standard Deviation
P	:	Phosphorous
PAR	:	Photosynthetically Available Radiation
PC	:	Personal Computer
r	:	Correlation coefficient
Rrs	:	Remote sensing reflectance
RMSE	:	Root Mean Square Error
SEAWIFS	:	SEA-viewing WIde Field of view Sensor
Si	:	Silicate
USEPA	:	United States Environmental Protection Agency
VBA	:	Visual Basic for Applications
VNIR	:	Visible and Near Infrared
WFD	:	Water Framework Directive
WWTP	:	WasteWater Treatment Plants
Z_{euph}	:	Euphotic zone depth
Z_{mix}	:	Mixing zone depth

Index

Index of Figures

Index of Tables

Index of Annexes

1. Introduction

Transitional waters are surface water bodies near river mouths which are partly saline as a result of their proximity to coastal waters and are substantially influenced by freshwater flows (Chen et al., 2004). These systems are important and valuable in terms of biodiversity, ecology, support to human populations and role in the connection between terrestrial and aquatic ecosystems. Furthermore, over 50% of human populations live in coastal zones (e.g. Richardson & Ledrew, 2005). Estuaries, included on this surface water category, are highly productive ecosystems usually enriched with nutrients, in comparison with most offshore waters (e.g. Ketchum, 1967 in Liu, 2005), and have multiple sources of organic carbon to sustain populations of heterotrophs. Colored dissolved matter, suspended sediments and phytoplankton typically have higher concentrations in estuaries, when compared to oceans (e.g. Richardson & Ledrew, 2005). Estuaries are highly sensitive to climate variability, although, their communities are well adapted to temporal variability and spatial gradients such as salinity or temperature (e.g. Gameiro, et al 2007).

In estuaries there are three main types of producers: phytoplankton, benthic algae and vascular plants, which ensure maximum utilization of light and nutrients, mixed by the water movement due to tidal action and freshwater flow (e.g. Trancoso, 2002). Producers are the basis of the trophic chain supporting countless ramifications. In most estuaries, phytoplankton is usually the most relevant contributor to total production (e.g. Day et al., 1989) and, therefore, it is a key component in these systems providing an essential ecological function for all aquatic life (e.g. Lucas et al., 1999a). The consequent intense bacterial activity promotes rapid cycling of nutrients, which along with the hydrodynamic conditions, gives estuaries the unique capacity of self-depurating systems (e.g. Trancoso et al., 2005). The central biological variable for phytoplankton is upper-layer chlorophyll-a concentration (hereafter chl-a), which can be used to estimate phytoplankton standing stocks and productivity throughout the photic zone (e.g. Behrenfeld et al., 2006).

Phytoplankton is responsible for up to 90 percent of Earth's oxygen production, nearly all the energy necessary for the oceanic food webs, and provides the basis for life on planet Earth (http://www.livephytoplankton.com/). Scientific focus is placed upon phytoplankton when a management plan or an assessment of ecosystem health is needed (e.g. Monbet, 1992; Cloern 1999; Sin et al., 1999). Because they play an important role in the oceanic biological stimulation for carbon dioxide uptake (e.g. Behrenfeld & Falkowski, 1997), some scientists

have suggested that phytoplankton can be a solution to reverse the accumulation of anthropogenic carbon dioxide (CO_2) in the atmosphere (Richtel, 2007). Everyday more than $100x10^6$ tons of carbon, in the form of CO_2, are fixed into organic material by phytoplankton and a similar amount of organic carbon is transferred to aquatic ecosystems by sinking and grazing (Behrenfeld et al., 2006). There is still great uncertainty in the scientific community concerning the overall magnitude of global primary production, with estimates varying from 27.1 (Eppley & Peterson, 1979) to 50.2 Gt Cy^{-1} (Longhurst et al., 1995). Considering only coastal ecosystems' global production, estimates range between 8.9 and 14.4 Gt Cy^{-1} (Longhurst et al., 1995). Day et al. (1989) estimated an average phytoplankton production in estuaries of 256 gCm^{-2} y^{-1}, well above typical values (100 gCm^{-2} y^{-1}). In temperate estuaries, the typical primary production rates are 160 gCm^{-2} y^{-1} and lower values may indicate light limitation (Heip et al., 1995). Estuarine productivity can sometimes be deceiving, where annual phytoplankton production can be less than that of other marine environments (Cloern, 1987). In fact, Borges et al. (2006) stated that estuaries are significant sources of CO_2 to the atmosphere, at an average rate of 49.9 molC m^{-2} yr^{-1}, corresponding to a scaled emission over Europe, of 67.0 TgC yr^{-1}.

Phytoplankton information may be relevant for many applications, such as water ecology (e.g. Nobre et al., 2005; Ferreira et al. 2003; Richardson & Laurie, 2006), carbon budgets (e.g. Borges et al., 2006; Longhurst et al., 1995), socio economy (e.g. Duarte et al., 2003; Keppler et al., 2005; Richardson & Laurie, 2006), aesthetic and health issues (e.g. Lucas et al., 1999a; Zhang et al., 2006), and management of marine resources (IOCCG, 2006). Many of these applications interact with each other, for instance, a harmful algae bloom (HAB) will potentially affect aesthetic and health aspects, having negative economic impacts on existing culture stocks with multiple ecological consequences. There is particular relevance in understanding the factors that drive estuarine eutrophication and lead to changes in phytoplankton bloom dynamics (frequency, duration, magnitude, species composition), as a response to growing anthropogenic pressures (Anderson & Garrison, 1997). Also, because of growing public and scientific concern about global climate change, the effect of climatic factors on the distribution of phytoplankton biomass is of crucial importance to the assessment of long term changes in aquatic ecosystems (e.g. Gates, 1993 in Simas et al., 2001). Increased knowledge about the phytoplankton's seasonal and spatial distribution, as well as its magnitude, is thus of great relevance and can be used both for investigative and monitoring purposes, including a variety of present and future applications.

Regular monitoring of surface water status is fundamental to obtain estuarine information and to better understand its dynamics. Monitoring is carried out by assessing a range of quality parameters, which usually varies both, in time and space. Logistical and financial resource limitations are important factors controlling the scope and range of monitoring activities. It is necessary to develop robust and low cost tools, which support monitoring activities, ensuring that objectives are accomplished and enabling optimisation, quality and reliability (Ferreira et al., 2007b).

The Water Framework Directive (WFD), approved by the European Union (E.U.), establishes a set of water quality objectives and the overall goal is to achieve good water status for all E.U. waters by the year 2015. In the scope, application and practical implementation of the Directive, regular monitoring is stated as fundamental and determines water bodies classification and the need for additional measures to achieve its objectives. Member States must establish monitoring plans to regularly assess their aquatic ecosystems ecological status, determining their compliance, and must report to the European Environmental Agency (EEA) every two years (Chen et al., 2004; Ferreira et al., 2007b). According to the WFD, phytoplankton is considered to be a key biological quality element for transitional and coastal waters. The main parameters are composition, abundance and biomass (i.e. chl-a concentration), which also integrate other relevant indicators (Bricker et al., 1999; Bricker et al., 2003; ICES, 2004; Ferreira et al., 2005a & 2007b).

Estuarine phytoplankton information can be achieved by using in-situ samples, model application or remote sensing data. Several studies have been conducted in estuaries using in-situ data both for long and short term assessment (e.g. Cloern, 1987 & 2001; Conley, 1999; Monbet, 1992; Brogueira & Cabeçadas, 2006). In the Tagus estuary, specifically, there is extensive data from the 80's, but reduced coverage in the following decades. Data is disperse and results from punctual campaigns usually with short term objectives. Since 1999, there is an ongoing monitoring programme, with monthly sampling, aimed at long term monitoring of the most relevant quality parameters (Cabeçadas, 2003 in Brogueira & Cabeçadas, 2006; Gameiro et al., 2007). Most of the in-situ data is not free and\or confidential being, therefore, unavailable to the scientific community. Monitoring based on in-situ samples has high cost, which, in a limited resource context, can be a serious limitation to program implementation. Moreover, in-situ sampling provides limited spatial and temporal coverage and is a very time consuming task (e.g. Chen et al., 2004). In Portugal, the cost of a sample ranges from 1.500 to 2.000€ in inshore transitional waters and approximately 6.300€ in open coast waters. In an

annual monitoring program, the former can reach up to approximately 90% of the total cost due to the higher number of inshore water bodies, number of sampling stations and monitoring frequency (Ferreira et al., 2005b).

To overcome some of the limitations of in-situ sampling, modelling is used to develop hypotheses and understanding the ecosystem's dynamics, through simulation of the main processes. This is accomplished by using mathematical modelling that typically investigates the influence of each factor and then combines it in an ecosystem approach. Monitoring provides the necessary data to model setup, calibration and validation, while models provide knowledge on systems and processes that may improve the monitoring programme (Ferreira et al., 2005b). Furthermore, it enables the simulation of several scenarios thru testing and prediction (Ferreira et al., 2005b; Neves et al., 2000 in Trancoso et al., 2005), and spatial and temporal filling of information blanks. Therefore, modelling and monitoring are tightly coupled and the former may improve the efficiency by reducing the need for resources whilst achieving the defined objectives (Ferreira et al., 2007). Several studies have been conducted using modelling approaches (e.g. Trancoso et al., 2005; Nobre et al., 2005; Nunes et al., 2003; Ferreira, et al., 2007a) and specifically in the Tagus estuary (e.g. Antunes, 1998; Saraiva, 2001; Trancoso, 2002; Ferreira, 1989; Portela, 1996; Alvera-Azcárate et al., 2003). Data availability is still considered to be the most important factor limiting the development of operational water quality models (James, 2002) while the compilation of a database for comparison purposes and system understanding is mainly being limited by scarce spatial and temporal data (Monbet, 1992). Modelling accuracy is limited by the calibration and validation data and, although a valuable tool, does not provide real system information.

Remote sensing is currently one of the best methods to obtain systematic spatial and temporal information on coastal waters characteristics and to assess changes in relation to other factors (e.g. Gitelson et al., 2007; Zawada, et al., 2007; Wynne et al., 2006; Chen et al., 2007; Tzortziou et al., 2007; Chen et al., 2004; Hu et al., 2004). Since the 1970s, remotely sensed data has been used to estimate water quality characteristics of rivers, lakes and both coastal and open sea waters (Zhang et al., 2002b; Chen et al., 2004). One major advantage of remote sensing, over traditional in-situ measurements, is the provision of surface water information with higher spatial and temporal resolution (Lindell et al., 1999 in Zhang et al., 2002b). Considering resource limitation for monitoring activities, as stated previously, remote sensing technology can provide regular and synoptic low-cost solutions (Lindell et al., 1999 in Zhang et al., 2002b; Chen et al., 2004). Other benefits include the provision of observations with

associated continually expandable historical archives, the detection and spatial distribution of changes in water bodies. Remote sensing can also establish information datasets regarding point and diffuse sources of pollution mapping relevant to emission control and support the establishment of river basin management plans. Particularly under the WFD, these benefits have high potential to support the establishment of the monitoring programmes', and thus, to assist EU states meet their obligation under the very demanding timetable and resource limitation (Chen et al., 2004).

Remote sensing has been widely used in monitoring Case 1 waters, in which the principal component is chl-a usually in low concentrations. There is a growing concern in using remote sensing to monitor optically complex Case 2 waters. By using current advanced satellite sensors, a large number of water quality variables can be monitored on a regular basis, for instance, chl-a, total suspended sediment, type of particulate content, yellow substance or *gelbstoff*, turbidity, Secchi disk depth, wave height, colour index and surface water temperature (e.g. Zhang et al., 2002b; Chen et al., 2004). Proposed parameters and their frequencies for surveillance monitoring according to the WFD are described in Ferreira et al. (2007). Table 1 exhibits only the parameters with potential for direct or indirect remote sensing acquisition.

Table 1 - Monitoring Frequencies for possible remote sensing parameters (adapted from Ferreira et al., 2007b)

Water Bodies	Quality Type	Parameter	Frequency
Open Coastal water bodies	Biological	Phytoplankton	Seasonal/ Six Months
	Physico-chemical	Turbidity	Seasonal
		Temperature	Seasonal
Coastal and transitional water bodies	Biological	Phytoplankton (biomass & abundance)	Monthly
		Phytoplankton species composition	Six Months
	Physico-chemical	Temperature	Monthly

Chl-a concentration is the most widely used product derived from remote sensing ocean-colour data. It has been used to study and monitor open coast and sea systems (e.g. Carder et al., 2004; Vander Woude et al., 2006; de Souza et al., 2006; Zhang et al., 2006; Lavender et al., 2004) and inshore transitional systems (e.g. Hu et al., 2004; Wynne et al., 2006; Tzortziou et al., 2007; Gitelson et al. 2007). The approach used by Ciotti and Bricaud (2006, see also Ciotti et al., 2002) showed potential remote estimation of phytoplankton cell size in open coast waters with a good accuracy providing valuable ecological information on species

composition. Suspended particulate matter (SPM) can be estimated thru remote sensing in coastal waters with good accuracy (e.g. Miller and Mckee, 2004; Doxaran et al., 2002a & 2002b; Li et al., 2003; Doerffer and Schiller, 2007; Zawada et al., 2007; Chen et al., 2007; Hu et al., 2004), providing frequent synoptic maps of turbidity. Water surface temperature has been estimated using remote sensing techniques, mainly in deep sea and open coast systems (e.g. Zhang et al., 2002b; Zhang et al., 2004; Chan and Gao, 2005; de Souza et al., 2006; Vander Woude et al., 2006; Barré et al., 2006), and scarcely in transitional inshore systems (e.g. Davies, 2004; Li et al., 2001) The principal aim of surface temperature is to study global scale temperature dynamics, for instance for climate change assessment and research purposes.

The role of remote sensing technology is presently under scrutiny and several conceptual and practical requirements need to be fulfilled, such as an incomplete technical and scientific basis, to optimize the support for regional and global scale water status monitoring (Ferreira et al. 2007b, Chen et al., 2004). Remote sensing provides information mainly on the surface layer and thus, when vertical sampling is necessary it provides valuable but incomplete information. Another limitation is related to operational constraints on systematic remote sensing monitoring. According to some authors, accessibility, poor management, inadequate trained staff and knowledge transfer need to be improved to facilitate further research, training and education in remote sensing practical applications (Rosenqvist et al., 2003; Kalluri et al., 2003 in Chen et al., 2004). The cost of remotely sensed data can also, in some cases, be a major limitation. Low resolution and product accuracy are important issues concerning reliability and practical implementation, especially in inshore systems (e.g. Tzortziou et al., 2007; Chen et al., 2004). There is a trade-off between remote sensing data cost, quality and application coverage. For instance, the MODIS sensor provides traditionally 1km resolution data at no cost, whilst, the MERIS sensor provides 300m resolution data but with use restrictions.

It is fundamental that remote sensing retrievals are statistically assessed and validated in order to become a robust, reliable and valuable systematic tool for water bodies monitoring. Results for individual scenes are not very consistent showing large variability in the determination coefficient, varying from 0.59-0.98 (Lindell et al., 1999 in Chen et al., 2004). For that purpose, in-situ measurements are necessary to the development of robust and accurate algorithms (Chen et al., 2004). Due to the high costs of in-situ measurements and its synoptic limitations, it is important to develop tools and methods capable of regularly monitoring

phytoplankton temporal and spatial dynamics in estuaries. For estuarine applications, one of the major challenges is to develop multisource monitoring procedures, associating different sources of information, thus, minimizing their limitations and flaws (Prandle, 2000).

This work assesses the usefulness of remote sensing in the systematic monitoring of chl-a in the Tagus estuary. The assessment focus on an ecosystem scale and monthly to seasonal chl-a monitoring. This large Portuguese estuary has scarce and interspersed available data, concerning phytoplankton biomass, in the last 20 years. The implementation of the WFD requires that Portugal, as well as other State Members, should develop robust tools to ensure a regular and accurate monitoring of its water bodies in order to fulfill its obligations. This work was a first step to assess the feasibility of remote sensing data to provide accurate phytoplankton data, at a low cost, particularly, for monitoring purposes. The approach proposed is innovative in Portugal, concerning chl-a. The work objectives are:

(1) Assess the accuracy and reliability of the remotely sensed chl-a, comparing it with the simulations of an extensively tested ecological model.

(2) Define the conceptual and methodological framework to use remote sensing data for monitoring purposes in the Tagus estuary.

(3) Evaluate and compare Case 1 chl-a algorithms, extensively developed, and regionally calibrated Case 2 algorithms, proposed for other estuaries.

(4) Identify the major potentialities and limitations of remote sensing as a monitoring tool for chl-a in estuaries.

(5) Identify further work needed to ensure that remote sensing is a robust, accurate and systematic method to monitor the Tagus estuary.

Firstly, the state of the art in remote sensing of estuarine chl-a is described. In chapter 2.1, estuarine dynamics, concerning its relevant features, are addressed and in chapter 2.2, remote sensing techniques, sensors and algorithms are briefly described. The case study, the Tagus estuary, is presented in section 3.1, regarding the relevant features mentioned previously. Conceptual issues of model calibration and assessment are addressed in section 3.2, in the context of the modelling approach used in this work.

Due to the scarcity and limited spatial coverage of the in-situ data, direct comparison with remote sensing data, is limited and not feasible. The EcoWin2000 (hereafter E2K) ecological model was used to simulate phytoplankton on an ecosystem and seasonal scale. The E2K was

developed using an object-oriented (OOP) approach and as proved to be a useful tool for the understanding of temporal and spatial annual and inter annual phytoplankton patterns on an ecosystem scale. The estuary was divided in 13 coarse model boxes and, the main simulated features were hydrodynamics, suspended matter, dissolved nutrients and phytoplankton (chl-a) (section 3.3). The E2K was calibrated for the Tagus estuary using 1998 and 1999 in-situ data (section 3.4). The model was validated using the scarce in-situ data for 2000 and 2002, available in two system extremes, the upstream zone (Northern Channel) and the ocean inlet channel (section 4.1).

To assess the use of remote sensing products to monitor systematically the Tagus estuary at an ecosystem and seasonal scale, comparison was performed with the E2K model simulations. The remote sensing data from the Moderate Resolution Imaging Spectroradiometer (MODIS) instrument aboard the Terra (EOS AM) satellite was available since late February 2000 and was used in this assessment. Chl-a retrievals from various existing algorithms and remote sensing reflectances (hereafter Rrs) were generated for the Tagus estuary. The factors that influence their retrieval were briefly investigated, like atmospheric correction, quality control and geometry conditions, defining a conceptual and methodological framework for the further use of remote sensing data. For comparison purposes the remote sensing products were temporally composited, in 16 day periods, and spatially, according to the 13 E2K model boxes (chapter 3.5). The development of regional empirical algorithms for Case 2 waters, based on relations found in the literature, was addressed and tuned up using the year 2000 E2k simulations (chapter 3.6). All algorithms, existing and regionally tuned, were preliminary assessed using the E2K simulations, as ground truth, for the years 2000 and 2001 (chapter 4.2).

Finally, all existing remote sensing products and regionally tuned algorithms were assessed comparing them with an independent data set, the E2K chl-a simulations for the year 2002. Although the latter are not classic ground truth data (in-situ), usually used when testing and tuning remote sensing algorithms, the comparison allowed to assess the degree of accuracy, concerning magnitude and temporal patterns, in the chl-a estimation (chapter 4.3). Work limitations were addressed in chapter 5. Special emphasis was laid upon the sources of errors in the whole process, the expectable future use of remote sensing for estuary monitoring and on the necessary future work. In chapter 6 the main conclusions are exposed.

2. Remote sensing of estuarine chl-a: State of the Art

2.1 - Estuarine Dynamics

Water quality in an estuary is governed by the combination of physical, chemical and biological processes and their interdependence. Parameters like light, salinity, suspended particulate matter, nutrients and dissolved oxygen distribution, influence biological activity introducing large complexity in estuarine ecosystems (EPA, 1985). The physical, chemical and biological dynamics in shallow estuaries are mainly influenced by land freshwater runoff, the exchange of water with the sea and internal processes. The freshwater inputs influence estuarine hydrography driving salinity gradients, stratification and large import of silt, organic and inorganic substances (Flindt, 1999). In estuaries quality properties have steep gradients between the upstream and the estuary mouth. Downstream, characteristics are mainly oceanic and nitrogen is the main limiting factor, while upstream light availability is the most important limiting factor (e.g. Antunes, 1998).

The magnitude and spatial distribution of phytoplankton biomass in estuaries is controlled by (1) local mechanisms, governing the production-loss balance for a water column at a particular spatial location, and (2) transport-related mechanisms, which govern biomass distribution determining its spatial distribution (Lucas et al., 1999a & 1999b). It mainly depends on grazing, productivity factors, like temperature, light and nutrient availability, and also on hydrodynamic factors like resuspension, deposition, tidal amplitude and freshwater flow (e.g. Underwood and Kromkamp, 1999; Nybbaken, 1993; Valiela, 1995, Lucas et al., 1999b). Spatially, phytoplankton biomass is usually heterogeneous and patchy due to the combination of two major processes. Firstly, spatial variability in population dynamics is due to horizontal variations in local conditions and combinations of water column height, turbidity, grazing rates, among others (Lucas et al., 1999a). Thus, local conditions control population growth rates, i.e. if a bloom is possible. Secondly, spatially variable transport, in hourly and weekly time scales, determines bloom biomass concentration and distribution. Thus, large-scale transport processes control where a bloom occurs (Lucas et al, 1999b).

Eutrophication is an increasing problem in estuaries, stimulating the growth of primary producers, leading to oxygen depletion and structural changes which result in oscillations between the aerobic and anaerobic states (Flindt et al., 1999, Cloern, 2001). Eutrophication does not stimulate the total primary production per unit area but shifts the main productivity

from the benthic to the planktonic community. Oxygen production is then restricted to the surface layer and spatially and temporally separated from oxygen consumption (Flindt, 1999).

Grazing by zooplankton has a strong indirect regulatory effect on phytoplankton biomass, independently of the photosynthetic rates achieved (Nybakken, 1993). Grazing may provide a top–down control of eutrophication symptoms (e.g. Cloern, 1982; Lucas et al., 1999b) and its control on phytoplankton varies indirectly with water column height and is negligible for deep water columns (Lucas et al., 1999a). Due to anoxic conditions, induced by eutrophication, potential phytoplankton grazing is reduced greatly and for long periods (Flindt, 1999). Temperature is generally not a critical factor in the growth of phytoplankton in coastal waters (Valiela, 1995; Nybakken, 1993), being an indirect regulatory factor with influence on other factors, like nutrient bacterial regeneration and predatory activity, influencing directly the metabolic rates (Valiela, 1995; Day et al., 1989). Temperature increase coupled with sea-level rise will have an important impact on the benthic component of estuaries, through inundation, and pelagic production, through net photosynthesis increase, as well as a rise in respiration rates (Gates, 1993 in Simas et al., 2001).

Among the more relevant factors are nutrients and light availability, influencing primary production, and hydrodynamics, influencing transport and water column mixing, both with ecological impacts (Nybakken, 1993). The following sections will focus on these three main factors with particular focus on their impact on phytoplankton dynamics.

2.1.1 - Light

Primary production by phytoplankton is a light dependent process that provides the energy to drive the food web being limited to the uppermost layers of the water column (Liu, 2005). The depth to which about 1% of surface light penetrates is denominated as euphotic zone and its extent is determined mainly by the (1) incident surface radiation, and its consequent attenuation thru the water column. The efficiency in the conversion of radiation to energy by producers is governed by their (2) photosynthetic response to light.

2.1.1.1 - Incident Surface Radiation and Sub Surface Attenuation

Radiation fluxes at the Earth's surface play important roles in many ecological, climatological, and hydrological systems. In ecological processes solar radiation often acts as the key driving

force (Brock, 1981) because biological activity is strongly dependent on radiative transfer directly through the interaction between phytoelements and radiant energy emitted by the sun (Oliphant, 2006). The physical and chemical factors that influence incident surface radiation are particularly relevant in primary production forcing, stimulating photosynthesis. Because remote sensing depends on surface radiation reflectance, thus primarily on incident radiation, this section will provide deeper insight to the significant factors that influence the latter.

The solar constant is the energy received per time at the Earth's mean distance from the Sun and its seasonal magnitude is influenced by the Earth's ellipticity during its revolution around the Sun. This movement around the Sun also determines the angular distance at solar noon between the former and the Equator. These factors, when combined, drive, for instance, higher spring and summer primary production due to higher light availability. Besides the motion around the Sun, the Earth's daily rotation around itself influences, for instance, daylength. From the winter to the summer solstice the daylength increases, thus average daily radiation, stimulating photosynthesis and forcing spring and summer blooms (Brock, 1981). Incident surface radiation also depends on geometric conditions. The zenith angle is defined by the angle between zenith, the point vertically above one specific geographical position, and the Sun position (e.g. Lillesand et al., 2004). The zenith angle is related to the intensity of solar radiation on a flat surface and determines the incident surface angle at which the light strikes the surface of the water, and consequently, the amount of back-reflectance (Oliphant, 2006). Geometric conditions influence mainly photosynthesis dynamics on a daily basis, with respect to the diurnal curve of solar radiation.

Radiation at the surface of the Earth is composed by two components, the direct and diffuse. Their sum is the global incident radiation at one specific geographical position. The direct component of solar radiation is the result of incident Sun rays, whilst the diffuse component is the result of scattering from atmospheric particles (Brock, 1981). Solar radiation is attenuated during its passage thru the atmosphere due to scattering, absorption and turbidity. Scattering is mainly due to small particles which change radiance intensity and directionality. According to the Rayleigh theory, scattering is highly wavelength dependent and varies as $wavelength^{-4}$. Scattering does not remove photons but increases their mean path length and the probability of being absorbed (e.g. Lillesand et al., 2004). Absorption is mainly performed by gases such as ozone, water vapour and carbon dioxide and changes radiance intensity (e.g. IOCCG, 2006). In the ultraviolet region of the light spectrum, absorption is mainly due to ozone and in the infrared region, due to water vapour (Brock, 1981). Turbidity is related to large particles,

for instance aerosols (Brock, 1981) and can play a major role in solar radiation attenuation, especially in urban and industrial areas. Moreover, optical transmissivity and cloud conditions influence radiation pathway, and thus, magnitude (Oliphant, 2006). The attenuation of solar radiation limits surface light availability on a daily, and specially, on a seasonal basis. Solar radiation variability is relatively low considering small temporal scales, days to weeks, and is particularly relevant considering large scales, months to seasons, with the latter playing a crucial role in the variability of ecosystem functioning (e.g. Oliphant, 2006).

Potential production is not always reached in estuaries due to light attenuation and/or due to the very fast renewal rate of the system. The former, due to water turbidity, is frequently the major factor controlling phytoplankton production and the turnover rate in estuaries (e.g. Cole et al., 1992; Cloern, 1987; Harding et al., 1986; Irigoien and Castel, 1997). Suspended particulate matter (SPM) is highly related to vertical light attenuation, and its spectral distribution, absorbing and scattering the radiation beams. Typical high SPM concentrations in estuaries confine the photic zone to a small shallow fraction of the water column, attenuating light rapidly and thus reducing phytoplankton photosynthesis, as well as, net water column productivity due to higher biomass loss driven by respiration (Cloern, 1987). Absorption and refraction by water, dissolved matter and SPM, determine the quantity and spectral quality of light at a given depth (Jerlov 1976 in Liu, 2005; Prieur and Sathyendranath, 1981). Detailed understanding of the interaction between estuarine turbidity and phytoplankton dynamics requires good understanding of vertical mixing and phytoplankton production and respiration.

Riverine inputs of SPM and/or tidally driven resuspension of bottom sediments act as mechanisms that influence the spatial and temporal variability of estuarine turbidity (Cloern, 1987). High tidal amplitudes, typical of spring tides, are associated with strong tidal currents which stimulate small scale resuspension (Portela, 1996). Wind effects also play a key role in water mixing and resuspension (Gameiro et al., 2004; Cloern et al., 1985). Recent studies suggest that tidal runoff and erosion from intertidal mudflats can also be important contributors (Prahl and Coble 1994 in Prahl et al., 1997). Anthropogenic activities influence SPM concentration through waste dumping and sewage discharges (Mutua et al., 2004). Phytoplankton in-situ production can also act as a source of SPM (Small et al., 1990), however, in highly turbid systems, this component of particulate matter only accounts for a small percentage and is not a major determinant of turbidity (Alvera-Azcárate et al., 2003).

Some authors have proposed an indicator of favourable conditions for phytoplankton growth, thus bloom initiation and development, using the ratio between mixing (Z_{mix}) and euphotic depth (Z_{euf}), determining the time spent by cells in the light (e.g. Alpine and Cloern, 1988; Gameiro et al., 2007). The time scale of mixing influences photoadaptation and inhibition of phytoplankton cells (Lewis et al., 1984 & Gallegos and Platt, 1985 in Duarte and Ferreira, 1997). Sverdrup (1953) proposed the ''critical mixing depth'' approach which assumes that the phytoplankton population is homogeneously distributed over depth and that growth depends mainly on light. It indicates whether net growth is possible or not (Platt et al., 1991), i.e. if the ratio is lower than 1 the entire water column is located within the euphotic zone and a ratio of 5 is the upper limit for net growth and bloom initiation (Lucas et al., 1998).

Therefore, SPM distribution vertically regulates estuarine phytoplankton dynamics, according to variations in the photic and mixed depth ratio and longitudinally, due to resuspension and both, ocean and river inputs (Cloern, 1987; Liu, 2005; Prahl et al., 1997). Moreover, it affects both biological and physico-chemical processes and can serve as a source or sink of carbon and nutrients (Mutua et al., 2004).

2.1.1.2 - Photosynthetic Response

Photosynthesis is the process by which producers use carbon dioxide, water and nutrients to convert incident radiation in chemical energy producing biomass. It depends on how producers interact with light and their energy conversion efficiency. Phytoplankton synthesize less chl-a if more light is available, so the chlorophyll to carbon ratio (chl:C) decreases as irradiance increases. Assimilation of new cellular carbon is faster if more light is available, thus the depth-averaged rate of photosynthesis increases as irradiance increases (Cloern et al., 1995). Therefore, for a given light attenuation coefficient, as the water column height increases the chl:C increases and photosynthesis decreases (Lucas et al., 1999a).

The photosynthesis-irradiance (P-I) relationship is related to the phytoplankton response to the light and nutrient availability. It is fundamental to estimate phytoplankton productivity (e.g. Macedo and Duarte, 2006) and several mathematical models have been proposed (e.g. Steele, 1962; Platt et al., 1980; Eilers and Peeters, 1988; Janowitz and Kamykowski, 1991). Most of the models are based on empirical relationships determined experimentally and only a few are deduced from the physiology of photosynthesis (e.g. Fasham and Platt, 1983; Eillers and Peeters, 1988). Increases in light intensity lead to increased production until a maximum

is reached and producers can no longer use more light because the enzymes involved in photosynthesis cannot act fast enough to process light quanta any faster (e.g. Trancoso, et al., 2002). The rate of photosynthesis, reaches therefore an asymptote, which is the maximum productivity (P_{max}) with a corresponding optimal light intensity (I_{opt}).

During the day, algal photosynthesis closely follows the variation in light intensity, the optimal light intensity is reached, from which the P-I relation becomes increasingly more nonlinear (e.g. Marra and Heinemann, 1982). When light intensity remains critical for a long time, photoinhibition relevance increases (Duarte and Ferreira, 1997). Some models assume a saturation curve in which production reaches a constant value when optimal light intensity is reached (e.g. Webb et al., 1974; Franks and Marra, 1994). Others consider photoinhibition where carbon fixation declines at high irradiance (e.g, Eillers and Peeters, 1988; Duarte and Ferreira, 1997). Models can be divided into static and dynamic, depending on whether the parameter values ruling the P-I relationship are respectively considered steady-state or time-dependent (Macedo and Duarte, 2006; Duarte and Ferreira, 1997). The static formulations are the most widely used (e.g. Steele, 1962; Webb et al., 1974). Dynamic formulations consider the effects of time exposure to light on photosynthetic responses, including the development of photoinhibition (e.g. Duarte and Ferreira, 1997; Janowitz and Kamykowski, 1991).

Recent evidence shows that parameters used in the P-I curves change over time due to the physiological adaptation to light in different time scales (Duarte and Ferreira, 1997). Phytoplankton can maintain a high production rate during the first minutes after initial exposure to critical irradiance during the day (Marra, 1978a in Macedo and Duarte, 2006). At night they adapt themselves to shading, exhibiting a higher photosynthetic efficiency in low light and, in both cases, variations in the initial P-I slope (Falkowski and Wirick, 1981 in Duarte and Ferreira, 1997). In coastal systems and estuaries, the assumption of static P–I curves might lead to a 21 to 72% underestimation of phytoplankton primary productivity (Macedo et al., 2002), corresponding to an increase in global primary production of 3.8-6.2 Gt Cy^{-1} (Macedo and Duarte, 2006). However, considering dynamic behaviours is more relevant in high light conditions and/or in the absence of vertical mixing (Duarte and Ferreira, 1997).

2.1.2 - Nutrients

Nutrient dynamics in estuaries strongly depend upon their external supply and internal regeneration. Organic matter is produced by a large variety of primary benthic and pelagic

producers (Flindt, 1999). The temporal and spatial variability of nutrients in estuaries is important in the control of producers' growth. These are determined by riverine fresh water and ocean tidally driven inputs, runoff, atmospheric precipitation, waste loads and also by internal recycling of nutrients (e.g. Gameiro et al., 2004; EPA, 1985). The macronutrients required for their growth are carbon, phosphorous, which is available in the form of phosphate, and nitrogen, which is available in the inorganic forms of ammonia, nitrate and nitrite. Moreover, micronutrients like calcium, potassium, sulphur iron, manganese, sulphur, zinc, copper, cobalt, and molybdenum are also required and are naturally abundant in marine ecosystems (EPA, 1985). Some producers, like diatoms, also require silica for growth which limits production mainly in fresh waters (Boney, 1975).

The nitrogen (N) cycle is a complex set of mechanisms and processes. Dissolved inorganic nutrients are removed from the water column by producers during photosynthesis. They are regenerated and distributed through soluble excretions, death of all organisms, the decomposition of suspended organic detritus and sediments, and the hydrolysis of dissolved organic nutrients (EPA, 1985). The processes involved depend not only on biological aspects but also on pH and temperature (Wetzel, 1993). Nitrogen can be assimilated by producers mainly as ammonia (NH_4^+) and nitrate (NO_3^-) forms. There seems to be a preference for the former form, because it is more reactive and nitrate assimilation implies conversion to ammonia, leading to higher energy spending (Portela, 1996; Wetzel, 1993).

In most salt-water systems phosphorous (P) is released from sediments and behaves essentially as a conservative tracer of benthic decomposition. The lower efficiency of salt-water sediments in binding and sequestering phosphorous, when compared to freshwater systems, is large enough to influence the often cited difference in phytoplankton nutrient limitation between both systems. Thus, it is usually abundant in estuarine systems, playing a smaller role in production limitation (Portela, 1996; Conley, 1999; Nixon, 1996; Caraco et al., 1990). Furthermore, phytoplankton cells are capable of accumulating phosphorous reserves and zooplankton excretion products may also be an important source (Boney, 1975).

Previous studies indicate that N is usually the primary limiting nutrient in coastal systems (e.g. Howarth, 1988; Mallin, 1994; Portela, 1996; Nixon, 1996; Conley, 1999). However, some studies suggest that in some estuaries P limits during spring and N limits during summer (D'Elia et al., 1986 in Conley, 1999). The former is often weaker than the latter and more pronounced near the freshwater inlets (Malone et al., 1996 in Conley, 1999). Redfield (1934)

demonstrated a relatively constant atomic proportion in oceanic algae exhibiting, respectively, a molar element ratio 106:16:1 for carbon (C), nitrogen (N) and phosphorus (P). Estuarine phytoplankton have a similar composition and, when nutrients are not limiting, the N:P ratio is about 16 (in atoms). The Redfield ratio depends on life strategy being a general average rather than a specific requirement for phytoplankton growth (Arrigo, 2005).

High freshwater inputs can stimulate primary production by importing nutrients into the system (e.g. Harding, 1994). Human activities have increased N and P fluxes and fertilization of coastal ecosystems is a growing environmental problem, disrupting the balance between the production and metabolism of organic matter (Cloern, 2001). According to Conley (1999), nutrient loading to estuarine systems has increased 6–50 and 18 to 180 times, for N and P respectively. Eutrophication can lead to the death of aquatic organisms, which stimulates significant internal nutrient loading due to their microbial mineralization (Flindt, 1999).

2.1.3 - Hydrodynamics

Estuaries are characteristic because of their shallow water column, often well mixed and thus resulting in coupled benthic and pelagic processes (Flindt, 1999). Due to their shallowness, estuaries are specially influenced by wind, inducing vertical mixing, tidal fluctuations, and broad meteorological conditions, influencing general water circulation (James, 2002). The connection to open marine areas imposes large scale physical and chemical forcing due to tidal water exchange, insuring large transport (Berner, 1996 in Flindt, 1999).

Phytoplankton blooms are driven by population responses to changing physical dynamics and production occurs preferably between unstable and stable hydrodynamic conditions (Legendre and Demers, 1985). Unstable conditions are represented by vertical mixing which leads to a homogeneous nutrient concentration driven by resuspension, on a tidal scale, or by riverine water input, mainly on a seasonal scale. Stable conditions are caused by stratification, driven by low tidal mixing and fresh water flow, which induces phytoplankton growth. The stability of the water column depends on tidal and seasonal cycles (e.g. Cloern, 1991). The balance between fresh and saline water, along with tidal currents, contributes to the existence or absence of vertical stratification (e.g. Gameiro et al., 2004; Monbet, 1992).

The mechanical energy driving vertical mixing in estuaries is produced by tides, wind stress, and freshwater runoff (Monbet, 1992) inducing vertical transport of organic and inorganic

matter (Flindt, 1999). Tidal fluctuations regulate the amount of turbulent mixing present in the water column to counter the stabilizing effects of freshwater inputs. A strong tidal influence coupled with typical shallow depths typically results in vertically well mixed conditions and stratification only occurs in punctual situations (Lucas et al., 1999a). Moreover, the extent of vertical mixing processes is more pronounced in macrotidal estuaries (Monbet, 1992). Intense vertical mixing can produce changes in light conditions that change faster than the phytoplankton physiologic adaptation (Marra, 1980 & Demers et al., 1986 in Monbet, 1992). Huisman et al. (1999) showed that critical turbulence is a mechanism for the development of phytoplankton blooms, leading to a possible bloom if turbulent mixing rates are lower than a critical point. This condition is irrespective of the depth of the water column, demonstrating that, in the absence of water column stratification, bloom development is possible, particularly in shallow estuaries.

The *residence time* reflects how long a material is maintained in a region (Lucas et al., 1999b) and has been pointed out as an important factor in bloom development (e.g. Huzzey et al., 1990; Muylaert et al., 1997; Valiela et al., 1997). It is mainly governed by fresh water advective physical forcing and temporal shifts can change the residence time influencing the export rate of phytoplankton biomass. Water *residence time* has also been pointed out as a possible mechanism regulating species composition and biodiversity by physically limiting the capacity of phytoplankton to grow faster than it is flushed. The higher the system's residence time the lower the P_{max} needed to maintain a phytoplankton specie, and vice-versa. Therefore, a reduction in freshwater input may induce changes in phytoplankton composition and biodiversity with several negative impacts (Ferreira et al., 2005a). Material can be transported to a region thru *import*, leading to biomass accumulation in an unproductive region if the export and local losses are relatively lower. The existence of a *main channel* can play a key role as a large scale conduit for wide biomass transport and dispersion. This process is driven by a larger inertia:friction ratio in the channel, which results in greater tidal excursions and velocities. The channel productivity can significantly enhance or constrain the large-scale distribution of phytoplankton biomass. These three mechanisms, *residence time*, *import* and the *role of a main channe*l, are low frequency subtidal transport processes which occur over time scales of days or weeks (Lucas et al., 1999b).

High frequency mechanisms occur on tidal or hourly time scales. For instance, *lateral sloshing* is a tidal-scale-mechanism which forces material out of a shallow region and into a deep channel region on ebb tide, and then back into the shoal during flood tide. It depends on

the width of the shoal, bathymetry and lateral tidal excursion. The *phasing* between tidal-time-scale changes in transport can induce a shift in mass transport and local growth, particularly in shallow zones, where growth rates are more sensitive to water column height variation (Lucas et al., 1999b). Hydrodynamic variations in water column height, due to bathymetric and tidal variations, affect the distribution of phytoplankton sources and sinks in a shallow estuary, as well as transport-related mechanisms controlling system-level bloom dynamics. For a given light attenuation coefficient, pelagic production decreases as column height increases because depth-averaged irradiance varies inversely with the former. The effects of the tidal cycle on growth rates in deeper waters are mainly consequence of light limitation, whereas in shallow waters, are consequence of the photoinhibition and benthic grazing. The influence of the latter increases as column height decreases because phytoplankton is more accessible to the benthos. For instance, the combination of low turbidity and high benthic grazing may lead to negative growth rates during low tide and positive during high tide (Lucas et al., 1999a).

The spring-neap cycle induces oscillations which influence phytoplankton production, mainly enhancing or dampening the effect of other factors already mentioned. For instance, grazing effects in shallow regions have a higher impact during spring-ebb tide than during neap-ebb tide, thus, day-averaged growth rates are typically negative in the former and positive in the latter (Lucas et al., 1999a). Spring tides increase vertical and turbulent mixing leading to lower photosynthetic activity and chl-a concentration because producers spend less time in the photic zone (Monbet, 1992). Neap-tide blooms are mainly due to reduced turbulent mixing (Cloern, 1991), reduced suspended sediment concentrations (Cloern et al., 1985; Thompson 1999 in Lucas et al., 1999a) and dampened low-tide benthic grazing (Lucas et al., 1999a).

Factors such as water residence time (e.g. Ketchum, 1954; Tett et al., 2003), tidal range (Alvera-Azcarate et al., 2003) and turbidity (May et al., 2003) are important drivers of the nature and magnitude of eutrophication symptoms (Ferreira et al., 2005a). Excessive phytoplankton biomass, nuisance or toxic algae are generally more probable in systems with lower flushing rates (Ferreira et al., 2004). For instance, dinoflagellates, frequent in harmful algal blooms, have maximum growth rates significantly lower than those of diatoms (Smayda, 1997; Furnas, 1990) and thus may only have the capacity to grow in estuaries when the water residence time increases (Ferreira et al., 2005a).

2.2 - Remote Sensing Techniques

2.2.1 - Remote Sensing of Ocean Colour

Remote sensing of ocean colour was initially focused on retrieving the concentration of chl-a in the open oceans and to date it has been the most successful and widespread application. Either as a cause or consequence, space-borne remote sensors have been designed and implemented with the principal aim of ocean monitoring (e.g. Richardson and Ledrew, 2006; Chen et al., 2004). Significant progress has been achieved and there has been growing concern in understanding and retrieving the inherent optical properties (hereafter IOPs), namely the scattering and absorption. The IOPs are clear indicators of changes in the water mass and its constituents, both dissolved and suspended material (IOCCG, 2006).

The study of coastal and transitional aquatic ecosystems could benefit greatly from the usefulness of remote sensing technologies, including synoptic quantitative regional and global data sets, repeated and continuous sampling and, in many cases, historical data. The limitations of remote sensing include costs, suitability for detailed monitoring, revisit time, accessibility to data, and poorly developed and validated algorithms (Richardson and Ledrew, 2006; Chen et al., 2004; Lee and Carder, 2005; Chen et al., 2007). Algorithms are mainly driven by the optical and biological complexity of these systems, such as, typical shallowness, which induces bottom reflectance, benthic optical contribution and highly variable spectral signatures (Richardson and Ledrew, 2006). Moreover, temporal and spatial dynamics are much more relevant features in coastal systems than in oceans and chl-a, CDOM and SPM are usually in higher concentrations in the former.

Contrary to in-situ methods, which measure separately the physical or chemical components of water, remote sensing acquires both based on the spectral appearance, in a process called spectral remote sensing (e.g. Lee and Carder, 2005). Passive remote sensors use the solar irradiance as the “power source”, whilst active sensors provide their own source, for instance, radar technology (e.g. Lillesand et al., 2004). Radiance received at spacecraft is driven by sunlight, passing through the atmosphere and being reflected, absorbed and scattered by the water and its constituents. Waves, sun glint, white caps, bubbles and surface slicks also affect the redistribution of penetrating light. Radiance is transmitted back through the atmosphere to the space-borne passive sensor being modified by scattering and absorption processes from the air, like Rayleigh scattering, suspended particles in the air, like Mie scattering and

selective absorption by ozone and water vapour (Clark, 1997; Lillesand et al., 2004). The IOPs affect the spectrum and radiance distribution of the light emerging from the ocean, hereafter referred to, as water leaving radiance. The IOPs do not depend on the radiance distribution but are highly wavelength dependent (IOCCG, 2006; Zaneveld et al., 2005). The normalized water-leaving radiance (nLw) is defined as the upwelling radiance just above the sea surface, in the absence of an atmosphere, and with the sun directly overhead. The remote sensing reflectance (Rrs) is the nLw divided by the solar irradiance, i.e. the relative fraction of radiance that reaches the sensor (http://oceancolor.gsfc.nasa.gov/). Remote sensing of water bodies relies in the assumption that if a successful removal of the atmosphere and surface effects is performed, it is possible to retrieve the scattering and absorption characteristics and estimates of dissolved and particulate concentrations, through the inversion of the Rrs acquired by the sensor (e.g. Zaneveld et al., 2005; IOCCG, 2006). One major difference between land and water remote sensing is the sensitivity needed in the retrieval of the water leaving optical signal, which is typically between 0 to 10%. Therefore, a sensor must be accurately calibrated to provide a high signal-to-noise. For instance, a 5% error in at-sensor radiances may result in a 50% Rrs error (Chen et al., 2007; Franz et al., 2006)

The spectral quality and quantity of the water leaving radiance is mainly determined by the IOPs and algorithms usually look for a combination of signals at different wavelengths in order to find a mathematical relation concerning a specific water constituent. The coefficients of this relation are usually derived using data collected at various spatial and temporal scales, therefore, minimising the associated noise. Due to the complexity of processes involved, the water mass is often considered as a black box, diminishing the IOPs relevance (IOCCG, 2006). Algorithms can be empirical or analytical, the former are based on simple relationships derived from Rrs data using the black box approach and the latter on the retrieval of process information i.e. the IOPs (e.g. Chen et al., 2004; IOCCG, 2006). Currently, the analytical approach is in fact semi-analytical because IOP determination is based on empirical relations at one or more wavelengths (e.g. Carder et al., 1999; Maritorena et al., 2002).

Water colour is determined by the IOPs, being chl-a only one of the active components, and therefore, its determination is followed by a larger uncertainty than that of the IOPs themselves. Improvements in this area will be driven primarily by enhanced understanding on how reflectance and the IOPs relate and, secondarily, by how the latter relate to dissolved and suspended water constituents (IOCCG, 2006). This will potentially enable and optimize a reliable remote sensing utilization and application. Approaches based on radiative transfer,

both in the forward and inverse way, are essential to obtain further improvements. Detailed description of the latter is beyond the scope of this work but a recent review can be found in Zaneveld et al. (2005). Briefly, the two key IOPs relevant to the water leaving radiance are the total absorption a (m^{-1}) and scattering b_b (m^{-1}) coefficients, often separated into, dissolved and particulate fractions, and water (Equation 1 and 2). The subscripts "g", "p", and "w" represent respectively dissolved, particulate matter, and water. On the other hand, subscripts "ph" and "d" represent respectively, the algal and non-algal components of the particles. Scattering can occur in back and forward directions, with subscripts “b” and “f” respectively. The beam attenuation coefficient is determined by the sum of absorption and backscattering (Zaneveld et al., 2005; IOCCG, 2006). Note that, only the term α_{ph} relates to chl-a concentration.

$$a = a_w + a_{ph} + a_d + a_g \qquad \textbf{Equation 1}$$

$$b_b = b_{bw} + b_{bp} \qquad \textbf{Equation 2}$$

In Case 1 waters, optical properties are primarily determined by phytoplankton and related CDOM and detritus degradation products which covary. In coastal Case 2 waters, light attenuation is greater due to optical complexity in the form of inorganic particulates, and due to a greater variety and higher concentration of dissolved and particulate organic matter which do not covary with phytoplankton (e.g., Mobley et al., 2004). Therefore, given this non covariance and the fact that the IOPs are not all a function of phytoplankton, deriving simple chl-a and reflectance relationships will often lead to incorrect results (Zaneveld et al., 2005). Moreover, chl-a can be determined with greater accuracy if there is a full understanding of all the optical processes involved (IOCCG, 2006). Note that the IOPs in Case 2 waters are typically two to four orders of magnitude different from Case 1 waters (Schalles, 2006).

Radiative transfer equations describe the interactions between the inherent optical properties, or IOPs and apparent optical properties (AOPs), remotely acquired (Schalles, 2006; IOCCG, 2006). With simple approximations, the Rrs acquired by the sensor can be generically expressed directly in terms of the IOPs:

$$R_{rs} = \frac{L_u(0^-)}{E_d(0^-)} = g\,\frac{b_b}{a} \qquad \textbf{Equation 3}$$

where, L_u (0^-) and E_d (0^-) are respectively, the upwelling radiance and downwelling irradiance just below the sea surface. Therefore, the Rrs which reaches the sensor, after the removal

atmospheric effects, is directly proportional to backscattering and inversely proportional to absorption (IOCCG, 2006). The proportionality factor *g* depends on how backscattering is related to its coefficient and on geometrical conditions, thus containing the directional effects of radiative transfer (Morel and Gentili, 1993; Lee et al., 2004). The equation above is the starting point for many current semi-analytical inversion algorithms (e.g. Carder et al., 1999; Maritorena et al., 2002; Lee et al., 2002). Moreover, optical modelling can also be used to model the Rrs using a set of IOPs, resolving Equation 3 in the forward direction (e.g. Feng et al., 2005; Bricaud et al., 1998 & 2004).

Besides optical modelling and radiative transfer equations, which have been widely used in Case 1 waters, the Case 2 algorithms development has been frequently addressed using the spectral signatures approach (Tzortziou et al., 2007; Gitelson et al., 2007; Richardson and Ledrew, 2006; Schalles, 2006). This is driven by the very different optical properties between both, because phytoplankton, CDOM and SPM concentrations are typically one or two orders of magnitude higher in Case 2 waters. These components have strong effects on the water leaving signal when they are present in high concentrations. Algorithms developed for Case 1 waters are not accurate under high concentrations of phytoplankton and/or SPM, which can lead to significant under or over estimation of the former (e.g. Richardson and Ledrew, 2006; Gitelson et al., 2007; Stumpf et al., 2000; Tzortziou, et al., 2007).

2.2.2 - Remote sensing of Case 2 waters

The advantages and main challenges of remote estimation of chl-a in Case 2 waters are well defined. However, operational monitoring programs are not fully developed and need further sensor and algorithm improvements (IOCCG, 2000). Approaches in these types of waters are based on the sunlight absorption by algal pigments (pigment-specific) in the presence of light scattering and absorption by algal and non-algal particles. This combination and diversity of optically active constituents partially masks fundamental phytoplankton absorption and scattering relationships, producing graded responses in the water leaving optical signals. The Case 1 algorithms are based on a simple relation: as phytoplankton concentrations increase, pigment absorption increasingly dominates at blue wavelengths, causing decreased reflectance, while scattering dominates at mid-green wavelengths causing a reflectance increase. Therefore, simple blue green ratios work relatively well in Case 1 waters. This relationship becomes less sensitive when chl-a concentrations are high and/or when CDOM

and SPM are significant and/or when the chl-a to total algal pigments ratio deviate from standard assumptions (Schalles, 2006).

Chl-a has a prominent absorption peak at the blue wavelengths and a secondary red absorption peak (Figure 1). The variety and packaging effect of phytoplankton pigments have overlapping spectral absorptions, particularly in the blue region, affecting chl-a estimation. However, chl-a can be distinguished by the characteristic narrow red absorption peak (~680nm), discernable when its concentration is higher than 1 μgl^{-1}, where water absorption is also high. Besides the relative contribution of accessory pigments and their packaging, the phytoplankton absorption spectrum is also influence by taxonomy, the size structure and physiological state of algal populations (Bricaud et al., 2004; Ciotti and Bricaud, 2006; Carder et al., 1999; Ciotti et al., 2002). The latter author states that the phytoplankton population size explains more than 80% of the variability in its spectral absorption shape.

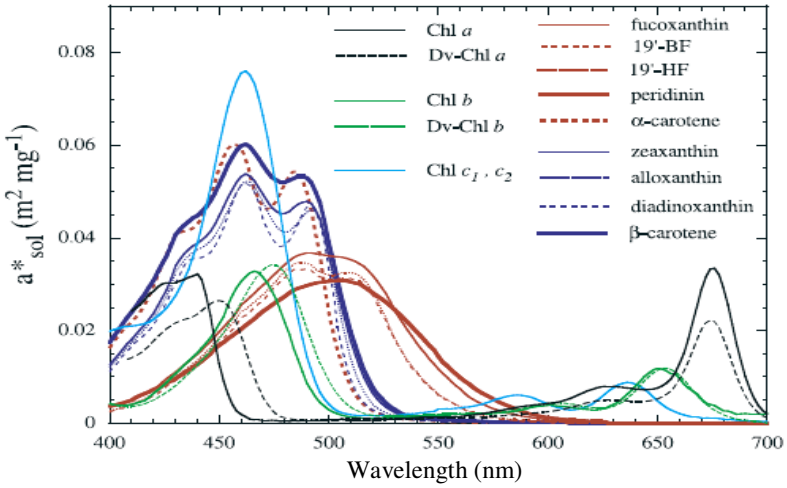

Figure 1 - In vivo weight-specific absorption spectra of the main pigments, a*sol,i(λ) in m^2 mg^{-1} (taken from Bricaud et al., 2004).
Photosynthetic and non photosynthetic carotenoids are shown in red and blue, respectively.

Colored dissolved organic matter (CDOM), also called gelbstoff or gilvin, is largely composed of humic substances, which result from the decomposition of plant materials from land inputs or in-situ production. At wavelengths greater than 300nm absorption by CDOM is inversely related to wavelength and described by an exponential decay curve (Figure 2) (Schalles, 2006; Keith et al., 2002; Ciotti and Bricaud, 2006). Although CDOM absorbs especially in the blue region, in very high concentrations it can affect reflectance over the whole visible spectrum, particularly attenuating the prominent green peak (Schalles, 2006).

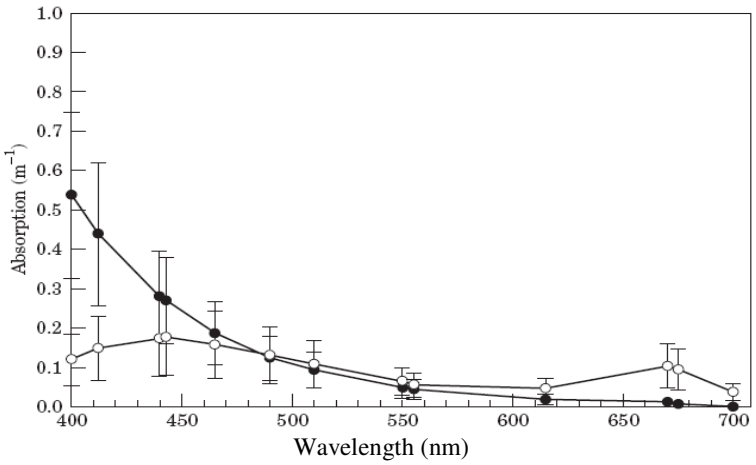

Figure 2 – Average CDOM (filled) and chlorophyll-specific (clear) absorption spectra for Narragansett Bay (taken from Keith et al., 2002).

Scattering is driven by the interaction, mainly reflection, of light with inorganic and organic suspended particles. Scattering increases reflectance decreasing monotonically with increased wavelength, but, in turbid waters the photon emergence at infrared is not negligible (Figure 3) (Mobley, 1994 in Schalles, 2006). Therefore, the "black pixel" assumption, frequently used in atmospheric correction over the ocean, does not work in turbid waters and can lead to errors in the chl-a estimation (e.g. Chen et al., 2007; Miller and McKee, 2004; Schalles, 2006; Siegel et al., 2000). The combination of CDOM, phytoplankton and SPM signals enhances the complexity of Case 2 waters and spectral signatures analysis have been used to discern the combined effects (Gitelson et al., 2007; Schales, 2006; Doxaran et al., 2002a).

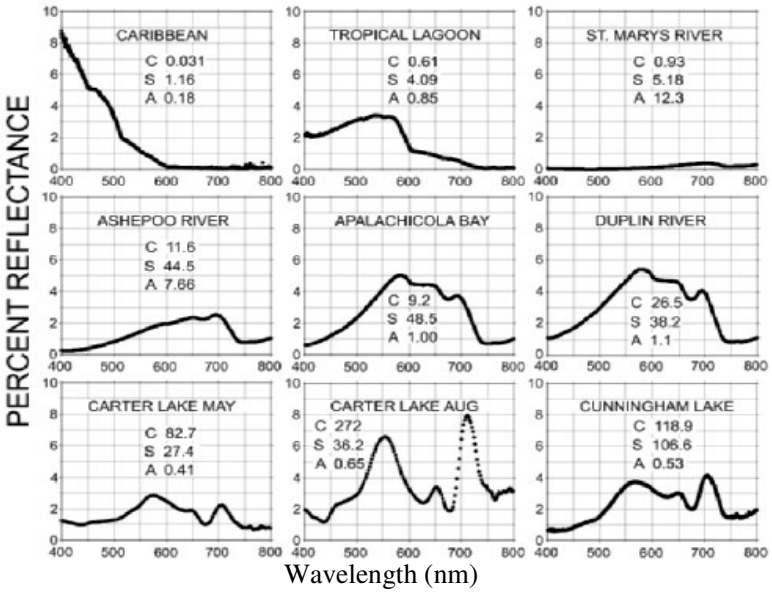

Figure 3 – Water reflectance spectra measured at various coastal, estuarine, and inland locations representing a broad range of optically active constituents.
Note: C = µg chl-a l^{-1} of; S = mgl^{-1} of SPM; A = m^{-1} of CDOM absorption at 440 nm (taken from Schalles, 2006)

Schalles (2006) provides an excellent review of the spectral effects of these components: Concerning only phytoplankton, at wavelengths below 510nm, reflectance decreases with increasing cell density due to pigment absorption and increases above it, resulting in a hinge point near 510nm. With the addition of SPM, the hinge point shifts towards higher wavelengths. Because scattering decreases monotonically with increased wavelength, the SPM increase leads to increase reflectances, particularly, in the blue and green regions. High CDOM concentrations can suppress the dominant scattering in the green region and flatten the reflectance spectra (Figure 3). When phytoplankton concentration increases a green peak, near 550nm, becomes evident at chl-a above 4 μgl^{-1}, with a slight proportional wavelength shift. With increasing concentration, a well defined minimum (through) develops near 670nm, associated with specific chl-a absorption, as well as the adjacent reflectance maximum (peak) near 700nm. The peak is due to increased cell scattering and/or chl-a fluorescence phenomenon. The chl-a increase drives a shift in the peak position from 685 (not noticeable) to higher wavelengths (about 5-10nm), due to a shift in the position of minimum combined absorption by pigment and water (Figure 4). The shift is due to increased phytoplankton cell scattering and is relatively independent of fluorescence. Therefore, over the VNIR spectrum, spectral analysis is done by inspecting the appearance and intensification of peaks and troughs with increasing chl-a concentration (Figure 3). Reflectance troughs coincide with stronger pigment and/or water absorption, while peaks appear in spectral regions where absorption is minimum and biological scattering plays an important role. These features are the starting point for remote sensing retrieval of chl-a in Case 2 waters. Algorithms for these types of systems should be based in the red absorption and NIR reflectance peak feature. A band ratio using both features can potentially isolate the chl-a signal from other absorption features.

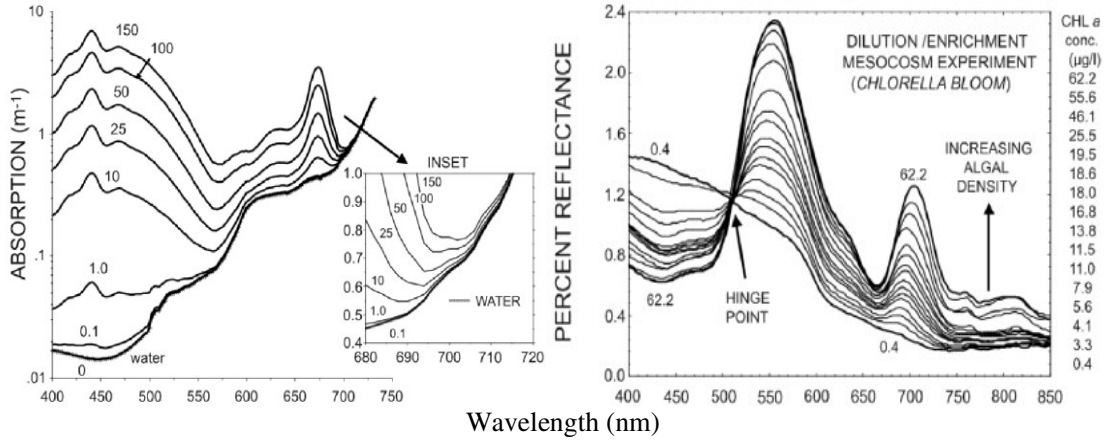

Figure 4 – On the *left*: Combined absorption coefficients for water and phytoplankton pigment at different concentrations (Bidigare et al., 1990 & Smith and Baker, 1991 in Schalles, 2006). On the *right*: Graded series of reflectance spectra for different chl a levels for a dilution/enrichment scheme experiment (taken from Schalles et al., 1997 in Schalles, 2006)

2.2.3 - Remote Sensing Sensors and Algorithms for chlorophyll monitoring

Space-born optical sensors observe aquatic systems since the Coastal Zone Color Scanner (CZCS) was launched in October 1978, which contributed significantly to the understanding of Case 1 waters. The follow-on sensors SeaWiFS (Sea-viewing Wide Field of view Sensor) and the newer instrument MODIS (MODerate resolution Imaging Spectroradiometer) aboard the Terra spacecraft, launched in 1997 and 1999 respectively, stimulated further improvements. The MODIS flown aboard the Aqua spacecraft aimed at obtaining information on the Earth's water cycle was launched in May, 2002 (http://aqua.nasa.gov/). Also in 1999, the Landsat ETM+ instrument was launched following his predecessors since the early 70's, providing high resolution imagery (30m) with the revisit time of about 16 days (http://landsat.gsfc.nasa.gov/). The long revisit time and possible cloud cover, along with data cost, limit its application to highly dynamic systems like estuaries (e.g. Gitelson et al., 2007). In contrast, SeaWiFS and MODIS sensors have shorter revisit time, for instance near daily overpasses, but the coarse and low spatial resolutions, about 1.2 and 1km respectively, also limit their application. The MODIS sensor, in particular, has bands with finer resolution (250 and 500m), which were designed especially for land and atmosphere applications. In 2002 the European Medium Resolution Imaging Spectrometer (MERIS) was launched with full-resolution of 300-m bands, with near-daily coverage. Its good trade-off between spatial and temporal resolution is limited by the cost of the acquisition (e.g. Chen et al., 2007). Particularly, MODIS and MERIS are able to optically measure the radiance leaving surface water in six or more bands in the visible and near-infrared (VNIR) region (e.g. Chen, et al., 2004; Zhang, et al. 2002b). In the future, the combination of optical and SAR technologies is expected to greatly improve the chl-a estimation. Although both technologies have co-existed for over than a decade, few discussions have been made on the combined use of these two very different technologies (Chen et al., 2004; Lindell et al., 1999; Zhang et al., 2002b).

Due to the combination of temporal contextualization, data availability, technical support, high temporal frequency, free access to data and widespread application, the MODIS Terra images were chosen for this work. The MODIS instrument provides high radiometric sensitivity in 36 spectral bands, ranging in wavelength from 0.4 μm to 14.4 μm and supporting land, atmosphere, and ocean applications. Two bands are imaged at a nominal resolution of 250 m at nadir, with five bands at 500 m, and the remaining 29 bands at 1 km. Data from MODIS Terra is available since 24 February 2000 (http://modis.gsfc.nasa.gov/). The principal aquatic scope of MODIS Terra was global ocean monitoring and therefore the

bands centred at relevant wavelengths have a 1km resolution. As already mentioned, this can be a limitation in finer coastal and transitional systems. Recently, several studies, have demonstrated the potential of high and medium resolution bands to monitor these systems (Hu et al., 2004; Miller and Mckee, 2004) using MODIS Aqua data. Terra high resolution bands are not well-calibrated, contain significant noise (Hu et al., 2004) and the sensor itself has suffered severe band degradation since 2003, with particular impact in the Rrs retrievals. Specifically, the radiometric response of the 412-nm band has degraded by more than 40% up to 2006, with similar but less extreme changes in the longer wavelengths rising significant cross-scan artifacts, mirror-side differences, and detector-to-detector striping in the retrieved water-leaving radiances (Franz et al., 2007). Two different approaches have been proposed to explore high resolution capabilities from MODIS data. Franz et al., (2006) proposed to correct 1km bands for atmospheric effects using high-medium resolution SWIR bands. Shuttler et al. (2007) proposed a method for radiance interpolation from low to medium resolution bands.

There are several algorithms developed for the retrieval of chl-a using Rrs. It was beyond the scope of this work to make a deep review of existing algorithms, which can be found in detail in IOCCG (2006). Furthermore, the algorithms described below can be found in the NASA Ocean Color Group processing software, SeaDas (http://oceancolor.gsfc.nasa.gov/seadas/) and in specific Case 2 waters literature (e.g. Gitelson et al., 2007; Tzortziou, et al., 2007). The majority of algorithms have been developed for Case 1 waters due to their optical simplicity and scope (e.g. Gordon and Morel, 1983; Morel and Prieur, 1977 in Zhang et al., 2002b). Some of them are theoretically also applicable to Case 2 waters with some restrictions, for instance, the Carder algorithm, although some studies have reported its inaccuracy when applied to these systems (e.g. Tzortziou et al., 2007). The chl-a algorithms selected for application in this work are the following:

- OC3M Empirical (O'Reilly et al., 2000)
- Clark Empirical (Clark, 1997)
- Carder Bio-Optical (Carder et al., 1999)
- GSM Bio-Optical (Garver and Siegel, 1997; Maritorena et al., 2002)

Because the above algorithms are more fit for chl-a retrieval in Case 1 waters and because they are complex, with multiple equations, describing these algorithms thoroughly is beyond the scope of the work and the reader should address the literature cited for the remaining. Carder et al. (1999) found a significant increase in prediction accuracy when the MODIS

ocean color algorithms were adapted to 3 bio-optical sets, suggesting that regional calibration may improve greatly the accuracy of globally tuned algorithms (see also Ciotti and Bricaud, 2006). Therefore, for simplicity, the OC3M algorithm will be selected for this task (see 3.6) and only its governing equation will be showed in detail. All these Case 1 algorithms will be tested in the estuary in order to assess their accuracy and limitations (see 4.2 and 4.3).

The OC3M empirical chl-a algorithm is a 4th order polynomial which relates the greater of the blue and green ratios, Rrs_{443}/Rrs_{551} or Rrs_{488}/Rrs_{551} to [chl-a]:

$$[chl-a] = 10^{a+bR3M+cR3M^2+dR3M^3+eR3M^4} \qquad \textbf{Equation 4}$$

where $R3M = \log_{10}\left(R_{550}^{443} > R_{550}^{490}\right)$ and the letters are the coefficients

The Clark empirical chl-a algorithm was originally based on an empirical 3rd order polynomial derived from chl-a measurements and blue and green reflectance ratios Rrs_{443}/Rrs_{551} or Rrs_{488}/Rrs_{551} in Case 1 and Case 2 waters (Clark, 1997). The algorithm uses different polynomial constants for waters with high and low [chl-a]. A recently proposed version of the algorithm (updated 19 March 2003, D. Clark, personal communication in Tzortziou et al., 2007) is a 5th order polynomial with potential improved performance in very high and very low [chl-a] environments.

The Carder bio-optical chl-a algorithm is based on a bio-optical model that relates [chl-a] with measured IOPs. It relates Rrs to backscattering and absorption by phytoplankton and a combined term for CDOM and non-algal particles (Carder et al., 1999). However, when [chl-a] is higher than 1.5-2.0 μgl^{-1}, the algorithm switches to an empirical 3rd order polynomial relating [chl-a] and to the ratio Rrs_{488}/Rrs_{551} (Carder et al., 2002). Therefore, the algebraic portion is for oceanic low absorption waters and the empirical portion is for high absorption coastal waters (IOCCG, 2006). The polynomial constants are adjusted dynamically (based on information on the sea surface temperature) in order to account for pigment packaging effects ('packaged', 'un-packaged', and transitional cases) in nutrient-replete and nutrient-deplete conditions (Carder et al., 2002). For mathematical details see Carder et al. (1999 and 2002) or IOCCG (2006).

The GSM algorithm is also bio-optical chl-a algorithm based on the quadratic relationship between the Rrs and, the absorption and backscattering coefficients. The algorithm parameters were optimized from a large global Case 1 in-situ data set. However, in waters where optical

characteristics differ strongly from those used to tune the model, i.e. coastal Case 2 waters, the model performance can be significantly lower (IOCCG, 2006). Both Carder and GSM algorithms have base equations similar to Equation 3, differing in the IOP determination procedure and parameters used.

Simple band ratios, developed for Case 2 waters and based on spectral signatures analysis, were also be employed and discussed regarding their suitability to retrieve chl-a in the Tagus estuary. Varied forms have been proposed and the majority are based on the ratio between the NIR reflectance peak and the red absorption (e.g. Gitelson et al., 2000 & 2007; Schalles, 2006). Tzortiziou et al. (2007) proposed a different approach using a ratio between the red reflectance and the green peak. There is no general equation, but relationships between reflectance ratios and chl-a are generally defined thru regression analysis, resulting mainly in linear, power, logarithmic, exponential and polynomial forms. Most of the algorithms proposed, avoid the blue region and explore the key optical feature in Case 2 waters, the reflectance peak corresponding to the chl-a fluorescence and cell scattering, in the upper red and lower NIR spectral region. Schalles et al. (2006) provides a good review of some of those relationships. Some algorithms are currently used in operational monitoring of Case 2 waters (see Ruddick et al., 2003 & Kallio et al., 2003 in Schalles, 2006; Gitelson, et al., 2000).

3. Methodology

3.1 - Study area: The Tagus Estuary

3.1.1 - General Description

Tagus estuary is one of the largest estuaries in the western coast of Europe, covering an area of 320 km^2 (e.g. Bettencourt et al., 1980 in Antunes, 1998), located in the most populated area of Portugal, the great Lisbon, with about 1.6-2.3 million inhabitants. About 120 km^2 (35-40%) corresponds to intertidal zones, of which 19 km^2 are occupied by salt marsh vegetation, and 81 km^2 are mudflats (www.aml.pt; Ferreira et al., 2003). This mesotidal estuary has a longitudinal extension of about 50 km, from the upstream boundary defined by tidal excursion, near Muge, to the downstream boundary, near São Julião da Barra - Cova do Vapor (Bettencourt, 1990 in Fernandes, 2005). Morphologically, the estuary is divided into three very distinct sections: upstream, middle and downstream (Ferreira et al., 2003; Brogueira and Cabeçadas, 2006). The upstream shallow section is located between Vila Franca de Xira and the Alcochete/Sacavém section. It has an average depth of 2m and includes most of the mudflats and salt marshes (Figure 5). This section is fresher and nutrient enriched with some small permanent islands (Mouchões), which separate this section into a wider and a small channel, the Northern Channel (or Cala do Norte) from Alhandra to Santa Iria da Azóia.

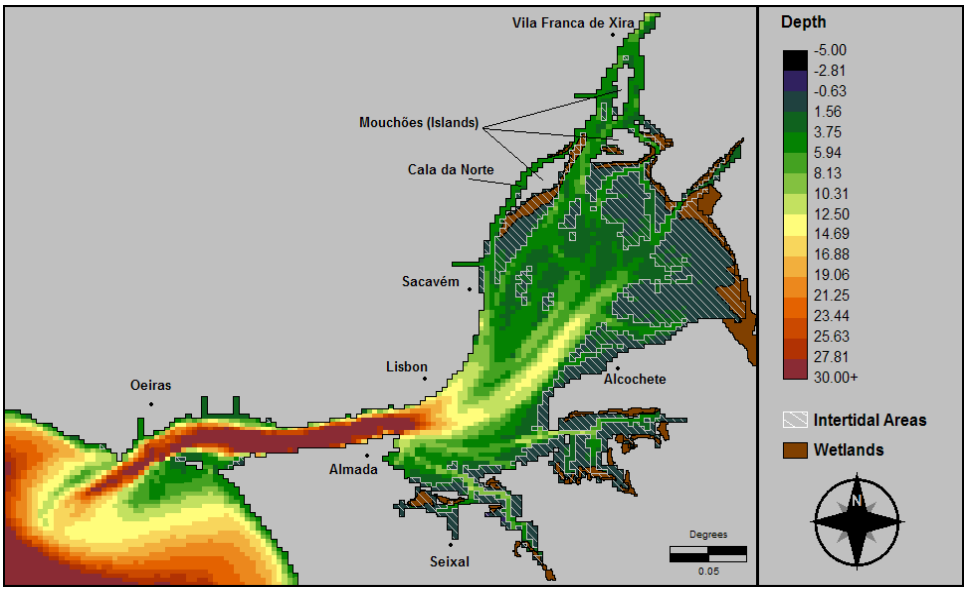

Figure 5 - Bathymetry, Intertidal Areas and Wetlands in Tagus estuary

The middle section, Mar da Palha, is wider and deeper, with an average depth of 7m, containing a higher average phytoplankton biomass (Brogueira and Cabeçadas, 2006). The downstream section is narrower, more saline, with low nutrient concentration and deeper, reaching depths of 46m and is currently the main navigation channel (Ferreira et al., 2003).

The mean air temperature is 16 ºC and the total average annual precipitation is 700 mm. Between 1999 and 2006, air temperature ranged from 6.4 ºC in the winter and 33.5ºC in the summer. The monthly mean wind speed is on average 3 ms^{-1} and higher in the summer (3-4.6 ms^{-1}), with dominant wind generally from N and NW (Gameiro et al., 2007).

The Tagus River is the largest of the Iberian Peninsula and drains an area of 86 000 km^2 acting as the major pollution source, mainly due to agriculture and industrial activities in the watershed upstream (Figure 6). The Tagus river has an annual average flow of approximately 300-400 m^3 s^{-1} with high seasonal variability, ranging from 145, in the summer, to 813 m^3 s^{-1} in the winter. Therefore, the residence time is highly variable, in average 23 days and 8 to 26 days for the seasonal flows mentioned (Cabrita and Brotas, 2000; Martins et al., 1984 in Brogueira and Cabeçadas, 2006; Gameiro et al., 2007; Câmara et al., 1987). Extreme events, like droughts and floods can cause flows of 30 and 2000 m^3 s^{-1}, respectively (Loureiro, 1979 in Saraiva, 2001; Câmara et al., 1987).

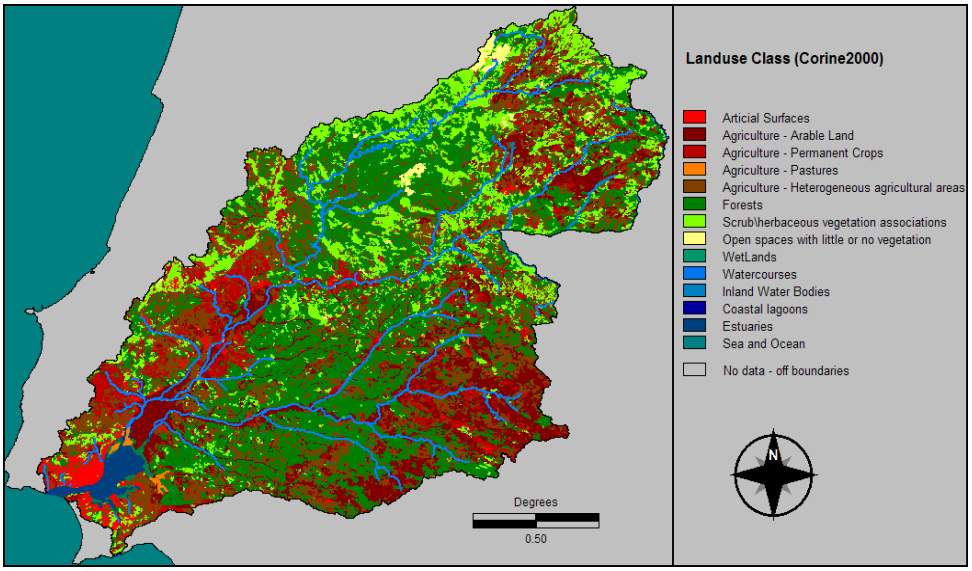

Figure 6 - Tagus river watershed land use Corine2000

The main pollution sources are the Tagus river, the tributaries Sorraia and Trancão rivers, punctual domestic and industrial effluents, with or without wastewater treatment plants (WWTP), and nearshore diffuse pollution (Annex III). The Sorraia and Trancão rivers are significant nutrient contributors to the system but of very distinct origins. The former, has a

catchment mainly influenced by agricultural activities and the latter, by industrial and domestic activities. Moreover, small tributaries also contribute to freshwater and nutrient inputs, like the Barcarena, Laje, Jamor, Moita creeks and the rivers, Coina and Judeu. In 2003, 17 WWTP adjacent to the estuary had secondary treatment, with a mean efficiency of about 70% in the removal of nitrogen compounds. On the North shore, the sewage treatment plants serve 90% of the population and on the South shore, only 30% of the residents are served by a WWTP. Despite the high organic discharges, the estuary's mesotidal characteristics and high dilution potential (Ferreira et al., 2003) induce a high estuarine export, maintaining the system in equilibrium (Câmara et al., 1987). In what concerns eutrophication risk, Ferreira et al. (2003), using the NEEA methodology, states that the overall eutrophic condition is Moderate or Low.

3.1.2 - Hydrodynamics

Hydrodynamics in the Tagus estuary are mainly driven by tidal forcing and wind. The latter influences vertical mixing and surface currents. In the lower section, topography tends to dampen the dominant N-NW wind effect (e.g. Fernandes, 2005). The upper section of the Tagus estuary is mainly intertidal, and in the midsection the water column height changes (on average) by 35-45%, thus the tidal scale variability is an important feature.

Physically, salinity influences the existence of vertical gradients, conditioning vertical diffusion and, therefore, sediment transport and primary production. Chemically, salinity influences suspended particle flocculation leading to increased sedimentation and thus influences light penetration in the water column (e.g. Antunes, 1998). Biologically, salinity influences mainly species composition within an estuary (e.g. Gameiro et al., 2004; Ferreira et al., 2005a). Salinity in the Tagus estuary is mainly driven by the degree of mixing between tidal and freshwater flow and, in the summer, specifically by heat exchanges in the surface, evaporation and precipitation (Antunes, 1998). Annually, salinity tends to be lower in the winter and higher in the summer (e.g. Gameiro et al., 2004; Grillot and Ferreira, 1996) due to variations in the rainfall and freshwater input, especially in the upper section. Furthermore, variations in salinity in the upper section are more pronounced than closer to the mouth and salinity shows a significant inverse correlation with the river discharge (Grillot and Ferreira, 1996; Gameiro et al., 2007). Salinity differences between the bottom and surface are not significant in the estuary (e.g. Martins and Duffner, 1982 & Martins et al., 1983a & Martins et al., 1983b in Antunes, 1998; Gameiro et al., 2004). Salinity's vertical distribution is more

homogeneous in the downstream estuary, reaching a maximum gradient in the Mouchões region, thus potentially presenting some stratification (Portela, 1996).

On average hydrological and tidal conditions, in flood tide, salinity varies from 36‰ to 27.5 ‰ downstream, immediately after the Mouchões. Upstream, the gradient is steep, reaching null salinity at 50 km from the ocean, near Muge. In ebb tide, in the ocean inlet channel, salinity is about 30‰, maintaining the steep gradient upstream (Câmara et al., 1987). The Tagus estuary can be divided into three main regions according to salinity. The first one is located upstream of Vila Franca de Xira, with an average salinity lower than 3‰ driven by the riverine influence (oligohaline). Midstream, between Vila Franca de Xira and the Póvoa Mouchão, salinities ranges from 15 to 20‰ (mesohaline to polyhaline). Salinity progressively increases towards the ocean with average salinity around 36‰ and vertical homogeneity (euhaline) (e.g. Antunes, 1998).

Tides are semi-diurnal (12h25m cycle) with an average amplitude of 2.4 m, ranging from 0.9m, at neap tide, to 4.1 m, at spring tide (e.g. Gameiro et al., 2004; Ferreira, 1988). For average tide, the tidal prism is about 750 x 10^6 m^3 and the average volume is 1.9 x $10^9 m^3$ (Vale, 1990 in Antunes, 1998). According to Portela (1996), the freshwater flow is typically two orders of magnitude lower than tidal flow, in the mid and lower sections of the estuary. Also, in the average tidal cycle, the maximum flow near the ocean inlet is $40x10^3$ m^3s^{-1}, during flood and $50x10^3$ m^3s^{-1}. Ebb currents are faster due to a temporal shift in ebb and flood tides that increases with the distance to the ocean. In the midsection, during spring tides, the maximum current velocities are 1.0 ms^{-1} during the flood and 1.2 ms^{-1} during the ebb. In neap tides, currents decrease significantly. Near the ocean, the current velocities are tidally driven, reaching a maximum of 1.3 ms^{-1} during flood and 1.7 ms^{-1} during the ebb, and sometimes reaching 2.3 ms^{-1} (Bettencourt et al., 1980). Moreover, current intensity generally decreases from the surface to the bottom (Portela, 1996).

River flow variability rules the degree of separation between brackish and fresh water and thus the upstream extension of saline intrusion. Brogueira and Cabeçadas (2006) stated that three homogeneous regions had different delimitations based on the magnitude of the winter flow. For instance, in high flow conditions, the more oxygenated river influenced zone extended downstream and the marine influenced area is restricted. As a consequence of high flow and transport conditions, materials tend to remain entrained in a limited area nearby extensive salt marshes in the mid section of the estuary, potentially favouring the

accumulation of suspended particles, as well as nutrients and phytoplankton (Cartaxana, 1999 in Brogueira and Cabeçadas, 2006).

Using the NEEA methodology, Ferreira et al. (2003) classified the Tagus estuary as having a High dilution potential and a Moderate flushing potential, resulting in overall Low susceptibility to dilute and flush nutrients. The combined factors of low average depth, strong tidal currents, and low input of river water make this a well-mixed estuary, with stratification occurring only in specific situations, such as neap tides or after heavy rains (Ferreira et al., 2003; Vale and Sundby, 1987 in Antunes, 1998; Bettencourt et al., 1980).

3.1.3 - Light and Suspended Particulate Matter

In the Tagus estuary the main driver of SPM concentration is the tidally driven bottom resuspension, followed by the riverine inputs, although the former is typically several orders of magnitude higher (Ferreira, personal communication). Gameiro et al. (2004) reinforced the idea that riverine input, mainly due to upstream erosion and highly flow dependent, is an important source of SPM in the Tagus estuary. High tidal amplitudes, typical in spring tides, are associated with high tidal currents, which may be an important source of SPM driven by bottom resuspension (Portela, 1996). Due to the erosion of the intertidal areas and consequent sediment transport, SPM concentrations are higher in ebb tide than in flood tide (Vale and Sundby, 1987 in Antunes, 1998). The concentration in the Tagus estuary can vary from $20mgl^{-1}$, in ebb tide, to more than 140 mgl^{-1}, in flood tide (Castanheiro, 1985 in Antunes, 1998). Longitudinal variations are especially due to the tidal amplitude and the maximum turbidity zone is located in the upper section, reaching concentrations higher than $200mgl^{-1}$ in spring tide. Transversal variations are also due to tidal amplitude, in neap tides the estuary is transversally homogeneous and, in spring tides, suspended matter tends to increase in the south half, where the majority of intertidal areas are located (Antunes, 1998).

Seasonally, concentrations tend to be slightly higher in the winter, probably due to riverine input but, globally, are relatively constant throughout the year. Boundary concentrations are on average below $5mgl^{-1}$ for the ocean, and approximately $10mgl^{-1}$ from the river (Ramos, 2002). Spatially, suspended matter, and thus turbidity, is higher in the middle and upper sections of the estuary and lower in the downstream section (Brogueira and Cabeçadas, 2006). In the lower estuary concentrations vary between 5 and $10mgl^{-1}$, in the downstream narrow channel, to $15mgl^{-1}$ near Cacilhas (Almada). Upstream, differences are even steeper increasing

20mgl^{-1} from the latter point to the mid section (Ramos, 2002; Gameiro et al., 2004; Fernandes, 2005). Ramos (2002) reported average values in the Northern Channel of 20 to 35 mgl^{-1} and Gameiro et al. (2004) reported higher values ranging from 40 to 50 mgl^{-1}. According to the latter, the wider mid section has SPM values between 20 and 25mgl^{-1}. To summarise, typical SPM concentration increases proportionally with the distance to the ocean, rising from average values of 5mgl^{-1}, in the inlet channel, to more than 40mgl^{-1} in the mid section, in the intertidal areas. This increase follows roughly an exponential function translating into large and rapid variations (Fernandes, 2005). The most significant variations are due to bottom resuspension driven by tides and SPM can reach very high concentrations in spring tide (Ferreira, personal communication).

SPM is especially important to phytoplankton production due to the light limitation imposed. Gameiro et al. (2007) reported that light attenuation coefficients ranged from 0.4 to 8.0 from 1999 to 2007, and suggested that turbidity was mainly due to SPM rather than phytoplankton cells, thus they probably do not shade themselves. The same author, indicates that the Zmix:Zeuf ratio was similar for all seasons, ranging from 0.4 to 4.1 and in only 22% of the samples the entire water column was located within the euphotic zone. Thus, light limits production in some extent. However, the ratio of 5 was never reached, which according to Cole and Cloern (1984) is the upper limit for net primary productivity.

3.1.4 - Nutrients

In recent years, the total annual nitrogen loading was around 26 000 tons (Cabrita and Brotas, 2000). According to Ferreira et al. (2003), the nutrient load to the estuary is 39ton N d^{-1} and about 12ton P d^{-1}. According to the same author, the Tagus river is the major source respectively introducing approximately 65% and 46% of N and P, mainly due to agriculture activities in the watershed. Average dissolved inorganic nitrogen (DIN) for the Tagus estuary is about 40 μmol l^{-1} and, in the last 20 years, concentrations have not changed significantly probably due to the low population increase and the equilibrium between increased effluent discharges and improvements in sewage coverage and treatments Approximately 30% of the population originates untreated effluents, which are responsible for 15-20% of total nutrient input. Treated effluents introduce 15% of total nitrogen and about 40% of phosphorus because of to the type of treatment used in most WWTP, which does not remove the latter from the effluents. In the south margin about 70% of the population is not covered by WWTP, whereas

in the north margin, only 10% is not covered (Gameiro et al., 2004 & 2007; Cabeçadas et al., 2000 in Brogueira and Cabeçadas, 2006; Ferreira et al., 2003).

Considering nitrogen inputs, nitrate is mainly supplied by freshwater inflow (Cabrita and Moita, 1995, Cabrita, 1997 in Gameiro et al., 2004; http://www.maretec.mohid.com) as is the case also in other estuaries (Malone et al., 1988; Mallin et al., 1993; Selmer and Rydberg, 1993). Therefore, nitrate input is highly flow dependent, typically with higher in the winter and lower in the summer, exhibiting a marked seasonal variation. Concentrations are higher in the spring (25-125 μmol l^{-1}), reaching extremely low values in the summer (0-10 μmol l^{-1}) and increasing in the autumn and winter due to river flow (Gameiro et al., 2004 & 2007). The seasonal pattern of nitrite is similar to nitrate, in spring it reaches 6-12 μmol l^{-1}, remaining constant throughout the year, with an average concentration of 4μmol l^{-1} in the upper and mid sections (Gameiro et al., 2004). Concentrations usually do not limit production, however, some authors have suggested that, especially in the mid estuary and during the summer, nitrogen can limit phytoplankton growth (Antunes, 1998; Gameiro et al., 2007). Spatially, average annual nitrate concentrations are lower with increased distance to the river, with average values of 40μmol l^{-1} in the upstream section, decreasing to values of 13μmol l^{-1} in the middle section, and even lower values near the mouth (Gameiro et al., 2004).

Ammonia has highly variable concentrations with no clear seasonal pattern and appears to be spatially related to sewage inputs and sediment resuspension. Lower peaks tend to be related to higher consumption by producers (Gameiro et al., 2004 & 2007; Brogueira and Cabeçadas, 2006). The WWTP and the Trancão River are responsible for up to 60% of total ammonia load, whilst the remaining is distributed by the Tagus and Sorraia rivers (http://www.maretec.mohid.com). The total nutrient removal by WWTP has negligible effects on primary production at an ecosystem scale (Saraiva, 2001). However, locally, it is relevant as reported by Gameiro et al (2004) in the Northern Channel (Cala do Norte) where ammonia concentrations are typically higher than 12μmol l^{-1} reaching up to 900μmol l^{-1}, mainly due to industrial and domestic activities upstream (Antunes, 1998), significantly higher than the mid and lower sections (Ramos, 2002). Gameiro et al. (2004) reported that ammonia concentrations, in 1999 and 2000, fluctuated between 0 and 30μmol l^{-1}, specifically, with average annual values of 8μmol l^{-1} and 20μmol l^{-1} in the upstream section and the Northern Channel, respectively. Brogueira and Cabeçadas (2006) reported that the upper section has ammonia values lower than the mid and lower sections, specifically an average of 3μmol l^{-1}, in the summer, and 5μmol l^{-1}, in the winter against 8 and 9μmol l^{-1}, respectively.

Phosphate concentrations typically decrease as depth increases suggesting that, similarly to other estuaries, they are mainly driven by sediment dynamics (Câmara et al., 1987) and salinity (Gameiro et al., 2007). Phosphate is higher in the upper section, where salinity is low (Neves et al., 1991 in Antunes, 1998), and lower in the downstream section estuary, with average values of 3-4μmol l^{-1} (Brogueira and Cabeçadas, 2006; Gameiro et al., 2007). According to the latter author, phosphate lower limit concentrations were never reached between 1999 and 2006. Ferreira et al. (2003) states that, according to the NEEA eutrophication assessment methodology, the Tagus estuary susceptibility to nutrient inputs is Low, mainly due to hydrodynamic conditions, and the progressive increase in waste water treatment, especially in the south margin, will probably improve the present situation.

3.1.5 - Phytoplankton

The total number of species in the Tagus estuary is around 300-350 (Ferreira et al., 2005a). The composition is mainly dominated by diatoms, contributing on average to about 60%, well represented by Skeletonema costatum, Thalassiosira minima and Detonula pumila (Gameiro et al., 2004 & 2007). Specifically, in the mid and upstream sections, Bacillariophyceae and Cryptophyceae, species below 20μm in diameter, represent more than 90% of the phytoplankton bulk (Gameiro et al., 2004). Spatial and temporal distribution varies for the different taxonomic groups, mainly due to physical preferences, like salinity (Gameiro et al., 2007), residence time (Ferreira et al., 2005a), precipitation patterns, stream flow (e.g. Lehman, 1992 in Gameiro et al., 2007), vertical turbulence (Huisman et al., 1999) among other factors. These drive bloom timing and localization with different contributions for total chl-a (Gameiro et al., 2007). Dinoflagellates, morphologically buoyant species, have a higher contribution during summer, when vertical turbulence is low and the water residence time is higher, which favours them over typical sinking species like diatoms (Huisman et al., 1999). Also, according to Gameiro et al. (2007), these species are more frequent downstream, while diatoms are predominant in upstream fresh waters, as also found in other estuaries (Marshal and Alden, 1990). Cloern (1996 & 2001) indicates a progressive shifting from diatom dominance to other taxa such as flagellates and dinoflagellates in European estuaries. However, Gameiro et al. (2004 & 2007) reveals that the Tagus estuary is still balanced. The Tagus has a typical residence time higher than one week and would, therefore potentially, be capable of accommodating phytoplankton species with a P_{max} of about 1 day^{-1} or lower, consistent with reference values for dinoflagellates (Ferreira et al., 2005a).

Average annual chl-a values for the whole estuary are typically between 4-8 μgl^{-1} and range between 1 and 35 μgl^{-1} (Gameiro et al., 2004 & 2007; Ferreira, 2000). The nature of the spring/summer blooms changes from year to year. External climatic factors are the principal drivers for long term biomass fluctuations, whilst short scale processes, strongly dependent on tidal variations which play a major role on intra annual bloom development (Gameiro et al., 2007) as stated for other estuaries (e.g. Lucas et al., 1999a & 1999b). Therefore, chl-a concentration has a strong seasonal variation and biomass peaks are spatially and temporally heterogeneous. Higher values occur during the summer, peaking from May to July, but, can also occur in August/September, in the same year, but in different locations of the estuary (Antunes, 1998; Gameiro et al., 2004 & 2007). The summer increase is probably due to relatively stable conditions in the water column and a more adequate light climate, as productivity is often light limited. Chl-a decreases and reaches very low values during the winter (Brogueira and Cabeçadas, 2006; Cabeçadas, 1999 in Gameiro et al., 2007).

According to Ferreira et al. (2003), maximum chl-a occurs in the tidal freshwater and mixing zone, being classified according to NEEA methodology as High, whilst the lower values occur in the seawater zone, classified as Medium. Gameiro et al. (2007) indicated a general 7 year pattern, in which unimodal blooms were more frequent in the upstream region and occurred in the late spring and summer months. Upstream typical values, were about 2-3 $\mu g\ l^{-1}$ in the winter and above 10 $\mu g\ l^{-1}$ in the summer. Some occasional bimodal peaks occur, especially in the middle section, which as annual average chl-a of 5 to 10 μgl^{-1} and peaks reach 15 to 20 μgl^{-1} (e.g. Antunes, 1998; Grillot and Ferreira, 1996). Although the average time spent by phytoplankton cells in the euphotic zone is similar in both, according to Gameiro et al. (2007), the more frequent upstream blooms were essentially due to nutrient availability and taxonomic composition. In the Northern Channel, values are highly variable and range from 3 to 8 μgl^{-1} (e.g. Ramos, 2002; Gameiro et al., 2004) and peaks higher than $10\mu gl^{-1}$ have been reported (Grillot and Ferreira, 1996). In the downstream section of the estuary, the average annual chl-a values are 1 and $5\mu g\ l^{-1}$ in the winter and summer months respectively (e.g. Brogueira and Cabeçadas, 2006; Grillot and Ferreira, 1996) and late spring peaks higher than 10 $\mu g\ l^{-1}$ have been observed (Antunes, 1998). The variability of the collected chl-a values suggests that phytoplankton dynamics are highly dependent on measurement methodology, environmental forcing and local conditions, thus were addressed with caution.

3.2 – Procedures of Model Calibration and Assessment (adapted from Janssen and Heuberger, 1995)

Models are based on mathematical approximations of the processes that occur in a given system and contain various quantities like parameters and boundary conditions. These quantities are often not totally known or directly measurable and therefore require information to make accurate performance inferences. Calibration is a crucial phase and depends on the aim and intention of the model. Calibration consists in comparing model results with measurements and prior knowledge, adjusting and determining the model parameters and/or structure, which provide adequate output matches. Calibration can be done manually, by tuning up some parameters until the model predictions match the data observations adequately. This subjective trial-and-error approach can be successful when models have few parameters but lack exactness and objectivity, leads to inconclusive results, and limits reproducibility and uncertainty management. A structured and systematic calibration approach can substantially improve reproducibility, objectivity, diagnosis information and the quality of the calibrated model and its results.

Comparisons between measurements and model predictions can be performed qualitatively or quantitatively. Qualitative approaches are done by visual comparison between observed and predicted data, for instance, using scatter plots, pairs of time series, histograms, among others. Quantitative approaches analyze numerically the agreement between observed and predicted data using performance measures (misfits), which are functions of the error between both. The model is adjusted so that the agreement between data and model is satisfactory, for a given aim, reducing the initial uncertainty and providing adequate model inference.

Solving the model calibration problem successfully will mainly depend on the intended aim, characteristics of the model, prior knowledge, and the nature, availability and quality of the data. Prior information on the model quantities (e.g. parameter ranges, constraints) should be explicitly incorporated, indicating their nature, characteristics, reliability and quality. The characteristics of the data define the quality boundaries of model calibration. Before calibration, it is recommended to analyse and treat data in order to detect and remove inadequacies and noise, and to discover important features and relationships. Also, it is recommended to reduce the number of calibrated parameters. For instance, by performing sensitivity analysis, in order to prevent unnecessary computational problems, identify the relevance of calibration and relevant model parameters and outputs. Parameters whose

variations have low influence on the model outcomes can be fixed establishing boundaries to the calibration effort.

The characteristics of the model should be exposed by addressing the following:

(a) aim and scope of the model;

(b) model principles and major processes involved;

(c) model components (i.e. features of parameters, initial and boundary conditions, state variables, model inputs and outputs);

(d) governing equations;

(e) technical information (numerical schemes, input data requirements, programming language, hardware requirements, run time etc.);

(f) status of the model;

(g) documentation.

In the definition of the calibration problem certain issues must be addressed, such as, the uncertainty or variability present in the data, level of accuracy required for model application and availability of adequate numerical techniques. One of the major problems in calibrating environmental models is the imbalance between their complexity and data availability. This can be driven by different temporal and spatial scales addressed and will probably set the calibration limits.

Misfits should be defined according to the intended use addressing the relevant model quantities. This will depend on data characteristics, prior parameter information and the error structure. One should specify, the parameters considered being candidates for calibration and denote prior knowledge, the outputs to be included and the methods used. Many parameter combinations can have a suitable agreement with the data but some of them will be more probable than others (Klepper and Hendrix, 1994 in Janssen and Heuberger, 1995). Misfit(s) can be employed in two different ways in the subsequent calibration:

(a) In a direct way, directly expressing the *'degree of approximation'* of the model.

(b) In an indirect way, expressing the *'likelihood'* of the model in relation to the available measurements and prior information on the model parameters.

Calibration can be defined as a problem of *optimization*, *set-identification*, *multi-criteria* and/ or explicit *evaluation of the posterior likelihood*. The *optimization problem* is used when it is appropriate to use one overall misfit function and it is meaningful to find parameters which

minimize it. The non-uniqueness of the optimal model parameters and the existence of various local misfit minima should be considered. The *set-identification problem* is used when it is inadequate to search for one specific optimal model and one should find a set of parameters. This can be driven by prominence of errors and/or uncertainties in the data and the future use of such set should be considered. The *multi-criteria problem* is a multiple simultaneous optimization procedure which minimizes several misfits and involves a trade-off between them. The non-uniqueness of minima is once again a critical issue. The *explicit evaluation of the posterior likelihood* incorporates prior knowledge in model parameters to assess the posterior likelihood. The availability of efficient numerical techniques is an issue that should be considered in all the approaches defined above.

Model quality assessment is an ongoing process and model accuracy should be determined to make meaningful inferences and predictions with the model. Generally, there are three main aspects in model evaluation and assessment. Firstly, the ability of the model to reproduce the system behaviour should be assessed, preferably using an independent data set and bearing in mind the desired accuracy. It is recommended that techniques should be less data-oriented, and to check if the model incorporates the relevant processes adequately and if calibrated parameter values are realistic. Secondly, the suitability of the model for the intended use should be assessed, for instance, prediction of long range or episodic events. Thirdly, model robustness should be assessed, by comparing model simulations with different data sets under varied conditions and/or different misfit functions. If the model exhibits small differences in its simulations, than it is probable that it is robust and represents the relevant processes. Different model evaluations will lead to different conclusions and inferences. If the model is unsatisfactory, improvement may be obtained by:

(i) Additional experimentation or data collection;

(ii) More adequate calibration (e.g. other misfit measures, alternative search techniques, new data sets);

(iii) Model adaptation (e.g. reparametrization, parameter aggregation or reduction).

If the model is satisfactory its uncertainty should be taken into account for further applications. An adequate calibration should, therefore, provide relevant information on parameters and outputs uncertainty, which should be appropriately accounted for in further model applications. Calibration choices should be a mixture of sound judgement, insight, prior knowledge and the availability of suitable techniques. Subjective judgement is an indispensable component in the whole process.

Misfits quantitatively express the deviation between model predictions and will be used in a direct way, expressing the 'degree of approximation' of the model. In this work, both for calibration and assessment purposes, the mean absolute error in percentage (*MAE %*), the root mean square error (RMSE) and correlation coefficient (*r*) will be used. The *MAE (%)* was adapted to provide a normalized positive error measure (Equation 5) i.e. the average absolute difference between predictions and observations normalized according to the latter. Note that, *Pi* and *Oi* denote respectively the predicted and observed value and *N* is number of observations. This misfit provides a performance measure at an *average level* over the whole time span considered, providing only rough and incomplete information of the model-data discrepancy because averaging smooths out the dynamic features.

$$MAE(\%) = \frac{\sum_{i=1}^{N}\left(\frac{|P_i - O_i|}{O_i}\right)}{N} \times 100 \qquad \textbf{Equation 5}$$

The RMSE measures the error in a quadratic way and is very sensitive to outliers (Equation 6). If the model accurately describes the noise-free data, the RMSE should be approximately equal to the standard deviation of the measurement noise.

$$RMSE = \sqrt{\frac{\sum_{i=1}^{N}(P_i - O_i)^2}{N}} \qquad \textbf{Equation 6}$$

The correlation coefficient indicates, in an absolute sense, the degree and strength of the relationship between the independent (*Oi*) and dependent (*Pi*) variables, i.e. the tendency of the variables to increase or decrease. The sign reflects the relationship direction i.e. if it is direct or inverse. This misfit renders information on a *population level* and varies between -1 and 1 (Mansfield, 1986). When appropriate, the coefficient of determination (r^2) will also be computed and shown (Equation 7).

$$r = \frac{N\sum_{i=1}^{N} O_i P_i - \sum_{i=1}^{N} O_i \sum_{i=1}^{N} P_i}{\sqrt{N\sum_{i=1}^{N} O_i^2 - \left(\sum_{i=1}^{N} O_i\right)^2}\sqrt{N\sum_{i=1}^{N} P_i^2 - \left(\sum_{i=1}^{N} P_i\right)^2}} \qquad \textbf{Equation 7}$$

Besides quantitative analysis, qualitative assessment will be performed using time series and scatter plots of measured *versus* modelled values, among others. Furthermore, regression analysis was performed rendering the associated information like the regression line and coefficients.

3.3 - Ecological Model Calibration

3.3.1 - General Considerations

E2K was used to simulate phytoplankton spatial and temporal distribution in the Tagus estuary between 1998 and 2002. This approach was chosen due to lack of in-situ data to calibrate and assess the remote sensing products. Phytoplankton was simulated as chl-a concentration (in μg chl-a l^{-1}), assuming that the latter is the predominant pigment and therefore representative of the pelagic producer's biomass distribution in the whole estuary. The seasons were defined considering that Winter includes January, February and March.

The first challenge was to identify the significant environmental variables which affect phytoplankton biomass. SPM, nutrients and zooplankton were the principal state variables and the ecosystem was forced by light, water temperature, hydrodynamics and the Tagus river flow. The second challenge was to resolve the main interrelations between state variables and chl-a, and also, between separate physical, chemical and biological processes. The model includes physical processes, such as the transport of nutrients, SPM, phytoplankton and zooplankton, through the system boundaries and between model boxes, and biological processes, namely, phytoplankton and zooplankton dynamics. The model aims towards a common structure that may be calibrated with a different set of parameters depending on regional and temporal characteristics (Ferreira et al., 2007a). Presently, E2K does not incorporate an automated method to perform sensitivity analysis and, therefore, the latter was performed manually regarding the impact on chl-a of main objects and parameters (3.4.1).

Phytoplankton biomass, as mentioned previously, is mainly influenced by hydrodynamic processes and both light and nutrient availability. Incident radiation at the surface was simulated using Brock (1981) formulations. SPM was simulated, due to its influence on sub surface light availability, providing a rough description of its dynamics in the estuary. Nutrients are essential to primary production, and ammonia, nitrate, nitrite, DIN, phosphate and silicate were considered. Zooplankton was simulated providing a production control which limits phytoplankton biomass. Regarding hydrodynamics, the ecosystem was assumed to be vertically homogeneous (e.g. Gameiro et al., 2004 & 2007) and divided into 13 boxes. The transport of particulate and dissolved substances between boxes and system boundaries was calculated using an upwind 1-D transport scheme, which simulates large scale advection and dispersion.

The most significant boundaries are the ocean and the Tagus river. The former is tidally averaged, importing and exporting substances to the system. The latter exports substances to the estuary through its upstream flow. Moreover, 27 boundaries were defined corresponding mainly to WWTP effluents, small creeks and the tributaries, Trancão and Sorraia rivers, providing a relevant ammonia input to the system. The boundary conditions, i.e. the substances concentration in the boundaries, were averaged in order to provide a constant value, defined object by object, concerning each boundary and representative of one or more years.

Calibration was addressed as a multi criteria problem with the aim of optimizing the model according to the different statistical information the three misfits provided and accounting for the trade-off involved. Multiple variables were calibrated separately and with different timings. Forcing functions were calibrated first, followed by the state variables, and the phytoplankton object in last, assuming that it did not significantly influence any other objects. This assumption is necessary, although it is obvious that, for instance, phytoplankton influences the ammonia concentration in each model box.

Due to its relevance, the phytoplankton object was calibrated using a slightly different procedure. A cost function was used in order to aggregate the different information that each misfit provides, into one global error indicator. The misfits were individually normalized according to their range, i.e. 1 gives the maximum cost or error and 0 gives the minimum. Note that the correlation coefficient was inverted to correspond to the scale defined above. Misfits were then average into a global error or cost, varying between 0 and 1. The aggregation method tended to smooth extreme performance measures. It was used with the aim of identifying sets of parameter combinations and areas with higher probability of parameter choice, i.e. the parameter combinations which corresponded to local minima.

A simple semi-automate procedure, developed in Visual Basic for Applications (VBA), run in Microsoft Excel environment, was used to accomplish the tasks and steps defined above. It consisted in loading E2K outputs box by box, in spreadsheets, and comparing them to the respective measurements. E2K outputs were exported with a time step of half a day and the matches, exactly at noon, were used for comparison. The hour was chosen due to ecological relevance, the average behaviour of the model and especially because the remote sensing data is acquired close to solar noon. Finally, misfits were calculated and qualitative information was generated. The cost function was implemented in MatLab R2006a using exported misfits.

Data assimilation was carried out using the BarcaWin2000^{TM} (B2k) software, which manages relational databases. B2k has been developed since 1985 and used in multiple research projects (Ferreira, et al., 2007b). In the present work, the available data was scarce and resulted from two different campaigns which represent 4 years (Table 2). Only surface measurements (depth < 1m) were considered. Data availability limits the level of accuracy provided by the model, however, the uncertainty associated with the sampled data was not accounted for due to lack of information. Therefore, with scarce and uncertain data, one must address the calibration and evaluation effort with caution. Prior knowledge on model parameters and simulated variables provide relevant information for this task and were stated case by case in the following sections.

Table 2 – In-Situ Data Characteristics

Year	Campaign Name	Samples (N)	Spatial Coverage (Boxes and Boundaries)	Parameters
1998	IH 1998	19	4; 11; 12; River ; Ocean	Chl-a; Nutrients* SPM; Temperature; Salinity
1999	IH 1999;	19	4; 11; 12; River; Ocean	Chl-a; Nutrients* SPM; Temperature; Salinity
1999	IPIMAR - DGA	8	1; 3; 6; 8; 10; 11; 13; Ocean	Chl-a; Nutrients* except nitrite; SPM; Salinity Temperature;
2000	IH 2000	15	4; 12; River; Ocean	Chl-a; Nutrients* SPM; Temperature; Salinity
2002	IH 2002	5	4; 11; River; Ocean	Chl-a; Nutrients* SPM; Temperature; Salinity

* Nutrients include: ammonia, nitrate, nitrite, silicate and phosphate.

E2K was calibrated using 1998 and 1999 data and evaluated using 2000 and 2002 data. The objects defined for the Tagus estuary in the E2K shell were the following:

- Forcing functions (River Flow; Light; Water Temperature; Hydrodynamics)
- Nutrients
- Suspended particulate matter
- Zooplankton
- Phytoplankton

The parameters suitable for calibration, prior knowledge and analyzed outputs were indicated object by object in the following sections. The quantitative and qualitative analyses performed reflected the intended use of the model i.e. to assess the accuracy of remote sensing products in the Tagus estuary, at an ecosystem spatial scale and at a monthly to seasonal temporal scale.

3.3.2 - EcoWin2000 Description (adapted from Ferreira, 1995)

E2K is an ecological model which simulates processes in aquatic systems, developed using an object-oriented programming (OOP) approach, which represents the different ecosystem compartments and their interactions. Incorporated components, like hydrodynamics, biogeochemistry and population dynamics, consist in a series of self-contained objects, rather than multiple sub-models.

E2K has two basic parts: a shell module and objects. The shell deals with the interface with the user, communication between the various objects, management of model inputs and outputs and general maintenance tasks. The ecological objects (or classes) encapsulate attributes (or properties/variables), with methods (or functions), which act upon them. Conceptually, an object resembles an actor whose actions (methods) are driven by its characteristics (attributes). For instance, phytoplankton, has as one of its attributes a standing crop and as one of its methods, productivity.

OOP is implemented as a set of class hierarchies, in a way that, descendants inherit the ancestor's attributes and methods, and may in turn modify the inherited properties. For instance, diatoms will inherit the properties of the phytoplankton ancestor and extend them in order to require silica for growth. Each object is self contained and groups together one or more related state variables that can be extended without affecting any other part of the model, avoiding error propagation. Moreover, the methods which control state variables within objects may easily be changed, due to inheritance and encapsulation properties.

An object has public sections which are used for initialization and communication, both with the shell and between objects, together with flexible private sections conceptualized in three types: active, passive and neutral methods. For instance, for the phytoplankton object, growth is a typical active behaviour; grazing by zooplankton is a passive behaviour and transport, due to advection and diffusion mechanisms, is a neutral method. All are processes which affect the attributes of an object.

The underlying structure is based on a box-model approach which typically divides the system into boxes, which may vary only with time (zero-D), or may vary also in space: longitudinally (one-D), in two dimensions (two-D), or in layers (three-D) and performs simulations at the system scale. This approach for system division has been used in previous

studies (e.g. Raillard and Menesguen, 1994). The shell and the objects have been implemented in C++ and objects use Euler numerical integration.

The advantages of using OOP for ecological modelling are the ease of development and flexibility associated with their inherent object properties: encapsulation, modularity, inheritance and polymorphism. Also, it provides a much greater conceptual approximation between natural ecosystems and interacting objects, in comparison with conventional structured programming methods, insuring reliability and re-usability. It insures improved model construction, flexibility and extensibility and adaptation of the objects to particular ecosystem characteristics. Since objects are encapsulated and have inheritance properties it is easy and feasible to develop modified or extended descendents according to their role in the ecosystem. The maintenance of a particular model is therefore simplified because new updates can be coded as descendants and polymorphism eases new code development.

Objects may be switched on or off improving and facilitating the analysis of the model's sensitivity to different components by altering the characteristics of the ecosystem. The model is not computer intensive: for a simulation of one year with all objects on and an hourly time step takes only about 10 seconds, on a 2 GHz PC.

E2K provides a platform for integration of the various other models, and adds functionality of its own. Although it can be used to run short-term simulations (e.g. Duarte and Ferreira, 1997), it has mainly been used to run multi-year models involving simplification of some finer-scale system processes, capturing event-scale phenomena such as seasonal variability (e.g. Ferreira et al., 2007a; Nunes et al., 2003; Alvera-Azcárate et al., 2003). At the present, no documentation is available for the E2K. This model has been developed and extensively tested over the last 15 years proving to be a potentially useful tool for supporting an ecosystem approach to sustainable aquaculture development, research on nutrient loading and ecological assessment. Some examples of model application will be briefly discussed.

E2k was used for short-simulations to assess phytoplankton photosynthesis dynamic behaviour in order to improve its estimation (Duarte and Ferreira, 1997), particularly in the Tagus estuary (Macedo et al., 1998). The majority of applications includes long term studies concerning aquaculture, response to environmental and culture changes, and anthropogenic driven impacts on wild species (Kianirad et al., 2006). It has been used in the SPEAR project (http://www.biaoqiang.org/) for interpretation of the coastal structure and dynamics

accounting for watershed interactions, ecological structure and human activities, with particular emphasis on aquaculture in China (Duarte et al., 2003). Moreover, it was applied in the Catchment To Coast (C2C) project in Southern Africa (http://www.ecowin.org/c2c/) to assess the influence of the different components of the system on the ecology of commercially exploited shrimp resources and to describe the dynamics and health of the mangrove forests (Franco et al., 2005). In the SMILE project, it was used to examine the effects of aquaculture on key ecological variables and evaluate sustainable carrying capacity from an ecosystem perspective (Ferreira et al., 2007a). Nunes et al. (2003) applied the model to simulate shellfish polyculture in the Sanggou Bay (Northern China). Currently, E2K is being used for ecosystem-scale carrying capacity modelling in the ECASA ongoing project aimed at understanding the effects of aquaculture on the environment (http://www.ecasa.org.uk/). In an eutrophication assessment, using a hybrid approach, E2K outputs were used to drive the ASSETS screening model and simulate different nutrient loading scenarios (Nobre et al., 2005; http://www.eutro.org). Alvera-Azcárate et al. (2003) used E2k to assess the role of intertidal seaweeds in the primary production of the Tagus estuary, whilst Simas and Ferreira (2007) studied the nutrient enrichment and role of the Tagus salt marches. Grillot and Ferreira (1996) and Ferreira and Duarte (1994) used the E2K to model phytoplankton in the Tagus estuary.

3.3.3 - Spatial Domain

According to WFD article 2.10, a water body is "a discrete and significant element of surface water such as (…) a transitional water or a stretch of coastal water" considered as a "sub unit in the river basin" that "will be used for reporting and assessing compliance" (WFD Guidance on Monitoring in Ferreira et al. 2005b). According to the same document, the water bodies' identification must be done to "enable the status to be accurately described and compared to environmental objectives" and "must be capable of being assigned to a single ecological class". In other words, transitional water ecosystems must be divided into homogeneous water bodies, enabling a focused environmental management according to the WFD objectives.

Estuaries should be divided according to their natural and human dimensions. In the former, the key factors are morphology, affecting hydrodynamics and mixing, and salinity, controlling biogeochemical processes (Ferreira et al., 2005b). Because ecosystem models rarely require the spatial and temporal resolution needed for accurate hydrodynamic calculations, hydrodynamics were averaged over time and space (e.g. Bird and Hall 1988, Chen and Smith,

1979 in Raillard and Menesguen, 1994). Moreover, for simplicity purposes, work scope and references using the same delimitation as used hereafter, the extensive methodology proposed by Bettencourt et al. (2003) was not considered. Brogueira and Cabeçadas (2006) proposed the Tagus estuary delimitation into three main homogeneous zones which varied, regarding their spatial extension, according to the magnitude of the river flow suggesting that a coarse grid is suitable for model simulations. Therefore, process simulation at the ecosystem scale was done using a coarse grid of 13 model boxes defined heuristically according to Grillot and Ferreira (1996) (Figure 7).

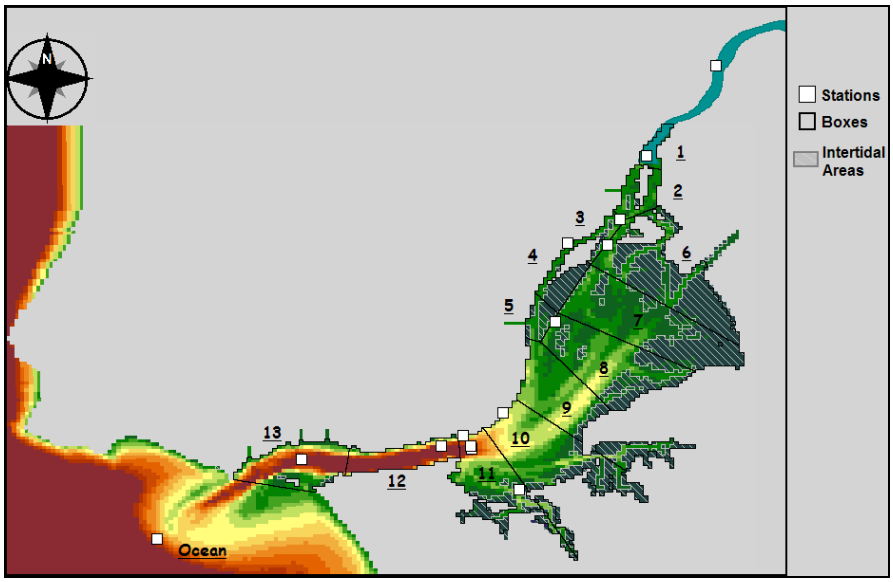

Figure 7 - Model boxes and station sampling locations

Two assumptions arose in the use of such model boxes in the Tagus estuary. Firstly, the compartments were assumed as "black boxes" i.e. boxes were homogeneous and representative of a determined spatial and temporal scale. Secondly, due to the numerical constraints in the advection-dispersion object, no lateral transport between boxes occurred i.e. transport was only done horizontally. For the latter assumption, in particular, the downstream flow in box 2 was distributed, in a 9:1 reason respectively, to boxes 6 and 3. Moreover, boxes 3, 4, and 5, in the Northern Channel were considered to have no connection with boxes 6, 7 and 8, being divided by a Mouchão and by intertidal areas. The numerical integration of variables is done according to the defined E2K boxes.

After box definition and delimitation, morphology was defined using a Tagus bathymetry with approximately 30m pixel resolution. E2K was used to simulate the tidal height between 1998 and 2002, with an hourly time step, establishing the lower and upper tidal limits, 0.2m and 4.2m respectively. Bathymetry was transformed considering the hydrographic zero to be

the lowest simulated tidal height, thus ranging from 0 and 4m. Due to numerical constraints in the advection-dispersion object, box volumes were constant throughout simulations. Mean depth was defined according to mean tide (2m). Box volumes were determined pixel by pixel, using the pixel area (i.e. the bathymetry resolution) and mean depth, and integrated at a box scale (Table 3).

Table 3 - Model Boxes: Description and morphology

Box	Description	Surface area (km^2)	Length (km)	Intertidal area (km^2)
1	Upstream channel (Vila Franca)	3.9	3.8	2.3%
2	Upstream channel (Alverca)	7.7	4.8	6.8%
3	Cala do Norte (Povoa Sta. Iria)	4.5	4.4	23.7%
4	Cala do Norte (centro)	8.5	4.8	71.1%
5	Cala do Norte (EXPO98)	5.5	3.3	54.4%
6	Mouchões (Pancas)	41.3	4.7	67.7%
7	Mouchões (Alcochete)	50.9	4.3	42.1%
8	Mouchões (Montijo)	41.6	4.5	31.8%
9	Mar da Palha (Olivais-Barreiro)	36.9	4.4	23.6%
10	Mar da Palha (centro)	43.8	4.6	26.0%
11	Mar da Palha (Almada-Lisboa)	28.3	4.1	26.9%
12	Outlet Channel (ponte 25 de Abril)	14.9	7.7	0.6%
13	Outlet Channel (Barra)	24.0	6.5	2.3%
Total	Tagus Estuary	311.8	49.5	34.4%

Sampling stations used in calibration and validation are shown in Figure 7 and correspondence with model boxes was assessed thru visual inspection. Note that in Figure 7 and Table 3, the intertidal areas correspond to those observed in the lowest tidal height.

3.4 - EcoWin2000 Object Calibration

3.4.1 - Sensitivity Analysis

Sensitivity analysis provides increased insight on the model and identifies the relevance of the calibration process. It provides a good overview of the most sensitive components in the model concerning the state variables, forcing functions and parameters (Janssen and Heuberger, 1995; Jørgensen, 1994). Performing a thorough sensitivity analysis on each object is out of scope for simplicity reasons and because the main goal is to accurately simulate chl-a. Therefore, only the phytoplankton object was analysed at a parameter level.

Reference conditions for each object were adapted from Ferreira and Duarte (1994). The E2K does not have an automate sensitivity analysis method and, therefore, parameters in each object were varied and the outputs expressed in terms of percentage of variation regarding the reference run. Variation was annually averaged and normalized to a fifty percent range and the impact on phytoplankton biomass was registered. This threshold was chosen to be high due to expectable, and previously referenced, extreme ranges in the simulated variables. For instance, flow can vary inter and intra annually in several orders of magnitude as referenced previously. The same happens with SPM, where estuary values range from 5 to 250 mg l^{-1} (e.g. Brogueira and Cabeçadas, 2006; Gameiro et al., 2007). Thus, the objects' relevance depends on their natural and model variability. The model was run for two years and four boxes were used in order to provide a spatial insight of possible variations on each object's impact (Table 4).

Table 4 - Sensitivity Analysis: Forcing Functions and State Variables (in %)

Variable	Range	Box 1	Box 4	Box 7	Box 11	Global
Flow	*+50*	2.0	11.5	13.6	9.2	**9.1**
	-50	-8.8	-18.2	-19.5	-14.2	**-15.1**
Light	*+50*	1.6	8.3	9.3	8.6	**7.0**
	-50	-1.9	-10.6	-11.2	-10.4	**-8.5**
Water Temperature	*+50*	0	0	0	0	**0**
	-50	0	0	0	0	**0**
SPM	*+50*	-2.2	-5.2	-8.7	-6.2	**-5.4**
	-50	1.6	4.0	5.5	4.6	**4.5**
Zooplankton	*+50*	-1.6	-14.5	-13.6	-19.3	**-12.8**
	-50	1.0	6.6	7.4	12.9	**6.9**

The variation in the four boxes was averaged providing a broad global impact indicator. The water temperature object has no effect on chl-a concentration, thus the object was excluded regarding further simulations. River flow had the higher impact on chl-a, consistent with

Brogueira & Cabeçadas (2006), followed by zooplankton and light availability. With the exception of SPM, objects had different impacts according to the signal of the variation, for instance, a flow decrease had a higher impact that an increase. Spatially, the upstream box 1 was less sensitive to variations in all objects. Different impacts from box to box were probably due to their morphology (e.g. volume) and transport.

The dissolved substances object has no parameters, however, some variations were imposed. Two simulations were performed: (1) Riverine nitrate concentration (constant throughout the year) was varied (2) Smaller boundaries concentration (constant throughout the year) was varied (see Annex III). Note that, the phytoplankton object settings, particularly Ks, play an important role in the rate of nutrient consumption. Nevertheless, these simulations provided a broad insight on the nutrient load impact on phytoplankton biomass (Table 5).

Table 5 - Sensitivity Analysis: Dissolved Substances Object (in %)

Variable	Range	Box 1	Box 4	Box 7	Box 11	Global
Nitrate	*+50*	0.21	0.50	0.71	0.58	**0.50**
	-50	0.48	0.79	1.16	0.88	**0.82**
Ammonia	*+50*	0.03	0.34	0.50	0.53	**0.35**
	-50	0.05	0.50	0.69	0.73	**0.49**

Compared to the other objects, the variation in nitrate and ammonia loads had significantly lower impacts, suggesting that nutrients were not limiting. Globally, nitrate increase had a higher impact than ammonia due to transport and higher associated flow. The phytoplankton object was analysed at a parameter level (Table 6). The more relevant parameters were maximum production (P_{max}), followed by death loss and optimum light intensity (I_{opt}). The half-saturation constant had the lowest impact but its relevance depends on the simulated nitrogen concentrations.

Table 6 - Sensitivity Analysis: Phytoplankton Object (in %)

Parameter	Range	Box 1	Box 4	Box 7	Box 11	Global
P_{max}	*+50*	3.2	5.8	7.8	6.1	**5.7**
	-50	-4.2	-17.8	-20.3	-18.6	**-15.2**
K_s	*+50*	-0.3	-1.3	-2.0	-1.9	**1.4**
	-50	0.3	1.4	2.0	2.0	**1.4**
I_{opt}	*+50*	-1.1	-3.8	-4.9	-4.3	**-3.5**
	-50	1.3	3.9	5.0	4.4	**3.6**
Death Loss	*+50*	-1.6	-6.1	-8.2	-9.1	**-6.2**
	-50	1.4	4.0	5.4	6.6	**4.3**

In model calibration, the sensitivity analysis performed determined, at an object level, the degree of accuracy intended and the degree of detail considered. For the phytoplankton object, it provided information on the level of detail used in the parameter variation when searching for the best suitable set.

3.4.2 - Light

The goal was to simulate the average available radiation at the water surface, temporally at a month to seasonal scale and spatially at an ecosystem scale. Photoperiod and incident surface radiation were calculated by the light object using standard formulations described in Brock (1981). Modelling incident solar radiation simplifies programming and reduces the necessity of extensive, and sometimes limiting, solar radiation data. The light object simulated incident surface radiation in Wm^{-2}, enabling local adjustments in cloud cover and latitude.

A dynamic periodic function of cloud cover, which varies from 0 to 1, was used to force a seasonal limitation on the top of the atmosphere radiation. No random clouds were included. Sub surface radiation and photic depth were calculated using the light attenuation coefficient *k*, provided by the SPM object. Measured values at Monte da Caparica (20D/01C) and Vila Franca de Xira (22B/01C) INAG meteorological stations were used for calibration. Both stations have temporally consistent recorded values since 2002. In order to fill punctual gaps of the Monte da Caparica station, the radiation values measured at the Vila Franca de Xira station were defined as a function of the former, thru linear regression presenting good agreements, $r > 0.90$ (Annex I). An average year was defined averaging hourly radiation from 2002 and 2003. Calibration was performed adjusting the parameters to match aggregated daily averaged radiation measurements (e.g. Grillot and Ferreira, 1996). The best parameters fitted (Annex I) exhibit a good agreement in an average sense, $r = 0.93$ (N=365), *MAE* =19% and *RMSE* = 616 Wm^{-2}, although some outliers are evident (Figure 8).

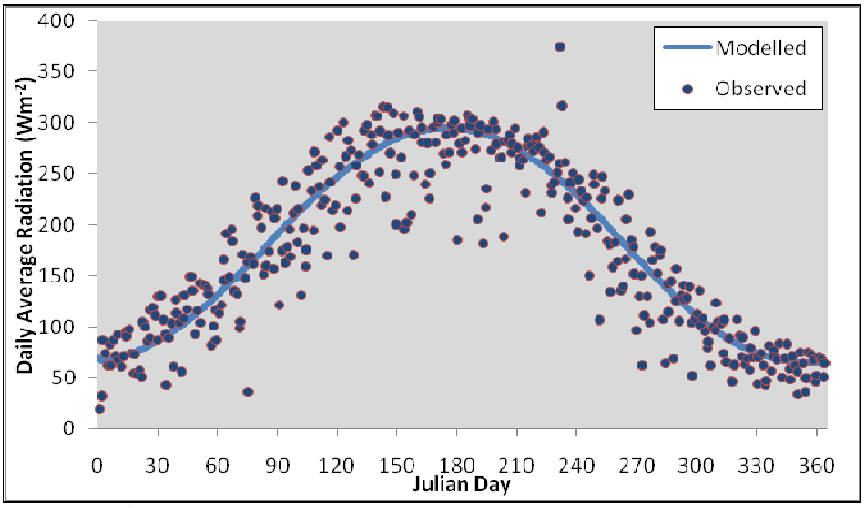

Figure 8 - Daily average radiation: observed *vs.* simulated

3.4.3 - River Flow

The river flow was simulated in m^3s^{-1}, using an empirical relationship between the time of the year and river flow, established by using field data. This object was responsible for computing freshwater flows into the model boxes and their temporal variation, using a cosine function based on the modal flow, the amplitude variation and a daily random flow (Ferreira, 1995).

The flow object was calibrated using data from the INAG Ómnias (18E/04H) station, considered representative of the Tagus river flow due to the estuary proximity. However, this station only has recorded data since 2002. The Almourol INAG station (17G/02H), about 40 kilometres upstream the former, with data since 1999, was therefore, used to model earlier flow values for the Ómnias station, using the 2002 and 2003 coincident data. The relationship derived follows a power law function with good agreement, r = 0.90 (N=674), enabling simulation of flow data at the Ómnias station from 1998 to 2001 and later years gap filling (AnnexI). Data was independently clustered to annual periods.

E2K typically simulates flow using a relatively smooth function assuming average conditions. In particular for the Tagus river: average annual flow of 300-400m^3s^{-1} with a monthly discharge of about 100-200 m^3s^{-1}, in the summer, and about 800-1000 m^3s^{-1} in the winter (Grillot and Ferreira, 1996; Gameiro et al., 2004 & 2007; Brogueira and Cabeçadas, 2006). For instance, from 1999 to 2007, Gameiro et al. (2007) reported about 950 m^3s^{-1} average monthly discharges with a 1200 m^3s^{-1} standard deviation. The first months of simulation were characterized by extreme flow, about 10 fold that of the homologous months in 1999 (Table 7). The river flow in the year 1998 was about 3 to 4 fold that of the year 1999. One can thus, state that they represent respectively a wet and a dry year. Note that, in 1999 the average month flow is 150 m^3s^{-1}, significantly lower than the referenced average flow.

Table 7 - Statistics of modelled flow values (m^3s^{-1}) in the calibration years

	1998					1999				
Season	**Wt**	**Sp**	**Su**	**Au**	**Year**	**Wt**	**Sp**	**Su**	**Au**	**Year**
Total	3884	620	540	368	5412	263	339	238	961	1801
Monthly Average	1295	207	180	123	451	88	113	79	320	150
Standard Deviation	894	84	51	30	638	17	59	9	102	115

The letters stand for: Wt: Winter; Sp: Spring; Su: Summer; Au: Autumn.

The choice of including two very heterogeneous years in the calibration process is done with the expectation of accommodating this variability in posterior model application, and thus potentially improving the model capability of reproducing system behaviour under different

forcing conditions. Due to the high variability and extreme flow measurements, the smooth averaged behaviour of the E2K cosine function had poor accuracy and agreement, especially after the year 2000, where $r < 0.22$ (Annex I). Therefore it was chosen, for simplicity and temporal relevance reasons, to use the modelled flow values at the Ómnias station, following the approach described above, and aggregate them to monthly average flows. Polynomial equations were adjusted to the former and inserted in the E2K code regarding independent annual periods (Figure 9), with good agreement, r >0.90, and reasonable errors (MAE~30%, RMSE~100m^3s^{-1}, see Annex I).

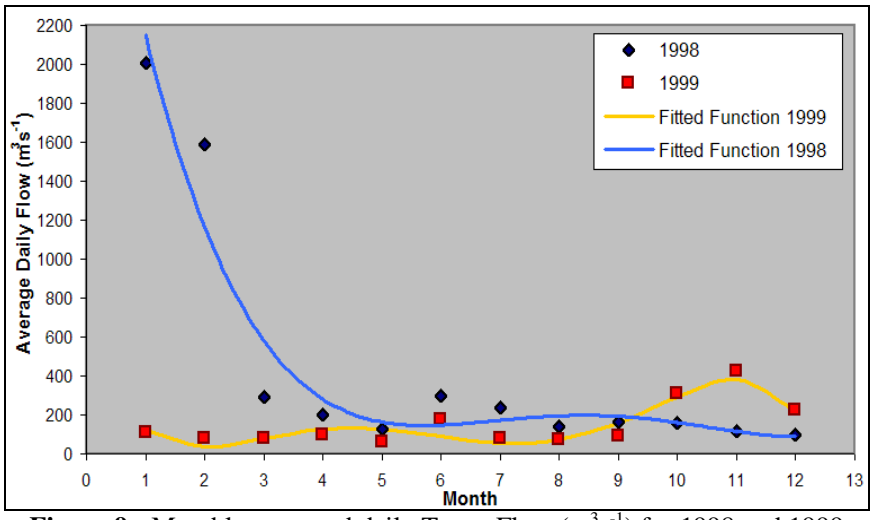

Figure 9 - Monthly averaged daily Tagus Flow (m^3s^{-1}) for 1998 and 1999

3.4.4 - Hydrodynamics

In natural waters, kinetics and transport are the main processes influencing how substances behave (Chapra, 1997). The latter was handled by the transport object which had the role of horizontally transporting other objects' state variables, redistributing dissolved and particulate substances within the model boxes. The transport was solved simultaneously for all boxes calculating all advective-diffusive fluxes across box boundaries and integrating them for all state variables and model boxes (Ferreira, 1995).

The object hasd two basic components: advection and dispersion. The former was modelled explicitly and the latter was modelled considering that, at a longer time scale, tides transport water cyclically and this motion could be classified as diffusive (Chapra, 1997). Hydrodynamics were, therefore, tidally averaged, modelling tidal transport using diffusion coefficients. Advection results from unidirectional flow and does not change the identity of the transported substance and mass is moved from one position to another, specifically, forced

by the Tagus river flow. Advection was modelled using Equation 8 where Q was the flow (m^3s^{-1}), S was the concentration of a conservative substance (e.g. mg m^{-3}, psu) and x was the distance (m) across one axis (Chapra, 1997).

$$Advection = \frac{\partial(QS)}{\partial x} \qquad \textbf{Equation 8}$$

Diffusion is the mass movement due to random water motion or mixing, which causes substances to spread out and dilute over time. On a small scale, molecular diffusion is due to the random Brownian motion of water molecules. On a larger scale, turbulent diffusion results from eddies. Both have negligible movement of the centre of mass and tend to minimize concentration gradients by moving mass from regions of high to low concentration. Diffusion was modelled, adapting Fick's First Law, following Equation 9, where E was the diffusion coefficient (m^2s^{-1}) and A was the cross-sectional area (m^2) of the interface between two model boxes. The first term was defined as the bulk diffusion coefficient (E') proportional to the concentration gradient and the cross-sectional area, between two model boxes (Chapra, 1997).

$$Diffusion = \frac{\partial(EA)\,\partial S}{\partial x} \qquad \textbf{Equation 9}$$

An estuary can be treated as a series of coupled well-mixed reactors. The estimation of mass balances was solved in a coupled way and the equations were solved simultaneously using numerical methods assuming steady state, i.e. the reactors volume did not change over time, $V\frac{\partial S}{\partial t} = 0$ (Chapra, 1997). For this type of transport models, a conservative substance is needed to define the diffusion coefficients, E2K specifically uses salinity. Typical average salinities, per box, were inserted and the E2K calculated the bulk diffusion coefficients stepwise up to downstream assuming steady state (Ferreira, personal communication). Calibration was performed by adjusting the mean salinities per box and comparing the model outputs (salinity) with available measurements.

For any model box, the change of a state variable with time may be calculated by adding the total advective flows in/out of the box, and the total dispersive flows in/out of the box, and adding a term which represents non-conservative processes, sources and sinks, calculated by other objects (Ferreira et al., 1998). Both advection and diffusion are expressed in mass fluxes, gs^{-1}, or $gm^{-3}s^{-1}$, if Equation 10 is expressed according to the derivative of concentration variation with time.

$$V\frac{\partial S}{\partial t} = Advection - Diffusion + (Sources - Sinks) \qquad \textbf{Equation 10}$$

A total of 27 samples, representing 7 different boxes, mainly collected during neap high tides were available. Mean box salinities were adjusted, thus adjusting the bulk diffusion coefficients, to account for the highly variable flow patterns in both calibration years. A reference run was performed using box mean salinities and initial box concentration, according to Ferreira and Duarte (1994) (Annex I). Using the reference situation, mean salinities were adjusted increasing the object accuracy in about 10%, maintaining a fair agreement, $r = 0.70$ (N = 27). Usually salinity is higher in the summer and lower in the winter (e.g. Grillot and Ferreira, 1996) due to the higher freshwater input in the latter and higher evaporation rates in the former. This flow dependency was evident in the simulations (Figure 10) as sampled salinity was low in 1998, a wet year, and more stable and higher in 1999, a dry year. It should be noted that the model 'spin up' was done in about 2 months.

On a box scale, significant errors were observed, specifically for boxes 1 and 4 (Table 8). For the latter, measured salinity was, on average, about 60% lower than modelled, in 1998, which had a total flow 4 times higher than 1999. Low salinities (<20psu), probably due to the model 'spin' up and the high flow in winter and spring months in 1998, were the main reason for the accuracy achieved (Annex I). This suggested that hydrodynamics would be accurate in an average-dry year, after 'spin up'.

Table 8 - Transport object performance statistics: box by box and ecosystem scale

	Box 1	**Box 3**	**Box 4**	**Box 6**	**Box 8**	**Box 11**	**Box 12**	**Global**
Matches	1	1	8	1	1	8	7	**27**
RMSE	12.77	0.2	8.0	1.84	1.4	3.0	2.7	**5.4**
MAE (%)	66%	1%	52%	7%	4%	10%	8%	**23%**
r	-	-	0.80	-	-	0.88	0.92	**0.70**

In sum, the hydrodynamics were calibrated with an average 23% error and with a reasonable agreement, $r = 0.70$ (N=27). Salinities, especially in 1998, were overestimated by about 5 psu.

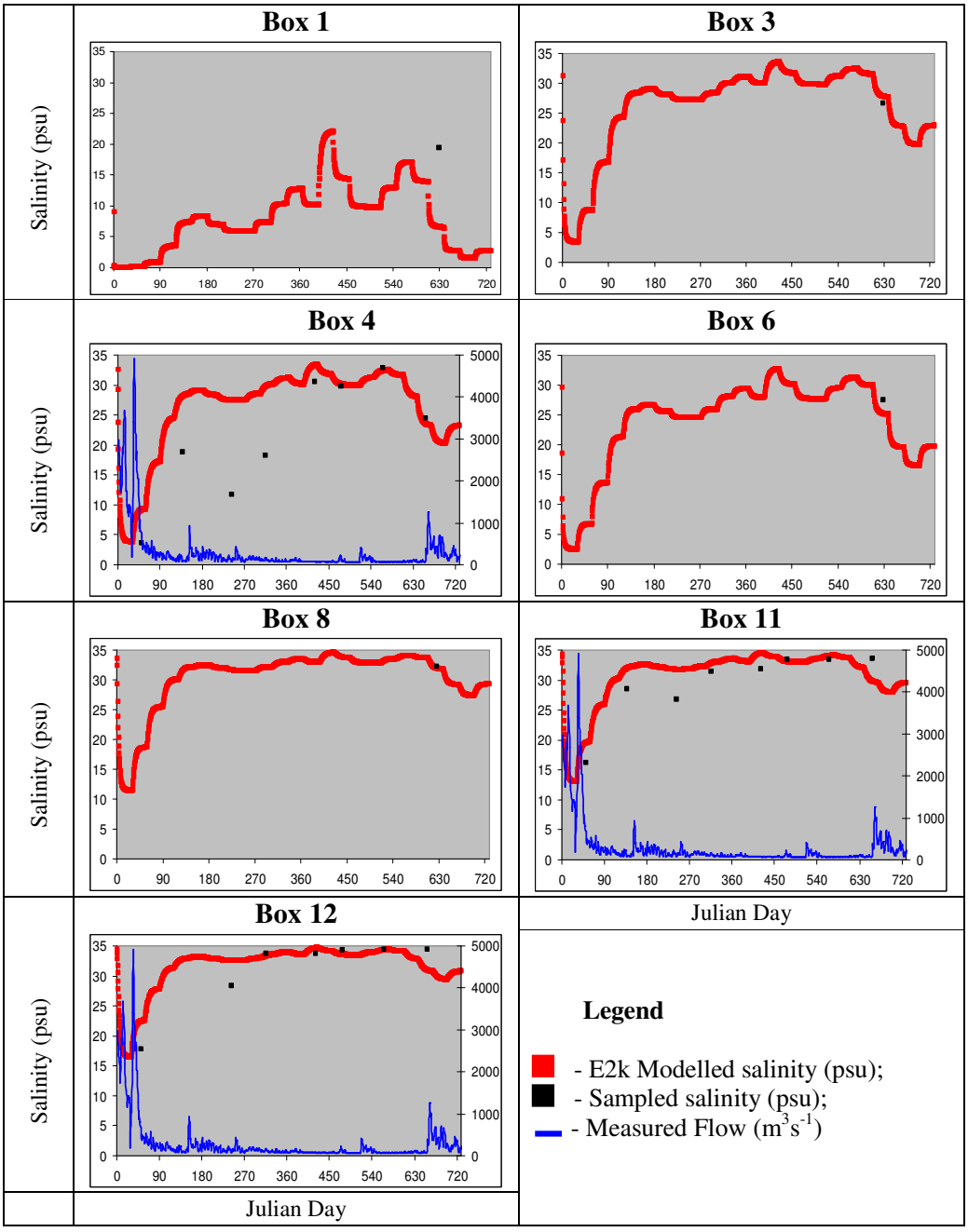

Figure 10 - Salinity time series box by box: sampled *vs.* modelled

3.4.5 - Dissolved Substances

The dissolved substances object encapsulates the attributes and methods for all dissolved nutrients in the system. Nutrients like ammonia, nitrite, nitrate, DIN (contribution of all nitrogen dissolved forms), phosphate and silicate were simulated and expressed in µmol l^{-1}. Concentration is modified by transport, consumption, driven by phytoplankton production, and addition, driven by boundary loads and mortality. The particulate organic detritus are remineralized and dissolved nutrients are returned as ammonia followed by nitrification, using

a fixed rate of oxidation of reduced forms of DIN (Ferreira, 1995). Boundaries introduce nutrients and other substances into the system with different dynamics. The Tagus river freshwater inputs introduce nutrients into the estuary which depend on the flow and upstream concentrations (e.g. driven by diffuse pollution). Concentration was constant throughout the simulation, defined as the annual average using monthly water quality measurements from the INAG station, Valada do Tejo (19E/02). Silicate data was not measured at the INAG station and was therefore taken from B2k, as well as, the average concentration for all nutrients in the ocean boundary. A total of 27 smaller boundaries were defined, corresponding to small rivers and WWTPs nearby the estuary (Ferreira, personal communication; INAG, 2002). These introduced nutrients only in the form of ammonia due to relevance and model requirement, being modelled with a constant flow and concentration throughout the year (Annex III).

Phosphate, silicate and DIN were used to determine the limiting nutrient for primary production in the Tagus estuary. When nutrients are not limiting, the molar element ratio C:N:P in most phytoplankton is 106:16:1 (in atoms). Diatoms need in addition silicate and the respective Redfield nutrient ratio is C:Si:N:P = 106:15:16:1 (Redfield, 1934). The N:P, N:Si and Si:P ratios were analysed and Figure 11 shows two different patterns. In 1998, the system is P limited, whilst in 1999 it is mainly N limited. The visual inspection of the N:P ratio in the validation years (not shown) suggested a smaller, but still consistent P limitation. The Si:P ratio exhibited a pronounced silicate limitation, which also occurred in the validation years (not shown). The N:Si ratio suggested the same (Figure 12). It is recalled that, besides requiring silicate to grow, diatoms are the most relevant form of phytoplankton in the Tagus estuary, especially in the mid-upstream zones (Gameiro et al., 2004 & 2007).

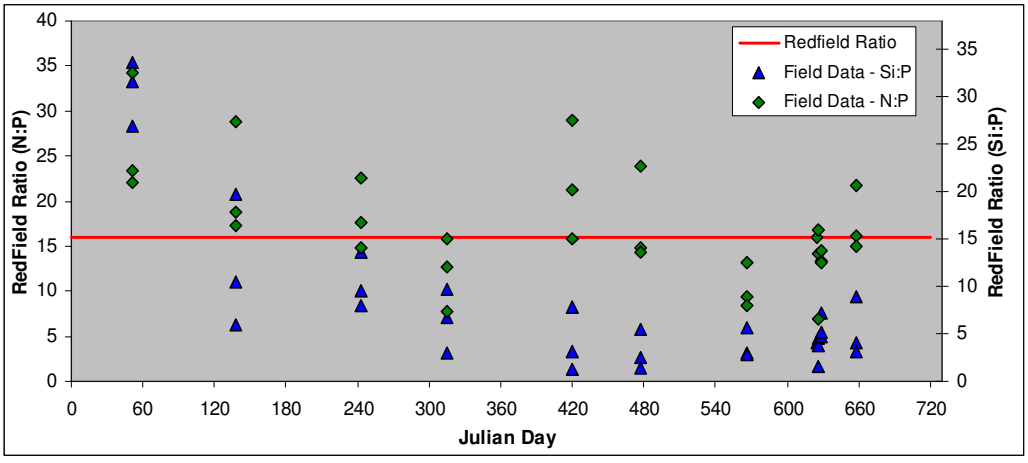

Figure 11 - Nitrogen to Phosphate (N:P) and Silicate to Phosphate ratio (Si:P)

This type of information is critical to the modelling process determining the governing nutrient limitation equations in the phytoplankton object and future accuracy issues. The previously implemented phytoplankton object code only considered N limitation and, therefore, Si and P limitation were not considered. Moreover, historical data, taken from B2k with higher temporal and spatial resolution, indicated that N was the main limiting nutrient.

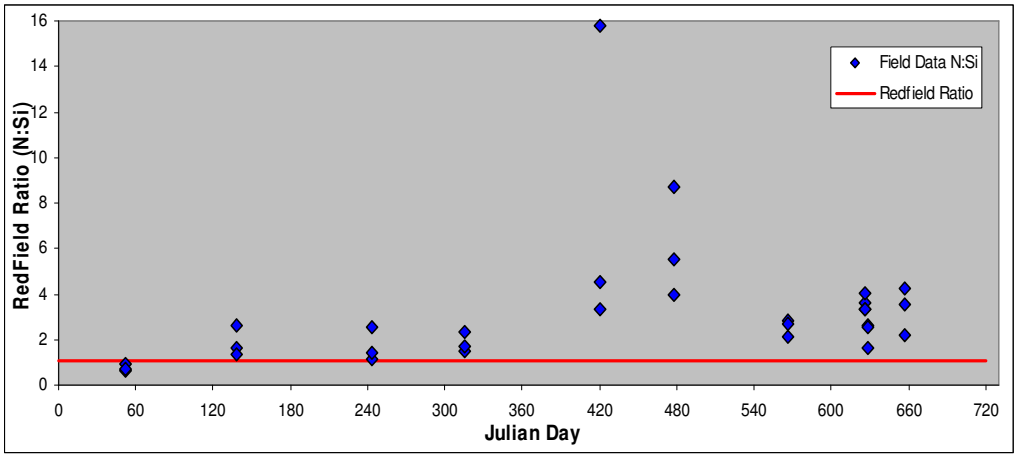

Figure 12 - Nitrogen to Silicate ratio (N:Si) in atoms

The dissolved substances object does not have parameters to perform calibration and, therefore, boundary loads were adjusted using auxiliary information and the phytoplankton object was kept with reference parameters. Initial box concentrations were defined according to Ferreira and Duarte (1994) and the nutrient simulation was compared with measured samples, for ammonia (Figure 13 and Table 9) and for the remaining nutrients (Annex III).

Globally, the model significantly underestimated ammonia concentration in about 70% or 45 µmol l^{-1}. Boxes, 4, 11 and 12 had more than one match in the calibration period, thus the analysis was focused upon these. Box 4 and Box 11 had the largest errors, with about 60% model underestimation. Note that, box 4 had the higher ammonia values in the estuary, with two particularly high values in 1998, one of them above 200 µmol l^{-1}. These drove a high global RMSE and a box error over 80 µmol l^{-1}. The boxes referred, are near highly populated areas and probably the boundary loading was underestimated or other sources of ammonia were not included. Other spatial inferences were not feasible due to the low number of samples, particularly in the mid estuary.

Ammonia concentration tended to have a regular annual distribution, atypical of sewage discharges, exhibiting low temporal correlation. However, it roughly tended to be smaller in the summer and higher in the remaining seasons, consistent with producer growth.

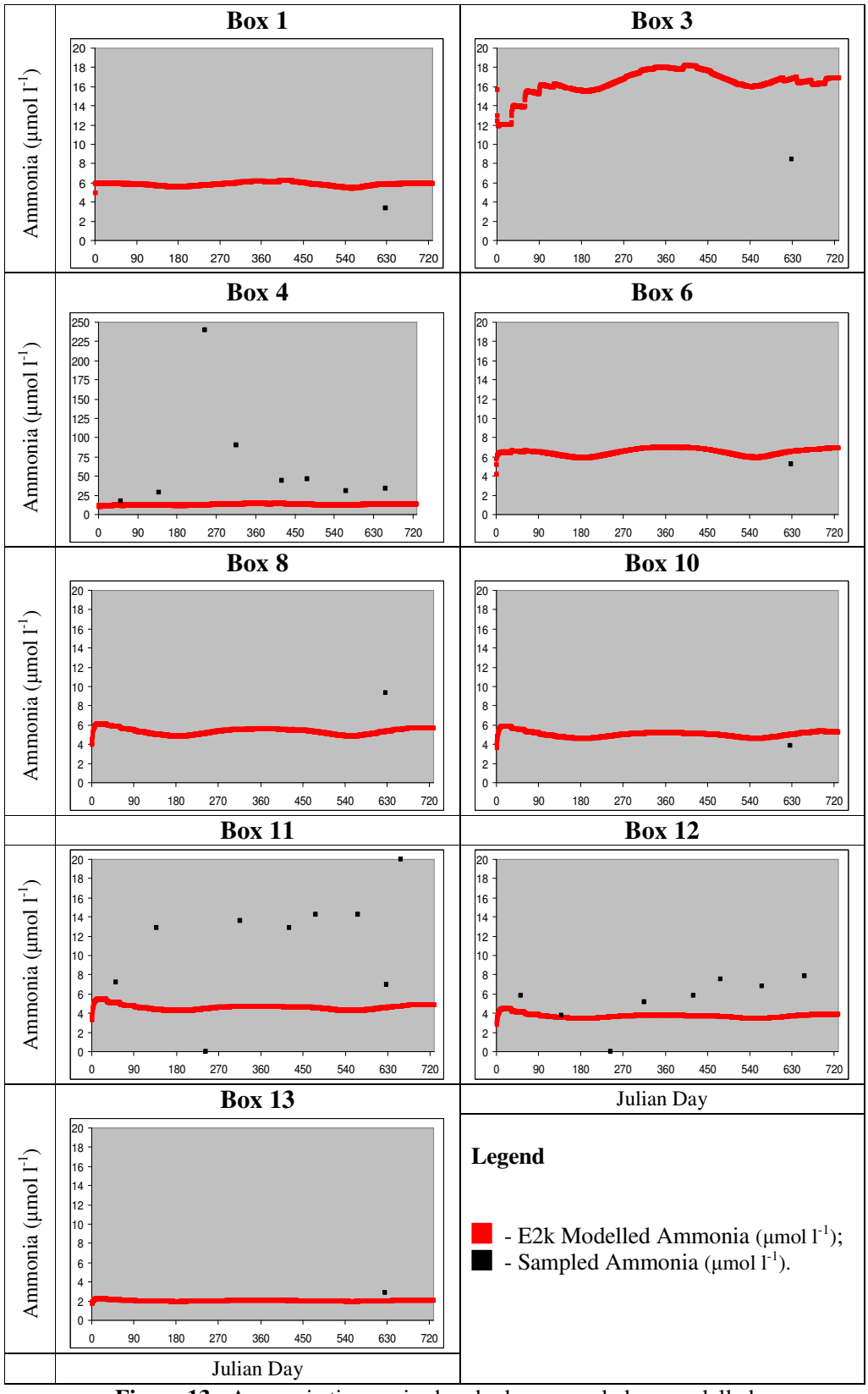

Figure 13 - Ammonia time series box by box: sampled *vs.* modelled

The remaining nutrients, silicate and phosphate, were modelled with approximately 50% underestimation error, while nitrate was underestimated by about 80%. One visible pattern

regards boxes 4 and 11, which underestimated all nutrients especially during the year 1998. Note that for all nutrients, except nitrate, there were two very high values in the summer and autumn samples during the year 1998 (Annex III).

Table 9 - Ammonia Calibration: performance statistics box by box and ecosystem scale

	Box 1	Box 3	Box 4	Box 6	Box 8	Box 10	Box 11	Box 12	Box 13	Global
Matches	1	1	8	1	1	1	9	8	1	**31**
RMSE	2.5	8.3	86.8	1.3	4.1	1.1	9.2	2.9	0.9	**44.4**
MAE (%)	75%	98%	66%	24%	43%	28%	91%	64%	30%	**70%**
r	-	-	0.06	-	-	-	0.04	0.22	-	**0.49**

Due to the lack of resolution in the samples used, the comparison of modelled and sampled values reported by other authors was considered very important. Simulated nutrients were underestimated according to Brogueira and Cabeçadas (2006) and Gameiro et al. (2007). The best agreements regarded phosphate in the winter and summer, with some underestimation in the mid estuary. Ammonia was punctually overestimated in the whole estuary and summer periods were better modelled than winter both in average and wet conditions. Gameiro et al. (2004) performed a study from March 1999 to March 2000 in the mid and upstream zones of the estuary. Comparing it to with the former simulations, for the year 1999, ammonia seemed well modelled, especially in box 4, and nitrate was underestimated by about 100%. Nitrite had good agreement in the upstream zones, while in the mid estuary had lower agreement. Globally, simulated DIN was underestimated by about 10 μmol l^{-1} (Ferreira, 2000). Specifically, boxes 2 and 3 were in good agreement with the reported DIN values in Martins and Duffner (1982), Silva et al. (1986) and Gameiro et al. (2004). In box 8, DIN was in good agreement with the latter author, but underestimated by about 10 μmol l^{-1} in comparison with the former.

Table 10 exhibits a seasonal comparison with averaged monthly values reported by Gameiro et al. (2007) between 1999 and 2007 concerning boxes 2, 3, 4, 7 and 8. Silicate and DIN were underestimated by about 100% throughout the whole year, with the exception of summer, regarding the latter nutrient. Phosphate was relatively well simulated, but also underestimated.

Table 10 - Comparison of simulated nutrients with Gameiro et al. 2007

	DIN		**Phosphate**		**Silicate**	
	Gameiro et al. 2007	*This Study*	*Gameiro et al. 2007*	*This Study*	*Gameiro et al. 2007*	*This Study*
Spring	65 (32)	29	3.5 (1.4)	1,6	48 (32)	19
Summer	27 (19)	27	3.9 (1.6)	1,4	32 (22)	17
Autumn	67 (36)	34	4.5 (3.0)	1,9	73 (50)	24
Winter	84 (33)	37	3.4 (1.1)	2,9	62 (45)	40
All	57 (55)	32	3.8 (3.5)	1,9	51 (44)	23

3.4.6 - Suspended Particulate Matter

The SPM object is responsible for calculating the SPM concentration and the light extinction coefficient in each model box. The deposition of suspended matter is calculated by the object's methods (see Eq.1 in Ferreira et al., 1998). The settling speed is calculated according to Stokes' law and the density of the water-column is based on the salinity and temperature in each box. Particle settling is related to grain-size, and the size distribution is mainly related to flocculation processes. The sedimentation rate is calculated using the ratio between the settling speed (m day^{-1}) and the box depth, leading to a decrease in the SPM flux (Ferreira et al., 1998). Turbulence prevents settling of suspended matter and is simulated using an empirical coefficient, which reduces the downward flux of suspended matter. The deposition coefficients were used according to the parameterization used by the latter author regarding information in Stumm and Morgan (1981). Resuspension depends on the shear-stress at the sediment-water interface, and on the nature and compaction of the sediment. The light extinction coefficient *k* is estimated using an empirical relationship between SPM concentration in the water column and *k* values, expressed in Equation 11, where k is the light extinction coefficient (m^{-1}) and SPM is the suspended particulate matter concentration (mg l^{-1}) (Ferreira, et al., 1998).

$$k = \frac{1.7}{\exp(2.034)} \times e^{(0.734 \ln(SPM))} \qquad \textbf{Equation 11}$$

The SPM object had two parameters, turbulence with ecosystem scale influence and SPM resuspension at a box scale. Because values were spatially significantly different, varying the turbulence had low effect on the global accuracy of the modelled values. Thus, varying the box resuspension was necessary to simulate such box to box differences. Initial concentration in the model boxes was defined according to Ferreira and Duarte (1994). Naturally, hydrodynamics transported SPM from these to other boxes with low values leading to a somewhat ambiguous calibration effort. Therefore, it was important to understand if the measured SPM values regarding the calibration years were representative at longer time scale, taking into consideration other studies, prior knowledge and other data sets.

Calibration was performed comparing sampled with simulated SPM (Figure 14) and the best fitted parameters were detailed in Annex II. Three boxes had higher number of samples, boxes 4, 11 and 12 and were in good agreement in what concerned magnitude although the average error was relatively high. The remaining boxes, especially in the mid estuary, were

significantly underestimated. Globally, the SPM was simulated with an average error of 70%, a 9.6 mgl^{-1} error and correlation of $r = 0.65$ (N = 31) (Table 11).

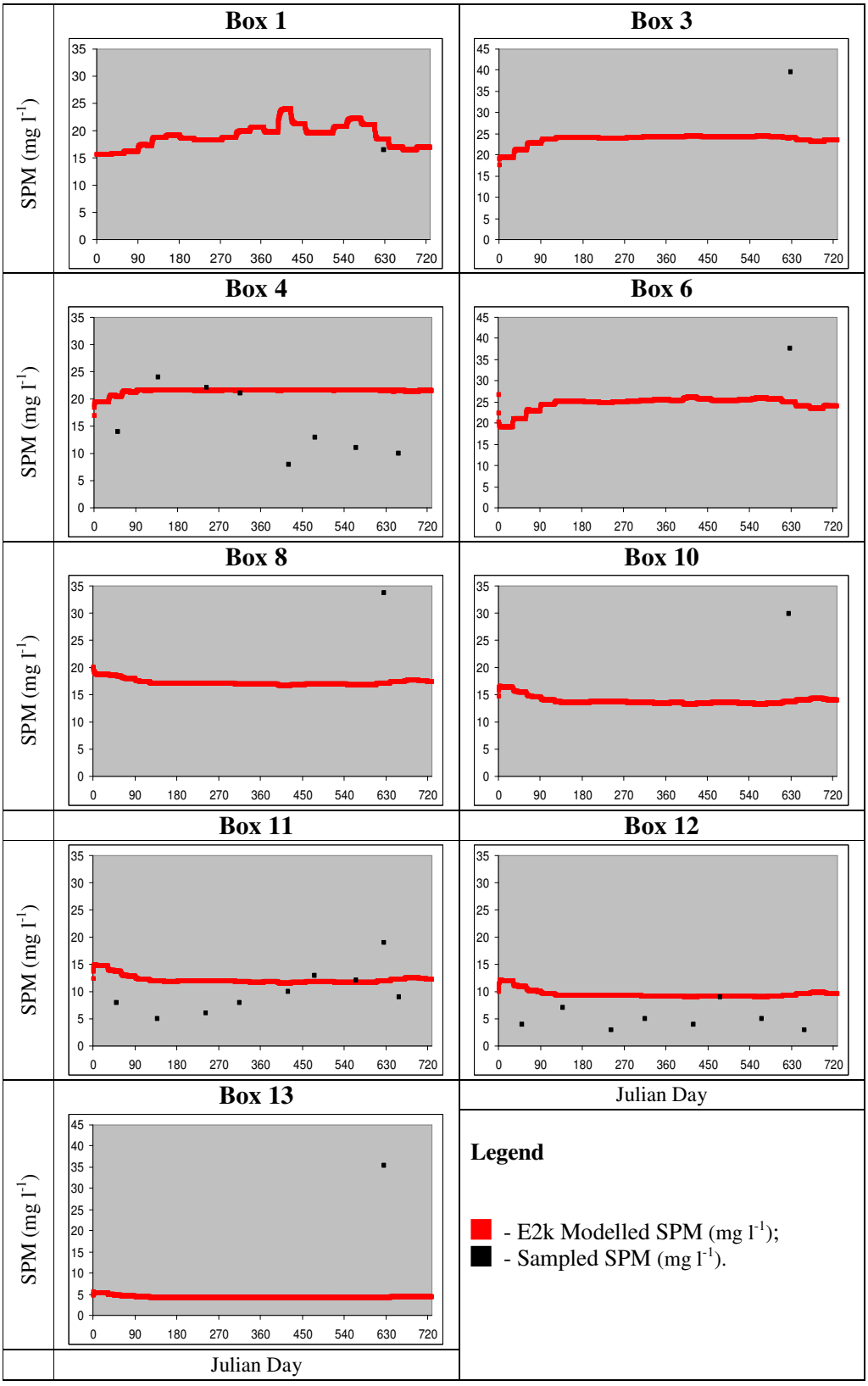

Figure 14 - SPM time series box by box: sampled *vs.* modelled

Spatially, comparing simulations with average monthly values in 1999 reported by Gameiro et al. 2004, boxes 2, 3 and 4 were two fold underestimated, whilst boxes 7 and 8 were in good agreement. However, Fernandes (2005), in these two latter boxes, reported higher values and overestimation in the downstream boxes. Calibration suggested that the model did not reproduce the longitudinal exponential SPM gradient according to the distance to the ocean (Fernandes, 2005), particularly in the mid estuary, where errors were above 12 mg l^{-1}.

Table 11 - SPM object performance statistics: box by box and ecosystem scale

	Box 1	Box 3	Box 4	Box 6	Box 8	Box 10	Box 11	Box 12	Box 13	Global
Matches	1	1	8	1	1	1	9	8	1	**31**
RMSE	2.0	15.7	8.3	12.7	16.7	16.3	4.9	4.9	31.1	**9.6**
MAE (%)	12%	40%	63%	34%	49%	54%	51%	116%	88%	**70%**
r	-	-	0.12	-	-	-	-0.21	-0.27	-	**0.65**

Temporally, comparing with Gameiro et al. 2007, values were within range but consistently higher than simulations. The best agreements were for summer and autumn but it was clear that the E2K object did not reproduce annual dynamics (Table 12). This was consistent with the comparison by Brogueira and Cabeçadas (2006), where the only fair agreement was achieved in the summer concerning the downstream boxes. Ramos (2002) stated that measured values near box 10, between 1994 and 1998, were highly variable, typically around 10-15 mg l^{-1} and occasionally higher than 20 mg l^{-1}.

Table 12 - Comparison of simulated SPM with Gameiro et al. 2007 (adapted)

	Gameiro et al. 2007	*This Study*
Spring	26 (18)	20
Summer	36 (15)	20
Autumn	26 (17)	21
Winter	30 (21)	19
All	30 (24)	20

Calibration was performed with a parallel goal: to match E2K simulation with historical data and reference studies, box by box. The collected information and subsequent SPM ranges were summarised in Annex II. With the collected information, another calibration effort was performed. The priority was set on increasing the accuracy in the mid section of the estuary without compromising it's accuracy in the upper and downstream sections. Due to the average hydrodynamic behaviour and limitations of the SPM object, the temporal SPM dynamics were difficult to simulate, and therefore, the focus was set upon spatial magnitude.

Besides SPM, the light extinction coefficient was compared with values reported by Gameiro et al. 2004 & 2007. Data was available for boxes 2,3,4,7 and 8 for the year of 1999. Although simulated SPM was lower than those reported by this author, the light extinction coefficient

(k) was higher for all boxes mentioned. The best agreement was for box 4 and the remaining had differences close to 1 m^{-1}. Seasonally, comparing with values reported by Gameiro et al. 2007, simulated k was within range but consistently higher and its temporal dynamics were not reproduced.

A ratio Z_{mix}:$Z_{euphotic}$ lower than 1 indicates that the entire water column is located within the euphotic zone. Gameiro et al., (2007), for the up and mid estuary, indicates that the ratios ranged from 0.4 and 4.1, in average 1.3 and were similar for all seasons. Moreover, only in approximately 20% of the samples was the entire water column located within the euphotic zone, whilst the production upper limit (ratio=5) was never reached. Due to the vertical homogeneity, the Z_{mix} was considered as the constant box depth. The modelled ratio was within the reported range, describing an expectable average behaviour, which was below 1 in about 15% of the cases and the upper limit was never reached (Figure 11). Seasonally, a slight decrease in the light limitation during Spring, was observed in the simulations. This analysis suggested that light availability was reasonably well modelled, particularly where it was more relevant to production limitation i.e. the upper and mid estuary regions.

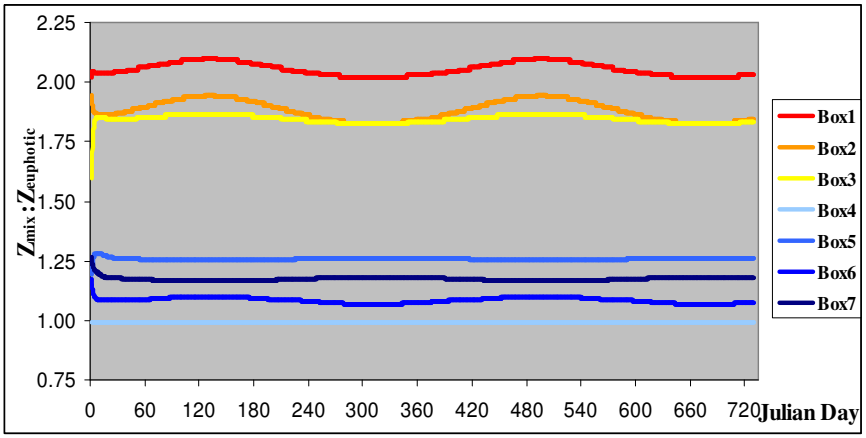

Figure 15 – Modelled Zmix:Zeuphotic in the upper and mid estuary model boxes

Calibration with sampled data provided extinction coefficients closer to the reported values for 1999, in the mid and upstream zones. Moreover, quantitative calibration is recommended over qualitative analysis, for reproducibility and uncertainty management in subsequent applications, and, therefore, were used for subsequent simulations.

3.4.7 – Zooplankton

No zooplankton data was available for the calibration and validation years. Therefore the goal when including this object in the model was to provide a phytoplankton grazing feature

enabling a production control. The object returns zooplankton biomass in mg m^{-3} of Fresh Weight. The parameters used were taken from Ferreira and Duarte (1994) and are described in Annex II. Initial concentration in the model boxes was defined according to the latter authors.

3.4.8 - Phytoplankton

The phytoplankton object returns biomass concentration in µg chl-a l^{-1}, along with gross and net primary productivity in mgC $m^{-3}d^{-1}$. Gross primary production (GPP or p_p) was estimated from maximum possible production, which was limited by light and nutrient (i.e. nitrogen) availability (Equation 12). The former was forced and calculated by the light and SPM objects and the latter, by the dissolved substances object. The light function or the photosynthetic response to light was defined by the P-I relationship taken from Steele (1962) and integrated over depth, whilst the nutrient function was calculated by a Michaelis-Menten function type (Equation 13), varying between 0 and 1, like a productivity limitation factor (Table 13) (Ferreira et al., 1998). It was assumed that growth is only limited by nitrogen.

Table 13 - Phytoplankton Productivity: Equations (Ferreira et al., 1998)

$$p_p = P_{\max} \frac{e}{k\ depth}\left(e^{-\frac{I}{Iopt}} - e^{-\frac{I\sup}{Iopt}} \right) f(N) \qquad \textbf{Equation 12}$$

where, $f(N) = \frac{n_{\lim}}{K_s + n_{\lim}}$ **Equation 13**

Parameter	Description	Value/Units
P_{max}	Maximum photosynthesis	Calibrated in h^{-1}
I	Light intensity at box depth	Calculated by the light object; m E m^{-2} s^{-1}
I_{sup}	Surface light intensity	Calculated by the light object; m E m^{-2} s^{-1}
I_{opt}	Optimum light intensity	Calibrated in m E m^{-2} s^{-1}
k	Light extinction coefficient	Calculated by the SPM object; m^{-1}
$f(N)$	Nutrient limitation	Calculated (adim)
n_{lim}	Nutrient concentration	Calculated by the dissolved substances object; µmol N l^{-1}
K_s	Half-saturation constant for limiting nutrient	Calibrated in µmol N l^{-1}

The object also calculates exudation and respiration. In the literature, estimates of dissolved organic carbon (DOC) loss and related factors are widely variable, ranging from almost zero to 90 % of carbon fixed (Jørgensen et al., 1991). Increased DOC losses may be driven by poor growth conditions (e.g. Ittekot et al., 1981 in Ferreira et al., 1998) and some authors indicate greater exudation at high productivity rates. The phytoplankton object calculates exudation and respiration as a fixed fraction of gross production, respectively 0.1 and 0.3 h^{-1}, converting

GPP into NPP (Net primary production) (Jørgensen et al., 1991). The main equations, parameters and processes regarding the phytoplankton object were described in Table 14.

Table 14 - Phytoplankton object : equations and processes (Ferreira et al., 1998)

$$\frac{\partial Phyt}{\partial t} = Phyt\left(p_p - e_p - r_p - m_p - gZoo\right) CarbontoClorophyll \qquad \textbf{Equation 14}$$

Parameter	Description	Value/Units
p_p	Phytoplankton gross photosynthetic rate	Equation 12 in h^{-1}
e_p	Phytoplankton exudation rate	Fraction of p_p in h^{-1}
r_p	Phytoplankton respiration rate	Fraction of p_p in h^{-1}
m_p	Phytoplankton mortality	Fraction of p_p in h^{-1}
gZoo	Zooplankton grazing pressure	Provided by the Zooplankton object in h^{-1}
CarbontoClorophyll	Conversion factor	0.03

Initial concentration in the model boxes were defined according to Ferreira and Duarte (1994). The object had four parameters that could be adjusted, P_{max}, I_{opt}, K_s and m_p. Calibration was performed in three stages. The information retrieved in the sensitivity analysis suggested that K_s was the parameter with less relevance and was, therefore, set to 1.19 μmol N l^{-1} (Ferreira and Duarte, 1994). Varying the death loss parameter in certain ranges introduced instability to the model and therefore this value was set to 0.1 h^{-1} for all simulations (Ferreira and Duarte, 1994). The photosynthesis parameters, P_{max} and I_{opt}, were varied within a given range according to literature values (Ferreira et al., 1998; Jørgensen et al., 1991; Jørgensen, 1994; Macedo and Duarte, 2006). The former was varied from 0.02 to 0.2 h^{-1} and the latter from 100 to 800 mE m^{-2} s^{-1}, both divided into 8 intervals resulting in a total of 64 combined simulations. A simple cost function was employed (Figure 16 and Annex IV).

The misfits provided different information suggesting that using only one performance measure would lead to ambiguity (Annex IV). Moreover, qualitative visual analysis was extremely important. The different parameter combination yielded several local minima regarding the cost function (Figure 16). Out of 64 simulations, 5 combinations were extracted for visual inspection and 2 (of the latter) were discarded due to model instability and lack of dynamic behaviour (not shown). The discarded simulations corresponded to P_{max} 0.2 and 0.1 h^{-1}, respectively, with I_{opt} 200 and 700 m E $m^{-2}s^{-1}$. Regarding P_{max}, it optimally ranged from 0.075 to 0.1 h^{-1}, while I_{opt} had a wider range, from 300 to 800 m E $m^{-2}s^{-1}$.

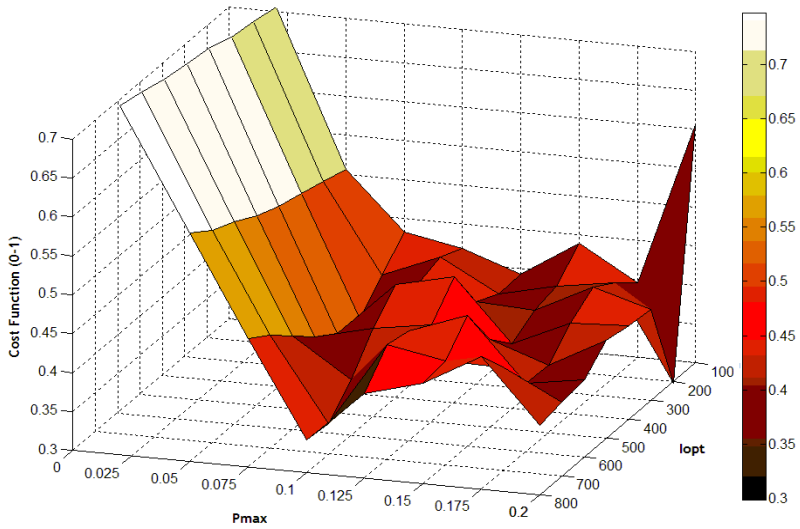

Figure 16 - Cost Function 3D plot: Parameter combination (P_{max} and I_{opt})

The remaining combinations were crossed with different K_s values, ranging from 0.2 to 2.4 µmolN l^{-1} and divided into 5 intervals. The variation of this parameter yielded low improvement, as would be expected, concerning the sensitivity analysis information. Moreover, simulated DIN was always well above the higher half saturation concentration used and was, therefore, set to the default value (Ferreira et al., 1998) for the remaining simulations. The parameter set that yielded the best agreement between predictions and observations was chosen solely regarding P_{max} and I_{opt}. Visual inspection of all boxes (not shown), the lower cost function value and the particularly lower MAE (%), lead to the choice of the combination P_{max} and I_{opt}, respectively, 0.1 h^{-1} and 800 $mEm^{-2}s^{-1}$ (Annex IV). This set of parameters along with K_s = 1.19 and m_p = 0.1 was used in further simulations. The high I_{opt}, retrieved is consistent with data published by Valiela (1995). Figure 17 and Table 15 show the calibration time series and statistics.

Table 15 - Phytoplankton object performance statistics: box by box and ecosystem scale

	Box 1	Box 3	Box 4	Box 6	Box 8	Box 10	Box 11	Box 12	Box 13	Global
Matches	1	1	8	1	1	1	9	8	1	**31**
RMSE	0.6	3.4	3.9	3.8	11.4	0.8	3.6	8.7	0.2	**5.6**
MAE (%)	8%	43%	104%	45%	79%	48%	82%	73%	14%	**77%**
r	-	-	-0.66	-	-	-	0.09	0.16	-	**0.06**

From Figure 17, one can infer that the object was unstable in the first 90-120 days due to model *spin up* and due to extreme flow variability (see 3.4.3). In the upstream boxes, the impact of flow variation induced model instability, particularly evident, in the beginning and in the end of the simulation. Increases in flow anomalously simulated high chl-a due to higher input of riverine phytoplankton, rather than by modifying the internal estuary dynamics.

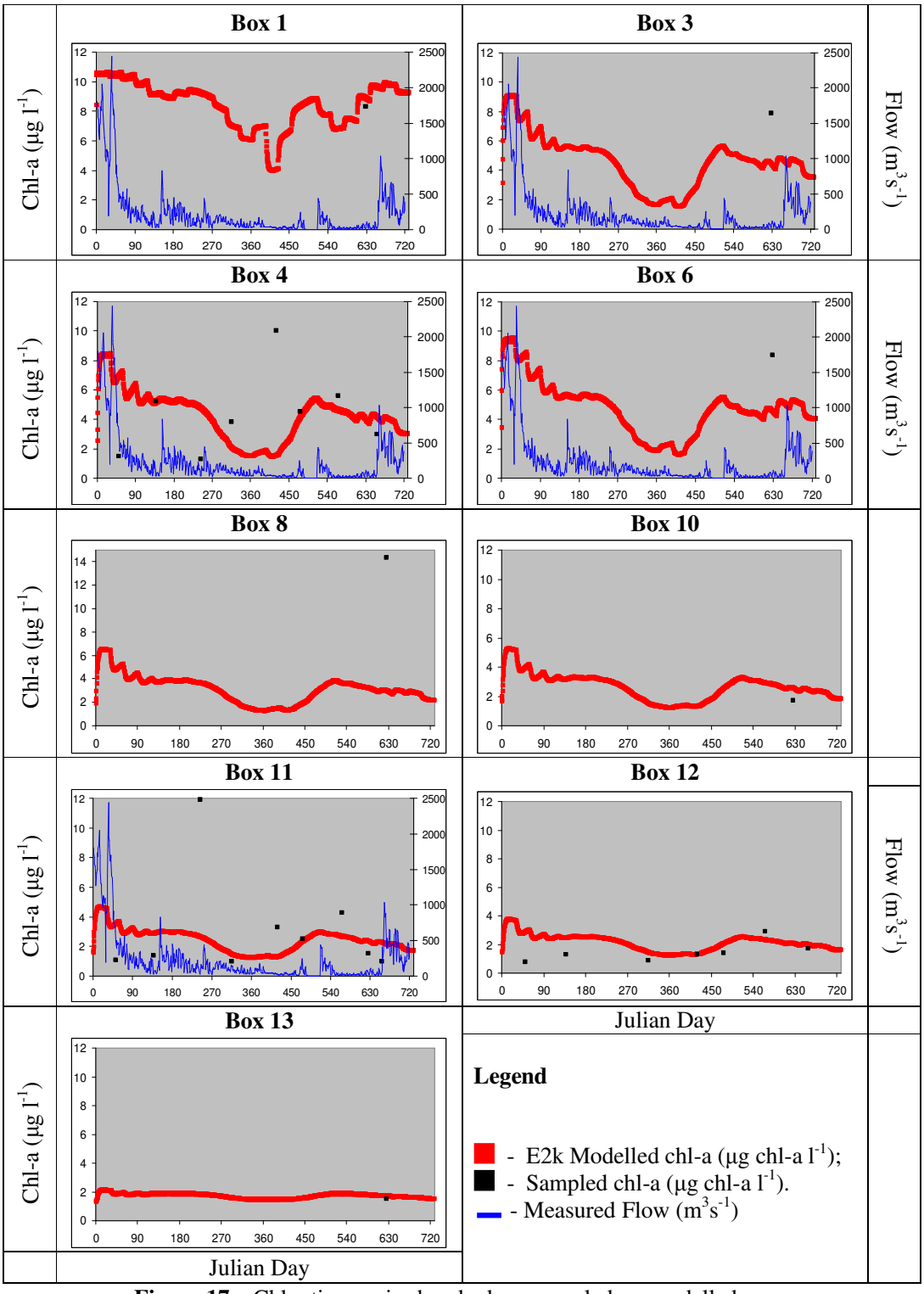

Figure 17 – Chl-a time series box by box: sampled *vs.* modelled

The phytoplankton object roughly translated the natural annual dynamics in the Tagus estuary, with a unimodal Spring bloom. In the upstream boxes, there was a late summer, early Autumn slight biomass increase which had been reported but for mid estuary regions. The flow increase and variability was probably the cause for the, early autumn, slight chl-a increase. The modal characteristics of chl-a peaks were consistent with those reported by

Gameiro et al. (2004), although, they were simulated slightly earlier (May). Furthermore, the spring blooms were simulated at the same time for all boxes, whilst the data reported by the latter author, suggested that the 1999 blooms occured between May and July with different timings concerning different sites. The sampled data suggested a later bloom, in July/August. It is recalled that, particularly in 1999, sampled data indicated a strong Si limitation (see Figure 11 & Figure 12) which was, as mentioned, required by the most relevant phytoplankton form in the upstream region: diatoms. This may explain why bloom dynamics were inaccurately reproduced.

The more pronounced blooms were not reproduced, probably due to the E2K large scale and multi year characteristics (see Box 4 and 11). Note that the chl-a peaks registered in box 11 and 12 corresponded to low peaks (near zero) of ammonia, suggesting a bloom event with extreme nutrient depletion. Furthermore, box 4 had an atypical winter bloom (in 1999), which was responsible for the negative correlation, which also occured, with lower magnitude, in box 11. The model reproduced fairly well, in an average sense, the spatial chl-a gradient, in which, chl-a increases with the distance to the ocean.

Although the mid estuary had only 3 samples (1 per box) and few boxes were represented, there seemed to be a significant underestimation, which also occured with nutrients and SPM. Calibration was not aimed at the optimization of these middle estuary boxes, because, spatial inference was not feasible due to data limitations. Compared with Gameiro et al. (2004), in 1999, the average concentration was slightly underestimated and the late Spring bloom was about three times higher than simulations. A previous study (Silva et al., 1986 in Gameiro et al., 2004) reported typical values within the simulated range, particularly for box 8. Moreover, compared with Brogueira and Cabeçadas (2006) for typical summer conditions, simulated values were underestimated in this estuary section. For the upstream boxes, chl-a values were within reported ranges for average winter and summer conditions (Brogueira and Cabeçadas, 2006). Particularly in the latter, boxes 1 and 2 suggested that river inputs were accurately simulated, in an average sense. However, for the year 1999, in boxes 2 and 3 chl-a was significantly underestimated (Gameiro et al., 2004) and, in the Northern Channel, were within the annual average reported by the same author, although the bloom was simulated 2/3 months earlier. According to Brogueira and Cabeçadas (2006), in the downstream section, chl-a was under and overestimated, respectively, for summer and winter average conditions.

3.5 - Remote Sensing Data Processing

For the purpose of remote sensing application, daily Level 1B (L1B) MODIS Terra data was acquired from the NASA Level 1 and Atmosphere Archive and Distribution System (LAADS), after visual inspection of cloud cover and scene coverage. Level 1B data concerns reflectances at full resolution without communications artefacts, radiometrically corrected and geolocated (http://ladsweb.nascom.nasa.gov/) in WGS84 coordinates. The full 1km resolution is provided at nadir view so that shifted pixels have lower resolution, resulting in data arranged in an irregular grid.

All data was processed with NASA Ocean Colour software, SeaDas 5.1, distributed freely and run in Linux environment (http://oceancolor.gsfc.nasa.gov/). MODIS scenes were subseted according to the study area delimitation to derive the Rrs from 412 nm to 869 nm. Atmospheric correction was applied to L1B data to derive the Rrs from 412 nm to 869 nm, which are the input for the majority of algorithms available, and in particular to all used in this work. Quality control flags were set in order to mask inaccurate pixels. The Rrs data was processed to L2, using several available chl-a algorithms, and exported to MatLab R2006a in *ascii* format. The second part of data processing was done in the latter software. Data was reprojected to a predefined 1km regular grid using the nearest neighbour method. All negative Rrs or chl-a retrievals were masked. The available bathymetry, with about 30m resolution, was resampled to 1km, using the bilinear method, to allow comparability and cross processing. Using tide simulations, provided independently by the E2K, daily water masks were developed for the sensor acquisition hour and all data was filtered according to it.

In order to investigate the factors affecting the quality of chl-a retrieval in the Tagus estuary, several atmospheric procedures were tested, along with a variety of quality control flags combinations. These processing options influence the Rrs, which precede the chl-a retrieval. Specifically, very high and atypical chl-a values were identified and the processing options leading to better retrievals were assessed. Regarding the information gathered in 3.1.5 and 3.4.8, these probably corresponded to noise. Since no reference, measured or modelled, Rrs were available, the OC3 chl-a algorithm, with standard atmospheric correction and quality flag settings, was defined as the reference data set. For simplicity, it was assumed that the impact of different processing options did not depend on the algorithm but solely on the input Rrs. The OC3 algorithm was chosen due to its simplicity, because it is the default MODIS algorithm and its operational constraints are straightforward. If this evaluation objective was

not achieved, at least the factors which were not responsible for such evident noise and the potential methods to diminish their impact could be identified.

The atmospheric correction and quality control options were evaluated respectively in the sub-sections, 3.5.1 and 3.5.2. Daily processed products were transformed to 16day temporal composites and spatially aggregated to allow the comparison between E2K simulations and remote sensing chl-a retrievals, at a box scale (3.5.3). In a first stage, only boxes 4-13 were used, due to spatial resolution issues. The processing options which rendered improved accuracy were selected for further remote sensing analysis.

3.5.1 - Atmospheric Correction

Optical remote sensing data are affected by the atmosphere and from the direct reflectance of the water surface. These effects can be removed using suitable atmospheric corrections dependent on weather conditions. The choice of the atmospheric procedure is critical to the accurate retrieval of chl-a thru remote sensing techniques (e.g. Hu et al., 2005; Chen et al., 2007; Franz et al., 2006). The SeaDas processing software supports a wide variety of correction procedures and this feature was exploited given its relevance. The atmospheric correction procedures used are only presented briefly due to their complexity and the unavailability of in-situ Rrs data.

The standard atmospheric correction procedure used for global ocean, uses the NIR bands to determine aerosol type and concentration using the water-leaving radiance at 748 and 869nm (Gordon and Wang, 1994; Stumpf, 2003; Franz et al., 2006). In Case 1 waters, a simple iteration scheme can be used to predict the nLw in the NIR, adopting the "black pixel" assumption (Stumpf, 2003). However, in turbid waters, the assumption of negligible photon emergence at NIR wavelengths becomes invalid due to increased scattering and nLw are inaccurate, or impossible to estimate, leading to significant errors in chl-a retrieval (Siegel et al., 2000; Schalles, 2006). Relaxation of this assumption can significantly improve chl-a retrieval in waters with chl-a > 2 μgl^{-1} (Schalles, 2006). Recently, other atmospheric correction procedures have been developed over turbid or highly productive waters (e.g. Ruddick et al., 2000; Wang and Shi, 2005). Moreover, aerosol type and distribution in coastal waters differ greatly from those found in oceanic areas, influencing the accurate estimation of Rrs, thus chl-a (Siegel in http://oceancolor.gsfc.nasa.gov/forum/).

A set of atmospheric procedures was chosen and applied MODIS data of the year 2000 to assess their adequacy in chl-a estimation in the Tagus estuary (Table 16). All procedures are based on the 2-band atmospheric correction scheme proposed by Gordon and Wang (1994) varying humidity and the aerosol model. The MUMM procedure uses the same scheme with an alternative modification for NIR nLw (Franz in http://oceancolor.gsfc.nasa.gov/forum/).

Table 16 - Atmospheric correction procedures tested

Description	Processing Code	Reference
Multi-scattering with 2-band model selection and NIR correction	StandardOC3	Gordon and Wang, 1994; Stumpf, 2003
Multi-scattering with fixed model (Coastal, 70% humidity)	AtmCor1OC3	Gordon and Wang, 1994; Stumpf, 2003
Single Scattering - white Aerosols	AtmCor2OC3	Gordon and Wang, 1994; Stumpf, 2003
Multi-scattering with fixed model (Coastal, 99% humidity)	AtmCor3OC3	Gordon and Wang, 1994; Stumpf, 2003
Multi-scattering with 2-band model selection	AtmCor4OC3	Gordon and Wang, 1994; Stumpf, 2003
Multi Scattering with MUMM correction MUMM NIR calculation	AtmCorMUMM	Ruddick et al., 2000

The focus was set primarily on the magnitude of chl-a retrievals (i.e. errors) and, secondarily, on correlation because this may be mainly driven by algorithm performance. From the six atmospheric correction procedures used, three are clearly inadequate when compared with E2K simulations (Figure 18), with errors above 6 μgl^{-1}, overestimating chl-a over 200 % (Annex VI). Therefore, the *Standard*, *Atmcor1* and *Atmcor4* procedures were removed from further analysis. The remaining methods had similar performance so a finer analysis was necessary.

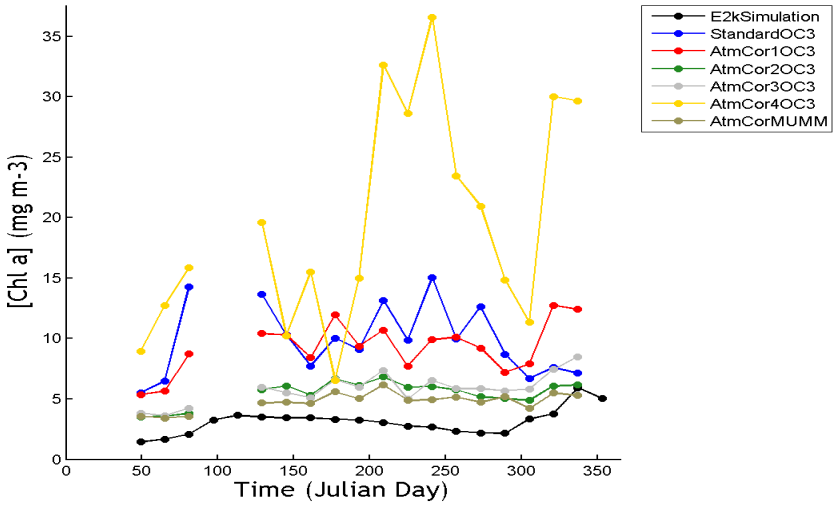

Figure 18 – Atmospheric correction procedure : Time series Box 10 - 2000

The *Atmcor2* and *Atmcor3* had similar error magnitude and temporal correlation for all boxes, and *AtmcorMUMM* exhibited the lowest errors but had slightly lower correlations (Figure 19 & Figure 20). Because the primary focus was set on magnitude and due to reasonable correlation, the MUMM procedure was chosen for the remaining remote sensing estimations.

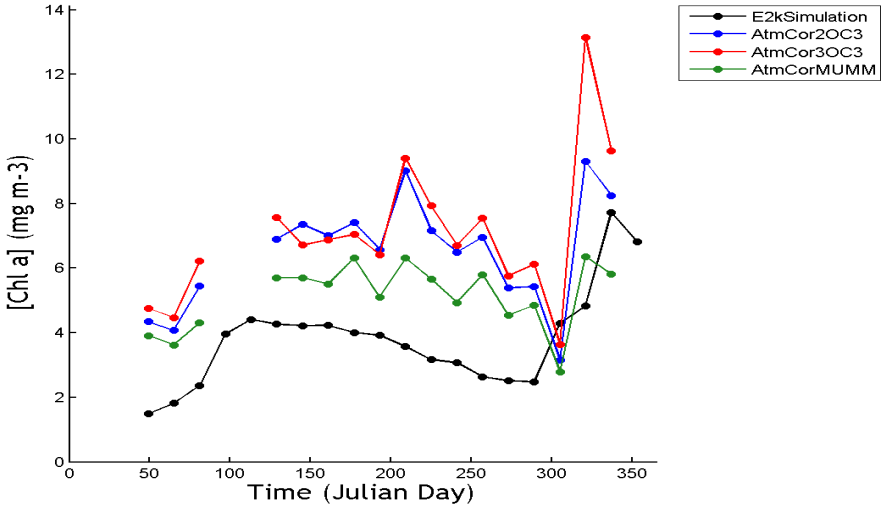

Figure 19 – Atmospheric correction procedure : Time series Box 8 - 2000

Discerning quantitatively the remaining two procedures may be ambiguous because, overall, errors and correlation are almost identical. A thorough analysis was presented in Annex VI. The *Atmcor3* was chosen as the secondary atmospheric correction procedure because, theoretically, the assumption of a coastal profile with 99% of humidity was more probable than the single scattering assumption. Furthermore, the second choice was made because it revealed higher correlation than the MUMM procedure. Both procedures were addressed in the preliminary assessment (see 4.2.1) in order to assess their impact in the chl-a retrieval using all Case 1 algorithms chosen previously.

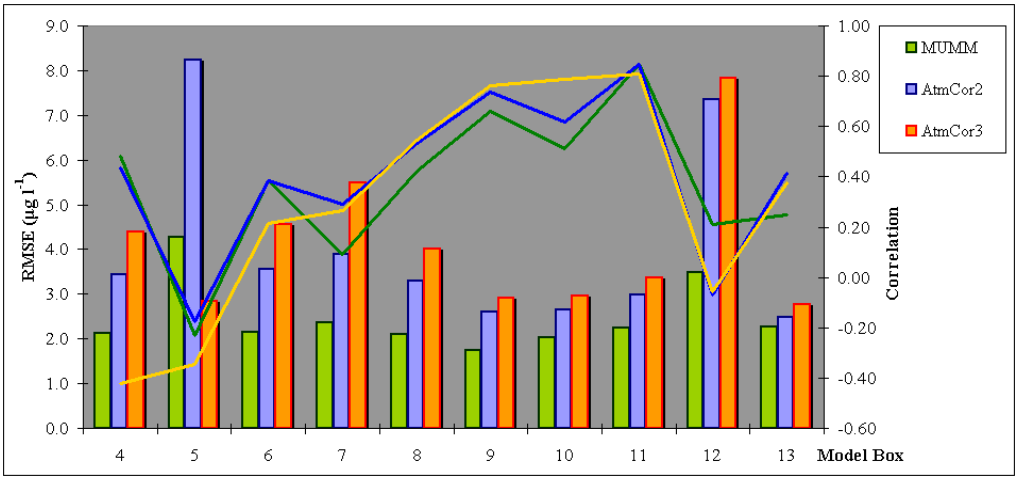

Figure 20 – Correlation and RMSE distribution, per box, using different atmospheric procedures : 2000

3.5.2 - Quality Control

Quality control is common to all MODIS products and applications. Flags are set based on mathematical equations or simple conditions regarding the L1B radiance information. For ocean applications and, specifically for the L2 products, the most relevant quality flags are described in http://oceancolor.gsfc.nasa.gov/VALIDATION/flags.html. Retrieved pixels are masked if a flag is set and this procedure is determined by the user in SeaDas.

For all simulations, high/saturated radiances and clouds/ice were masked. Pixels over shallow waters and over land were not masked in the SeaDas processing stage, because the available masks were coarse and static. To investigate the impact of quality options on the retrieval of chl-a, a set of simulations were performed, with different flag settings (Table 17).

Table 17 - Quality Control flags tested

Code Name	Flags or Restrictions
Standard	Mask Clouds and Saturated radiances
AngleMask	Solar and Sensor zenith angle above 60º and 70º respectively *
Mask Glint	Sun Glint *
Mask Stray	Straylight Contamination *
Mask All	All flags and restrictions set above

* Note that the standard flag masking is applied to all

As mentioned, the SeaDas land mask is static and does not vary according to the tidal height. Daily images were masked according to a land mask developed, in MatLab R2006a environment, using a reprojected 1km bathymetry and tidal simulations. The latter, had a 1 hour temporal resolution and, therefore, an interpolation was performed to match exactly the acquisition hour for a given day. All pixels with less than 1m depth were also masked to avoid errors due to bottom reflection which could significantly affect chl-a retrievals (e.g. Schalles, 2006; Hu et al., 2004; Chen et al., 2007). Gameiro et al., (2007) reported light extinction coefficients (k) between 1.7 and 2.1 m^{-1}. Estimating euphotic depth at 4.6/kpar, the minimum and maximum depths that light reaches were respectively 2.2 and 2.7m. Assuming that the bottom is a lambertian surface and that the down and upwelling paths are the same, the minimum depth at which bottom reflection would be perceived is approximately between 1.1 and 1.4m. Since the bottom is not a lambertian surface the minimum depth used provided, theoretically, a good agreement between simplicity and noise reduction. Higher wavelengths are less sensitive to bottom reflectance than lower wavelengths because of the greatly increased light attenuation by water at red and especially, at NIR region. It is recalled that

Case 1 chl-a algorithms typically use lower wavelengths potentially compromising their performance over shallow waters.

The different simulations regarding the different setting of quality flags are exhibited in Figure 21. The chl-a distribution increased when sun glint was masked, probably due to the elimination of erroneously augmented Rrs values which lead to lower absorption and higher concentrations. Hu and Carder (2002) suggested that this feature, unlike for land applications, should always be removed to correctly obtain the water signal. Therefore, this flag was set for further simulations assuming that sun glint was well identified during the SeaDas processing.

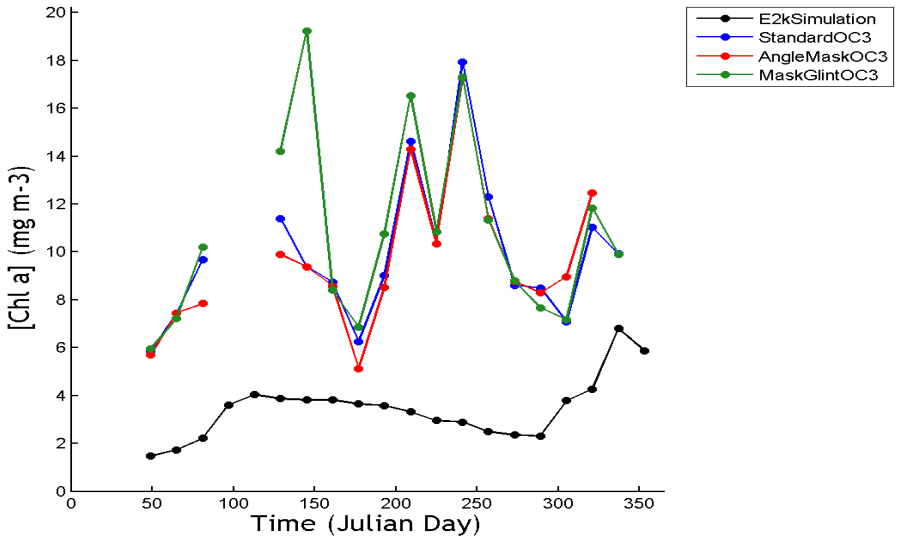

Figure 21 – Quality Flags and Restrictions : Time series for Box 9 – 2000

Masking the viewing angles had low impact in the chl-a estimation and values tended to be slightly lower. It would be expectable that higher solar and/or sensor zenith angles would lead to inaccurate chl-a retrievals due to the sensor field of view. Apparently, this did not occur in the data set used (Figure 22), reinforcing the idea that chl-a retrieval is relatively geometry independent in Case 2 waters (e.g. Wynne et al., 2006). Therefore, no geometry constraints were set in further simulations.

Straylight results from radiance contamination from adjacent pixels which is often near bright sources such as clouds, coastlines or sun glitter. The largest impact is to low Rrs values which can be particularly relevant in highly productive, and thus absorbing, waters. There is no pre-launch procedure for stray light correction for MODIS, so the custom solution is to increase the mask on the edge of possible sources (http://oceancolor.gsfc.nasa.gov/). This resulted in the elimination of almost all pixels within the estuary and, therefore, the *MaskStray* time series was not shown. The *MaskAll* version (not shown) had, thus, even lesser pixels. Several

atypical and high chl-a values were detected in near shore pixels. A simple procedure was applied, in MatLab R2006a, considering stray light from land. A 7x7 pixel window was set around each pixel adjacent to the shore defined by the daily tidal land mask. Any pixel outside the threshold defined by the average ± two times the standard deviation was excluded, and visual inspection indicated improvements although some high chl-a values were still present (Annex VII). The largest influence of stray light contamination probably occured in box 12 due to its narrowness and the topography of the adjacent land.

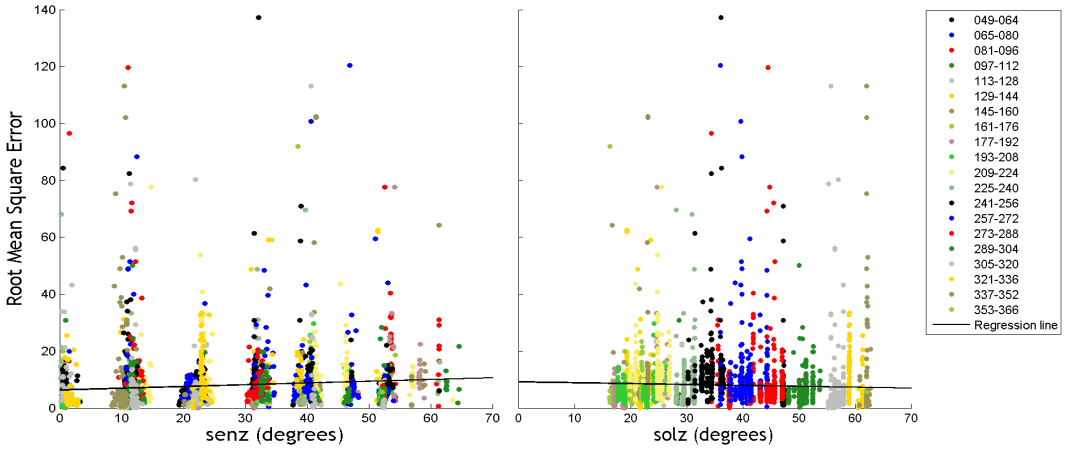

Figure 22 – Geometry (solar and sensor zenith angle) *vs.* Error : 2000
Note that, the legend indicates the compositing period i.e. the initial and final Julian day
Senz : Sensor zenith angle ; Solz : solar zenith angle

Annex VII thoroughly describes all the quality control analysis performed. In sum, saturated radiances, clouds and pixels with sun glint were removed at the top of the processing chain and a simple straylight removal procedure was used along with the daily tidal land masking.

3.5.3 - Data Temporal and Spatial Compositing

Cloud cover in optical satellite data acquisition seriously affects the usefulness of these data for surface water quality monitoring (e.g. Lavery et al., 1993 in Zhang et al., 2002b). Therefore, a time composite procedure was needed in order to enhance the geographical coverage, accumulating the information which was available during the compositing period. Data was composited assigning to a pixel the chl-a value closer to the average in the 16 day compositing period (Pinty et al., 2002). This temporal resolution was considered to be a good compromise solution between the E2K month to seasonal scale and the daily MODIS data. It should be noted that, the benefit of using composites is both spatial aggregation, in which clouds are a common problem, and temporal smoothing.

The best processing options identified above, which theoretically improved the accuracy of reflectance retrievals, were used in this section. Three temporal compositing options were tested independently. Firstly, during compositing, outliers for each pixel were removed using thresholds of 1 and 2 standard deviations. Secondly, daily data was filtered according to tidal state, both ebb/flood and high/low tide. Thirdly, chl-a values were crossed with the number of files in a composite in order to understand if the anomalously high composite values resulted from image scarcity within a given compositing period. Removing outliers and filtering files according to their tidal height and state had no apparent effect on accuracy (Annex VIII). Atypical high values were apparently related with the lower number of files in the compositing period (Figure 23). However, removing composites with few daily files would severely limit the number of samples in the dataset and, therefore, no filtering was applied. Moreover, from visual inspection of daily MODIS data (not shown), the low number of files also seemed to be related with correspondent low spatial coverage. The latter hypothesis was not investigated, but may be related to stray light from clouds. In sum, no temporal compositing restrictions were applied.

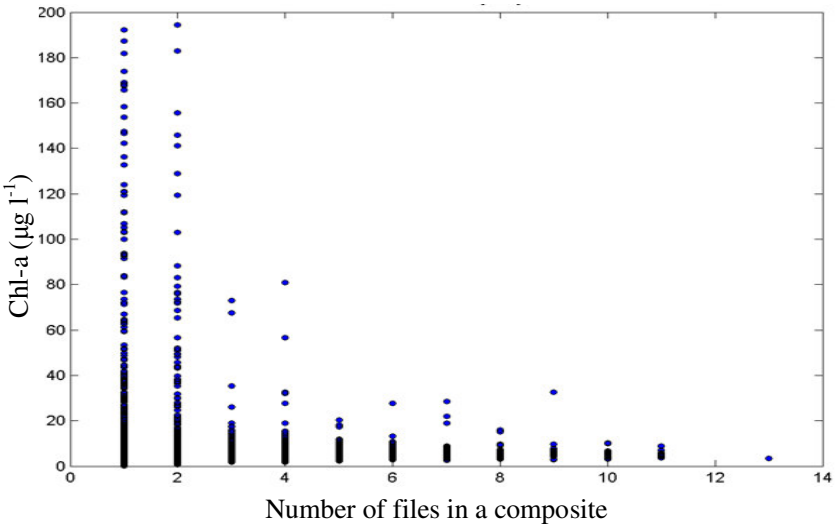

Figure 23 - Number of files in a composite *vs.* [chl-a] : 2000

Data was spatially aggregated according to the model boxes allowing comparison with E2K chl-a simulations. The main issue in this step concerned the mathematical method used for spatial aggregation and understanding the chl-a distribution within each box was, therefore, extremely important. For each model box, histograms were made and average chl-a, percentiles 10 and 90, were plotted (Figure 24). The histograms were made for each box for every composite period. For the majority of the periods, the chl-a distribution was normal, although there were some exceptions (Annex VIII). Some of the distributions were shifted towards lower values. Some values were exceptionally high and, as mentioned, were

considered as outliers. For instance, in the compositing period 241-256, there were low frequency values of about 40µg l^{-1}, which significantly increased the average. In fact, the average was higher than the percentile 90. A maximum threshold was defined as the percentile 90 of all pixels within each box. Every pixel above it was eliminated and the average value, computed without outliers, was assigned to a given model box. Values below the percentile 10 were not removed because there was no information suggesting they were outliers.

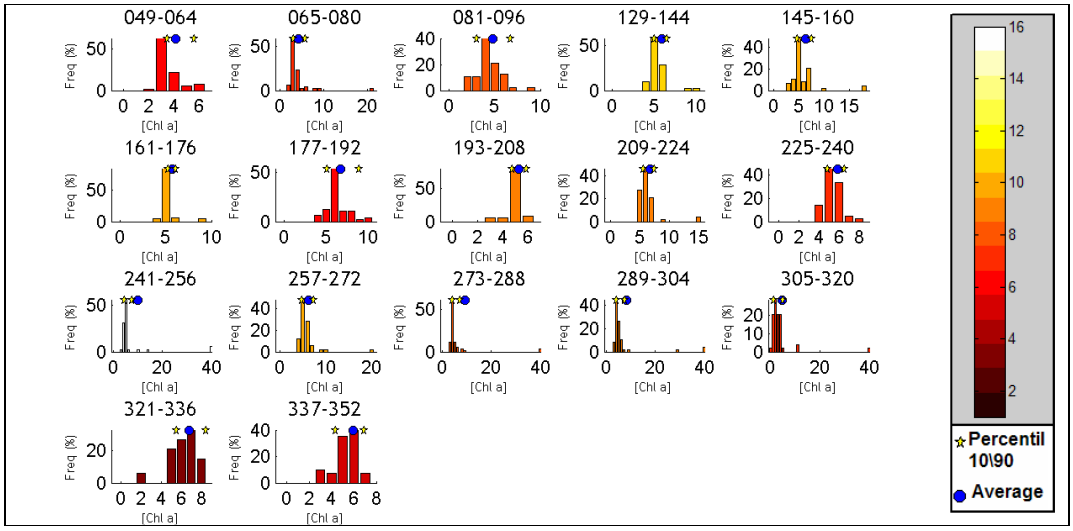

Figure 24 – Spatial histograms : Box 8 – 2000

The histograms have the value frequency (%) in y axis and chl-a concentration in the x axis
The scale bar represents the number of MODIS daily images in a composite

Figure 24 suggested that a high number of files in a composite did not smooth box distributions up to the point where outliers have no significant effect on the box average. For the remaining boxes, the temporal coverage had no apparent effect on the shape of the distribution (Annex VIII). The referred Annex showed that box 12, both for 2000 and 2001, had highly irregular distributions, as in box 4 and 5 (not shown). This was probably due to the low box surface area, thus high sensitivity to errors, as mentioned, and therefore, only boxes between 6 and 13 were used in further analyses. To maintain box spatial representativeness, when its pixel coverage was less than 20%, a single box value was not assigned.

3.6 - Remote Sensing Regional Calibration

The calibration of simple algorithms lead to two distinct assessments. Firstly, the calibration of regional Case 1 and Case 2 algorithms and the preliminary assessment of existing global Case 1 algorithms (see 4.2), were both done using the "best" processing options. Secondly, all algorithms were assessed using an independent data set (see 4.3). This choice was driven by the need of using a validated calibration dataset (2000) and an independent validation data set (2002) for accuracy related inferences. This section is divided in the regional calibration of the OC3 Case 1 algorithm and some Case 2 algorithms, proposed in literature.

Calibration is typically done by establishing mathematical relations between Rrs values, usually thru band ratios, and chl-a measurements. In-situ samples coincident with MODIS imagery occured only in the year 2002. In 2001, no sampled data was available and for 2000, only 6 samples were coincident with the MODIS Terra operation, because, despite being launched in 1999, data was only available since late February 2000. These six samples corresponded to the model boxes 4 and 12 which, as mentioned, had low potential for remote sensing estimation. In 2002 there was only one sample in box 11. Therefore, sampled chl-a was not used. It should be noted that there is a MODIS data gap in early spring of 2000, coincident with the simulated chl-a peak, which limited both the calibration and assessment of remote sensing chl-a when it was expected to be high.

The procedure already applied to chl-a processing (see 3.5) was also applied to Rrs, producing 16day box reflectances, between 412 and 748nm. The only difference was that the spatial aggregation was made without removing outliers because there was no prior and present information regarding Rrs in the Tagus estuary. Only the E2K chl-a simulations, for the year 2000, were used. Empirical relations were established between the MODIS Rrs and E2k chl-a simulations. It should be underlined that each box value was used as a "chl-a sample" because E2K simulations were representative at a box scale. Using every box pixel for calibration would resulted in a noisy procedure due to scale ambiguity between Rrs and simulated chl-a. Furthermore, in this calibration effort it was assumed vertical optical homogeneity within each model box.

Due to the, somewhat, stringent processing options, the coarse resolution of MODIS data, and the morphology of both, model boxes and the Tagus estuary, boxes 6 and 12 were removed from regional calibration. As mentioned, due to their low surface area the upstream boxes (1-

5), using 1km data, have low potential for remote sensing. Approximately 70% of Box 6 corresponds to intertidal areas (see Table 3) and therefore, it had few valid composites per year and was probably highly sensitive to bottom reflectance contamination. Box 12 was very narrow, had low surface area and was probably highly sensitive to straylight from adjacent land. The removal of these boxes improved the fitting of all regionally derived empirical relationships. The number of total "samples", for the year 2000, was reduced from 114 to 103. However, boxes 6 and 12 were included in the spectral signatures analysis, when relevant.

The OC3 empirical algorithm was regionally tuned by adjusting its coefficients to match chl-a E2K box simulations. As mentioned, its original coefficients were derived using a global Case 1 data set. Equation 4 was log scaled to determine the polynomial coefficients where the *x* variable was the R3M band ratio (Figure 25). The algorithm code was implemented in MatLab R2006a to produce 16day chl-a maps of the OC3 tuned Case 1 algorithm. The semi-analytical algorithms used in this work, could also be regionally tuned, but due to their complexity, code accessibility, and the need for in-situ Rrs and IOPs, this procedure was not performed.

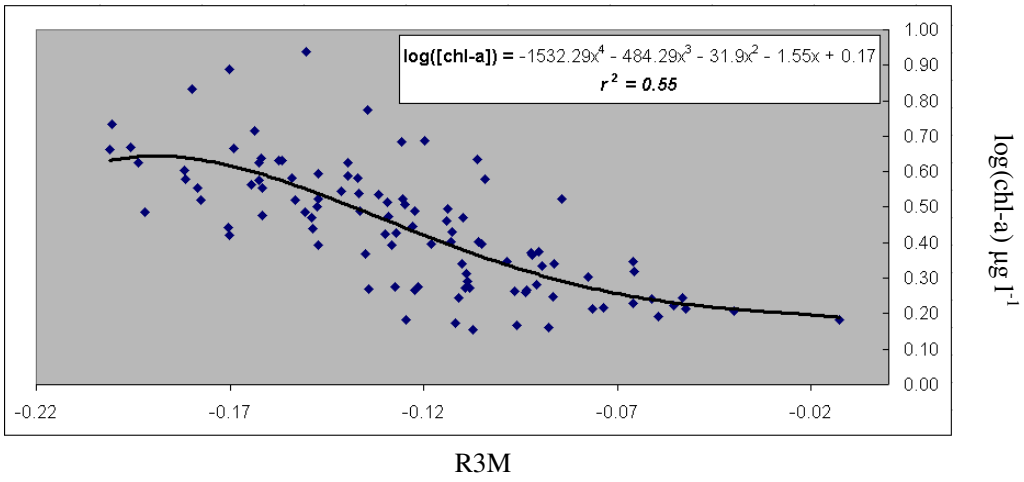

Figure 25 – OC3 regional calibration (2000)

The OC3 fitted equation showed a fair agreement, r^2=0.55 (N=103). A linear relationship produced the same agreement. It was evident that with the increase in concentration, dispersion also increased, indicating that higher chl-a was less accurately retrieved. The majority of high chl-a values were simulated in the winter (Annex IX) and, for reasons mentioned in 3.4.8 (and 4.1), the confidence in them was lower that in the remaining seasons. Therefore, the relationship could be more accurate than it apparently was. Furthermore, there was also significant dispersion around average and low chl-a values, particularly when the R3M tended to lower values.

The regional calibration of Case 2 algorithms was based on several band ratios, proposed in literature (Gitelson et al., 2007; Tzortziou et al., 2007; Schalles, 2006). These are based on three main spectral features: the green peak, the upper red and the NIR reflectances. The latter two regions are, theoretically, used to discriminate the chl-a specific absorption maximum in the red, and the upper red/NIR peak reflectance, usually associated with chl-a fluorescence and cell scattering. MODIS has three bands in these regions with centre wavelengths in 667, 678 and 748 nm. Therefore, reproducing these features is constrained by spectral resolution, and the number and position of the bands, which greatly affect the operational abilities to detect chl-a signals in different optical regimes. Furthermore, this is a particularly relevant limitation because it is known that the Rrs peak shifts from the upper red to NIR, around 700nm, with increasing chl-a due to increased cell scattering (Schalles, 2006).

A spectral signature analysis was performed plotting the 16day box Rrs, over the whole spectrum, for each compositing period, in order to understand the key optical features that could be exploited in the Tagus estuary (Figure 26). It should be noted that the lines result from a linear interpolation of the Rrs values for the discrete MODIS bands. The spectral signatures were highly variable over the whole year (Annex IX). There was a clear similarity with the reflectance spectra of Apalachicola bay and Duplin river presented in Figure 3.

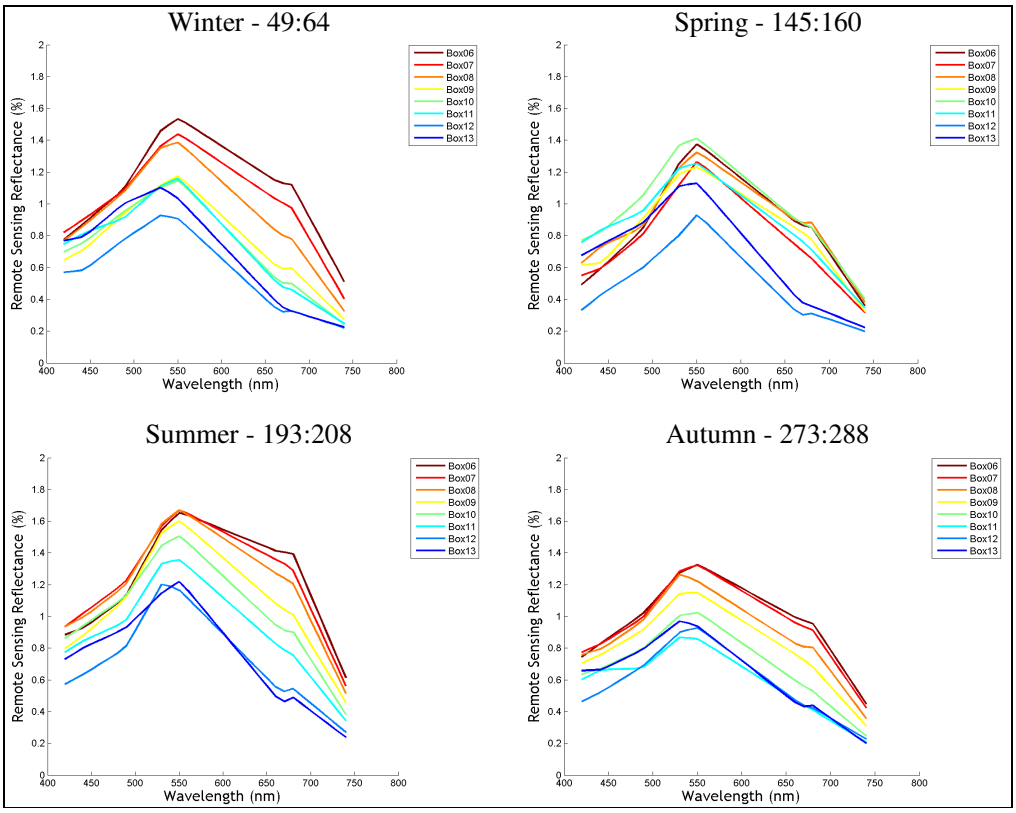

Figure 26 - Spectral Signatures for all boxes per season : 2000

Particularly for the former, the chl-a (9.2 µg l^{-1}) and SPM (48.5 mgl^{-1}) concentrations resembled those typically found in the Tagus estuary (see 3.1.3 and 3.1.5). This similarity suggested that the methodology used was robust and could be used in future works. According to Schalles (2006), the Ashepoo river had similar chl-a and SPM concentrations but with increased CDOM absorption (about $7m^{-1}$ against 1 m^{-1} in the former) lowering Rrs and smoothening the green peak to the point that it was no longer discernable. There was no information regarding CDOM absorption in the Tagus estuary, but, the spectral signature suggested, by comparison, that there was generally low CDOM absorption. The green peak was prominent and discernable in the majority of the compositing periods, which also suggested low CDOM absorption. The reflectance magnitude, over the whole spectrum and, particularly, in the green region, often increased with distance from the ocean suggesting spatial differentiation. This region, along with the NIR reflectance which, as mentioned, is not negligible in turbid waters, could potentially be used to establish SPM and Rrs relations (Schalles, 2006).

The upper red "shoulder" was discernable in some occasions, for instance, in box 6 in the winter and summer. It, however, also presented high variability and did not necessarily indicate high chl-a concentrations. This feature could potentially differentiate chl-a concentrations, for instance in the summer for boxes 6, 7 and 8 where the green Rrs was similar but the red "shoulder" was different, particularly evident in box 6 where higher chl-a was expected. From the beginning of autumn 2000 to the beginning of winter 2001, reflectances increased in about 2%. By the end of the year 2000, the red peak increased significantly, sometimes higher than the green peak, and returned to typical values, similar to the 2000 winter, in late winter 2001 (Figure 27).

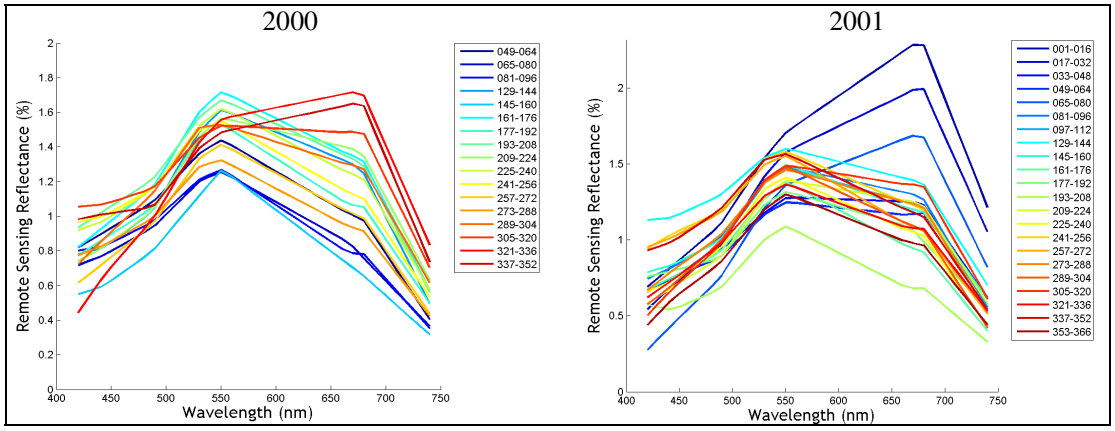

Figure 27 - Spectral Signatures over time for box 7

The legend and associated line colours indicate the composites Julian day range

This feature was more evident in the mid estuary boxes. During this peak shift, the green and red regions had, respectively, low and high variability suggesting that the increase in the latter was probably not due to an increase in overall scattering but due to cell scattering. Therefore, the winter chl-a peak could be in fact correctly simulated and was discussed later on. However, CDOM could result from run off which could be constraining the green peak increase.

Several Case 2 empirical relations, using different band ratios, were implemented using different approaches. Firstly, the fluorescence line height (FLH) was computed according to Letelier and Abbot (1996) formulations which rely on the 667, 678 and 748nm MODIS bands. One of these wavelengths was centred on the chl-a fluorescence maximum (approximately 683 nm) and the remaining were used to form a baseline below the fluorescence peak (Equation 15). The authors indicated that there was a strong agreement between the magnitude of the FLH and chl-a, although they could vary independently. All empirical relations developed hereafter had the condition that FLH>0, which eliminated 3 "samples".

$$FLH = Rrs_{678} - Rrs_{748} + \left(Rrs_{667} - Rrs_{748}\right)\left[\frac{(748-678)}{(748-667)}\right] \qquad \textbf{Equation 15}$$

Secondly, other two ratios were used, the Rrs_{748}/Rrs_{678}, proposed by Gitelson et al. (2007) and, the Rrs_{678}/Rrs_{551}, proposed by Tzortziou et al. (2007). The key features that they exploited were addressed previously (see 2.2.2). Thirdly, an altered version of the latter was proposed which added the NIR as follows: $R_{678}/(R_{551}+R_{748})$. Scattering is discernible in the NIR region and high CDOM absorption can smooth the prominent green scattering peak (Schalles, 2006). Therefore, this proposed alteration could, theoretically, provide a more robust representation of the non-cell scattering and isolate the cell scattering signal in the red region, thus chl-a. Several combinations of these features were derived thru function fitting or by multiple regression, and Table 18 showed the most relevant. The *y* variable was the retrieved chl-a.

The calibration plots (Annex IX) showed that dispersion was high and for the higher values the fitted functions were inaccurate, mainly because the majority of high values occured in the winter although some occured in the summer. Probably due to issues concerning the centre wavelength in the upper red/NIR, the band ratio proposed by Gitelson et al. (2007) had very low agreement (r^2 = 0.21). It, thus, presented high variability and dispersion, with even lower

agreement that the general Case 1 relations tested (r^2 = 0.39 and r^2 = 0.52). The low blue region had low spatial and temporal variability, probably due to pigment and CDOM overlapped absorption, being probably the reason for the better performance using the upper blue region (near 488nm).

Table 18 – Description and performance of regionally calibrated algorithms

Equation	Description	RMSE ($\mu g\ l^{-1}$)	r^2
$y = 0.937\ (R_{748}/R_{678})^{1.156}$	Adapted from Gitelson et al. 2007	1.21	0.21
$y = 4.857(R_{678}/R_{551})^2 - 0.083(R_{678}/R_{551}) + 1.031$	Adapted from Tzortziou et al. 2007	0.75	0.68
$y = 1.194\ (R_{443}/R_{551})^{-1.825}$	General Case 1 Relation	1.51	0. 39
$y = 1.054\ (R_{488}/R_{551})^{-3.382}$	General Case 1 Relation	1.02	0.52
$y = 1432882.186\ FLH^2 + 143.988\ FLH + 2.056$	Adapted from Letelier & Abbott, 1996	0.85	0.59
$y = 0.976 + 486.940\ FLH + 4.0835\ (R_{678}/R_{551})^2$	Combined Letelier & Abbott, 1996 ; Tzortziou et al. 2007	0.74	0.69
$y = -0.730 + 570.740\ FLH + 5.370\ (R_{678}/R_{551})$	Combined Letelier & Abbott, 1996 ; Tzortziou et al. 2007	0.77	0.67
$y = 20.493(R_{678}/R_{551}+R_{748})^2 - 11.544\ (R_{678}/R_{551}+R_{748}) + 3.4010$	Adapted from Tzortziou et al. 2007; NIR band added	0.70	0.71
$y = 10^{0.175-1.555R3M-31.874R3M^2-484.295R3M^3-1532.289\text{x}R3M^4}$	Tuned OC3 (O'Reilly et al., 2000)	0.99	0.55

The temporal shift in the red and green peaks from autumn of 2000 up to late winter of 2001, described previously, was probably the reason for the reasonable agreement (r^2 = 0.68) of the band ratio proposed by Tzortziou et al. (2007). This seemed to be a key optical feature in the Tagus estuary. The FLH approach, by itself, had lower agreement (r^2 = 0.59), which was increased when combined with the latter (r^2 = 0.69 and r^2 = 0.67). However, no significant improvement was accomplished when compared with the R_{678}/R_{551} ratio solely. The addition of the scattering contribution in the NIR region, however, provided a more robust empirical relationship and it was in fact the best agreement retrieved (r^2 = 0.71) (Figure 28). The accuracy assessment of the remote sensing retrievals, using the regionally tuned algorithms, was made in 4.2.1.

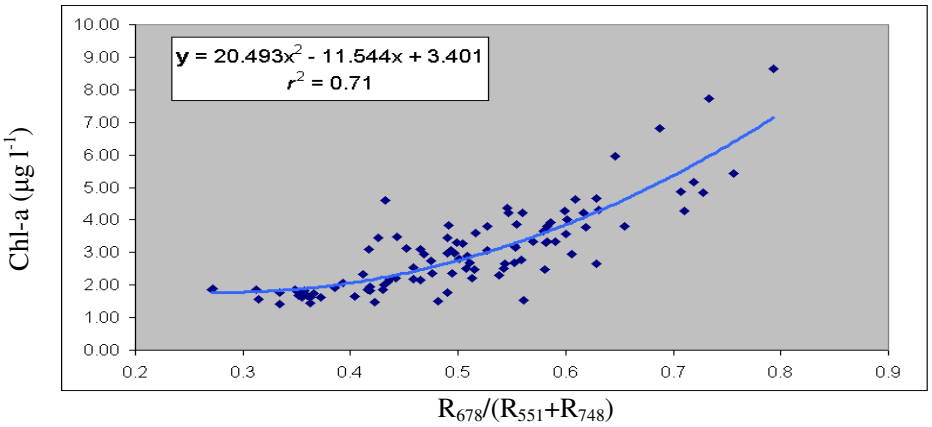

Figure 28 – Calibration plot using the ratio $R_{678}/(R_{551}+R_{748})$: 2000

The main methodological steps performed for the assessment of chl-a remote sensing products in the Tagus estuary are exhibited in Figure 29.

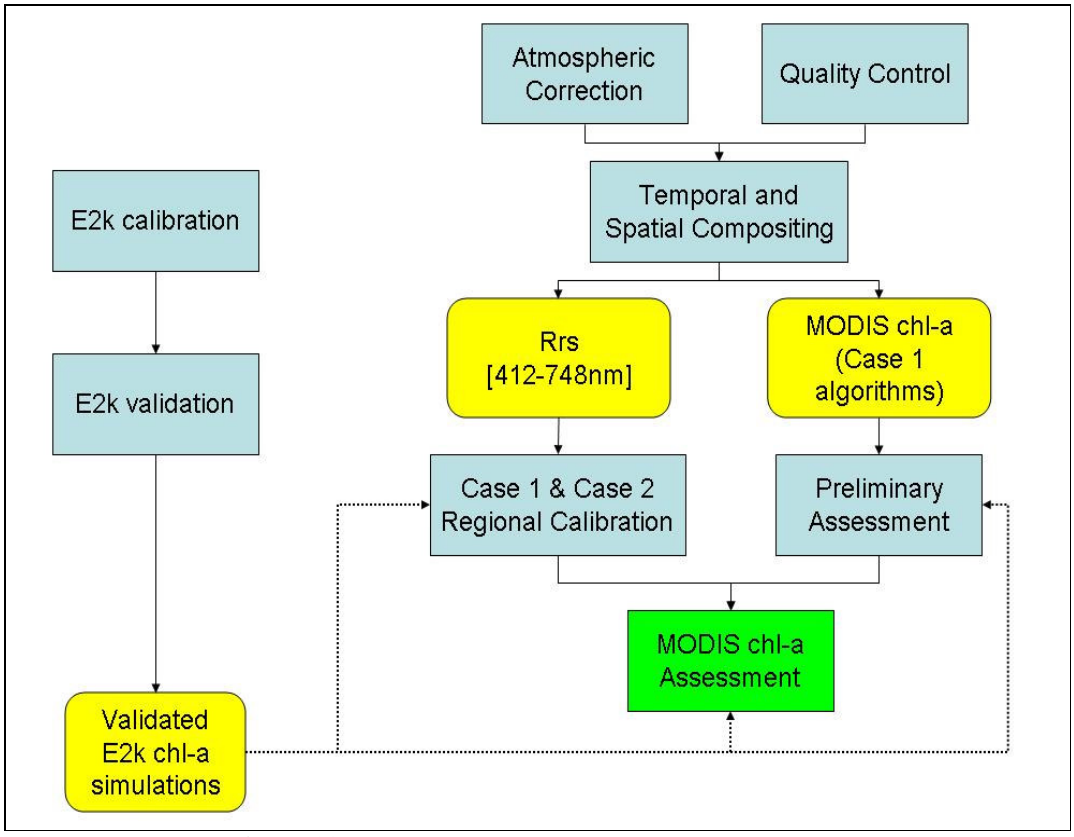

Figure 29 - Main methodological steps and connections

4. Results and Discussion

4.1 - Ecological Model Validation

The evaluation of the model accuracy was performed comparing simulations with sampled chl-a, available in five distinct dates, in the years 2000 and 2002, interspersed between boxes 4, 11 and 12. The year 2001 was also evaluated mainly because of the extreme winter chl-a peak simulated. Brief insights on the behaviour of nutrients and SPM were provided, for relevance, and model improvements were addressed later on (see chapter 5).

Model validation was addressed carefully due to the scarcity of data. The model presented reasonable accuracy, with a 57% or 8.0 µg chl-a l^{-1} error (Table 19).

Table 19 - Phytoplankton object performance statistics: box by box and ecosystem scale

	Box 4	Box 11	Box 12	Global
Matches	5	1	4	**10**
RMSE	10.9	0.6	2.8	**8.0**
MAE (%)	76%	43%	37%	**57%**
r	0.28	-	0.63	**0.37**

The correlation was very low (r = 0.37; N=10) but the number of matches was too scarce to make quantitative inferences. However, it was clear that the blooms that occured in the summer, both in box 4 and 12, were not reproduced (Figure 30 and Figure 31) leading to the high RMSE.

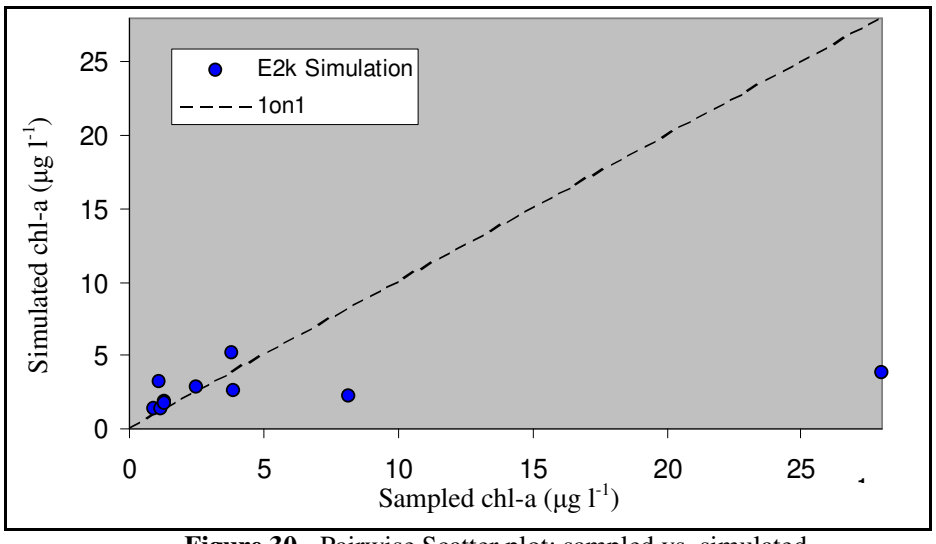

Figure 30 - Pairwise Scatter plot: sampled vs. simulated

In the remaining seasons, the chl-a simulations were in good agreement with the sampled data. The underestimation could be related with SPM overestimation, in about 100%, limiting

light availability, thus production. However, compared with the calibration (see 3.4.8), the Zmix:Zeuph ratio was simulated in a similar fashion suggesting that light availability is well reproduced, in an average sense. Ammonia seemed to be in agreement with sampled values. However, in box 4, samples were highly variable (from 6 to 76 µmol N l^{-1}), being over and underestimated. Nitrate concentrations were consistently underestimated (Annex V).

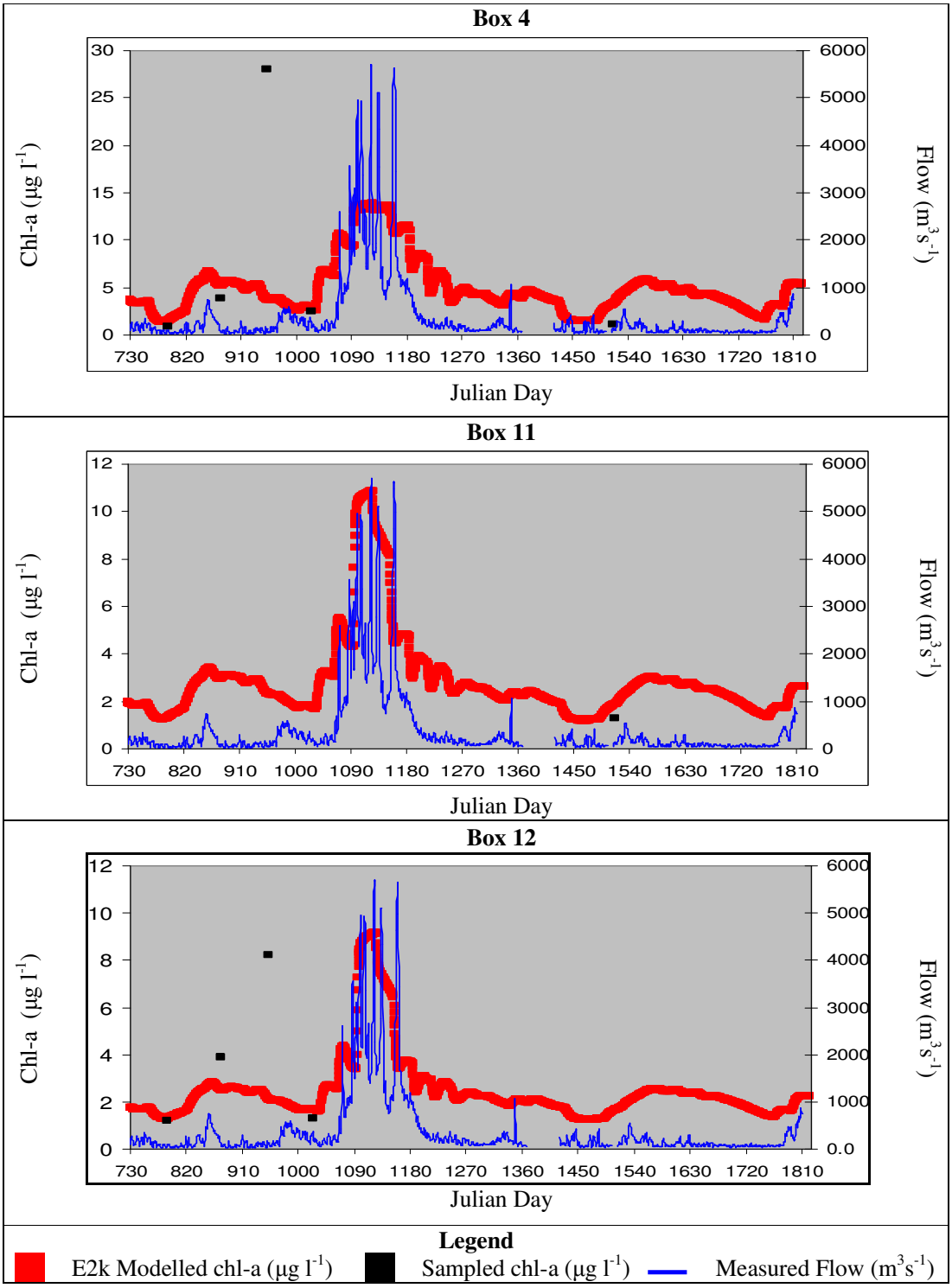

Figure 31 – E2k chl-a validation, time series box by box: sampled *vs.* modelled

Annual average chl-a for the whole estuary was in agreement with reported values by Gameiro et al. (2007) and Ferreira (2000). The annual dynamics suggested a different bloom distribution, while in the calibration years peaks appeared to be unimodal, in the validation years, data indicated a moderate spring peak followed by a higher summer peak. Sampled data was scarce and, therefore, the comparison of model estimations with values reported in literature was crucial. Comparing with the 7 year study performed by Gameiro et al. (2004), in 2000, the up and mid estuary boxes 3, 6 and 7 had bimodal blooms in late spring and late summer. Box 8 was an exception has the higher values occured only in the latter period. For these boxes, simulated chl-a was slightly underestimated, with the exception of the summer increase/bloom, which simply was not simulated.

The 2000 and 2002 winters were in good agreement with reported values (Gameiro, et al. 2004 & 2007). In 2002, in box 3 and 6 there was a spring increase, which was simulated, and chl-a values were slightly underestimated (about 1µg chl-a l^{-1}) throughout the year. The summer bloom of about 20µg chl-a l^{-1}, like in 2000, was not simulated. In the Northern Channel, the spring bloom was simulated, but it was about half the one reported by Gameiro et al. (2007). Chl-a values were significantly underestimated in spring and summer months. In box 7 and 8 a bloom occured in late spring, with a slight increase in the summer. The model simulated the former but not the latter, concomitant with was mentioned above. Seasonally, the comparison with Gameiro et al. (2007) is expressed in Table 20.

Table 20 - Comparison of simulated chl-a with Gameiro et al. 2007 (adapted)

	Gameiro et al. 2007	**2000**	**2001**	**2002**	**2000-2002**
Winter	1.4 (1.7)	1.8	11.3	1.8	5.0
Spring	4.5 (4.1)	2.0	3.4	1.7	2.4
Summer	8.0 (4.8)	1.7	1.6	1.6	1.6
Autumn	2.4 (1.7)	3.7	1.9	2.2	2.6

The values in parentheses indicate the standard deviation

The 2001 simulations were addressed with caution in the following sections because no quantitative evaluation was made. It was clear that the extreme modelled flow in 2001 had a large impact in simulated chl-a, driven by riverine import rather than by internal production. As a consequence, the simulated chl-a annual distribution departed from typical dynamics and there was no clear spring or summer bloom. Gameiro et al. (2007) reported data for 2001 with typical dynamics exhibiting bi-modal blooms in the up and mid estuary. According to Brogueira and Cabeçadas (2006), as mentioned, after extreme winter flows the upstream freshwater influenced region extends downstream limiting the marine influenced area.

However, according to data published by the same author, current simulations significantly overestimated chl-a values (over 6 μg l^{-1}), in the 2001 winter. One particular feature was evident, in box 7/8 reported concentrations were about 4 μg l^{-1} for chl-a and 11 μg l^{-1} for phaeopigments. The latter, were usually associated with the death of phytoplankton cells, which most likely occurred after such an extreme flow as the one modelled in 2001. This feature could relevant in the next sections because phaeopigment concentrations have been retrieved in the past, using remote sensing techniques (e.g. Esaias et al., 1998).

The reasons behind the underestimation of the chl-a peaks could be due to small scale phenomena which were not reproduced by the model, due to its average nature and, in particular, due to the large scale transport object used. The latter object could also be responsible for not simulating accurately the spatial chl-a gradient, with upstream underestimation and downstream slight overestimation.

In 2000, flow data showed a slight increase in late summer, coincident with the chl-a increase. This increase, along with the consistent Si limitation in the calibration and validation years, could explain why the model was not simulating the late summer blooms. It is recalled that, Si is mainly introduced by river flow and diatoms, which are predominant in the upstream regions require Si to grow. The Redfield ratio, for both 2000 and 2000, also indicated a P limitation, which was not considered in the phytoplankton growth. Nitrogen was the only nutrient limiting growth, being clearly underestimated, concerning nitrate, and the ammonia variability was not reproduced. Nutrients were probably one of the main reasons for the consistent chl-a underestimation.

In sum, the model did not simulate the summer blooms. It underestimated chl-a concentration in the spring and summer. In the winter and autumn, the low chl-a concentrations were fairly well simulated. Upstream boxes were underestimated and downstream boxes were slightly overestimated. The suitability for the intended use was limited, regarding the comparison made with data published by Gameiro et al. (2004 & 2007) and Brogueira and Cabeçadas (2006). Therefore, E2K simulations were addressed with caution in the following sections.

4.2 - Remote Sensing Preliminary Assessment

The preliminary assessment aimed at identifying the error and correlation magnitudes, and the potentialities and limitations of the remote sensing algorithms in retrieving chl-a concentration. The assessment was addressed spatially, at an ecosystem scale, and temporally, at a month to seasonal scale, comparing the E2K simulations with the MODIS chl-a products. The focus was set on the year 2000 because the 2001 data set was not quantitatively assessed and had an atypical, flow driven, chl-a peak in the winter (see 4.1). The existing Case 1 products, available in the SeaDas software, were compared with the E2K 16day box simulated chl-a in 4.2.1. The regionally calibrated Case 2 products were compared in 4.2.2. Included in this section, was the regionally tuned OC3 algorithm assessment, although it is based on Case 1 relationships. All products mentioned were assessed using an independent data set (2002) in chapter 4.3.

4.2.1 - Performance of Case 1 Algorithms (2000)

In broad terms, all algorithms seemed to increase the retrieved chl-a towards the spring, maintaining relatively high concentrations up to the end of the summer. During this period retrievals were highly variable, but in average sense, tended do decrease until autumn, achieving a generalized minimum. The atypical E2K autumn chl-a increase, discussed previously, was probably due to an artefact driven by extreme river flow. However, in most cases, the Case 1 algorithms retrieved a winter increase varying only the occurrence timing. For instance, the OC3 tended to start the increase before the Carder algorithm (Figure 32). Overall, the algorithms seemed to reproduce reasonably well the chl-a seasonal dynamics.

The OC3 and Carder algorithms had very similar temporal behaviours, because the latter used, for the majority of the compositing periods, the empirical form, which is similar to the former (Figure 32; Figure 33). Both consistently overestimated simulated chl-a in about 70-80%, or about 2.0 μg chl-a l^{-1} (Figure 34). The correlation was, in spatially averaged terms, about 0.50 with a maximum of about 0.80 in box 11 and a minimum in box 12 (discussed latter). The Carder algorithm had a slight better performance, concerning both error magnitude (-6% and -0.1 μg chl-a l^{-1}) and correlation (+0.05). Good correlations in box 10 and 11 occured ($r \geq 0.80$). Since only the OC3 algorithm was regionally calibrated it was expected that error magnitude decreased maintaining correlation (see 4.2.2).

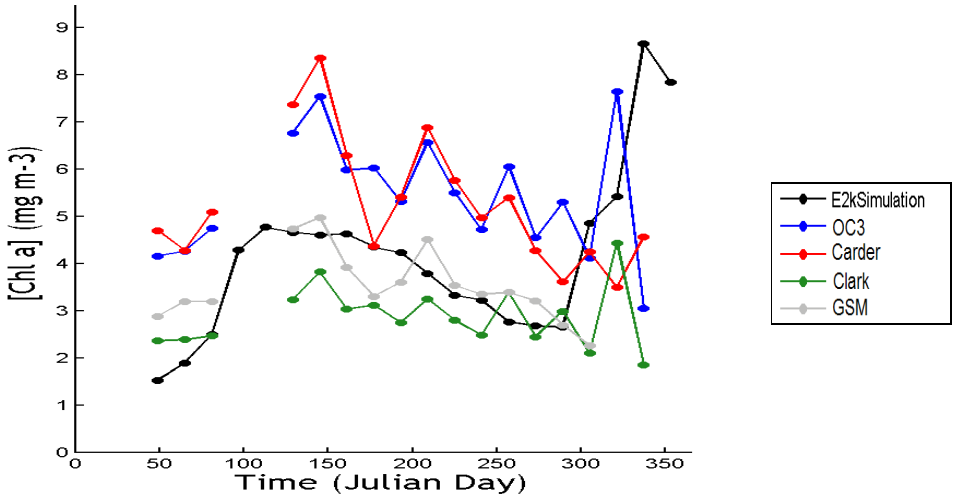

Figure 32 – Case 1 algorithms performance: time series for box 7 - 2000

The GSM algorithm exhibited correlation which ranged from $r < 0$, in the mid estuary boxes 6 and 7, to $r = 0.62$ in the estuary mouth, in box 13, showing an accuracy gradient which decreased with the distance to the ocean. Considering all boxes, average correlation was low, about r=0.34, due to the negative correlation in boxes 6 and 7. The magnitude of chl-a retrievals was similar to those simulated, with an average RMSE for all boxes of about 1.4 µg chl-a l^{-1} or about 30%, both under and over estimating. The distribution along the year increased from winter to spring, peaking despite the data gap, and decreased towards the summer. In the summer, a distinct peak above 4 µg chl-a l^{-1} occured, about 1 month earlier than the peak reported by Gameiro et al., (2007) for sampling sites near boxes 7 and 8. The relatively low correlation could be deceiving and also attributed to this feature. Following the peak, the GSM retrievals decreased followed by a winter data gap due to negative chl-a retrievals.

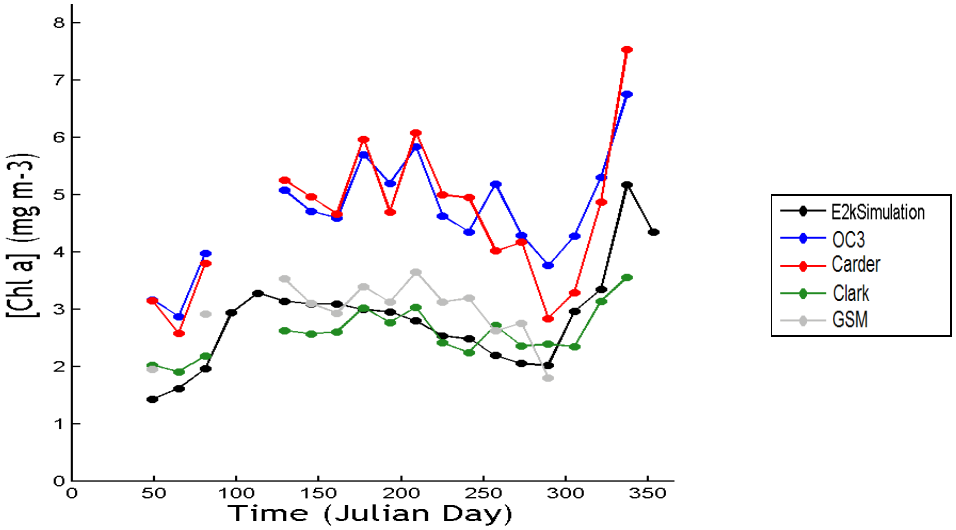

Figure 33 – Case 1 algorithms performance: time series for box 11 - 2000

In fact, the GSM algorithm was particularly unstable because it often retrieved negative chl-a values and punctually retrieved very high anomalous chl-a (not shown). This limited data availability because both were masked at the top of the processing chain. One particular spatial feature refers to the fact that this algorithm had the highest correlation and lowest errors in box 12, being the only algorithm which increased its accuracy in the downstream estuary (Figure 34).

The Clark algorithm had better correlations than GSM, particularly for boxes 10 and 11, increasing retrieved chl-a towards the winter and peaking slightly in late summer. However, this algorithm seemed to have less ability do reproduce the temporal dynamics and, despite the data gap, seemed unable to reproduce the first chl-a peak in spring. In comparison with GSM, the latter seemed to reproduce better the E2K spring bloom. Despite this, the Clark algorithm had the higher accuracy between box 9 and 11 and although his behaviour was smooth and flattened, there was a pronounced peak in box 12 in autumn (see Annex X). Note that, the Clark algoritm had a temporal distribution very similar to the OC3 algorithm but with different magnitudes, since the latter retrieved chl-a two times higher. Both are empirical polynomials which use the 443, 488 and 551nm bands. The difference relies on the fact that the Clark algorithm uses the three bands and the OC3 uses only two bands, depending on the highest band ratio (see 2.2.3).

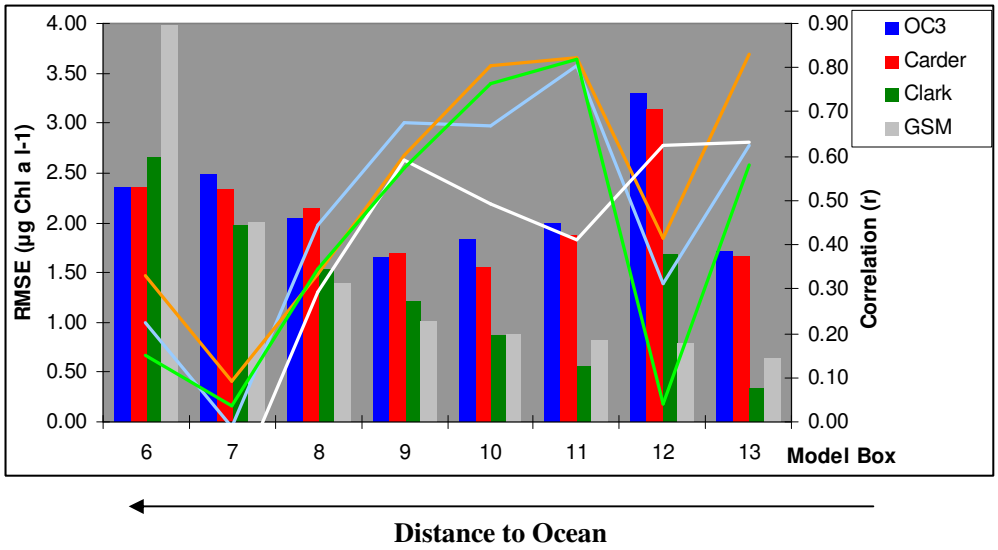

Figure 34 – Case 1 algorithms performance per box : 2000
Bars indicate RMSE and lines the correlation (*r*)

For all algorithms some spatial features were evident. As mentioned, boxes 6 and 12, due to their intertidal nature and narrowness, respectively, had lower potential for remote sensing chl-a estimation. As a consequence, both had the lowest agreements and the highest errors

(Figure 34). Moreover, box 6 had more temporal gaps, about 50 % of the composites were missing, because retrievals depended on the simulated tidal height at the MODIS acquisition time. Box 12, was potentially highly sensitive to contamination due to urban features, like boats and the 25 Abril bridge, and straylight because it was very close to land surfaces. Note that this box was situated in the main navigation channel of the estuary. This probably drove the irregular and inaccurate retrievals without a distinct temporal trend. Data with increased spatial resolution would probably increase data quality and quantity because the factors mentioned impact mainly on the retrieved Rrs.

Concerning the spatial distribution of errors, the GSM and Clark algorithm tended to have decreasing errors, both MAE(%) and RMSE, with decreasing distance to the ocean (Figure 35) with the exception of box 12. The high RMSE for box 6 was driven by a low retrieved chl-a in the winter whereas the E2K simulated a peak, explaining why the highest RMSE occured in the latter box whilst the MAE (%) was relatively low. For the remaining algorithms, OC3 and Carder, the error distribution was relatively independent of the distance to the ocean, except for the mentioned boxes 6 and 12. Near the ocean (box 13), where optical complexity should theoretically be lower and closer to the Case 1 waters definition, were particularly high, probably due to high SPM concentration. However, both algorithms had similar errors, comparing with the mid estuary retrievals, and GSM and Clark had the lowest errors. Estimates were variable along the year (Figure 1 in Annex X) and the latter algorithm seemed to have the best performance. It is recalled, that E2K seemed to slightly overestimate chl-a in the downstream boxes although taken this into account, the OC3 and Carder algorithms still overestimated chl-a. Also in the estuary mouth, the Carder algorithm correlation was high (r~0.80) whilst for the remaining algorithms, was reasonable (r~0.60).

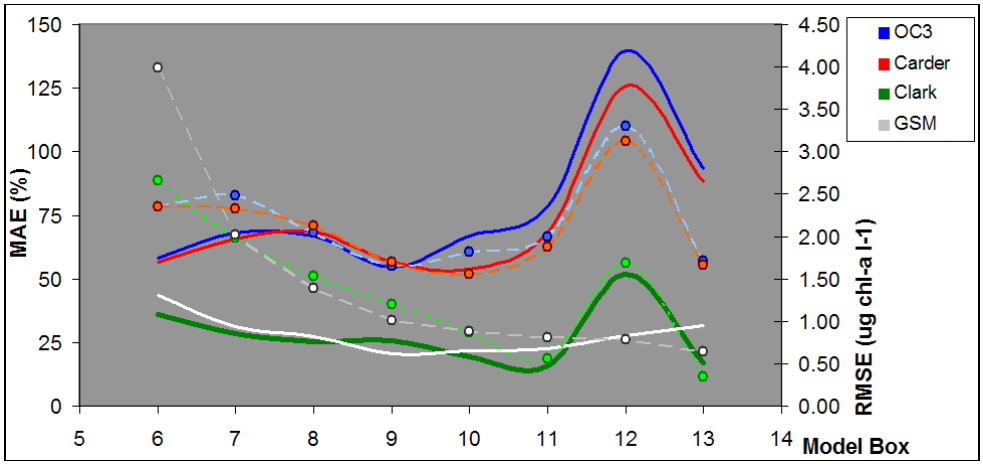

Figure 35 – Case 1 algorithms performance per box : 2000
Dashed and filled lines indicate respectively RMSE and MAE (%)

Gameiro et al. (2004), for a site corresponding to box 7, reported a late spring (180-210 Julian day) peak of about 4 µg chl-a l^{-1} which seemed to be reproduced by all algorithms used, although with different magnitudes. The GSM algorithm had retrievals closest to those reported (Figure 32). The same author, concerning the same box, indicated another peak in late summer (240-270) of about 6 µg chl-a l^{-1}. The Clark, Carder and OC3 algorithms retrieved a coincident peak and the latter with similar magnitude. However, the remote sensing retrievals of the OC3 and Carder algorithms were variable and during spring and summer exhibited 2 to 3 distinct peaks. Moreover, the highest peak was reported in the summer and remote sensing chl-a indicated that the highest peak was in Spring. These features may be driven by the different temporal resolution used: the MODIS data concerned 16day composites and, data from Gameiro et al. (2004 & 2007), concerned an individual sample representative of one month. Furthermore, it is recalled that the comparisons were made using data integrated at a box scale whilst samples represented one distinct point. The same author, for a site corresponding to box 8, reported a slight increase in chl-a in the summer (210-270 Julian day), ranging 2-4 µg chl-a l^{-1}. All the algorithms indicated, once again, that the highest values occured in Spring (see Figure1 in Annex X). The GSM and Clark algorithms had a slight distinct peak (near 210) with a coincident chl-a concentration.

The chl-a values tended to increase with increasing shallowness, which could indicate that the algorithm reproduced the expectable spatial chl-a distribution in the Tagus estuary (Figure 36). It could also indicate that bottom reflectances interfered with the remote sensing signal leading to incorrect inferences. Since the bottom reflectances were accounted for during data processing (see 3.5.2) it suggests that the spatial trend revealed a remote sensing potentiality or "strong point". Note that, the high chl-a values in deeper waters concerned box 12.

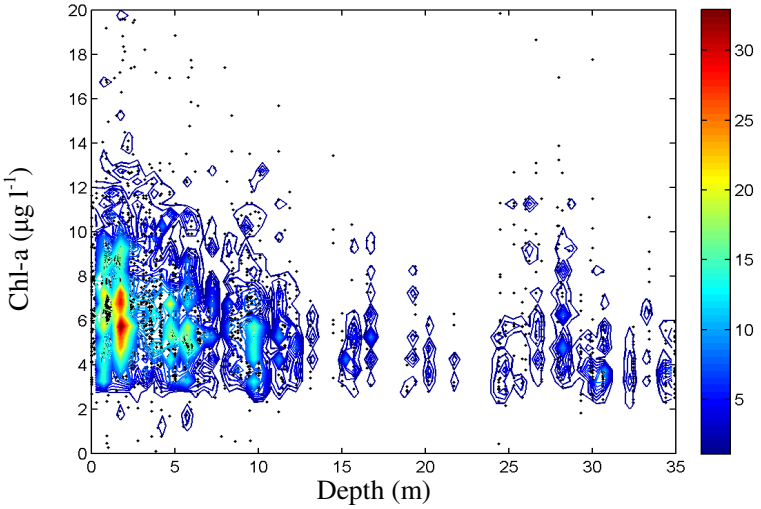

Figure 36 – Chl-a concentration vs. Depth: GSM algorithm 2000
The bar indicates frequency

In Annex X, the distribution of chl-a values against their distance to the ocean was plotted for the GSM algorithm using all 16day pixels i.e. without spatial aggregation. There was a clear spatial gradient: with increasing distance to the ocean, chl-a increased and the relation was steeper towards the summer. Temporally, the autumn distributions had high dispersion and in the upper boxes the algorithm reproduced high values in late spring and early summer. It is clear that between 5 and 10 km from the ocean (i.e. box 12) retrievals were dispersive and scarce producing a distinct gap and some atypical high chl-a values.

The RMSE distribution (Figure 37) exhibited two different patterns. Firstly, the OC3 and Carder algorithms had higher errors in the summer, as mentioned before, consistently overestimating the E2K simulations particularly in this season. As the E2K simulations peaked towards the end of the year, both algorithms tended to have lower errors. Secondly, the Clark and GSM algorithms followed the inverse trend and errors were more significant in the winter. It was expectable that remote sensing retrievals, both for land and ocean applications, due to atmospheric contamination and cloud limitation, had higher errors in late autumn and winter.

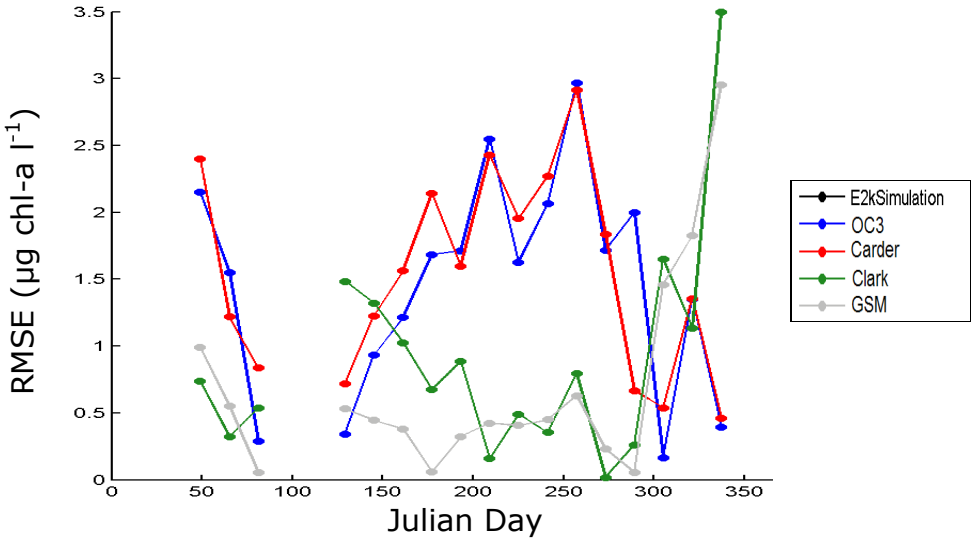

Figure 37 – Case 1 Algorithms RMSE distribution: box 9 2000

Concomitant with the analysis for the year 2000, in 2001, the OC3 and Carder algorithms had similar temporal behaviours and magnitudes, and both, GSM and Clark, were also very similar, reproducing two distinct types of retrievals. Following the wet winter in 2001, the OC3 and Carder algorithms retrieved high chl-a concentrations similar to the ones retrieved later in the year 2000 (see Annex X). Afterwards, concentrations slightly decreased, peaking in late spring/early summer and showing increased variability in the end of the year. The GSM apparently had an independent behaviour in the winter and was the only algorithm

without a clear winter chl-a peak, reproducing well the theoretical chl-a dynamics. Both GSM and Clark chl-a retrievals were within the 57% E2K simulation error for 2000. Comparing with Brogueira and Cabeçadas (2006), for the winter of 2001, between boxes 7 and 13, only the GSM estimates were within the range of reported chl-a. Comparing with Gameiro et al. (2007), the retrievals by the Carder and GSM algorithm in box 8 were similar to those reported, indicating two peaks in late spring and mid summer, both underestimated. Overall, the retrievals by all algorithms were fuzzier than in 2000, concomitant with the sampled data reported by the latter author. Comparing with Brogueira and Cabeçadas (2006), in the summer for boxes 7-13, only the OC3 and Carder retrievals were within reported chl-a range, although with a slight underestimation.

The extreme winter flow in 2001 probably flushed large quantities of riverine phytoplankton cells into the estuary. It was likely that these cells were dead when they reached the estuary because of their salinity tolerance and because the extreme flow acted faster than their reproduction rate. It is known that when phytoplankton dies or degrades, the phaeopigment concentration increases which has impacts on the remote sensing signal and have been estimated using MODIS and CSZS data (e.g. Esaias et al., 1998). Moreover, when excited at 420 nm, phaeopigments also emit fluorescence at 680 nm (e.g. Breves et al., 2003) which could explain the increases and peaks in the red reflectance during the shift from autumn 2000 to winter 2001 (see Figure 27). This fact, along with the increased absorption in the blue region, could be the reason for the high chl-a retrievals, during the mentioned period, by the Case 1 algorithms. To reinforce this idea, Brogueira and Cabeçadas (2006) reported concentrations of 4 $\mu g\ l^{-1}$ for chl-a and 11 $\mu g\ l^{-1}$ for phaeopigments near boxes 7 and 8. The increased flow could have also introduced a large SPM loading. According to Schalles (2006), this feature by itself, would probably lead to the underestimation chl-a. One possible reason to the increase in the retrieved chl-a was the higher concentration of CDOM, which strongly absorbs blue light, which could have been also introduced by the increased river flow.

To assess the accuracy impact of the chosen processing options, the error distribution per box for the year 2000 was plotted using the default processing options (Figure 38). The water tidal mask was also applied. The Clark algorithm was very sensitive to the different Rrs inputs, overestimating chl-a above 1000%. The GSM algorithm was unstable, as mentioned, and the high error in box 8 was probably related to erroneous pixels which were not flagged. This suggestion was driven by a fairly low error in the remaining boxes indicating that the magnitude of Rrs inputs should not be the "local" reason. For all algorithms, the errors and

correlations significantly increased and decreased respectively, using the standard processing options. However, the Carder algorithm was still the one with the best correlation in comparison with the remaining algorithms. The introduced processing options lead to an increase in accuracy over 200% or 6 µg chl-a l^{-1} and correlation of about 0.3. The performance of the OC3 algorithm using the AtmCor3 and MUMM atmospheric correction procedures was compared (Figure 9 in Annex X). The AtmCor3 retrieved higher correlation (+0.1-0.15) but with higher associated errors (+ 50%). The MUMM correction procedure was kept has the reference data set, due to lower chl-a errors, although both procedures were compared in the next sections. The analysis suggested that to monitor chl-a in Case 2 estuaries it is crucial to have an accurate atmospheric correction procedure and a strict setting of quality control flags to diminish the data set noise. The former, should be made using in-situ reflectances and vicariously calibrating the Rrs retrievals (discussed latter on).

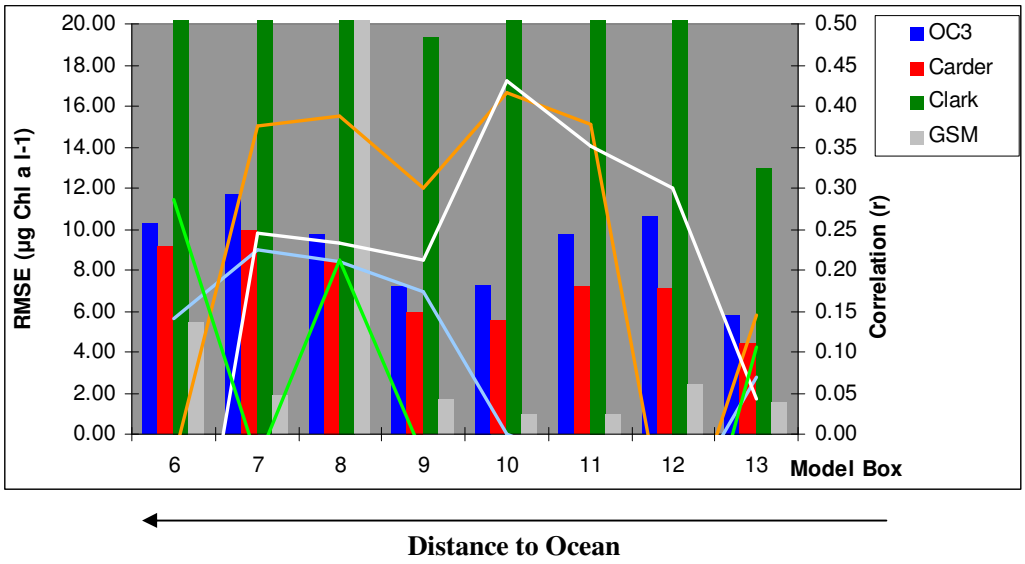

Figure 38 – Standard Processing options – Performance per box : 2000
Bars indicate RMSE and lines the correlation (*r*), per box

4.2.2 - Performance of Case 2 Algorithms (2000)

It is recalled that calibration was performed by adjusting the algorithms to match the E2K 16day box chl-a simulations, using only the year 2000 because it was quantitatively validated. Although the OC3 is a typical Case1 algorithm, it was regionally calibrated, along with the R_{488}/R_{551} and R_{433}/R_{511}, typical Case 1 band ratios. These were assessed to understand how they would reproduce chl-a in a Case 2 environment. Also, the aim was to show that using other spectral regions, such as the green, red and NIR, was more suitable for chl-a monitoring in optically complex waters.

The OC3 calibration for Case 2 waters adjusted the magnitude of chl-a retrievals, whilst the correlation was very similar because it mainly depended on the dependent variable i.e. the band ratio (Figure 39 and Figure 40). For the year 2000, there was a significant error decrease, about 60% or 1.1 µg chl-a l^{-1}, and a slight correlation improvement (r=0.55 *vs.* r=0.47), from a global estuary perspective. The OC3 algorithm, with adjusted coefficients for Case 2 waters, had good agreements between box 9 and 13 (r~0.80), where the higher improvements occured (Figure 40). The error temporal distribution was flattened, and the high summer and early autumn errors of the OC3 original algorithm were greatly decreased (Annex XI).

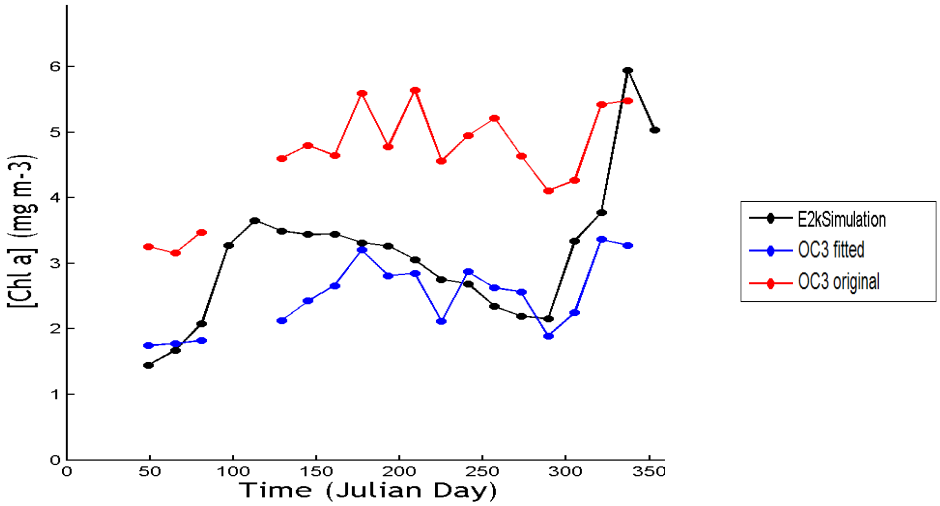

Figure 39 – OC3 fitted *vs.* original OC3 : box 10 – 2000

The tuned OC3 algorithm was compared with 2001 E2K simulations. Because OC3 was fitted using the 2000 data set its performance in 2001 was greatly reduced and the original form had higher accuracy (Figure 2 in Annex XI). The latter was derived from a large data set and, therefore is more robust, suggesting that an algorithm must be calibrated using an extensive Case 2 data set comprising large ranges of chl-a, SPM and CDOM concentrations.

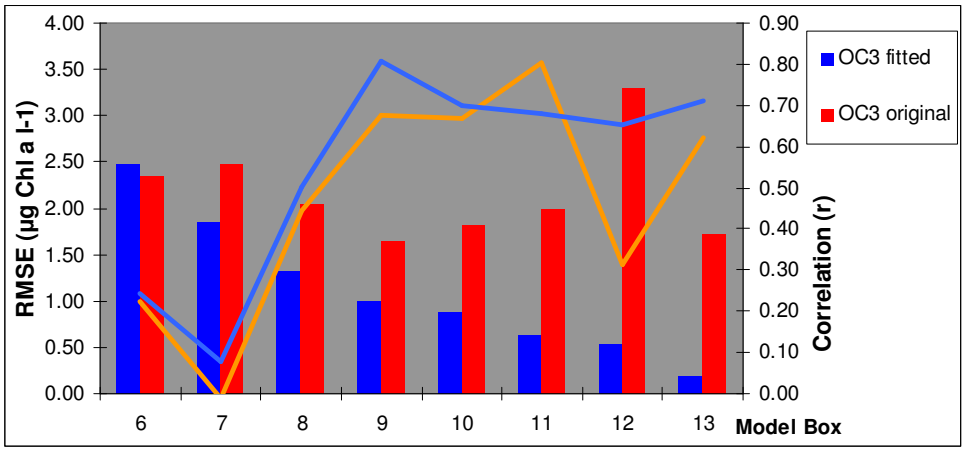

Figure 40 – Tuned OC3 performance : 2000
Bars indicate RMSE and lines the correlation (r)

The regional relationships developed using the typical Case 1 ratios, R_{488}/R_{551} and R_{433}/R_{511}, had similar performance compared with the tuned version of the OC3 algorithm, as expected, and differences were probably driven by the equation form (see Table 18 & Equation 4). The R_{488}/R_{551} had better performance than the typical R_{433}/R_{511} ratio (Annex XI), both exhibiting errors of approximately 20% or 1µg chl-a l^{-1}. The former ratio had good correlation in box 9 (r=0.76) (not shown). This analysis suggested that the low blue region, probably overlapped by CDOM, chl-a and other pigments absorptions, and scattering, was not suitable to reproduce chl-a in the Tagus estuary.

The band ratio proposed by Gitelson et al. (2007), which used the NIR and the upper red regions (R_{748}/R_{678}) (see Table 18), underestimated the E2K chl-a up to box 9 and, overestimated from box 10 to 13. The overall error was about 28% or 1.10 µg chl-a l^{-1} and correlation ranged from null, in box 7, to 0.89, in box 11, with an average agreement of r~0.50. The algorithm performance increases with proximity to the ocean (Figure 41). Theoretically the band ratio should have a band closer to the 700nm to accommodate the peak shift from the upper red to NIR with increasing chl-a (Gitelson, et al., 2007; Schales, 2006). MODIS Terra and Aqua do not have any band closer to 700nm and the low 748nm variability probably limited the algorithm performance. The relationship developed using the FLH adapted from Letelier and Abbott (1996) presented a higher accuracy than the latter algorithm. Its correlation ranged from 0, in box 13, to 0.89, in box 8, with fair inner estuary agreements (r~0.75, box 13 excluded).

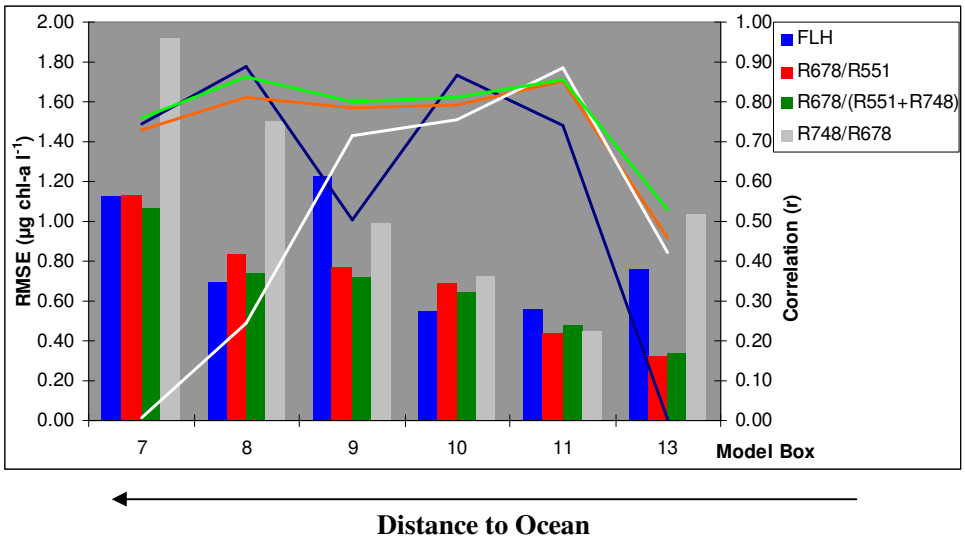

Figure 41 – Case 2 algorithms performance per box : 2000
Bars indicate RMSE and lines the correlation (*r*), per box

The band ratio proposed by Tzortziou et al. (2007), which related the green peak and the upper red region (R_{678}/R_{551}), had 19% error or 0.70 µg chl-a l^{-1} with correlation ranging from 0.46-0.85 and an average agreement of r~0.74. Particularly, this algorithm had good correlations in the mid estuary, from box 7 to 11 with r >0.73, usually near 0.80. The combined versions, using the FLH and the Tzortziou ratio (see Table 18), had similar performance introducing small improvements (not shown). The proposed ratio $R_{678}/(R_{551}+R_{748})$, which added the NIR reflectance to the Tzortziou ratio, also had similar performance. It is recalled that, that NIR reflectance is relevant and seemed to be coupled with total scattering (Figure 26 & Figure 27), possibly coupled with SPM distribution. This proposed ratio had the best performance of all Case 2 ratios tested, with errors of 18% or 0.66 µg chl-a l^{-1} and correlation which ranged from 0.53, in box 13, to 0.86, in box 8. The latter two ratios had performances slightly better than the OC3 algorithm in box 13, suggesting that the estuary mouth, probably due to SPM concentrations, was closer to the Case 2 definition than Case 1. Both had, as it was expected, better performances than the existing global Case 1 algorithms, which were not regionally calibrated.

Regarding temporal distribution, almost all of the band ratios used seemed to simulate a late spring/early summer peak followed by an autumn chl-a bloom. As a consequence of the calibration performed, the best fitted algorithms exhibited the lowest errors, thus had temporal distributions similar to those exhibited by the E2K simulations. Given the limitations of the simulated chl-a, namely the underestimation and non simulation of summer blooms in the mid estuary, the discussion was focused in the statistical "inaccuracies". In others words, the Case 2 algorithms were well fitted and it was important to understand the ability of remote sensing to fill the identified model flaws. The Case 2 ratios simulated late spring and summer peaks (Annex XI; Figure 42; Figure 43) which the E2k did not.

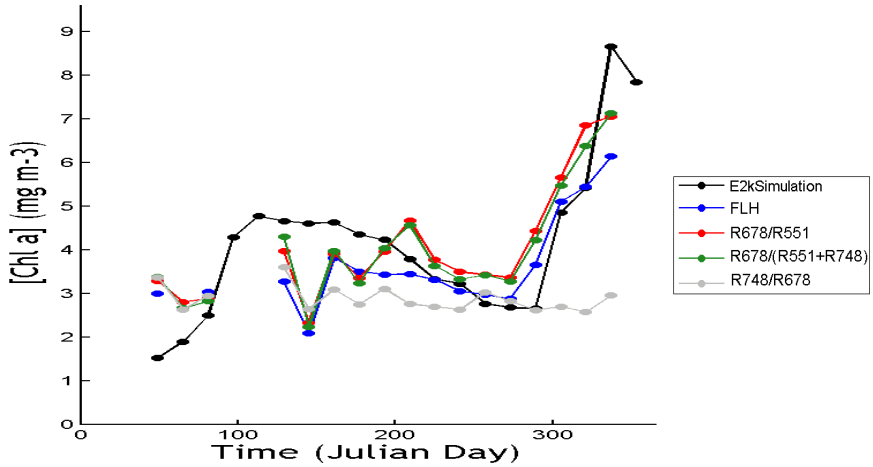

Figure 42 – Case 2 algorithms : time series for box 7 - 2000

Comparing with Gameiro et al. (2007), for box 7, the reported late spring peak (near Julian day 200) was retrieved using the Tzortziou ratio, its adapted version, and the tuned OC3 algorithm. The summer peak, reported by the same author for box 7, was only retrieved by the tuned OC3 version. For box 8, the late summer peak was not retrieved, although there was a slight increase in chl-a retrieved by the latter algorithm. It is recalled that the in-situ data used in the E2K validation also suggested a summer bloom (see 4.1). One spatial feature standed out, the Tzortziou and the adapted version retrieved a chl-a peak in the upper boxes (7-9), near Julian day 200, which was shifted, by about 16 days, in the downstream boxes (10 and 11) (Figure 43 and Annex XI). Considering the typical residence time of the Tagus estuary, this shift could be related to chl-a transported up to downstream sections.

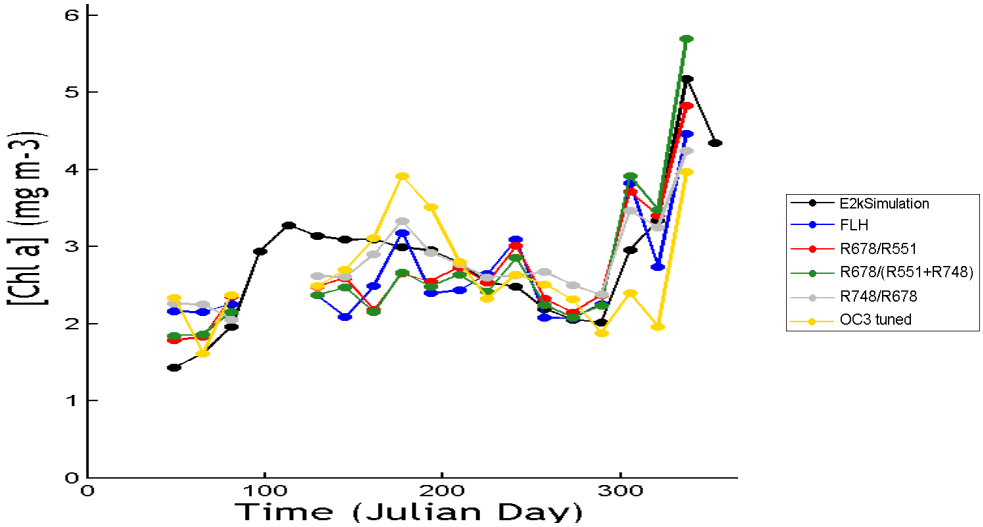

Figure 43 – Case 2 algorithms (all) : time series for box 9 - 2000

All the algorithms which used the green and red ratio retrieved an increase in chl-a concentration even sooner than the E2K (Annex XI). As seen in section 3.6, this increase was associated with a peak reflectance at 678nm, which sometimes exceeded the prominent green peak and did not occur in any other period (see Figure 26 & Figure 27). Extreme flows input large loadings of SPM, driven by upstream watershed erosion, and may have contributed to the increase of Rrs in the whole spectra, but presumably, it would not drive a higher red than green peak. Phaeopigments, as discussed previously, are associated with dead or degraded phytoplankton cells and as a consequence of the extreme run off, may have been massively introduced in the estuary. As stated by Breves et al. (2003), these pigments also exhibit fluorescence at 680nm and could be the cause of the extreme red peak. However, one particular feature must be taken into account: when the red peaking occured, the green reflectance was relatively unaltered but, the NIR reflectance also increased. As mentioned, the latter can be used to estimate SPM using remote sensing techniques. The red and NIR peaks

could be driven by increased SPM scattering, and the green peak could be flattened by the presence of high CDOM concentrations (see the the Ashepoo river example in Figure 3), which could also have been flushed out by the extreme river flow. So the possible combined effects of phaeopigments, SPM and CDOM, introduced by river flow, probably induced a higher red than green peak.

4.3 - Case 1 and Case 2 Algorithms: Independent Assessment (2002)

The remote sensing retrievals were compared with the equivalent E2K 16day box chl-a retrievals to independently attain their performance in the year 2002. Both, Case 1 and regionally developed Case 2 algorithms were compared. The E2K chl-a simulations had similar patterns, considering the years 2000 and 2002, regarding both temporal distribution and magnitude, probably due to their annual flow resemblances. Particularly, no extreme events occured contrary to 2001. Both years could be considered as "average" years and therefore it was expected similar performance regarding the remote sensing retrievals.

As occurred for 2000, during the simulated early spring peak, in 2002 there was also a MODIS imagery gap, limiting the analysis. The retrievals were highly variable and fuzzy with constant increases and decreases, except for the GSM algorithm (Figure 44). The latter was the only algorithm exhibiting a fair performance (Figure 45) with errors ranging from 15% to 32%, or 0.47 to 0.88 µg chl-a l^{-1}, and an average for the whole estuary of about 25% or 0.70 µg chl-a l^{-1}. It is recalled that, only boxes 6-11 and 13 were used in this analysis. The correlation ranges from 0.17 to 0.81, the latter is achieved in box 10. However, it should be underlined that the GSM is an unstable algorithm, as the often negative retrieved chl-a values reduce the available composites (see Annex XII) because they are masked during data processing.

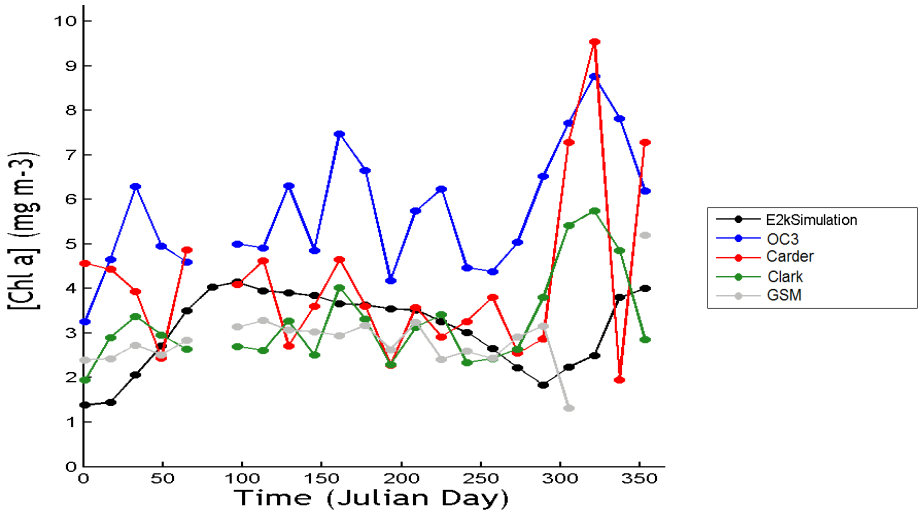

Figure 44 – Case 1 algorithms : time series for box 8 - 2002

The remaining algorithms had very low correlations, r<0.20. Both, Carder and OC3 algorithms had errors above 2 µg chl-a l^{-1}, consistently overestimating chl-a between 50 and 120%. The Clark algorithm had low errors, of 0.70 µg chl-a l^{-1} or 25%, despite the low correlation. Once again, the very low accuracy of the Case 1 algorithms in the near ocean box

13 suggested that this box optically resembled Case 2 waters. However, it is recalled that the E2K probably underestimated chl-a in box 13, particularly, in the spring/summer.

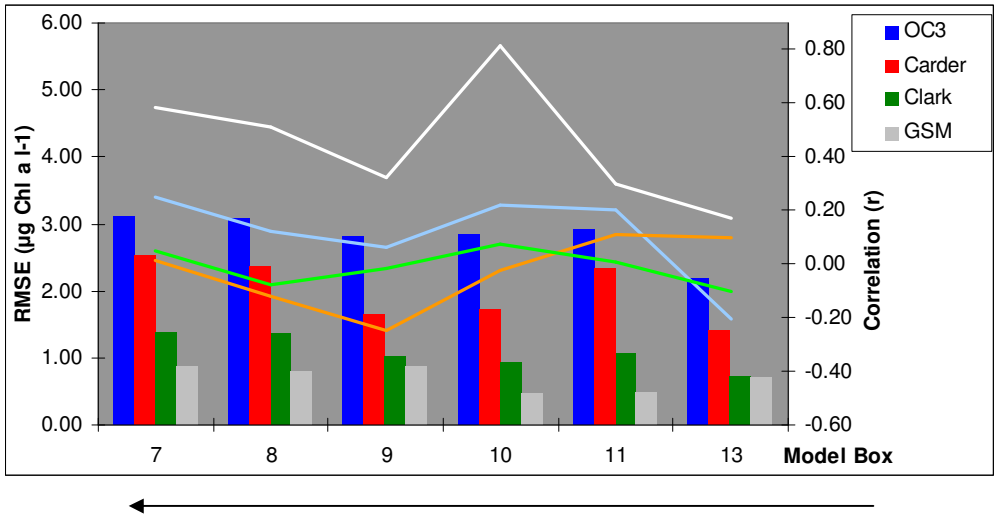

Figure 45 – Case 1 algorithms performance per box : 2002
Bars indicate RMSE and lines the correlation (*r*), per box

The error distribution showed similar patterns for the three algorithms, errors were higher in the winter and autumn (Figure 46), except for GSM, which had scarce data in the latter season. This may driven by factors such as, high water vapour, cloud coverage and other inadequate atmospheric conditions, which affected the accuracy of remote sensing retrievals. The retrievals were consistently above the simulations in the extremes of the year, and during spring and summer, values fluctuated with a few discernable peaks in late spring and mid summer but without any clear temporal trend. The GSM algorithm was the only algorithm with low variability, thus a flattened behaviour, presenting less discernible peaks, particularly in the mid spring when the other two algorithms also peaked (see also Annex XII). Compared with the year 2000, the Case 1 algorithm performance was significantly lower.

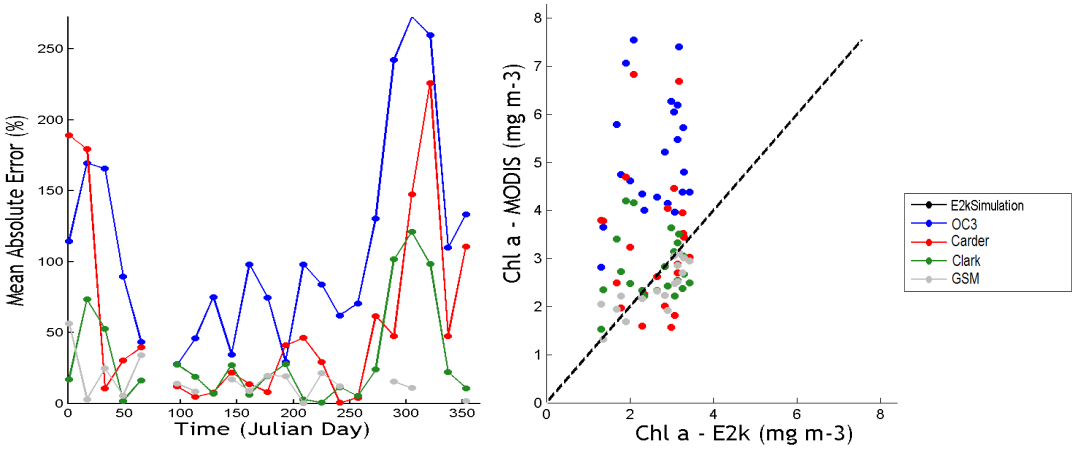

Figure 46 – Case 1 algorithms Pairwise and MAE(%) distribution for box 10 (2002)

Comparing with Gameiro et al. (2007), for a sampling site located in box 7 and considering only the spring and summer periods, the remote sensing estimates of the OC3, Carder and Clark seemed to reproduce the principal peak in May (120-150 Julian day). Moreover, they also seemed to reproduce the reported summer peak (180-210 Julian day). Concerning reported magnitude, the OC3 was the only algorithm which was within reported range. Comparing with the same author, but for box 8, the findings were similar to box 7, concerning a peak in June (150-180) (see Annex XII). The difference was that in the mid/late summer, algorithms reproduced a slight peak, which was not reported.

The spatial distribution of chl-a, for the GSM algorithm between 113-128 Julian days, is shown in Figure 47. Despite the coarse resolution and the low variability of the algorithm, spatial differences were discernable and were theoretically consistent. The map shows higher chl-a concentrations in the upper estuary, the south part of the intertidal areas near Alcochete and in the Montijo bay. The spatial gradient was evident as the distance from the ocean increased, generally, so did chl-a. Furthermore, the outlet plume was discernable along with the near shore chl-a gradient. The synoptic ability of remote sensing to reproduce the spatial distribution of chl-a is a major potentiality which cannot be achieved using in-situ data.

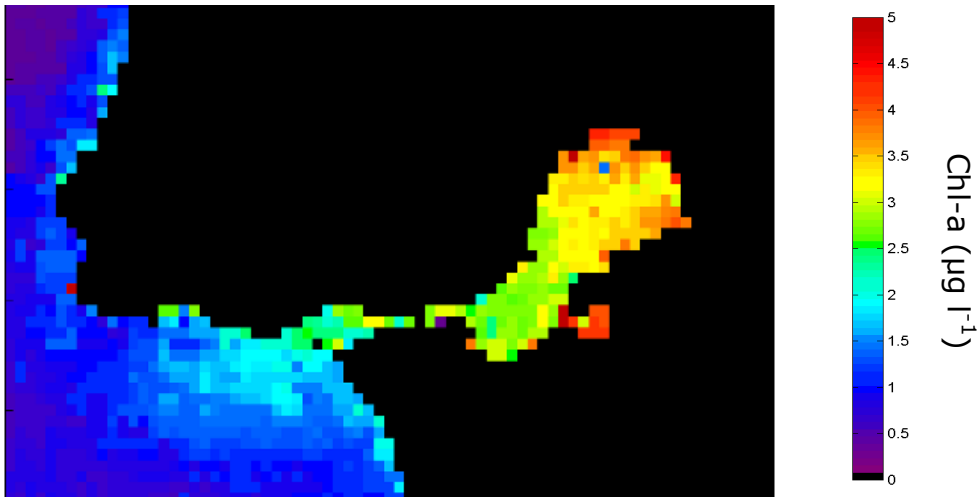

Figure 47 – GSM chl-a spatial 16day distribution: 113-128 (2002)

The spatial analysis arose an important feature: box variability. From visual inspection it was clear, for instance, that box 9 and 10 (see Figure 7) had great variability due to two very distinct chl-a ranges. The Montijo bay exhibited concentrations near 5 µg chl-a l^{-1}, whilst near the main channel, concentrations were about 50% lower. Some studies, which also used model boxes, divided the estuary delimiting the small bays in the south part of the estuary from the remaining boxes (Antunes, 1998; Pina, 2001; Saraiva, 2001). This could be a factor

that caused the high variability in chl-a retrievals, because the other algorithms (not shown) suggested a similar spatial pattern.

The performance of the regionally tuned Case 2 algorithms was lower than the Case 1 algorithms. Distributions were even more variable and one particular feature was common, the chl-a retrievals were higher in the winter and in the autumn, when the simulated chl-a was relatively low (Figure 48).

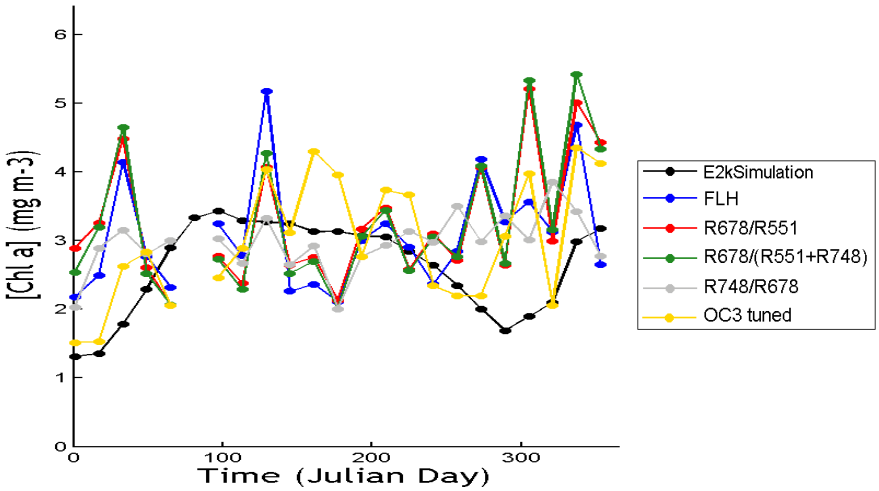

Figure 48 – Case 2 algorithms : time series for box - 2002

This similar trend could be driven by varied causes, namely:

1) Parallel internal processes could be more relevant in those periods and affect the IOP's of the Tagus estuary. The CDOM dynamics were poorly known in the Tagus estuary and may influence greatly the band ratios using shorter wavelengths. Note that, the ratio R_{748}/R_{678}, which used regions less sensitive to CDOM absorption, did not retrieve such high chl-a concentrations in the year extremes. Also, the SPM dynamics were simulated in an average sense and were poorly described.

2) The chl-a dynamics cannot be retrieved with the spectral regions used. This may driven by the distribution of the MODIS bands, which lack spectral resolution in the upper red and NIR regions (e.g. Schalles, 2006).

3) Atmospheric conditions, which are typically more adverse to remote sensing in both periods, could be influencing the accurate Rrs retrieval.

4) The MODIS Terra sensor, besides not being tailored for ocean application, is not calibrated according to it (Franz in http://oceancolor.gsfc.nasa.gov/forum/). Moreover, the pronounced sensor degradation mentioned before (Franz et al., 2007) could affect the Rrs retrievals. Note that in Figure 5 of the Annex XII it is clear that spectral signatures were

fuzzier and more variable, compared with the year 2000 and 2001 (see Figure 27), indicating that Rrs were probably the main cause for the lack of accuracy in 2002.

The error and correlation spatial distribution clearly showed that the tuned algorithms had a poor performance in 2002 (Figure 49). The accuracy was very low for all boxes and decreased with decreased distance to the ocean. In fact, correlation wass often negative indicating that the temporal trend retrieved was inverse to the simulated one. The OC3 fitted algorithm had a slightly better performance than the original form (see Annex XII), suggesting that the remaining Case 1 algorithms would probably have increased accuracy if they were tuned for the Tagus estuary conditions.

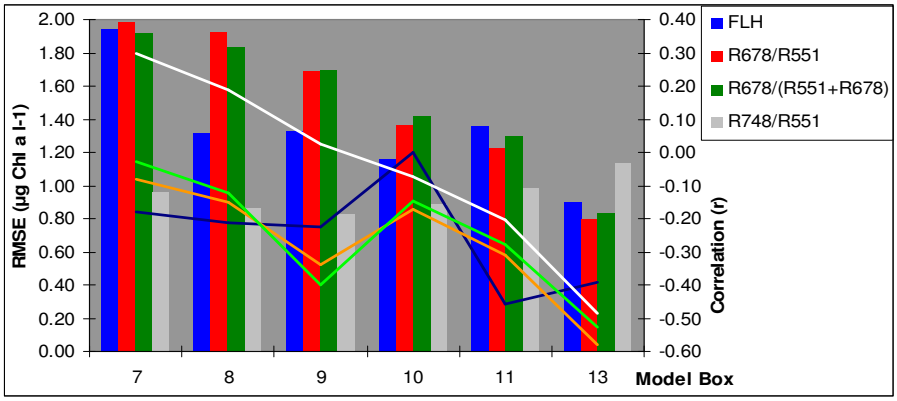

Figure 49 – Case 2 algorithms performance per box : 2002
Bars indicate RMSE and lines the correlation (*r*), per box

Comparing with Gameiro et al. (2007), for box 7, only the Tzortziou et al (2007) and its adapted version retrieved both the May and July peak, respectively. However, after the latter concentrations increased significantly contrary to reported dynamics. Also, comparing with the same author, but for box 8, both algorithms mentioned and the OC3 fitted algorithm retrieved a June peak (150-180 Julian days) although estimates were widely variable.

The analysis of seasonal spectral signatures of boxes 6 to 13, indicated some similar patterns between 2000 (Figure 26) and 2002 (Figure 50). The upper red shoulder was, in some periods and boxes, discernable and possibly indicated higher chl-a concentration. After the summer, this region increased its relative magnitude, exceeding in some occasions the green peak, producing a flat bound in the green-red region. Moreover, as the red reflectance increased so did the NIR. This suggested, like in 2000, that phaeopigments could be increasing the red Rrs thru fluorescence and/or cell scattering and/or, that, CDOM concentration increased in the year extremes flattening the green peak and masking the increased scattering. The NIR peak may be a good independent indicator of the SPM spatial gradient, and could possibly be used

in further work, instead of the green region. In fact, the Case 1 band ratios which used the NIR instead of the green region (e.g. R_{443} or R_{488} /R_{551} *vs.* R_{443} or R_{488} /R_{748}) had better performances. Between compositing periods, the spectral signatures were highly variable probably explainning the consistent "up and down" behaviour of retrieved chl-a. The magnitudes of Rrs also were widely variable suggesting that the retrievals were influenced, for instance, by atmospheric conditions, not accounted for.

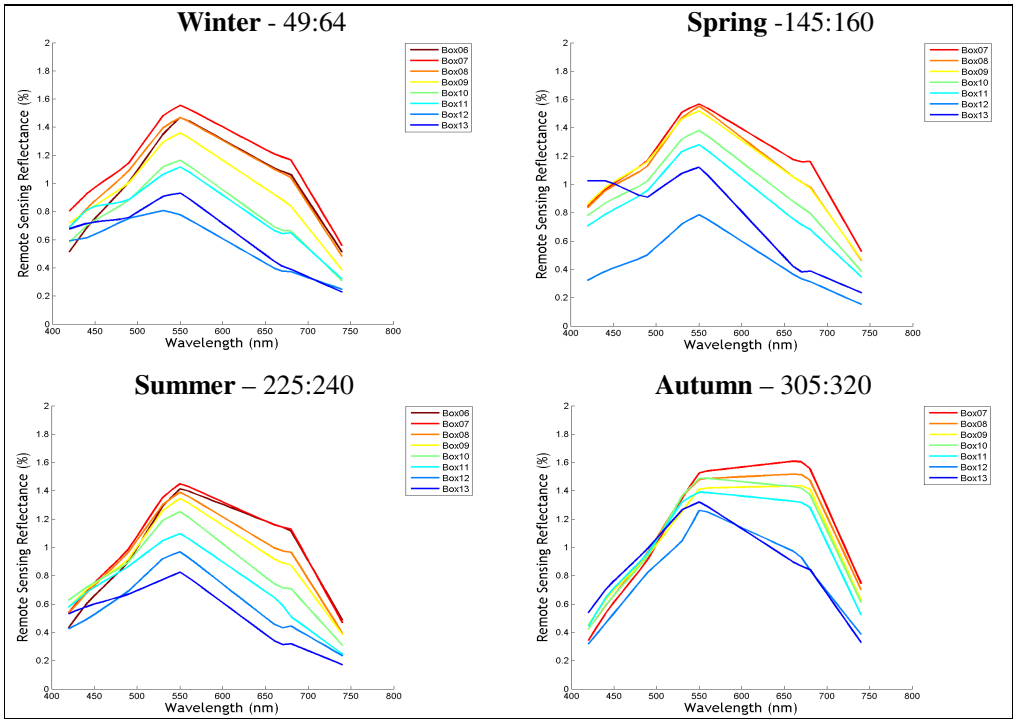

Figure 50 - Spectral Signatures for all boxes per season : 2002

In summary, both Case 1 and regionally tuned Case 2 algorithms had low performances for the year 2002 exhibiting high small scale variability and poor temporal trends when compared with the E2k simulations and the expectable chl-a distribution. The spectral signatures provided valuable information that should be exploited, in order to understand how to retrieve chl-a, and other variables, in the Tagus estuary. The development of a robust algorithm can only be achieved accommodating other regions of the spectra, like the red and NIR. Of all the algorithms tested, the GSM was the more constant and accurate among all. The reasons behind the better performance of GSM when compared, for instance, with the also used semi-analytical Carder algorithm, were poorly known. The different coefficients, inversion methods and slightly different equations, could have driven these differences and understanding them required a thorough analysis which was beyond the scope of this work. The necessity, expressed by many authors, of a particular regional calibration for Case 2 algorithms and the increased performance of the OC3 tuned algorithm, suggest that regional algorithms could be more suitable for chl-a monitoring in Case 2 waters.

5. Limitations and Future Work

This section was dedicated to identifying the major limitations of this work and point out the future work required to develop a robust method for remote sensing retrieval of chl-a in the Tagus estuary. The current work was based in two different, but complementary, components: ecological modelling and remote sensing of chl-a. This section, therefore, addressed the limitations and future work needed for each one and integrates both.

The use of an ecological model to compare and assess remote sensing retrievals of chl-a was an innovation. It attempted to assess the accuracy of remote sensing algorithms to monitor chl-a, using a large scale approach, both spatial and temporally. The overall assessment was constrained by the model accuracy and its limitations. The few and interspersed available samples were a major limitation to the ecological model development and for remote sensing assessment and calibration. For the latter, the majority of the studies performed in estuaries compare optical signals with chl-a, SPM and/or CDOM concentrations and/or IOPs (discussed later). A larger number of in-situ samples, with increased temporal and spatial resolution, along with a wider temporal coverage, would probably increase the model accuracy and applicability. An improved spatial coverage, particularly in the mid estuary where the available data was very scarce, would allow the model to be more robust where remote sensing data was more abundant. Future work should aim towards at using a large in-situ data set with finer spatial resolution, particularly to assess large scale trends, and at using large temporal series. Furthermore, most of the comparisons made throughout the work were based in published data regarding a coincident period. This comparison was complex and ambiguous for many reasons. Firstly, data was not accessible in spreadsheets or tables not allowing an objective comparison. In fact, in most of the cases, making accurate inferences from plotted data was very difficult and limited its potentialities. Secondly, the comparison was made subjectively matching the point sampling locations to the model boxes. Thirdly, the methodologies and objectives of the consulted works were very different.

As mentioned above, the ecological model had its major limitations where the remote sensing had its higher potential: the mid estuary zone. Besides the availability of in-situ data for model calibration and assessment, the model was also limited by its components. The more relevant were addressed. The major model limitation refered to its transport component suited for tidally averaged simulations, but unable to resolve small-medium scale hydrodynamic events, which may be crucial to both chl-a bloom development and its spatial distribution

(e.g. Lucas et al., 1999b). For 8 or 16 day periods this influence could be smoothened, but for instance, if a neap tide induced a bloom development and the remote sensing imagery had low temporal coverage, this effect would have enhanced the differences between the latter and the chl-a simulations. It should be noted that, the low temporal coverage was very often in the MODIS Terra data sets used, frequently having just 3 or 4 days without the full spatial coverage, per composite. In spite of the effect of high frequency events such as tides, an accurate hydrodynamic model should provide a good description of the main transport processes in the estuary. The impact of such processes, like lateral sloshing and the effect of the main channel, probably had higher impacts in the mid estuary. Therefore, the use of coarse transverse model boxes was by far a rough approximation to reality because the transport is probably disproportionate, considering the north and south parts of the main channel. The transport of materials is probably not done according to a homogenous longitudinal gradient and, therefore, transversal transport in the mid estuary is probably an important mechanism. For instance, a clear limitation was the assumed constrained communication between the highly productive Northern channel and the mid estuary. Another obvious limitation was the numerical necessity of assuming a constant box volume, which had impact on the definition of the transport fluxes and concentration of dissolved and particulate substances. This feature probably had higher impacts especially in the intertidal areas, key components of the estuarine chl-a dynamics, which are mainly located in the south mid estuary. Furthermore, the residence time computed by the transport model is important for bloom development and a more detailed approach would probably have increased the ecological model accuracy. For instance, Cartaxana (1999 in Gameiro et al., 2007) stated that, in the up-mid regions, the suspended materials remained entrapped and probably stimulated ammonia and phytoplankton production. In sum, the transport model may be suitable for inter annual comparisons (e.g. Ferreira et al., 2007a) but lacked in accuracy regarding intra annual, weekly or bi-weekly simulations, being the major limiting component. Furthermore, the model should have been calibrated prior to 1998 to allow the model to spin up, enhance the use of the sampled data for that year in the model calibration. The use of the more extensive in-situ data set of the 80's decade would have probably increased the model robustness.

Future work using the ecological model approach to assess remote sensing retrievals should focus on the use of a detailed transport model, which is crucial to attain robust ecological simulations. Currently, for the Tagus estuary, some studies have used MOHID, a detailed 3-D transport model, with good results and extensive validation (Trancoso et al., 2005; Antunes, 1998; Fernandes, 2005; http://www.maretec.mohid.com/). The incorporation of such a model

in the E2K shell, in a compatible fashion, would enhance the benefits of using ecological models to retrieve the chl-a concentration in the Tagus estuary and to assess the accuracy of remote sensing products. The transport model drove the definition of coarse model boxes for the ecological integration and the box definition used was an imperative limitation because the transport model did not allow lateral transport between boxes. The MOHID transport model has been integrated in the coarse box grid with a similar number of boxes, compared with E2K. However, it uses boxes with lateral transport with two main differences: it divides the mid estuary into a northern and southern part, evidencing the importance of the transversally disproportionate transport, driven by the existence of a main channel. Specifically, it divides the adjacent small bays (Seixal and Montijo) from the remaining estuary (http://www.maretec.mohid.com/). This work reinforced the idea that these particular (see section 4.3) areas should be separated because they have specific dynamics with higher intertidal nature and are dependent of the highly organic loading of adjacent streams. Furthermore, the MOHID model separates the intertidal area near Alcochete. Future work should use a different box definition coupled with a more detailed transport model.

The simulated river flow has proven to be a major limitation to this work. The E2K uses a periodic function, which may adapt to a fairly regular and average annual flow distribution, but clearly fails to reproduce the hydrological variability in the years used in this work. The flow impact on chl-a retrievals, using the implemented polynomial functions, introduced high instability, reaching high atypical peaks in autumn and winter. One of the main reasons was the discussed transport model, which would probably better redistribute the extreme water input and smoothen its effect on chl-a retrievals. The other main reason was the monthly polynomials adjusted to simulated data, which lack in temporal resolution and accuracy because they were fitted using a power law explainning the extreme flows. This major limitation had a pronounced impact on chl-a simulations, particularly in the year 2001, and also for the wet seasons of the other years used. The power law should be replaced, for instance, by a smooth linear function which does not amplify any high flows measured at the Almourol station. A promising improvement in future work would be to adapt the E2K model so as to use time series as an input, with the advantage of using real, or near real, measured data with a temporal resolution adequate to finer scale simulations. This was a major limitation because climatic factors are key forcing functions to phytoplankton production (e.g. Gameiro et al., 2007) and were specifically difficult to model accurately. Using sampled data surely diminishes the error propagation, when compared with using models over models.

The capability of using time series was also a limitation for boundary loads, ocean, river and smaller streams or WWTPs. For instance, the assumption of a constant nutrient and SPM riverine concentration over a simulation period was very rough and broad. Seasonal dynamics in flow and concentrations probably drove major impacts in estuarine phytoplankton (e.g. Gameiro et al., 2007). For the ocean boundary, dynamic models have been used in other E2K applications (Ferreira, personal communication) and remote sensing can, potentially, be a valuable tool in its quantitative characterization. In order to assess the remotely sensed chl-a retrievals, a fair description of SPM and CDOM dynamics is needed to understand the possible IOPs that underlie in a "black" model box. The analysis performed suggested that SPM were roughly described mainly because the transport model did not accurately simulate the particulate dispersion within the estuary (e.g. Cartaxana, 1999 in Gameiro et al., 2007) and also because it did not simulate the SPM resuspension in a tidal cycle. The latter has been pointed out as the major process ruling the SPM magnitude and distribution in the Tagus estuary. As mentioned, the constant riverine input concentration was also a limiting factor. Furthermore, the SPM model had limited parameters and a more detailed model is needed in future work.

The main limitation of the phytoplankton object was the fact that it only considered nitrogen limitation. Several authors have suggested that phosphorous and nitrogen limit production with different seasonal patterns. Furthermore, silicate limitation can indirectly drive the after spring chl-a decrease due to lower river flow and stimulate it, when river flow increases. The analysis of the Redfield ratio suggested that silicate was limiting, both in calibration and the validation years, probably causing a higher impact in the up and mid estuary regions where salinity was lower, diatoms were more abundant and silicate was, therefore, more relevant.

For the application of remote sensing techniques to monitor chl-a in the Tagus estuary, the main limitation were the data used due to the MODIS Terra band degradation which influenced ocean retrievals (Franz et al., 2007). Furthermore, the Terra data was not calibrated for ocean applications. These two factors coupled were a major limitation. Future work on retrieving estuarine chl-a should use the recent AQUA sensor data, which is expected to greatly increase the accuracy of Rrs retrievals. Concerning the processing options used, two major limitations were evident. Firstly, the assessment of the most adequate atmospheric correction procedure based on chl-a retrievals, and secondly, the procedure used to remove straylight contamination. As mentioned, in remote sensing of aquatic systems the atmospheric correction is critical to accurate Rrs retrievals because the optical signal is very low. In future

work, it is highly recommended to use in-situ radiometer samples to assess the most adequate atmospheric correction procedure in the Tagus estuary (e.g. Hu et al., 2004). Furthermore, specific aerosol and atmosphere profiles should be developed to insure a robust and potentially operational monitoring procedure in the Tagus estuary. The simple straylight procedure was a clear limitation because it did not completely remove contaminated pixels even if it insured that some were removed. No pre-launch procedure for straylight identification was developed for MODIS. The ocean applications, due to their global scale monitoring aim, are probably less sensitive to straylight errors. However, for estuarine applications, due to their smaller geographic scale, a more robust and accurate procedure should be developed in future work. The water daily water mask developed may not fully correct for bottom reflectance and intertidal contamination. Because tidal simulations were made for the port of Lisbon and there was a pronounced lag, for instance, when estimating the tidal height, for the same hour and day, in the 40km upstream intertidal areas. Therefore, assuming that the tidal height of box 6 was equal to the one simulated in the Lisbon port was a rough approximation. It was expected that spatial resolution would be a major limitation, but it was shown that it was not, theoretically reproducing the chl-a spatial dynamics. However, in future work, and to monitor the upstream zones, the Northern Channel, the intertidal areas and the main navigation narrow channel, increased resolution data would be of great benefit. The methods proposed by Shutler et al. (2006) and Franz et al. (2007) can be of great value, providing synoptic, near daily medium resolution data.

For future algorithm development, simultaneous in-situ samples of IOPs, Rrs and substances concentration are crucial. These must be compatible with the sensor characteristics and must allow a match comparison for vicarious calibration of Rrs and specific algorithm development. As demonstrated and stated by other authors, the spectral signature analysis was a valuable tool to understand dynamics in optically complex waters. These were highly variable and contain various overlapping signals “underneath” the “black box” driven by varying SPM, CDOM and chl-a contributions. For the SPM component, E2K clearly did not simulate it at the required scale. Therefore, reflectance spectra retrieved by radiometer sampling is very important in future work. However, the resemblance of the spectral signatures with those reported by Schalles (2006), for similar contents, indicated that the methodology used was robust and could be used in future works. Also, calibrating algorithms with average radiances may smooth temporal variability to a point that its impact is difficult to assess. In-situ samples should be used to calibrate further Case 2 algorithms and afterwards information may be aggregated for long term assessment purposes.

6. Conclusions

This work demonstrated that, an ecosystem scale assessment of remotely sensed chl-a was feasible in the Case 2 Tagus estuary, although with limitations. It was shown that several issues arise when using data sets which provide information at different spatial and temporal scales. The ecological model provided broad and average information on the chl-a dynamics in the estuary by using large model boxes and reproducing monthly to seasonal dynamics, whilst the remote sensing approach provided daily\weekly imagery with higher spatial resolution. A major task in this work was to make these different scale data compatible and comparable. The methods used provide a good and robust approximation to an ecosystem scale assessment, since they successfully removed the noise associated with remote sensing data, maintaining ecological significance.

The simulated chl-a concentration, using the E2k model, had a 57% error when compared with sampled data in the years 2000 and 2002. The availability of in-situ data and some model constraints limit its accuracy, thus the simulated chl-a. Further work is needed to improve the E2K chl-a simulations, namely the implementation of a detailed transport model which simulates transversal fluxes and tidal processes, the accommodation of phosphorous and silicate limitation in the phytoplankton object, as well as the incorporation of detailed river flow time series. The latter had a pronounced impact in chl-a simulations, driving an excessive and atypical winter chl-a peak in 2001 and in the wet seasons of 2000 and 2002.

The remote sensing of chl-a in the Tagus estuary is feasible but requires regionally developed algorithms, using in-situ data. As demonstrated, processing options such as atmospheric correction and quality control had a large impact on chl-a retrievals. The analysis performed for the year 2000, specifically showed an error reduction of more than 100% by using an atmospheric correction procedure more adequate for turbid waters. The MUMM algorithm was used successfully in this work but, in the future, work must aim at retrieving suitable water leaving radiances comparing top of the atmosphere reflectances with in-situ radiometer data and vicariously fitting an adequate atmospheric correction method. The quality control flags were also relevant, namely the sun glint and straylight correction were implemented successfully by removing noise thus improving accuracy. The latter needs a more robust and validated procedure but the simple method used provided reasonable improvements.

Remotely sensed chl-a was retrieved by using pre-existing Case 1 algorithms and regionally tuned algorithms. The latter were divided in the regionally tuned OC3 empirical algorithm and simple Case 2 band ratios relationships. In the Case 1 algorithms, the Carder algorithm revealed the higher correlations in both 2000 and 2001 (r~0.55), but retrieved chl-a with relatively high errors, about 2.5 μg chl-a l^{-1}, or 70% errors for the whole estuary. In the year 2002, this algorithm revealed a lower performance, inadequate for chl-a monitoring. The GSM was the algorithm with better and more constant performance for the analyzed years. In the year 2000, the GSM resulted in an accuracy of about 1.5μg chl-a l^{-1}, or 30% error for the whole estuary, with correlation of about r~0.40. In 2001, the performance was lower, as it was for all algorithms used. However, in 2002 the GSM algorithm had the best performance, but, still below the quality requisites needed for consistent, periodic and robust monitoring of chl-a in the Tagus estuary. The correlation was approximately 0.45, with average errors of about 30% or 1 μg chl-a l^{-1}. The Case 2 band ratios also had low accuracy, indicating that much work is needed to retrieve a robust Case 2 algorithm suitable for chl-a monitoring in the Tagus estuary.

Spatially, some remote sensing limitations were evident. The intertidal box 6 was poorly retrieved in terms of accuracy and in terms of temporal coverage due to the low number of composites analyzed. Box 12 was also very difficult to assess using remote sensing techniques due to its narrowness and high sensitivity to urban features and land contamination. The remote sensing of chl-a has its "strong point" in the mid region, between box 7 and 11 because it is wider and less "optically contaminated". The correlations peaked in this region and the errors were reasonable. Historically, this mid section has been less monitored than the remaining areas, such as the upstream region, the Northern Channel and the outlet channel. Therefore, information provided by remote sensing techniques could improve the spatial coverage of chl-a information over the Tagus estuary. Furthermore, the regional calibration of the OC3 algorithm dramatically increased its accuracy, namely by adjusting the magnitude of retrievals to the Tagus estuary reality, diminishing the absolute errors. However, it was demonstrated that when applied to other data sets, not used in its calibration, the accuracy diminished dramatically. This analysis suggestd that future work should be focused in the regional calibration of semi-analytical algorithms, such as, the GSM algorithm.

7. References

Alpine, A., Cloern, J., 1988. Phytoplankton growth rates in a light-limited environment, San Francisco Bay. Marine Ecology Progress Series 44:167-173.

Alvera-Azcarate, A., Ferreira, J., Nunes, J., 2003. Modelling eutrophication in mesotidal and macrotidal estuaries. The role of intertidal seaweeds. Est. Coast. Shelf Sci. 57 (4):715-724.

Anderson, D., Garrison, D., 1997. The ecology and oceanography of harmful algal blooms. Limnol Oceanogr 42:1009-1305.

Antunes, I., 1998. Modelação Matemática da Qualidade da Água no estuário do Tejo. Dissertação para a obtenção do grau de Mestre em Ecologia, Gestão e Modelação dos Recursos Marinhos. Instituto Superior Técnico. Universidade Técnica de Lisboa, p. 93.

Arrigo, K., 2005. Marine microorganisms and global nutrient cycles. Nature 437:349-355.

Barré, N., Provost, C., Saraceno, M., 2006. Spatial and temporal scales of the Brazil–Malvinas Current confluence documented by simultaneous MODIS Aqua 1.1-km resolution SST and color images. Advances in Space Research 37:770-786.

Behrenfeld, M., Falkowski, P., 1997. Photosynthetic rates derived from satellite-based chlorophyll concentration. Limnol. Oceanogr. 42:1-20.

Behrenfeld, M. , O'Malley, R., Siegel D., McClain C., , Sarmiento J., Feldman G., Milligan A., Falkowski P., Letelier R., Boss, E., 2006. Climate-driven trends in contemporary ocean productivity. Nature – Letters, 244(7):752-755.

Boney, A., 1975. Phytoplankton, The Institute of Biology's studies in Biology, No.52, Edward Arnold (Publs.) Ltd., England, p. 116.

Borges, A., Schiettecatte, L., Abril, G., Delille, B., Gazeau, F., 2006. Carbon dioxide in European coastal waters. Estuarine, Coastal and Shelf Science 70:375-387.

Breves, W., Heuermann, R., Reuter, R., 2003. Enhanced red fluorescence emission in the oxygen minimum zone of the Arabian Sea. Ocean Dynamics 53: 86–97

Bricaud, A., Claustre, H., Ras, J., Oubelkheir, K., 2004. Natural variability of phytoplanktonic absorption in oceanic waters: Influence of the size structure of algal populations. Journal of Geophysical Research 109:1-12.

Bricker, S., Clement, C., Pirhalla, D., Orlando, S., Farrow, D., 1999. National Estuarine Eutrophication Assessment: Effects of Nutrient Enrichment in the Nation's Estuaries. NOAA, National Ocean Service, Special Projects Office and the National Centers for Coastal Ocean Science. Silver Spring, p.71.

Bricker, S., Ferreira, J., Simas, T., 2003. An integrated methodology for assessment of estuarine trophic status. Ecol. Model. 169:39-60.

Brock, T., 1981. Calculating solar radiation for ecological studies. Ecolog. Modelling 14:1-9.

Brogueira, M., Cabeçadas, G., 2006. Identification of similar environmental areas in Tagus estuary by using multivariate analysis. Ecological Indicators 6:508-515.

Cabeçadas, G., Brogueira, M., Cabeçadas, L., 2000. Southern Portugal: the Tagus and Sado estuaries. In: Sheppard, C. (Ed.), Seas at the Millennium: an Environmental Evaluation. Elsevier Science Ltd. Oxford. UK, p. 151-165.

Cabrita, M., Brotas, V., 2000. Seasonal variation in denitrification and dissolved nitrogen fluxes in intertidal sediments of the Tagus estuary, Portugal. Marine Ecology Progress Series 202:51-65.

Câmara, A., Silva, M., Ferreira, J., Rodrigues, A., Remédio, J., Castro, P., Fernandes,T., Machado,V., 1987. Sistema de Gestão da Qualidade da Água do Estuário do Tejo. Relatório Projecto Tejo nº 15, Estudo Ambiental do Estuário do Tejo.

Caraco, N., Cole, J., Likens, G., 1990. A comparison of phosphorus immobilization in sediments of freshwater and coastal marine systems. Biogeochemistry 9(3): 277-290.

Carder, K., Chen, F., Lee, Z., Hawes, S., Kamykowski, D., 1999. Semianalytic Moderate-Resolution Imaging Spectrometer algorithms for chlorophyll-a and absorption with bio-optical domains based on nitrate depletion temperatures. J. Geophys. Res. 104: 5403-5421.

Carder, K., Chen, F., Cannizzaro, J., Campbell, J., Mitchell, B., 2004. Performance of the MODIS semi-analytical ocean color algorithm for chlorophyll-a. Advances in Space Research 33:1152-1159.

Chan, P., Gao, B., 2005. A Comparison of MODIS, NCEP, and TMI Sea Surface Temperature Datasets. IEEE Geoscience and Remote Sensing letters 2(3):270-274.

Chapra, S.C., 1997. Surface Water-Quality Modelling. McGraw-Hill. NY, p. 844.

Chen, Q., Zhang, Y., Ekroos, A., Hallikainen, M., 2004. The role of remote sensing technology in the EU water framework directive (WFD). Environmental Science & Policy 7:267-276.

Chen, Z., Hu, C., Muller-Karger, F., 2007. Monitoring turbidity in Tampa Bay using MODIS/Aqua 250-m imagery. Remote Sensing of Environment 109:207-220.

Ciotti, A., Lewis, M., Cullen, J., 2002. Assessment of the relationships between dominant cell size in natural phytoplankton communities and the spectral shape of the absorption coefficient. Limnol. Oceanogr. 47:404-417.

Ciotti, A., Bricaud, A., 2006. Retrievals of a size parameter for phytoplankton and spectral light absorption by colored detrital matter from water-leaving radiances at SeaWiFS channels in a continental shelf region off Brazil. Limnol. Oceanogr: Methods 4:237-253.

Clark, D., 1997. Bio-Optical Algorithms Case 1 Waters, MODIS Algorithm Theoretical Basis Document.

Cloern, J., 1982. Does the benthos control phytoplankton biomass in South San Francisco Bay? Mar Ecol Prog Ser 9:191-202.

Cloern J., Cole B., Wong R., Alpine A., 1985. Temporal dynamics of estuarine phytoplankton: a case study of San Francisco Bay. Hydrobiologia 129:153-176.

Cloern, J., 1987. Turbidity as a control on phytoplankton biomass and productivity in estuaries. Continental Shelf Research Vol7, 11/12:1367-1381.

Cloern, J., Powell, T., Huzzey, L. 1989. Spatial and temporal variability in South San Francisco Bay (USA). II. Temporal changes in salinity, suspended sediments, and phytoplankton biomass and productivity over tidal time scales. Estuar Coast Shelf Sci 28:599-6113.

Cloern, J., 1991. Tidal stirring and phytoplankton bloom dynamics in an estuary. J Mar Res 49:203-221.

Cloern J.E., Grenz C., Lucas L.V., 1995. An empirical model of the phytoplankton chlorophyll:carbon ratio-the conversion factor between productivity and growth rate. Limnol. Oceanogr. 40(7):1313-1321.

Cloern, J., 1996. Phytoplankton bloom dynamics in coastal ecosystems: a review with some general lessons from sustained investigation of San Francisco Bay, California. Reviews of Geophysics 34:127-168.

Cloern, J., 1999. The relative importance of light and nutrient limitation of phytoplankton growth: a simple index of coastal ecosystem sensitivity to nutrient enrichment. Aquatic Ecology 33:3-16.

Cloern, J., 2001. Our evolving conceptual model of the coastal eutrophication problem. Marine Ecology Progress Series 210:223-253.

Cole, B., Cloern, J., 1984. Significance of biomass and light availability to phytoplankton productivity in San Francisco Bay. Marine Ecology Progress Series 17:15-24.

Cole, J., Caraco, N., Peierls, B., 1992. Can phytoplankton maintain a positive carbon balance in a turbid, freshwater, tidal estuary? Limnology and Oceanography 37:1608-1617.

Conley, D., 1999. Biogeochemical nutrient cycles and nutrient management strategies. Hydrobiologia 410:87-96.

Day, J., Hall, C., Kemp, W., Arancibia, A., 1989. Estuarine ecology. Wiley, p. 558.

Davies, P., 2004. Nutrient processes and chlorophyll in the estuaries and plume of the Gulf of Papua. Continental Shelf Research 24:2317-2341.

de Souza, R., Mata, M., Garcia, C., Kampel, M., Oliveira, E., Lorenzzetti, J., 2006. Multi-sensor satellite and in-situ measurements of a warm core ocean eddy south of the Brazil–Malvinas Confluence region. Remote Sensing of Environment 100:52-66.

Doerffer, R., Schiller, H., 2007. The MERIS Case 2 water algorithm. Int. J. Remote Sensing 28(3-4):517-535.

Doxaran, D., Froidefond, J., Lavender, S., Castaing, P., 2002a. Spectral signature of highly turbid waters Application with SPOT data to quantify suspended particulate matter concentrations. Remote Sensing of Environment 81:149-161.

Doxaran, D., Froidefond, J., Castaing, P., 2002b. A reflectance band ratio used to estimate suspended matter concentrations in sediment-dominated coastal waters. Int. J. Remote Sensing 23:5079-5085.

Duarte, P., Ferreira, J., 1997. Dynamic modelling of photosynthesis in marine and estuarine ecosystems. Environ. Model. Assess. 2:83-93.

Duarte, P., Meneses, R., Hawkins, A., Zhu, M., Fang, J., Grant, J., 2003. Mathematical modelling to assess the carrying capacity for multi-species culture within coastal waters. Ecological Modelling 168:109-143.

Eilers P., Peeters, J., 1988. A model for the relationship between light-intensity and the rate of photosynthesis in phytoplankton. Ecol. Modelling 42:199-215.

EPA, 1985. Rates, Constants and Kinetics Formulations in Surface Water Quality Modelling (2nd Edition) Chapter 5 - Nutrients; United States Environmental Protection Agency, Report EPA/600/3-85/040, p. 231-278.

Eppley, R., Peterson, B., 1979. Particulate organic matter flux and phytoplanktonic new production in deep ocean. Nature 285:677-680.

Esaias, and 11 Coauthors, 1998. An overview of MODIS capabilities for ocean science observations. IEEE Transactions on Geoscience and Remote Sensing 36(4):1250-1265.

Fasham, M., Platt, T., 1983. Photosynthetic response of phytoplankton to light – a physiological model. Proc. R. Soc. Lond. 219(1217):355-370.

Feng, H., Campbell, J., Dowell, M., Moore, T., 2005. Modeling spectral reflectance of optically complex waters using bio-optical measurements from Tokyo Bay. Remote Sensing of Environment 99:232 – 243.

Fernandes, R., 2005. Modelação Operacional no Estuário do Tejo. Dissertação para obtenção do grau de Mestre em Ecologia, Gestão e Modelação dos Recursos Marinhos. Universidade Técnica de Lisboa – Instituto Superior Técnico. Lisboa, p. 106.

Ferreira, J., 1988. Mercúrio em algas macrófitas do estuário do Tejo. Estudo Ambiental do Estuário do Tejo. Dissertação para obtenção do grau de Doutor em Ciências do Ambiente. Faculdade de Ciências e Tecnologia. Universidade Nova de Lisboa. Lisboa, p. 307.

Ferreira, J., Duarte, P., 1994. Productivity of the Tagus Estuary - An application of the EcoWin ecological model. Gaia 8: 89-95.

Ferreira, J., 1995. ECOWIN - an object-oriented ecological model for aquatic ecosystems. Ecological Modelling 79:21-34.

Ferreira, J., Duarte, P., Ball, B., 1998. Trophic capacity of Carlingford Lough for oyster culture—analysis by ecological modelling. Aquat. Ecol. 31:361-378.

Ferreira, J., 2000. Development of an estuarine quality index based on key physical and biogeochemical features. Ocean and Coastal Management 43: 99-122.

Ferreira, J., Simas, T., Nobre, A., Silva, M., Shifferegger, K., Lencart-Silva, J., 2003. Identification of sensitive areas and vulnerable zones in transitional and coastal Portuguese systems. Application of the United States National Estuarine Eutrophication Assessment to the Minho, Lima, Douro, Ria de Aveiro, Mondego, Tagus, Sado, Mira, Ria Formosa and Guadiana systems. INAG/IMAR, 2003, p. 168.

Ferreira, J., Simas, T., Bricker, S., Wolff, W., Mason, A., Nobre, A., 2004. The use of ASSETS and phytoplankton species composition to define type-specific reference conditions for estuarine water quality management. In: ASLO/TOS 2004 Ocean Research Conference, Honolulu, Hawaii, 15–20 February, http://www.aslo.org/meetings/honolulu2004/files/aslo-tos- 2004-abstracts.pdf.

Ferreira, J., Wolff, W., Simas, T., Bricker, S., 2005a. Does biodiversity of estuarine phytoplankton depend on hydrology?. Ecological Modelling 187:513-523.

Ferreira, J., Abreu, P., Bettencourt, A., Bricker, S., Marques, J., Melo, J., Newton, A., Nobre, A., Patricio, J., Rocha, F., Rodrigues, R., Salas, F., Silva, M., Simas, T., Soares, C., Stacey, P., Vale, C., de Wit, M., Wolff, W., 2005b. Monitoring Plan for Water Quality and Ecology of Portuguese Coastal Waters (MONAE). INAG & IMAR, p. 141.

Ferreira, J., Hawkins, A., Monteiro, P., Service, M., Moore, H., Edwards, A., Gowen, R., Lourenço, P., Mellor, A., Nunes, J., Pascoe, P., Ramos, L., Sequeira, A., Simas, T., Strong, J., 2007a. SMILE – Sustainable Mariculture in northern Irish Lough Ecosystems – Assessment of Carrying Capacity for Environmentally Sustainable Shellfish Culture in Carlingford Lough, Strangford Lough, Belfast Lough, Larne Lough and Lough Foyle. Ed. IMAR – Institute of Marine Research, p. 100.

Ferreira, J., Vale, C., Soares, C., Salas, F., Stacey, P., Bricker, S., Silva, M., Marques, J., 2007b. Monitoring of coastal and transitional waters under the E.U. Water Framework Directive. Environ Monit Assess *In Press*

Flindt, M., Pardal, M., Lillebø, A., Martins, I., Marques, J., 1999. Nutrient cycling and plant dynamics in estuaries: A brief review. Acta Oecologica 20(4):237-248.

Franco, A., Ferreira, J., Nobre, A., 2005. A model for sustainable management of penaeid shrimp fishery – application to Maputo Bay, Mozambique. LOICZ II Inaugural Open Science Meeting, p. 12: http://www.loicz.org/public/loicz/osm2005/day1/franco.pdf

Franks, P., 1992. Phytoplankton blooms at fronts: patterns, scales, and physical forcing mechanisms. Rev Aquat Sci 6:121-133.

Franks, P., Marra, J., 1994. A simple new formulation for phytoplankton photoresponse and an application in a wind-driven mixed-layer model. Marine Ecol. Progr. Ser. 111: 143–153.

Franz, B., Werdell, P., Meister, G., Kwiatkowska, E., Bailey, S., Ahmad, Z., McClain, C., 2006. MODIS Land Bands for Ocean Remote Sensing Applications, Proc. Ocean Optics XVIII, Montreal, Canada, 9-13.

Franz, B., Kwiatkowska, E., Meister, G., McClain, C., 2007. The utility of MODIS-Terra for ocean color applications. Proc. SPIE, 6677, http://dx.doi.org/10.1117/12.732082

Furnas, M., 1990. In-situ growth rates of marine phytoplankton: approaches to measurement, community and species growth rates. J. Plankton Res. 12:1117–1151.

Gameiro, C., Cartaxana, P., Brotas, V., Cabrita, M., 2004. Variability in chlorophyll and phytoplankton composition in an estuarine system. Hydrobiologia 525:113-124.

Gameiro, C., Cartaxana, P., Brotas, V., 2007. Environmental drivers of phytoplankton distribution and composition in Tagus Estuary, Portugal. Estuar. Coast. Shelf Sci. In Press, 75(1-2):21-34.

Garver, S., Siegel, D., 1997. Inherent optical property inversion of ocean color spectra and its biogeochemical interpretation. Time series from the Sargasso Sea. J. Geophys. Res. 102:18607-18625.

Gitelson, A., Yacobi, Y., Schalles, J., Rundquist, D., Han, L., Stark, R., Etzion, D., 2000. Remote estimation of phytoplankton density in productive waters. Limnology and Lake Management – Archives for Hydrobiolia, Special Issues, Advances in Limnology 55:121-136.

Gitelson, A., Schalles, J., Hladik, C., 2007. Remote chlorophyll-a retrieval in turbid, productive estuaries: Chesapeake Bay case study. Remote Sensing of Environment 109:464-472.

Gordon H., Wang, M., 1994. Retrieval of water-leaving radiance and aerosol optical thickness over the oceans with SeaWiFS: a preliminary algorithm. Appl. Opt. 33:443-

Grillot, N., Ferreira, J., 1996. Modelo Ecológico da Cala do Norte do estuário do Tejo. ECOTEJO, Rel. A-8403-06-96-UNL, DCEA/FCT.

Harding L., Meeson, B., Fisher, T., 1986. Phytoplankton production in two East coast estuaries: Photosynthesis-light functions and patterns of carbon assimilation in Chesapeake and Delaware Bays. Estuarine, Coastal and Shelf Science 23:737-806.

Harding, L., 1994. Long-term trends in the distribution of phytoplankton in Chesapeake Bay: roles of light, nutrients and stream flow. Marine Ecology Progress Series 104: 267-291.

Harris, G., Lott, J., 1973. Light intensity and photosynthetic rates in phytoplankton. J. Fish. Res. Board Canada 30:1771–1778.

Heip, C., Goosen, N., Herman, P., Kromkamp, J., Middelburg, J., Soetaert, K., 1995. Production and consumption of biological particles in temperate tidal estuaries. Oceanography and Marine Biology: an Annual Review 1995 vol. 33:1-149.

Howarth, R., 1988. Nutrient limitation of net primary production in marine ecosystems. Annual Review of Ecology and Systematics 19: 89-110.

Hu, C., Carder, K., 2002. Atmospheric correction for airborne sensors: Comment on a scheme used for CASI. Remote Sensing of Environment 79:134-137

Hu, C., Chen, Z., Clayton, T., Swarzenski, P., Brock, J., Muller-Karger, F., 2004. Assessment of estuarine water-quality indicators using MODIS medium-resolution bands: Initial results from Tampa Bay, FL. Remote Sensing of Environment 93:423-441.

Huisman, J., van Oostveen, P., Weissing, F., 1999. Critical depth and critical turbulence: two different mechanisms for development of phytoplankton blooms. Limnology and Oceanography 44:1781-1787.

Huzzey L., Cloern J., Powell T., 1990. Episodic changes in lateral transport and phytoplankton distribution in South San Francisco Bay. Limnol. Oceanogr. 35(2):472-478.

ICES, 2004. Report of the Study Group to Review Ecological Quality Objectives for Eutrophication. ICES CM 2004/ACE:04. Copenhagen, p. 60.

INAG, 2002. Water quality in Portuguese Estuaries: Tejo, Mondego & Sado. p. 122. http://www.maretec.mohid.com/PortugueseEstuaries/Reports/Portuguese_EUDirectives.pdf

IOCCG, 2000. Remote sensing of ocean color in coastal, and other optically complex, waters. S. Sathyendranath (Ed), Report Number 3, p. 140.

IOCCG, 2006. Remote Sensing of Inherent Optical Properties: Fundamentals, Tests of Algorithms, and Applications. Lee, Z.-P. (ed.), Reports of the International Ocean-Colour Coordinating Group, No. 5, IOCCG. Dartmouth. Canada, p. 122.

Irigoien, X., Castel, J., 1997. Light limitation and distribution of chlorophyll pigments in a highly turbid estuary: the Gironde (SW France). Estuarine, Coastal and Shelf Science 44:507–517.

James, I., 2002. Modelling pollution dispersion, the ecosystem and water quality in coastal waters: a review. Environmental Modelling and Software, 17:363-385.

Janowitz, G., Kamykowski, D., 1991. An Eulerian model of phytoplankton photosynthetic response in the upper mixed layer. J. Plankt. Res. 13:988–1002.

Janssen, P., Heuberger, P.S.C., 1995. Calibration of process-oriented models. Ecological Modelling 83:55-66.

Jaworski, N., Howarth, R., Hetling, L., 1997. Atmospheric deposition of nitrogen oxides onto the landscape contributes to coastal eutrophication in the northeast United States. Environ Sci Technol 31:1995-2004.

Jørgensen, S., Nielsen, S., Jørgensen, L., 1991. Handbook of Ecological Parameters and Ecotoxicology. Elsevier. Amsterdam, p. 464.

Jørgensen, S., 1994. Fundamentals of Ecological Modelling (2nd Edition). Elsevier. Amsterdam, p. 628.

Keith, D., Yoder, J., Freeman, S., 2002. Spatial and Temporal Distribution of Coloured Dissolved Organic Matter (CDOM) in Narragansett Bay, Rhode Island: Implications for Phytoplankton in Coastal Waters. Estuarine, Coastal and Shelf Science 55: 705–717.

Keppler, C. , Hoguet, J., Smith, K., Ringwood, A., Lewitus, A., 2005. Sublethal effects of the toxic alga *Heterosigma akashiwo* on the southeastern oyster (*Crassostrea virginica*). Harmful Algae 4:275–285.

Ketchum, B., 1954. Relation between circulation and planktonic populations in estuaries. Ecology 35:191-200.

Kianirad, E., Bedoya, D., Ghosh, I., McGarvey, K., 2006. Review of Watershed Ecological Models. Center for Urban Environmental Studies Northeastern University. Boston,p.88.

Koseff, J., Holen, J., Monismith, S., Cloern, J., 1993. Coupled effects of vertical mixing and benthic grazing on phytoplankton populations in shallow, turbid estuaries. J Mar Res 51:843-868.

Lavender, S., Pinkerton, M., Froidefond, J., Morales, J., Aiken, J., Moore, G., 2004. SeaWiFS validation in European coastal waters using optical and bio-geochemical measurements. Int. J. Remote Sensing 25(7–8):1481–1488.

Lee, Z., Carder, K., Arnone, R. (2002). Deriving inherent optical properties from water colour: A multi-band quasi-analytical algorithm for optically deep waters. Appl. Opt. 41: 5755-5772.

Lee, Z., Carder, K., Du, K. (2004). Effects of molecular and particle scatterings on model parameters for remote-sensing reflectance. Appl. Opt. 43:4957-4964.

Lee, Z., Carder, K., 2005. Hyperspectral Remote Sensing. In: Remote sensing of Coastal Aquatic Environments. Miller, R., Castillo, C., McKee, B. (eds).Springer. Dordrecht, p. 347.

Legendre, L., Demers, S., 1985. Auxiliary energy, ergoclines and aquatic biological production. Naturaliste Canadien 112:5-14.

Letelier, R., Abbott, M., 1996. An Analysis of Chlorophyll Fluorescence Algorithms for the Moderate Resolution Imaging Spectrometer (MODIS). Remote Sens. Environ. 58:215-223.

Li, G., Tang, Z., Yue, S., Zhuang, K., Wei, H., 2001. Sedimentation in the shear front off the Yellow River mouth. Continental Shelf Research 21:607–625.

Li, R., Kaufman, Y., Gao, B., Davis, C., 2003. Remote Sensing of Suspended Sediments and Shallow Coastal Waters. IEEE Transactions on Geoscience and Remote Sensing 41(3):559-566.

Lillesand, T., Kiefer, R., Chipman, J., 2004. Remote Sensing and Image Interpretation – Fifth Edition. John Wiley & Sons, Inc. United States of America, p. 763.

Liu, W., 2005. Water column light attenuation estimation to simulate phytoplankton population in tidal estuary. Environ. Geol. 49:280–292.

Longhurst, A., Sathyendranath, S., Platt, T., Caverhill, C., 1995. An estimate of global primary production in the ocean from satellite radiometer data. J. Plankt. Res. 17:1245–1271.

Lucas, L., Cloern, J., Koseff, J., Monismith, S., Thompson, J., 1998. Does the Sverdrup Critical Depth Model explain bloom dynamics in estuaries? J Mar Res 56(2):375-415.

Lucas, L., Koseff, J., Cloern, J., Monismith, S., Thompson, J., 1999a. Processes governing phytoplankton blooms in estuaries. I. The local production-loss balance. Mar. Ecol. Prog. Ser. 187:1-15.

Lucas, L., Koseff, J., Monismith, S., Cloern, J., Thompson, J., 1999b. Processes governing phytoplankton blooms in estuaries. II. The role of horizontal transport. Mar. Ecol. Prog. Ser. 187:17-30.

Macedo, M., Ferreira, J., Duarte, P., 1998. Dynamic behaviour of photosynthesis-irradiance curves determined from oxygen production during variable incubation periods. Mar. Ecol. Prog. Series, 165:31-43.

Macedo, M., Duarte, P., Ferreira, J., 2002. The influence of incubation periods on photosynthesis-irradiance curves. J. Exp. Marine Biol. Ecol. 274:101-120.

Macedo, M., Duarte, P., 2006. Phytoplankton production modelling in three marine ecosystems-static versus dynamic approach. Ecological Modelling 190:299-316.

Mallin, M., Pearl, H., Rudek J., Bates, P., 1993. Regulation of estuarine primary production by the watershed rainfall and river flow. Marine Ecology Progress Series 93: 199-203.

Mallin, M., 1994. Phytoplankton ecology of North Carolina estuaries. Estuaries 17: 561-574.

Malone, T., Crocker, L., Pike, S., Wendler, B., 1988. Influences of river flow on the dynamics of phytoplankton production in a partially stratified estuary. Marine Ecology Progress Series 48: 235-249.

Mansfield, E., 1986. Basic Statistics with Applications. W.W. Norton & Company, Inc. United States of America, p. 214.

Maritorena, S., Siegel, D., and Peterson, A., 2002. Optimization of a semianalytical ocean color model for global-scale applications. Appl. Opt. 41: 2705-2714.

Marra, J., Heinemann, K., 1982. Photosynthesis response by phytoplankton to sunlight variability. Limnol. Oceanogr. 27:1141-1153.

Marshall, H., Alden, R., 1990. A comparison of phytoplankton assemblages and environmental relationships in three estuarine rivers of the lower Chesapeake bay. Estuaries 13:287-300.

May, C., Koseff, J., Lucas, L., Cloern, J., Schoellhamer, D., 2003. Effects of spatial and temporal variability of turbidity on phytoplankton blooms. Mar. Ecol. Prog. Ser. 254, 111-128.

Miller, R., McKee, B., 2004. Using MODIS Terra 250 m imagery to map concentrations of total suspended matter in coastal waters. Remote Sensing of Environment 93:259-266.

Monbet, Y., 1992. Control of phytoplankton biomass in estuaries: a comparative analysis of microtidal and macrotidal estuaries. Estuaries 15:563-571.

Morel, A., Gentili, B., 1993. Diffuse reflectance of oceanic waters II: Bidirectional aspects. Appl. Opt. 32: 6864-6879.

Mutua, A., Mavuti, K., Daro, N., Tackx, M., 2004. Spatial Distribution of Suspended Particulate Matter in Mtwapa Creek and Funzi Bay, Kenya. Western Indian Ocean J. Mar. Sci. 3(1):29-36.

Muylaert, K., Kerckvoorde, A., Vyverman, W., Sabbe, K. 1997. Structural characteristics of phytoplankton assemblages in tidal and non-tidal freshwater systems: a case study from the Schelde basin, Belgium. Freshw Biol 38(2):263-276.

Nixon SW and 15 Co-authors, 1996. The fate of nitrogen and phosphorus at the land-sea margin of the North Atlantic Ocean. Biogeochemistry 35:141-180.

Nobre.A., Ferreira, J., Newton, A., Simas, T., Icely, J., Neves, R., 2005. Management of Costal Eutrophication: Integration of field data, ecosystem-scale simulations and screening models. Journal of Marine Systems 56:375-390.

Nunes, J., Ferreira, J., Gazeau, F., Lencart-Silva, J., Zhang, X., Zhu, M., Fang, J., 2003. A model for sustainable management of shellfish polyculture in coastal bays. Aquaculture 219:257-277.

Nybakken, J., 1993. Marine biology: an ecological approach. Harper Collins College Publishers. USA, p. 462.

Oliphant A, Susan C, Grimmond B, Schmid H., Wayson, C., 2006. Local-scale heterogeneity of photosynthetically active radiation (PAR), absorbed PAR and net radiation as a function of topography, sky conditions and leaf area index. Remote Sensing of Environment 103 (3): 324-337.

O'Reilly, J.E., and 24 Co-authors, 2000. SeaWiFS Postlaunch Calibration and Validation Analyses, Part 3. NASA Tech. Memo. 2000-206892, Vol. 11, S.B. Hooker and E.R. Firestone, Eds., NASA Goddard Space Flight Center, 49 pp. Parsons, T.R.; Takahashi, M. & Hargrave, B., 1984. Biological oceanographic processes, 3rd. ed., Pergamon Press, Oxford, 330 pp.

Pina, P., 2001. An Integrated Approach to Study the Tagus Estuary Water Quality; Dissertaçao para obtençao do grau de Mestre em Ecologi, Gestao e Modelação dos Recursos Marinhos; Instituto SuperiorTécnico, Universidade Técnica de Lisboa.

Pinty, B., Gobron, N., Mélin, F., Verstraete, M., 2002. Time Composite Algorithm for FAPAR products Theoretical Basis Document. Institute for Environment and Sustainability Joint Research Centre, p. 8.

Platt, T., Gallegos, C., Harrison, W., 1980. Photoinhibition of photosynthesis in natural assemblages of marine phytoplankton. J. Mar. Res. 38:687-701.

Platt, T., Bird, D., Sathyendranath, S., 1991. Critical depth and marine primary production. Proceedings: Biological Sciences 246:205-217.

Portela, L. 1996. Modelação matemática de processos hidrodinâmicos e de qualidade da água no Estuário do Tejo, Dissertação para obtenção do Grau de Doutor em Engenharia do Ambiente. IST, Universidade Técnica de Lisboa. Lisboa, p. 240.

Prahl, F., Small, L., Eversmeyer, B., 1997. Biogeochemical characterization of suspended particulate matter in the Columbia River estuary. Marine Ecology Progress Series 160:173-184.

Prandle, D., 2000. Introduction operational oceanography in coastal waters. Coastal Engineering. 41:3-12.

Prieur L., Sathyendranath, S., 1981. An optical classification of coastal and oceanic water based on the specific spectral absorption curves of phytoplankton pigments, dissolved organic matter, and other particulate materials. Limnol. Oceanogr. 26(4):671-689.

Raillard, O., Ménesguen, A., 1994. An ecosystem box model for estimating the carrying capacity of a macrotidal shellfish system. Marine Ecology Progress Series 15:117-130.

Ramos, P., 2002. Modelação matemática da qualidade da água no estuário do Tejo. Dissertação para a obtenção do grau de Mestre em Ecologia, Gestão e Modelação dos Recursos Marinhos. Instituto Superior Técnico. Universidade Técnica de Lisboa, p. 70.

Richardson, L., Ledrew, E., 2006. Remote sensing and science, monitoring, and management of aquatic coastal ecosystems. In: Remote sensing of Aquatic Coastal Ecosystem Processes. Richardson, L., Ledrew, E., (eds).Springer. Dordrecht, p. 347.

Richtel, M., 2007. Recruiting Plankton to Fight Global Warming, New York Times.

Rosenqvist, A., Milne, A., Lucas, R., Imhoff, M., Dobson, C., 2003. A review of remote sensing technology in support of the Kyoto Protocol. Environ. Sci. Policy 6 (5):441-455.

Ruddick, K., Ovidio F., Rijkeboer, M., 2000. Atmospheric correction of SeaWiFS imagery for turbid coastal and inland waters. Applied Optics, 39(6):897–912.

Saraiva, A., 2001. Produção primária de biomassa no estuário do Tejo – Estudo da variabilidade das descargas. Trabalho Final de Curso da Licenciatura em Engenharia do Ambiente. Instituto Superior Técnico. Universidade Técnica de Lisboa. Lisboa, p. 170.

Schalles, J., 2006. Optical remote sensing techniques to estimate phytoplankton chlorophyll-a concentrations in coastal waters with varying suspended matter and CDOM concentratrions. In: Remote sensing of Aquatic Coastal Ecosystem Processes. Richardson, L., Ledrew, E., (eds).Springer. Dordrecht, p. 347.

Shutler, J., Land, P., Smyth, T., Groom, S., 2006. Extending the MODIS 1 km ocean colour atmospheric correction to the MODIS 500 m bands and 500 m chlorophyll-a estimation towards coastal and estuarine monitoring. Remote Sensing of Environment 107: 521-532.

Selmer J., Rydberg, L., 1993. Effects of nutrient discharge by river water and waste water on the nitrogen dynamics in the archipelago of Goteborg, Sweden. Marine Ecology Progress Series 92: 119-133.

Siegel, D., Wang, M., Maritorena, S., Robinson, W. 2000. Atmospheric correction of satellite ocean color imagery: The black pixel assumption. Applied Optics 39:3582- 3591.

Simas, T., Nunes, J., Ferreira, J., 2001. Effects of global climate change on coastal salt marshes. Ecol. Model. 139 (1):1-15.

Simas, T., Ferreira, J., 2007. Nutrient enrichment and the role of salt marshes in the Tagus estuary (Portugal). Estuarine, Coastal and Shelf Science 75:393-407

Sin, Y., Wetzel, R., Anderson, I., 1999. Spatial and temporal characteristics of nutrient and phytoplankton dynamics in the York River estuary, Virginia: Analysis of long-term data. Estuaries 22:260-275.

Smayda, T., 1997. Harmful algal blooms: their ecophysiology and general relevance to phytoplankton blooms in the sea. Limnol. Oceanogr. 42:1137-1153.

Steele, J., 1962. Environmental control of photosynthesis in the sea. Limnol. Oceanogr. 7:137-150.

Stumm, W., Morgan, J., 1981. Aquatic Chemistry: An Introduction Emphasizing Chemical Equilibria in Natural Waters, 2nd ed. New York: John Wiley & Sons.

Stumpf, R., Arnone, R., Gould, R., Martinolich, P., Ransibrahmanakul, V., Tester, P., Steward, R., Subramaniam, A., Culver, M., Pennock, J., 2000. SeaWiFS ocean color data for US Southeast coastal waters. In: Proceedings of the Sixth International Conference on Remote-Sensing for Marine and Coastal Environments. Veridan ERIM International. Ann Arbor, MI. USA, p. 25-27.

Stumpf, R., Arnone, R., Gould,R., Martinolich, P., Ransibrahmanakul, V., 2003. A Partially Coupled Ocean-Atmosphere Model for Retrieval of Water-Leaving Radiance from SeaWiFS in Coastal Waters, NASA/TM-2003-206892, Vol. 22NASA Goddard Space Flight Center. Greenbelt. Maryland, p. 51-59.

Sverdrup, H., 1953. On conditions for the vernal blooming of phytoplankton. Journal du Conseil pour l'Exploration de la Mer 29:130-135.

Talling, J., 1971. The underwater light climate as a controlling factor in the production ecology of freshwater phytoplankton. Mitteilungen Internationale Vereiningung fuer Theoretische und Angewandte Limnologie 19:214-243.

Tett, P., Gilpin, L., Svendsen, H., Erlandsson, C., Larsson, U., Kratzer, S., Fouilland, E., Janzen, C., Lee, J., Grenz, C., Newton, A., Ferreira, J., Fernandes, T., Scory, S., 2003. Eutrophication and some European waters of restricted exchange. Cont. Shelf Res. 23: 1635-1671.

Trancoso, A., 2002. Modelling Macroalgae in Estuaries. Trabalho Final de Curso da Licenciatura em Engenharia do Ambiente. Universidade Técnica de Lisboa – Instituto Superior Técnico. Lisboa, p. 87.

Trancoso, A., Saraiva, S., Fernandes, L., Pina, P., Leitão, P., Neves, R., 2005. Modelling macroalgae using a 3D hydrodynamic-ecological model in a shallow, temperate estuary. Ecological Modelling 187:232-246.

Tzortziou, M., Subramaniam, A., Herman, J., Gallegos, C., Neale, P., Harding Jr., L., 2007. Remote sensing reflectance and inherent optical properties in the mid Chesapeake Bay. Estuarine, Coastal and Shelf Science 72:16-32.

Underwood, G., Kromkamp, J., 1999. Primary production by phytoplankton and microphytobenthos in estuaries. Advances in Ecological Reser 29:93-153.

Valiela, I., 1995. Marine ecological processes. Springer-Verlag. New York, p. 686.

Valiela, I., McClelland, J., Hauxwell, J., Behr, P., Hersh, D., Foreman, K., 1997. Macroalgal blooms in shallow estuaries: controls and ecophysiological and ecosystem consequences. Limnol Oceanogr 42:1105-1118.

Vander Woude, A., Largier, J., Kudela, R., 2006. Nearshore retention of upwelled waters north and south of Point Reyes (northern California)—Patterns of surface temperature and chlorophyll observed in CoOP WEST. Deep-Sea Research II 53:2985-2998.

Walters, R., Cheng, R., Conomos, T., 1985. Time scales of circulation and mixing processes of San Francisco Bay waters. In: Hydrobiologia 129:13-36.

Wang, M., W. Shi, 2005. Estimation of ocean contribution at the MODIS near-infrared wavelengths along the east coast of the U.S.: Two case studies, Geophys. Res. Lett., p. 32.

Webb, W., Newton, M., Starr, D., 1974. Carbon dioxide exchange of Alnus rubra: a mathematical model. Oecologia 17:281-291.

Wetzel, R., 1993. Limnology 2nd edition. Fundação Calouste Gulbenkian. Lisboa, p. 1016.

Wynne, T., Stumpf, R., Richardson, A., 2006. Discerning resuspended chlorophyll concentrations from ocean color satellite imagery. Continental Shelf Research 26:2583-2597.

Zaneveld, J., Twardowski, M., Barnard, A., Lewis, M., 2005. Introduction to radiative transfer. In: Remote sensing of Coastal Aquatic Environments. Miller, R., Castillo, C., McKee, B. (eds).Springer. Dordrecht, p. 347.

Zawada, D., Hu, C., Clayton, T., Chen, Z., Brock, J., Muller-Karger, F., 2007. Remote sensing of particle backscattering in Chesapeake Bay: A 6-year SeaWiFS retrospective view. Estuarine, Coastal and Shelf Science 73:792-806.

Zhang, B., Zhang, Y., Song, K., Zhang, B., 2004. Detection of sea surface temperature (SST) using thermal infrared band data of AVHRR and MODIS in the Gulf of Bohain Sea of China. International Journal of Infrared and Millimeter Waves 25(1):129-137.

Zhang, C., Hu, C., Shang, S., Muller-Karger, F., Li, Y., Dai, M., Huang, B., Ning, X., Hong, H., 2006. Bridging between SeaWiFS and MODIS for continuity of chlorophyll-a concentration assessments off Southeastern China. Remote Sensing of Environment 102:250-263.

Zhang, Y. Pulliainen, J., Koponen, S., Hallikainen, M., 2002a. Detection of sea surface temperature (SST) using infrared band data of AVHRR in the Gulf of Finland. International Journal of Infrared and Millimeter Waves, 23(10):1407-1412.

Zhang, Y., Pulliainen, J., Koponen, S., Hallikainen, M., 2002b. Application of an empirical neural network to surface water quality estimation in the Gulf of Finland using combined optical data and microwave data. Remote Sensing of Environment 81:327-336.

Zhang,Y., Fu, F., Whereat, E., Coyne, K., Hutchins,D., 2006. Bottom-up controls on a mixed-species HAB assemblage: A comparison of sympatric Chattonella subsalsa and Heterosigma akashiwo (Raphidophyceae) isolates from the Delaware Inland Bays, USA. Harmful Algae 5:310-320.

INTERNET

http://www.livephytoplankton.com/ - General Phytoplankton Information, consulted in September, 2007.

http://www.maretec.mohid.com/PortugueseEstuaries/Tagus/DirectivesAplication/22_Tagus_WaterQualityConclusion.htm - Tagus Estuary - EU Directives, consulted in September, 2007.

http://www.ecowin.org/c2c/#Framework%20and%20Scope – Project Catchment to Coast, consulted in October, 2007.

http://www.ecasa.org.uk/ - Project Ecosystem Approach for Sustainable Aquaculture, consulted in October, 2007.

http://www.biaoqiang.org/ - Project Sustainable options for PEople, catchment and Aquatic Resources (SPEAR), consulted in October, 2007.

http://www.eutro.org - Assessment of Estuarine Trophic Status (ASSETS), consulted in October, 2007

http://en.wikipedia.org/wiki/Redfield_ratio - Redfield Ratio, 15 August, 2007

www.aml.pt - Great Lisbon Population; 2 September, 2007

www.insaar.inag.pt – National inventory of public supply systems and wastewater (Inventário Nacional de Sistemas de Abastecimento e Aguas Residuais – INSAAR), 20 September, 2007

http://aqua.nasa.gov/ - MODIS AQUA Project Science, 20 January, 2008

http://ladsweb.nascom.nasa.gov/ - Level 1 and Atmosphere Archive and Distribution System (LAADS) NASA, consulted between October 2007 and January 2008.

http://oceancolor.gsfc.nasa.gov/ - NASA Ocean Color Web, consulted between October 2007 and January 2008.

http://oceancolor.gsfc.nasa.gov/VALIDATION/flags.html - Level 2 Ocean Quality Flags, consulted in December 2008.

ANNEX I – FORCING FUNCTIONS CALIBRATION

1. LIGHT OBJECT CALIBRATION

In order to fill punctual gaps of the Monte Caparica station, the radiation values measured at the Vila Franca de Xira station were defined as a function of the former, thru linear regression. Both stations have radiation values since 2001, and the latter station, has scarce and interspersed data and was, therefore, excluded. The relationship derived presented good agreements (Table 1) providing confidence in data gap filling.

Table 21 - Regression statistics between Monte Caparica and Vila Franca de Xira stations

Year	Number of Samples (N)	Correlation (*r*)	RMSE
2002	8486	0.90	40.3
2003	8566	0.97	4.4
"Average Year"	8566	0.92	26.50

The figures below exhibit the scatter plot of coincident hourly radiation values measured at both stations for 2002 (Figure 51) and 2003 (Figure 52). Note that in 2002, there are some large radiation values will null correspondence.

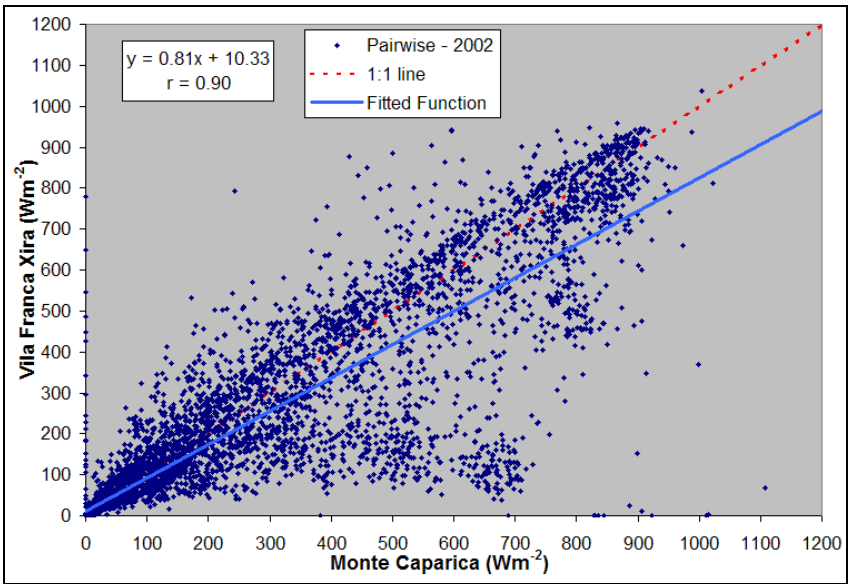

Figure 51 - Pairwise scatter plot: hourly radiation values (2002)

An average year was defined, has the arithmetic average of 2002 and 2003 hourly radiation values in Monte Caparica station, and aggregated into daily average radiation in order to simplify the light object calibration process, maintaining ecological significance (e.g. Grillot & Ferreira, 1996).

Moreover, this choice was made to account for error overestimation due to:

a) occasional night time radiation positive values;

b) systematic 1 to 2 hours shift between measured and modelled values

c) smoothing of errors in radiation measurement.

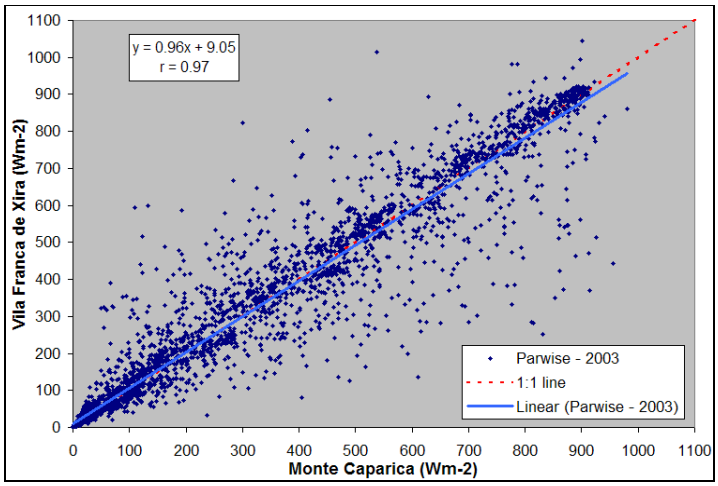

Figure 52 - Pairwise scatter plot: hourly radiation values (2003)

The three distinct daily datasets are shown in Figure 53.

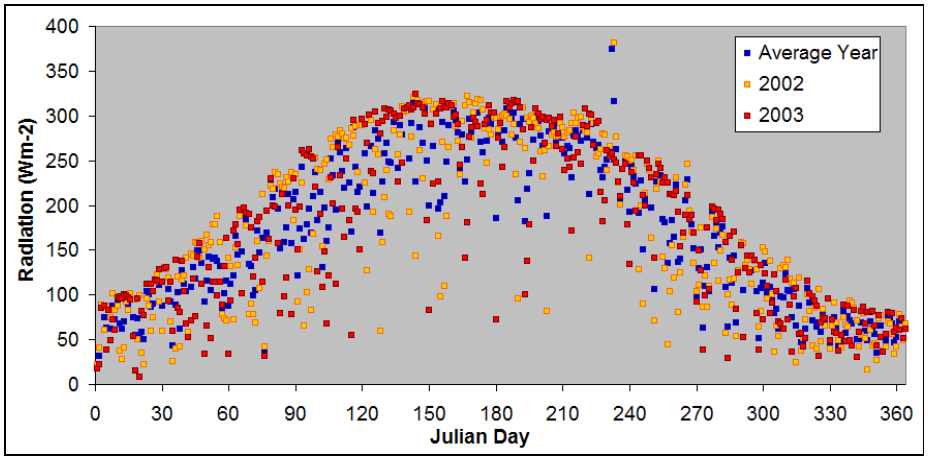

Figure 53 - Daily average radiation values distribution (Monte da Caparica)

Photoperiod and top of the atmosphere radiation were calculated by the light object and the latter was limited according to a fractional cloud cover, which varies from 0 to 1, defined by a dynamic periodic function, relating the time of the year (Julian day) with the cloud coverage (Equation 9).

$$CloudCover = ModalCloud + \cos\left(\pi \times \left(\frac{JulianDay + CloudPeak}{CloudPhase}\right)\right) \times CloudAmplitude \qquad \textbf{Equation 16}$$

The above function models the seasonal cloud distribution. The "average year" was set to represent all years used. Calibration parameters (Table 22) corresponded to 19.5% errors with good correlation, $r^2 = 0.93$ (N=365).

Table 22 - Set of parameters used in the light object calibration

Year	Latitude (º)	Modal Cloud	Cloud Peak (Julian day)	Cloud Phase (º)	Cloud Amplitude
Average Year	40.5	0.6	350	180	0.1

2. FLOW OBJECT CALIBRATION

Flow was modelled using a yearly cosine function based on the modal flow, the amplitude variation and daily random flow (Equation 17), typically calibrated using field data. T_{flow} is the river flow; T_{modal} is the modal flow; τ, the calculation timestep; λ a lag factor; maxh the maximum amplitude; f_r the random fluctuation (Ferreira, 1995).

$$T_{flow} = T_{modal} + \left(\cos\left(\frac{\pi \times (\tau - \lambda)}{180} \right) \times (\max h + f_r) \right) \qquad \textbf{Equation 17}$$

The Almourol INAG station (17G/02H), about 40 kilometers upstream the former, with data since 1999, was used to model flow values for the Ómnias station using 2002 and 2003 coincident data. The relationship derived follows a power law function, with good agreement r^2 = 0.82 (N=674), enabling flow simulation at the Ómnias station from 1998 to 2001 also used in latter years gap filling. Each year was treated independently. The agreement decreases when flows are higher than 600m^3s^{-1} (Figure 54).

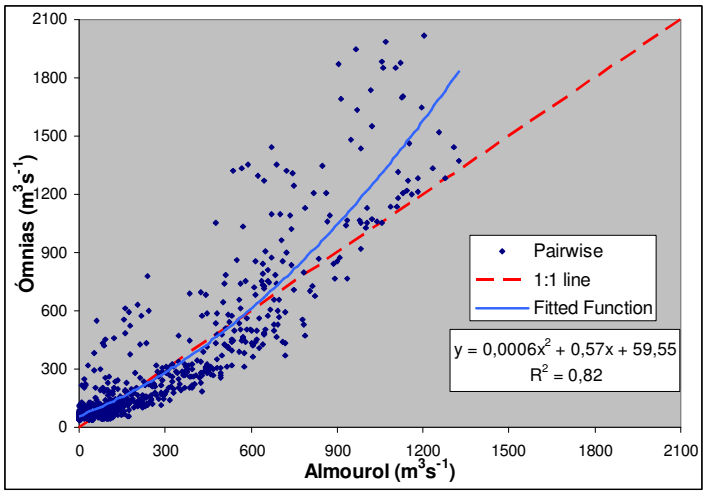

Figure 54 - Pairwise scatter plot : Daily flow m^3s^{-1} (2002 and 2003)

The function was fitted for a 0-2100 m^3s^{-1} range and when applied to flows outside this interval, the data confidence was lower. For instance, in the year 2001, the highest monthly flow, recorded in Almourol station, was 2900 m^3s^{-1} and the simulated flow was about 6700 m^3s^{-1}. This can potentially introduce significant errors. Firstly, the E2k flow standard object was compared with month average flows (Table 23). Random flow was set to null favouring model stability. High flow events in typically dry months (and vice versa) are examples of

phenomena which were not simulated accurately using the E2k flow function, and therefore, another approach was tested.

Table 23 - E2k flow simulation performance

	1998	1999	2000	2001	2002
RMSE	143	109	300	1000	205
MAE (%)	82%	69%	92%	336%	75%
r	0.55	0.63	0.63	<0	0.22

Secondly, polynomial equations were adjusted to daily flows, resulting in periods with negative simulated flow. Therefore, to simplify the programming effort, 4th and 5th order polynomial equations were fitted to monthly averaged daily flows and inserted in the E2k code leading to increased accuracy, however, with significant errors (Table 24).

Table 24 - Statistics regarding monthly averaged daily flows (polynomial)

	1998	1999	2000	2001	2002
RMSE	164	43	233	603	64
MAE (%)	29%	32%	89%	75%	160%
r	0.96	0.92	0.92	0.97	0.93

3. ADVECTION-DISPERSION

The advection-dispersion object was calibrated matching salinity samples, taken between 1998 and 1999, with E2K simulations. The first year had a significantly higher average salinity and total flow than the second, especially for the winter months. The calibration performed slightly increased the model accuracy (Figure 55) when compared with a reference run (Ferreira and Duarte, 1994) (Figure 56).

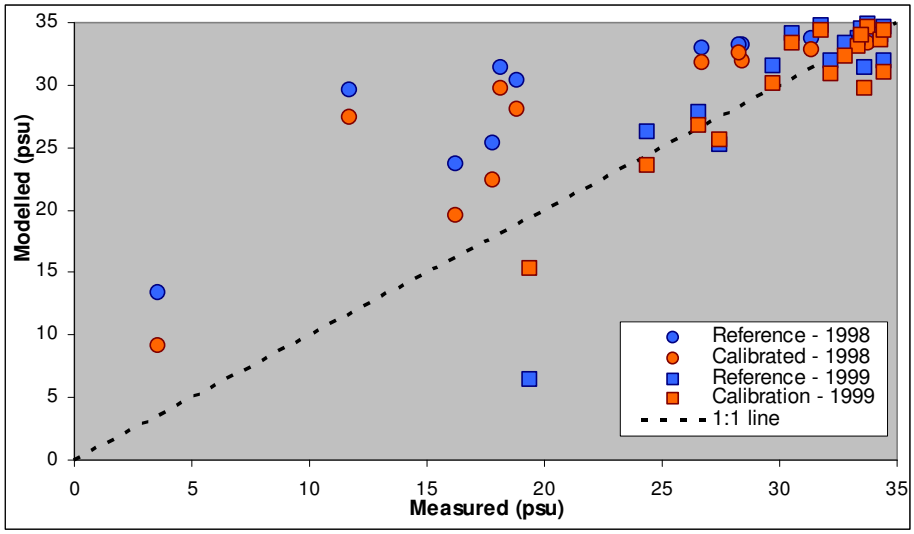

Figure 55 - Pairwise salinity comparison: measured *vs.* modelled

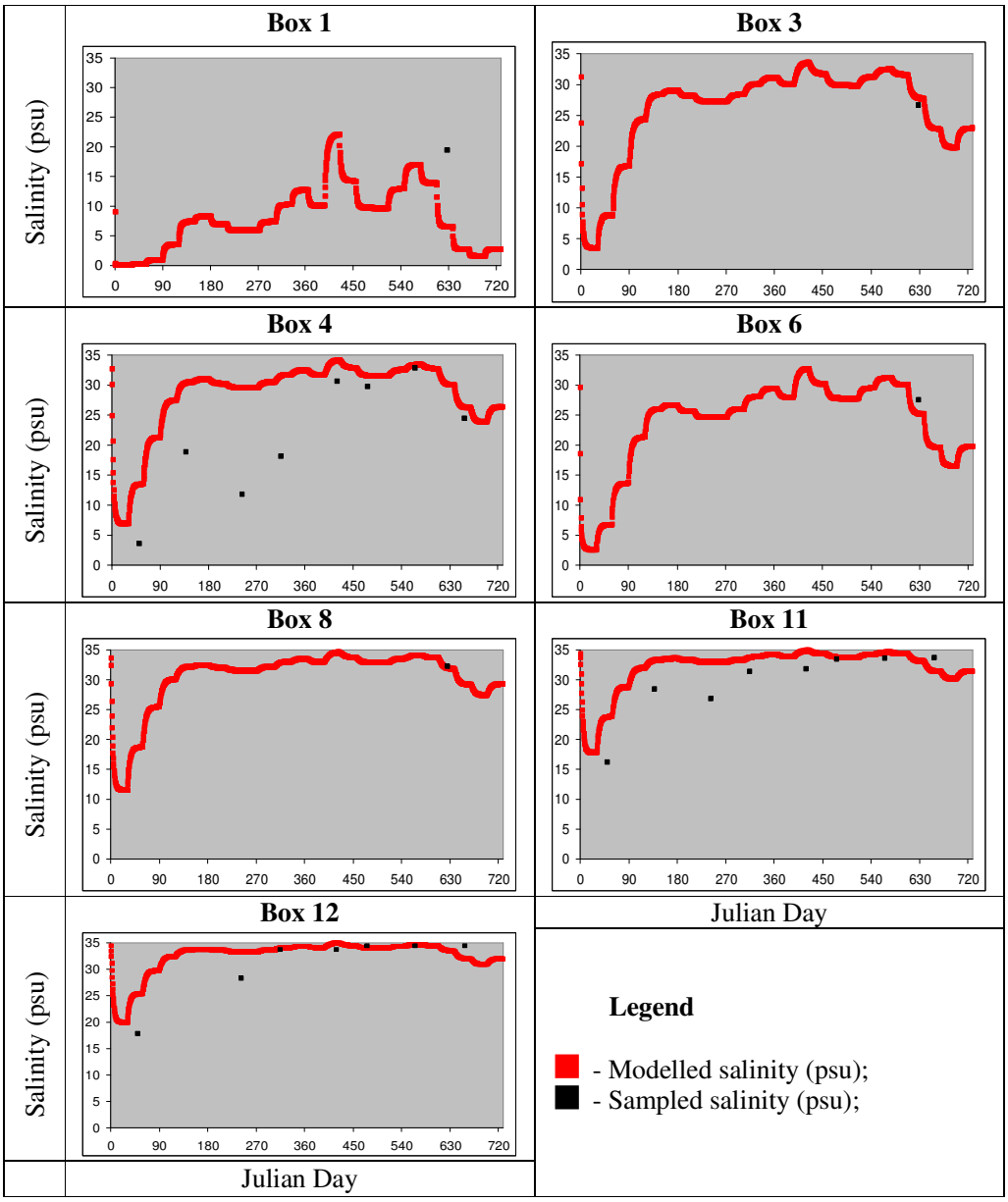

Figure 56 - Reference time series box by box: Sampled *vs.* modelled

ANNEX II – SPM AND ZOOPLANKTON CALIBRATION

1. SPM OBJECT CALIBRATION

SPM in-situ measurements were available for 9 boxes and system boundaries, the Tagus river and ocean. The best parameters achieved, concerning the calibration dataset were turbulence = 1.1 and box resuspension as detailed in Table 25.

Table 25 - Parameters achieved in SPM calibration (sampled data)

Box	1	2	3	4	5	6	7	8	9	10	11	12	13
Ressuspension (%)	0	0	4	0	0	6	5	0	0	0	0	0	0

The comparison with other studies, historical data and sampled data indicates that simulated SPM was significantly underestimated. Another calibration effort was performed to include a broader insight, temporal and spatially, using a mixture of historical data, reference studies and the calibration dataset (Table 26). The best parameters achieved are described in Table 27 considering the same turbulence. Quantitative assessment is not possible and therefore qualitative evaluation was made thru visual inspection of Figure 57.

Table 26 - Historical and reference studies comparison

	Historical data (1980-1995)	**Sampled 1998-1999**	**Gameiro et al. 2004**	**Fernandes, 2005**	**Brogueira and Cabeçadas, 2006**	**Proposed**
Box 3	65	40 (1)	40	-	40-50	40-50
Box 4	49	15 (8)	50	-	-	30-45
Box 6	97	38 (1)	-	-	35-50	40-50
Box 8	66	34 (1)	20	20-30	35-50	25-35
Box 10	49	30 (1)	-	5-15	10-40	20-35
Box 11	25	10 (9)	-	5-10	10-35	10-15
Boxes 12 & 13	16	8 (9)	-	5	10-35	10-15**

* The values in parenthesis mean number of samples
** Ramos (2002) was also considered (see text)

Table 27 - Parameters achieved in SPM calibration (historical and reference data)

Box	1	2	3	4	5	6	7	8	9	10	11	12	13
Ressuspension (%)	0	0	10	4	4	9	6	2	0	0	0	0	0

Simulated values are relatively within ranges and are in some cases significantly higher than the ones modelled according to measured data in 1998 and 1999. Still, the mid estuary is underestimated and the downstream boxes slightly overestimated, except for box 13. The simulation does not reproduce the longitudinal exponential SPM gradient from mid to downstream estuary (Fernandes, 2005).

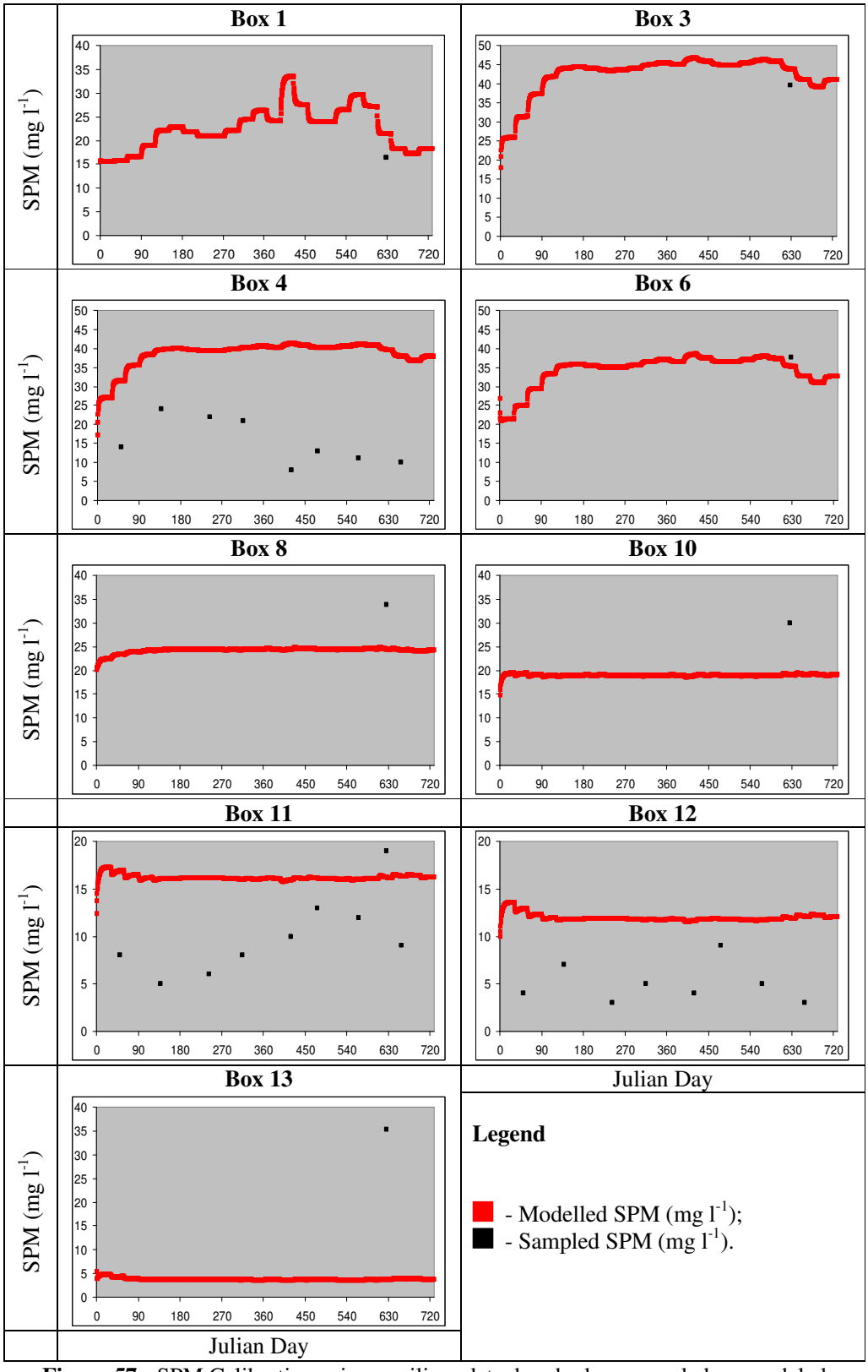

Figure 57 - SPM Calibration using auxiliary data, box by box: sampled *vs.* modeled

2. ZOOPLANKTON OBJECT CALIBRATION

The parameters used for the calibration of the zooplankton object, described in Table 28, were adapted from Ferreira and Duarte (1994). A thorough description of the equations and parameters used is provided in Parsons et al. (1984).

Table 28 - Parameters used in the zooplankton object

Parameter	Description	Units	Value
KGraze	Proportionality Constant for Zooplankton Ration	$(\mu g\ C\ l^{-1})^{-1}$	0,01
PhytoLowerLimit	Minimum Phytoplankton concentration at which feeding starts	$\mu g\ C\ l^{-1}$	40
Rmax	Maximum ration	mg FW $(mg\ FW)^{-1}$ day^{-1}	5
Death Loss	Death loss	day^{-1}	0,05
Metabolism	Fraction of energy used for zooplankton activity, internal maintenance, digestion and growth	%	0,75
MaximumDeathLoss	Maximum death loss	day^{-1}	0,75
KZooStarvedByPhyto	Proportionality Constant relating Zooplankton Death Loss and Phytoplankton concentration	$(\mu g\ Chla\ l^{-1})^{-1}$	0,1

ANNEX III - Boundary Conditions and Dissolved Substances Calibration

1. Boundary Conditions

This annex provides a brief description of the boundary conditions defined for the calibration process (1998, 1999), validation and model application (2000-2002). Three types of boundaries are considered in the model: Tagus river, ocean and smaller estuary affluents, such as small rivers, streams and WWTP's. The particulate and dissolved substances are nutrients, SPM, phyto and zooplankton. The E2k requires the definition of a constant concentration throughout the simulation period concerning each boundary. The substances loading into the Tagus estuary can be variable, for the river and ocean, or constant, for the smaller affluents. Loading behaviour is therefore driven by the boundary flow modelling. Advective river flow varies in a month scale concerning independent years. Ocean flow, from a tidally averaged standpoint, is done by diffusion transport. For the smaller affluents a constant flow and concentration were defined (Ferreira, pers.comm.; INAG, 2002; www.insaar.inag.pt). For the coincident boundaries concerning both data sources, modelled and measured ammonia were compared tuning flow and concentration within ranges and depending on the need to simulate higher or lower loadings, thus improving the nutrients object accuracy. Note that, this is highly dependent on phytoplankton concentration and therefore a reference simulation was defined to access if there were significant modelled to measured differences. For the three distinct periods, the concentration at the river and ocean is presented in Table 29 and

Table 30, for smaller affluents in Table 31 and Figure 58. Two different data sources were used. The INAG station Valada do Tejo (19E/02) with monthly measurements was used specifically for the Tagus river. The BarcaWin2000 software with punctual samples that result from campaigns performed in the Tagus estuary was used for both river and ocean. No zooplankton data was available and were defined according to Ferreira and Duarte (1994), 15 and 2 mgm^{-3} for river and ocean respectively.

Table 29 - Boundary conditions for the Tagus river and ocean – Calibration

Variable	Units	Tagus River		Ocean	
Ammonia	µmol l^{-1}	4.1	a	1.0	b
Nitrite	µmol l^{-1}	0.7	a	0.3	b
Nitrate	µmol l^{-1}	55.0	a	5.0	b
Phosphate	µmol l^{-1}	6.2	a	0.4	b
Silica	µmol l^{-1}	88.5	a	3.8	b
Phytoplankton	µg Chl*a* l^{-1}	10.1	a	1.7	b
Suspended matter	mg l^{-1}	15.4	a	2.0	b

The different letters refer to the data source: INAG station (a) and BarcaWin2000 (b)

Table 30 - Boundary conditions for the Tagus river and ocean – Calibration

Variable	Units	Tagus River		Ocean	
Ammonia	µmol l^{-1}	3.6	a	1.6	b
Nitrite	µmol l^{-1}	0.7	a	0.4	b
Nitrate	µmol l^{-1}	58.1	a	5.2	b
Phosphate	µmol l^{-1}	6.9	a	0.5	b
Silica	µmol l^{-1}	101.9	a	4.9	b
Phytoplankton	µg Chl*a* l^{-1}	13.6	a	2.1	b
Suspended matter	mg l^{-1}	13.5	a	1.5	b

The different letters refer to the data source: INAG station (a) and BarcaWin2000 (b)

Table 31 - Boundary description and setting for smaller estuary affluents (Ferreira, personal communication; INAG, 2002 and www.insaar.inag.pt)

Boundary	Description	Ammonia (µmol l^{-1})	Flow (m^3s^{-1})	Box connection
3	Sorraia River	43	39.50	6
4	Trancão River	1000	5.00	5
5	Portinho da Costa Caparica	3000	0.24	13
6	Almada	3000	0.25	11
7	Seixal	3000	0.24	11
8	Palhais	1029	0.79	11
9	Coina	3000	0.05	11
10	Pinhal do General	3000	0.03	11
11	Barreiro	3000	0.46	10
12	Moita	3000	0.11	9
13	Afonsoeiro	3000	0.13	9
14	Seixalinho	3000	0.17	9
15	Pegões Gare	3000	0.03	8
16	Pegões Velhos	3000	0.02	8
17	Faias	3000	0.02	8
18	Passil Terroal	3000	0.01	8
19	Atalaia	3000	0.00	8
20	Alcochete	3000	0.02	8
21	Alverca	3000	0.18	2
22	Granja Alpriate	3000	0.01	3
23	Ponte de Frielas	3000	0.69	3
24	Povoa da Galega	3000	0.00	3
25	Beirolas	3000	0.31	5
26	Chelas	3000	0.23	10
27	Alcantara	3000	0.53	12
28	S. João da Talha	3000	0.14	5
29	Quinta da Bomba	936	0.71	11

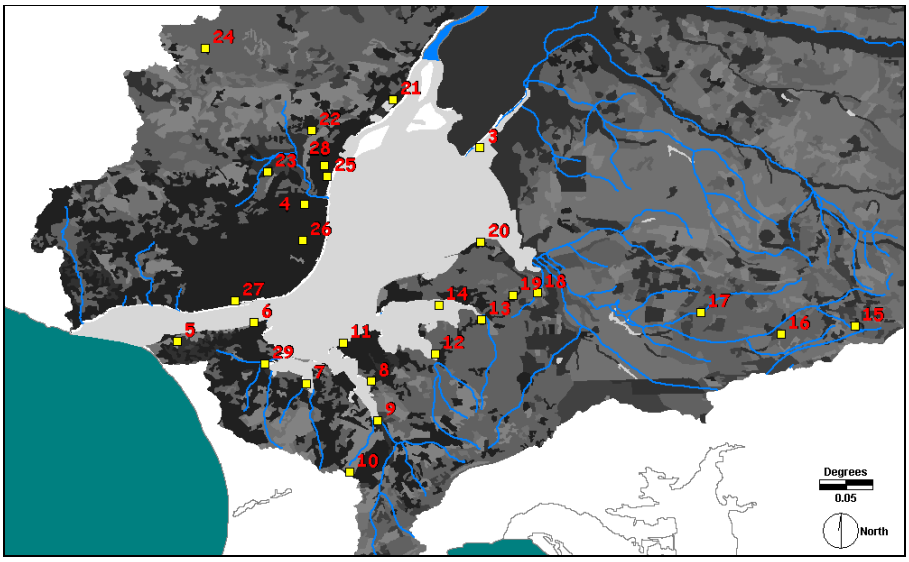

Figure 58 - Pollution Sources in the Tagus watershed

2. Dissolved Substances Calibration

The comparison of modelled with sampled nitrate, phosphate and silicate in the calibration years is exhibited in Figure 59, Figure 60 and Figure 61 respectively. Performance statistics in Table 32, Table 33 and Table 34. Nitrate is modelled with about 80% or 19 µmol l^{-1} error but exhibiting good temporal agreement, r=0.84. Phosphate is simulated with lower errors than the former, 51% and 2.8 µmol l^{-1} and silicate is with 47% and 25.2 µmol l^{-1}.

Table 32 - Nitrate Calibration : performance statistics box by box and ecosystem scale

	Box1	Box3	Box4	Box6	Box8	Box10	Box11	Box12	Box13	Global
Matches	1	1	8	1	1	1	9	8	1	**31**
RMSE	18.0	26.6	26.9	22.8	20.7	0.1	17.1	10.3	1.2	**18.8**
MAE (%)	35%	64%	151%	60%	66%	1%	79%	40%	16%	**80%**
r	-	-	0.82	-	-	-	0.74	0.86	-	**0.84**

Table 33 - Phosphate Calibration : performance statistics box by box and ecosystem scale

	Box1	Box3	Box4	Box6	Box8	Box10	Box11	Box12	Box13	Global
Matches	1	1	8	1	1	1	9	8	1	**31**
RMSE	1.0	2.0	5.0	1.5	2.1	1.2	1.9	0.6	0.2	**2.8**
MAE (%)	21%	50%	66%	41%	63%	53%	54%	39%	23%	**51%**
r	-	-	-0.15	-	-	-	0.09	0.63	-	**0.25**

Table 34 - Silicate Calibration : performance statistics box by box and ecosystem scale

	Box1	Box3	Box4	Box6	Box8	Box10	Box11	Box12	Box13	Global
Matches	1	1	8	1	1	1	9	8	1	**31**
RMSE	27.9	1.7	42.9	3.9	2.4	5.0	16.9	15.5	0.2	**25.2**
MAE (%)	77%	8%	60%	21%	18%	143%	40%	44%	6%	**47%**
r	-	-	0.67	-	-	-	0.97	0.96	-	**0.72**

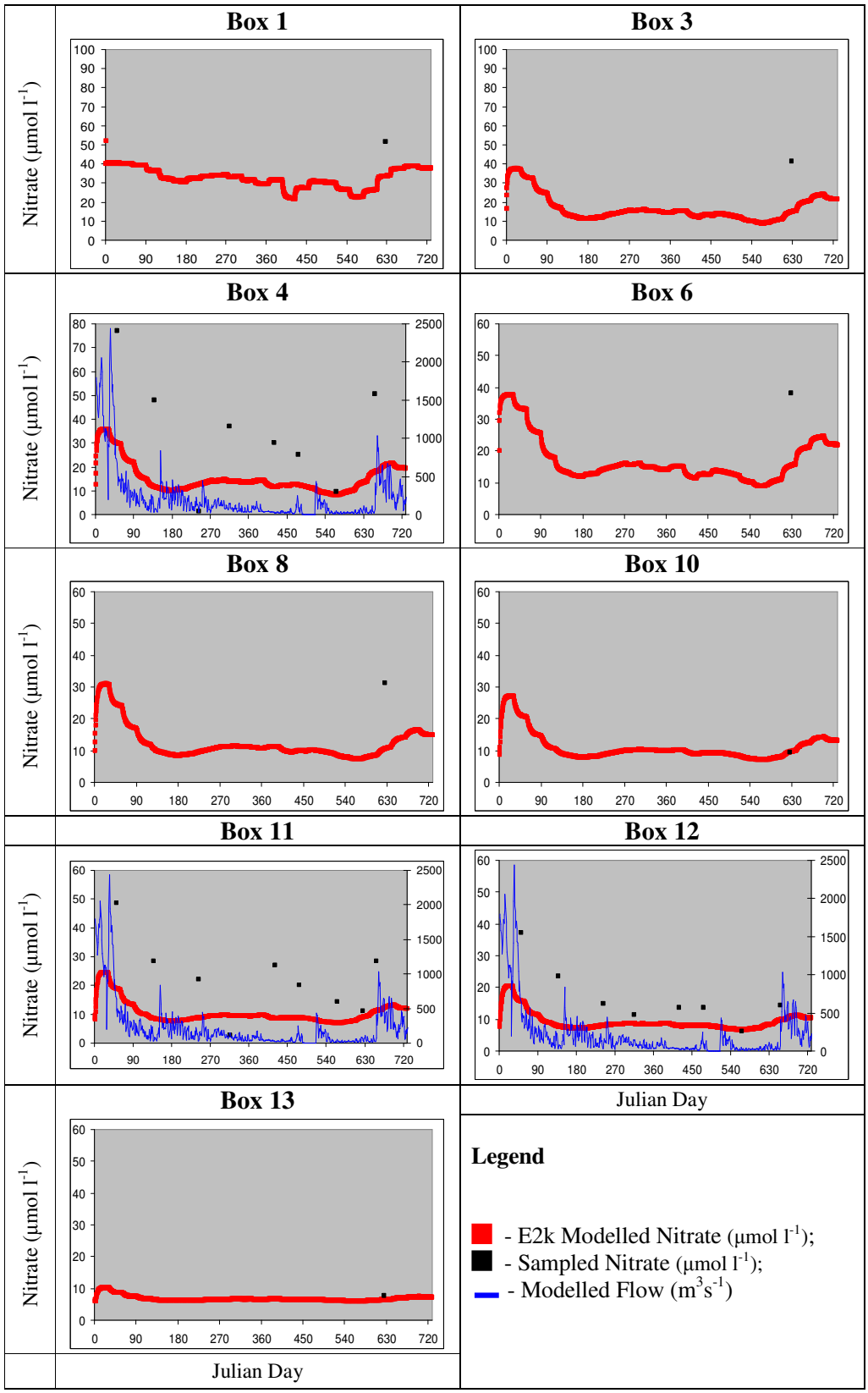

Figure 59 - Nitrate Calibration box by box: sampled *vs.* modelled

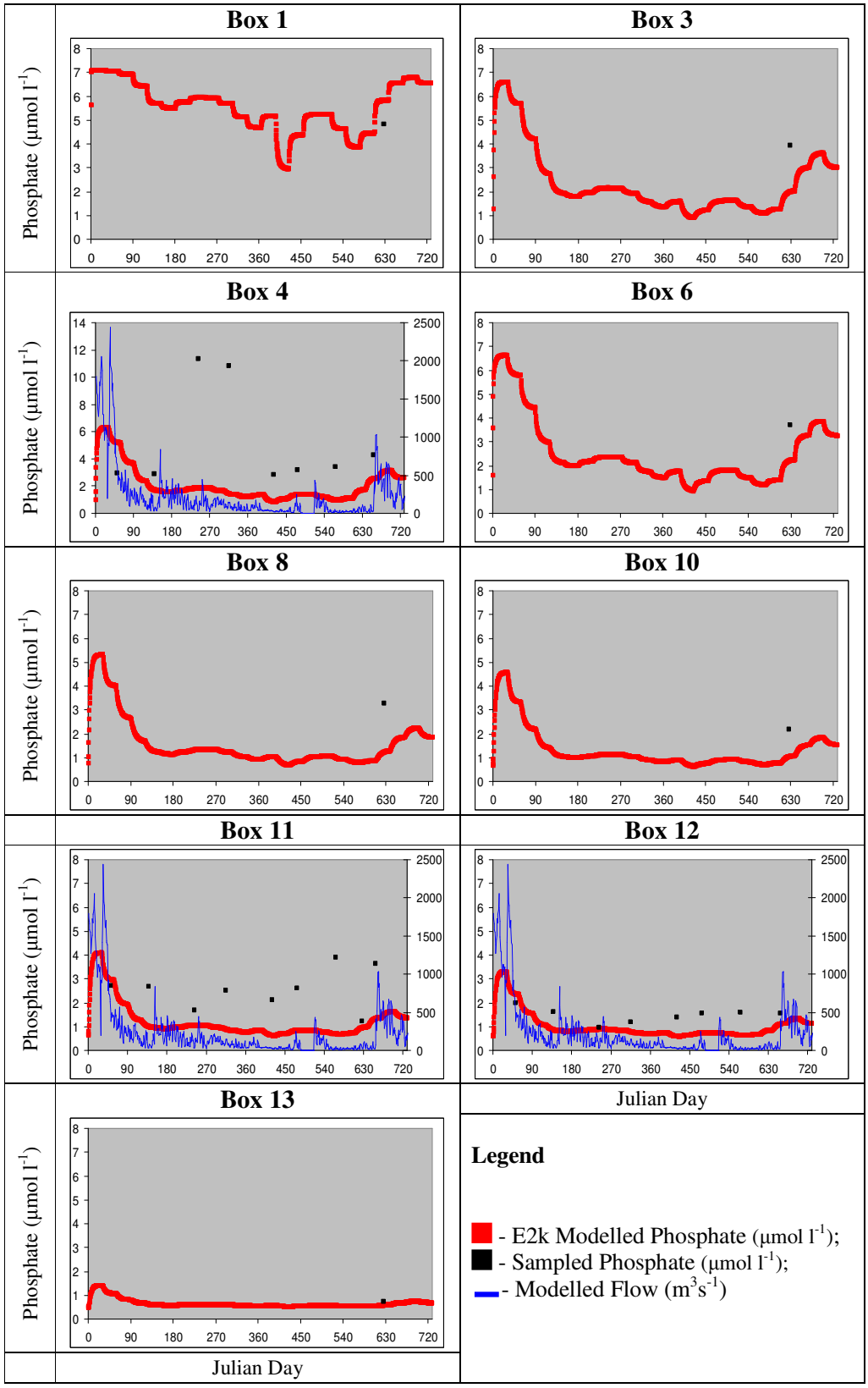

Figure 60 - Phosphate Calibration box by box: sampled *vs.* sampled

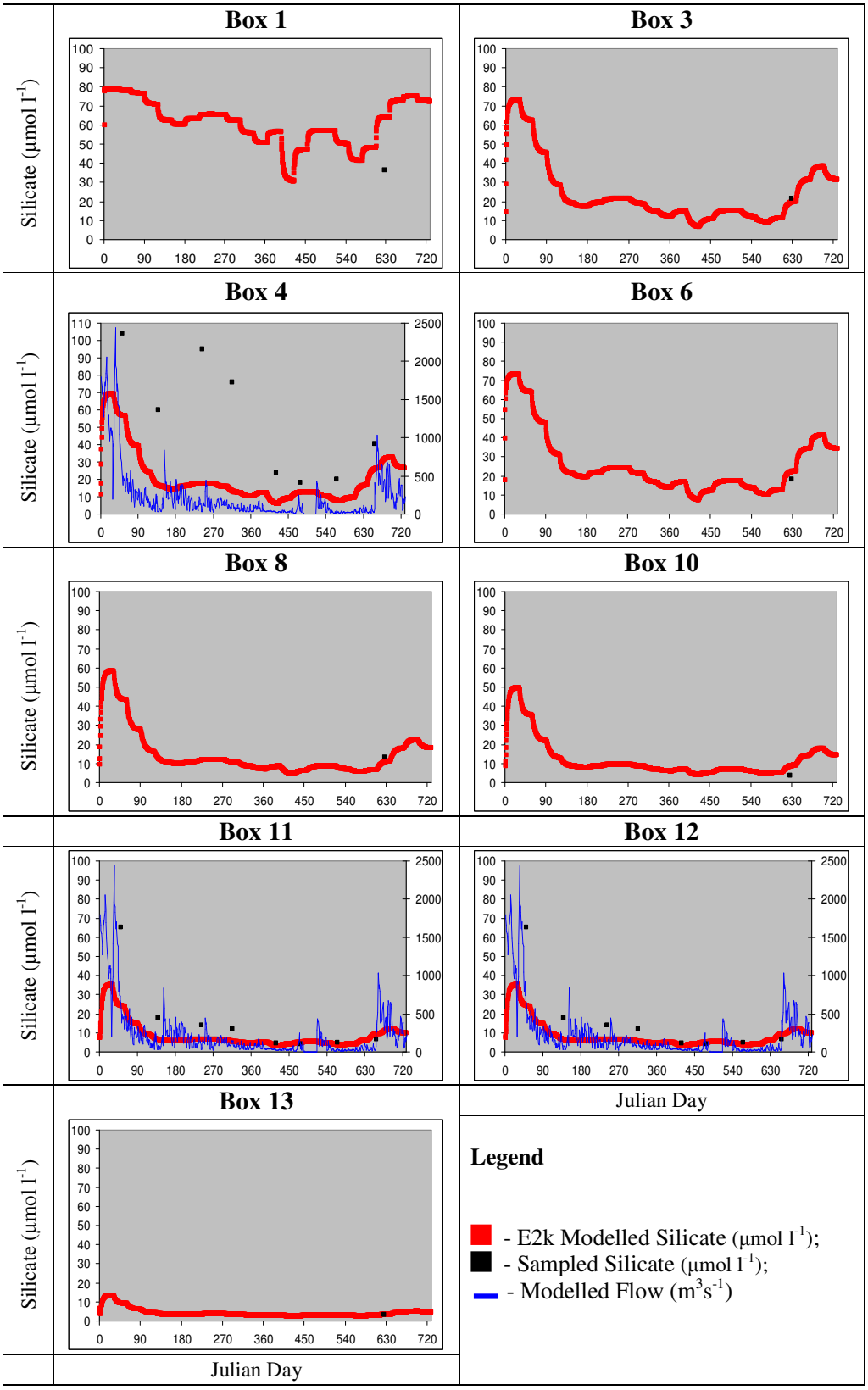

Figure 61 - Silicate Calibration box by box: sampled *vs.* modelled

ANNEX IV : PHYTOPLANKTON OBJECT CALIBRATION

The parameters P_{max} and I_{opt} were combined, within ranges, and performance measures were calculated (Figures 1-3; Tables 1-3). A simple cost function was employed which aggregates the normalized misfits in a 0-1 range. Table 38 shows the cost function for each combination and Table 15 and Table 40 exhibit the performance for two discarded simulations.

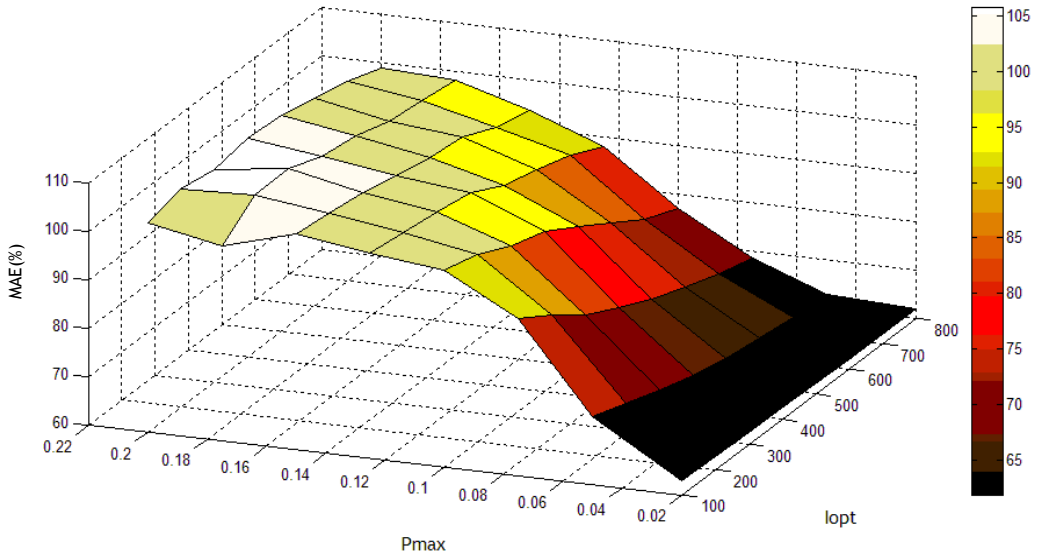

Figure 62 – MAE (%) 3D plot: Parameter combination (P_{max} and I_{opt})

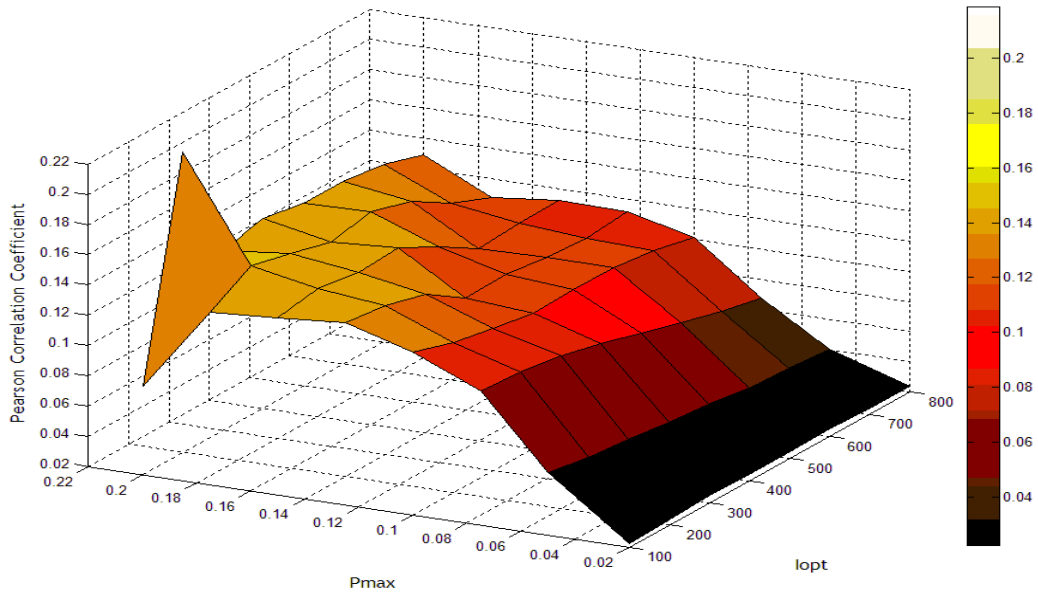

Figure 63 - Pearson correlation coefficient 3D plot: Parameter combination (P_{max} & I_{opt})

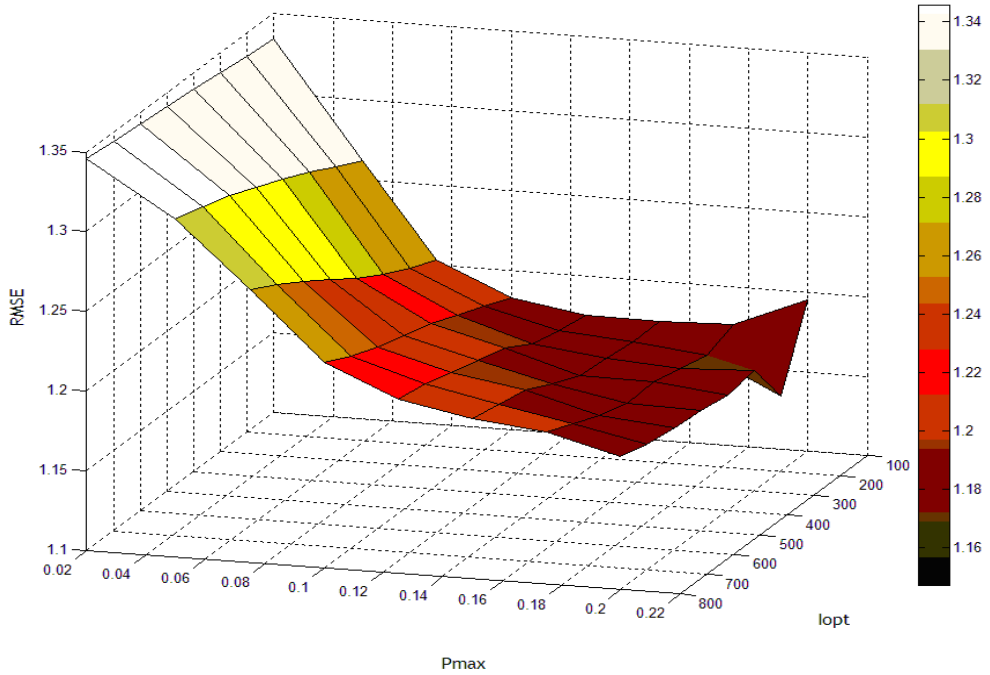

Figure 64 - RMSE 3D plot: Parameter combination (P_{max} & I_{opt})

Table 35 - MAE (%): Parameter combination (P_{max} & I_{opt})

Pmax \ Iopt	100	200	300	400	500	600	700	800
0.02	63	63	62	62	62	62	62	62
0.05	74	71	69	67	65	64	63	63
0.075	92	88	83	79	76	73	70	68
0.1	101	99	95	93	89	84	80	77
0.125	102	101	100	99	95	94	91	88
0.15	104	104	103	101	99	99	95	94
0.175	100	105	106	103	102	100	99	98
0.2	103	105	104	105	105	103	101	99

Table 36 - Pearson Correlation Coefficient : Parameter combination (P_{max} & I_{opt})

Pmax \ Iopt	100	200	300	400	500	600	700	800
0.02	0.02	0.02	0.02	0.02	0.02	0.02	0.02	0.02
0.05	0.06	0.06	0.05	0.05	0.05	0.04	0.04	0.04
0.075	0.11	0.11	0.10	0.10	0.09	0.08	0.07	0.07
0.1	0.13	0.12	0.11	0.11	0.11	0.11	0.11	0.10
0.125	0.14	0.14	0.13	0.11	0.11	0.11	0.11	0.11
0.15	0.14	0.14	0.14	0.14	0.13	0.11	0.11	0.11
0.175	0.13	0.15	0.14	0.14	0.14	0.13	0.12	0.11
0.2	0.08	0.22	0.14	0.15	0.14	0.14	0.14	0.13

Table 37 –RMSE**:** Parameter combination (P_{max} & I_{opt})

Pmax \ Iopt	100	200	300	400	500	600	700	800
0.02	1.33	1.34	1.34	1.34	1.34	1.34	1.34	1.35
0.05	1.26	1.27	1.28	1.29	1.30	1.30	1.31	1.31
0.075	1.20	1.21	1.22	1.23	1.24	1.25	1.26	1.27
0.1	1.18	1.19	1.20	1.20	1.21	1.21	1.22	1.23
0.125	1.18	1.18	1.18	1.19	1.20	1.20	1.21	1.21
0.15	1.17	1.17	1.18	1.18	1.19	1.19	1.20	1.20
0.175	1.18	1.17	1.17	1.18	1.18	1.18	1.19	1.20
0.2	1.20	1.15	1.18	1.17	1.18	1.18	1.18	1.18

Table 38 – Cost function: Parameter Combination (Pmax & Iopt)

Pmax \ Iopt	100	200	300	400	500	600	700	800
0.02	0.71	0.71	0.72	0.73	0.73	0.73	0.74	0.75
0.05	0.51	0.51	0.52	0.53	0.54	0.56	0.57	0.59
0.075	0.43	0.40	***0.37***	0.38	0.40	0.42	0.44	0.46
0.1	0.42	0.43	0.42	0.44	0.41	***0.37***	***0.34***	***0.34***
0.125	0.39	0.39	0.41	0.46	0.42	0.44	0.45	0.41
0.15	0.44	0.41	0.40	0.38	0.41	0.47	0.43	0.43
0.175	0.40	0.42	0.44	0.42	0.39	0.39	0.43	0.47
0.2	0.61	***0.30***	0.42	0.42	0.43	0.40	0.39	0.39

* local minima are identified as italic and bold in the Table

Table 39 - Phytoplankton object performance statistics for I_{opt} = 300 & P_{max} = 0.075

	Box1	Box3	Box4	Box6	Box8	Box10	Box11	Box12	Box13	Global
Matches	1	1	8	1	1	1	9	8	1	**31**
RMSE	0.4	4.0	3.9	4.3	11.9	0.4	3.7	8.8	0.1	**5.8**
MAE (%)	5%	51%	105%	51%	83%	25%	78%	68%	8%	**75%**
r	-	-	-0.71	-	-	-	-0.03	0.07	-	**0.06**

Table 40 - Phytoplankton object performance statistics for I_{opt} = 600 & P_{max} = 0.1

	Box1	Box3	Box4	Box6	Box8	Box10	Box11	Box12	Box13	Global
Matches	1	1	8	1	1	1	9	8	1	**31**
RMSE	0.9	2.73	3.9	3.1	10.9	1.2	3.5	8.7	0.3	**5.6**
MAE (%)	11%	35%	111%	37%	76%	70%	91%	82%	20%	**84%**
r	-	-	-0.68	-	-	-	0.08	0.15	-	**0.06**

ANNEX V: VALIDATION OF THE DISSOLVED SUBSTANCES AND SPM OBJECTS

Although the main goal of the modelling process was to access the accuracy of simulated chlorophyll a, the dissolved substances (ammonia and nitrate) and SPM were also be evaluated. This analysis provided auxiliary information for the validation process along with a broad idea of the accuracy achieved in the simulation of the system's components for future applications. Moreover, due to the interdependence of SPM and nutrients concerning the phytoplankton biomass production and distribution, theoretically if both were accurately simulated the probability of an accurate chlorophyll *a* simulation would be increased.

Nitrate is highly dependent of the freshwater flow as exhibited in Figure 65. Moreover, the nitrate concentration is underestimated consistently, in average about 100%, consistent with the information retrieved during calibration. Ammonia was in fair agreement with sampled values, however, in box 4, samples were highly variable (from 6 to 76 μmol N l^{-1}) being systematically over and underestimated (Figure 66). SPM was consistently overestimated in about 100% probably over limiting primary production (Figure 67). In sum, calibration and validation of both objects retrieved similar results.

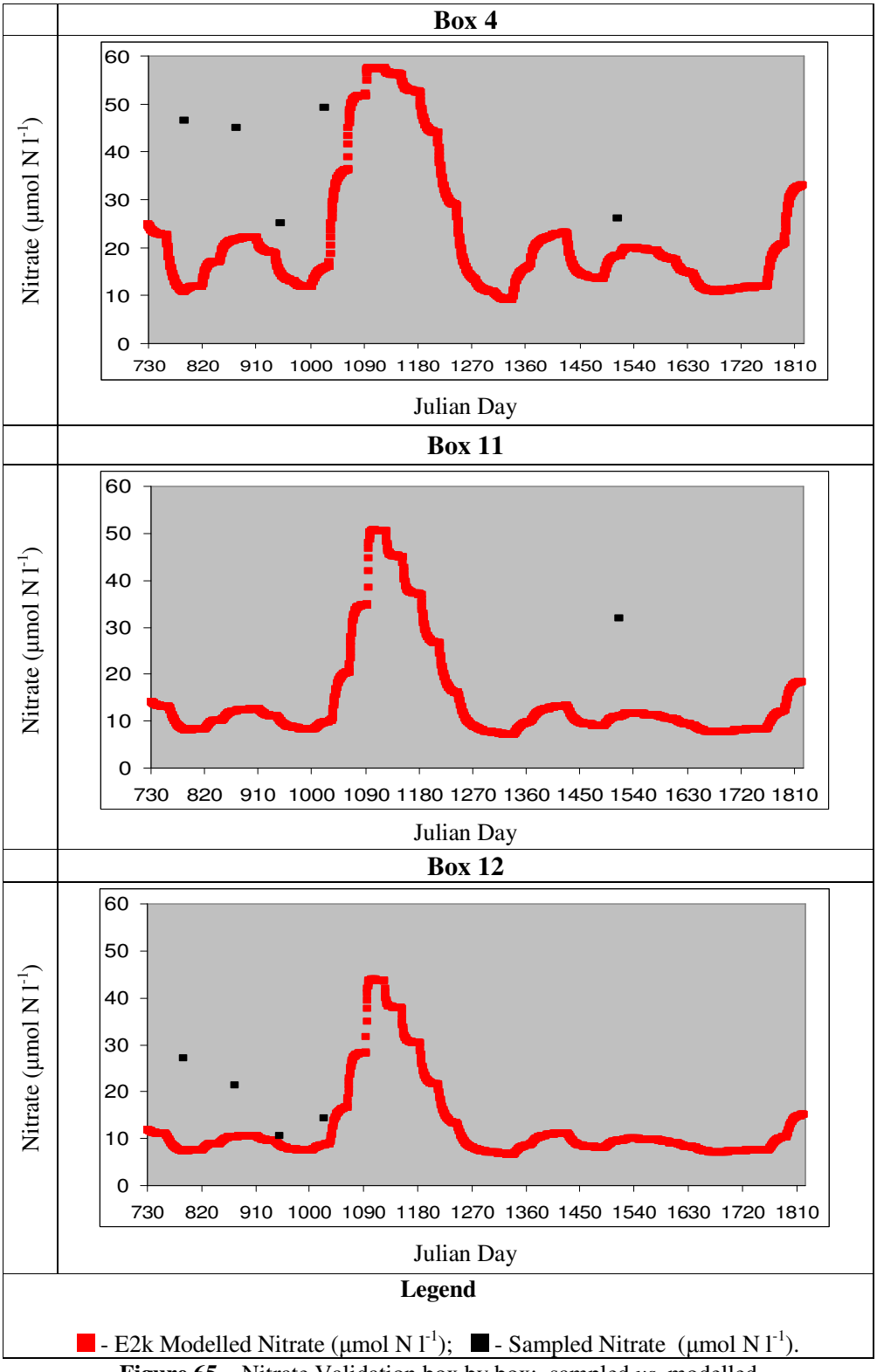

Figure 65 – Nitrate Validation box by box: sampled *vs.* modelled

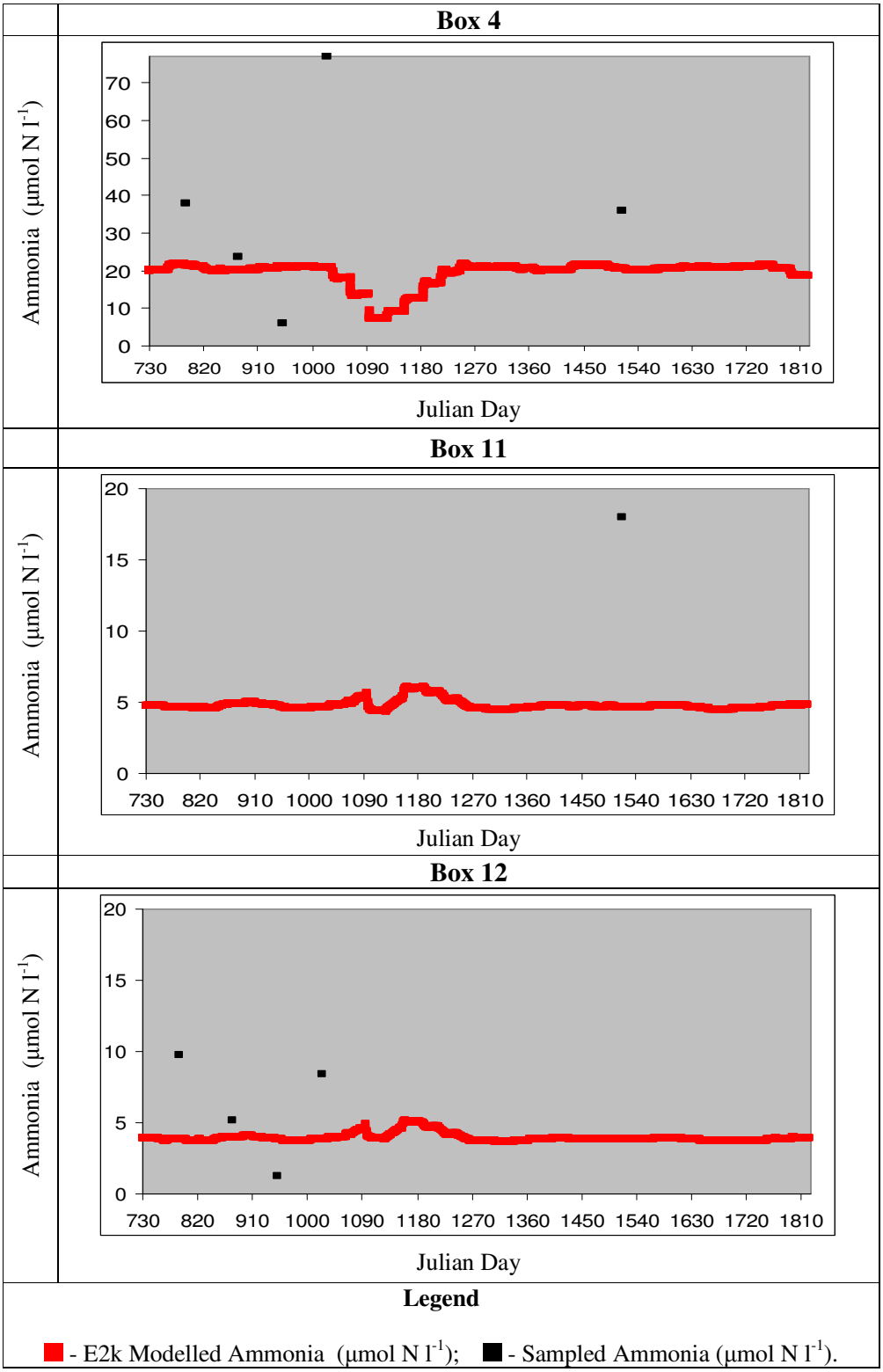

Figure 66 – Ammonia Validation box by box: sampled *vs.* modelled

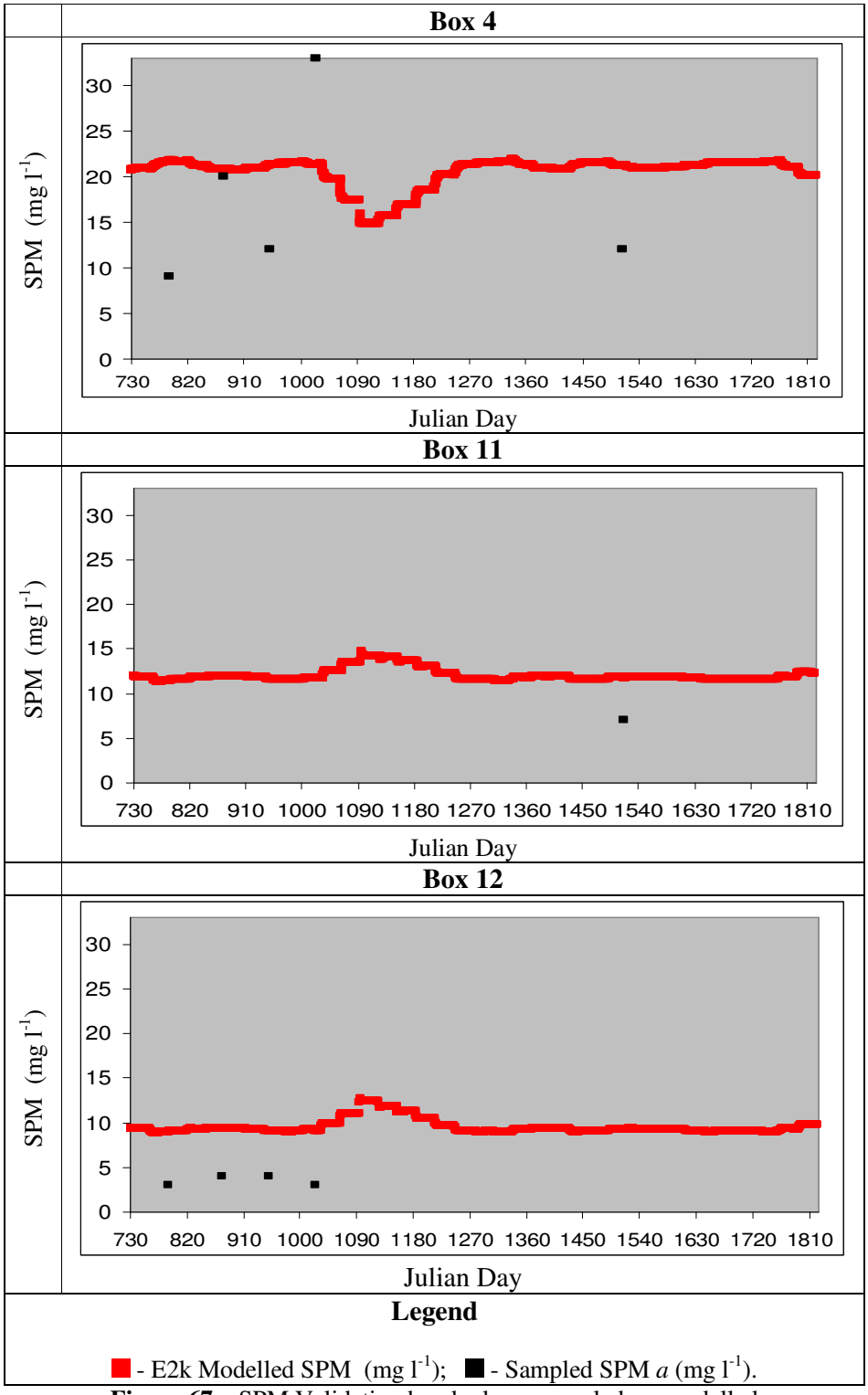

Figure 67 – SPM Validation box by box: sampled *vs.* modelled

ANNEX VI – ATMOSPHERIC CORRECTION PROCEDURES

To assess the atmospheric procedure(s) more adequate to chl-a estimation in the Tagus estuary. The analysis was performed comparing the E2k simulations with remote sensing retrievals using several atmospheric correction procedures. The OC3 algorithm was the reference data set and comparisons were made at a box scale for the years 2000 and 2001. Note that only the E2k simulations for the year 2000 were validated and therefore are considered more robust than those of the year 2001. Time series for specific boxes are presented thru Figure 5-4 and performance regarding RMSE (Figure 71) and correlation (Figure 72).

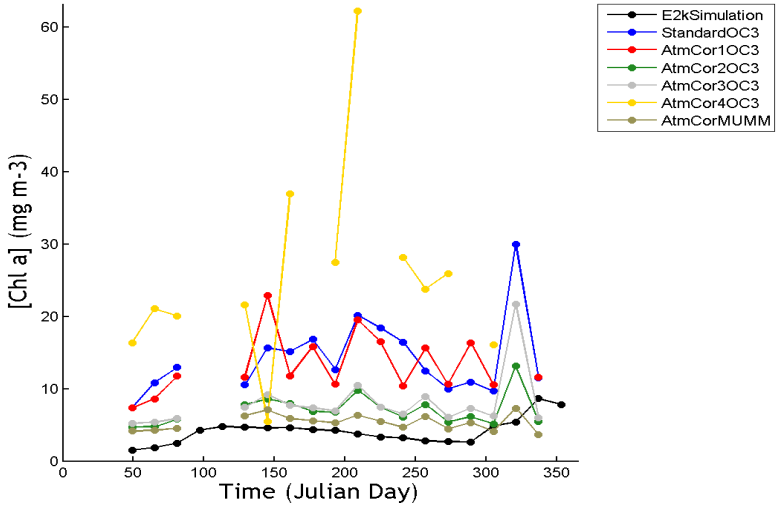

Figure 68 – Atmospheric correction procedure : Time series Box 7 - 2000

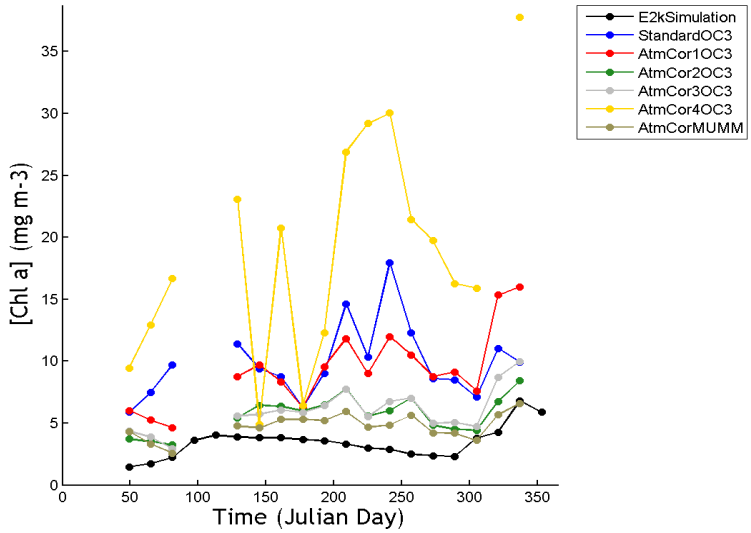

Figure 69 – Atmospheric correction procedure : Time series Box 9 - 2000

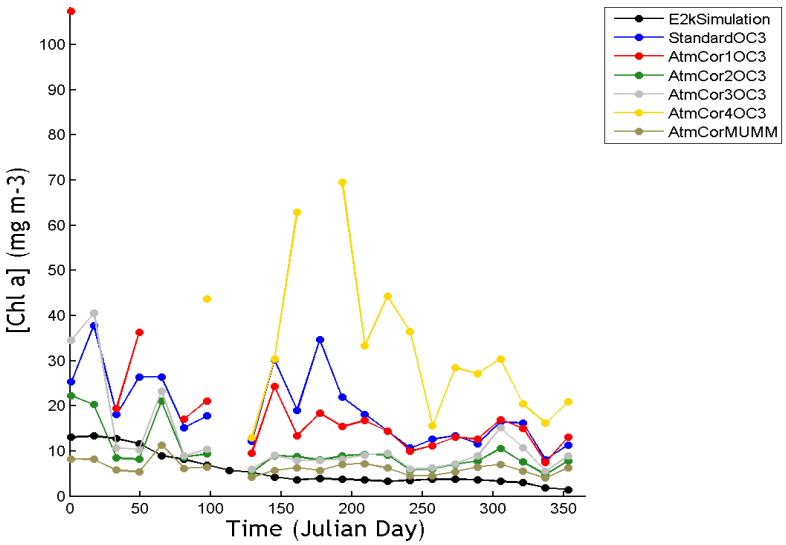

Figure 70 – Atmospheric correction procedure : Time series Box 7 - 2001

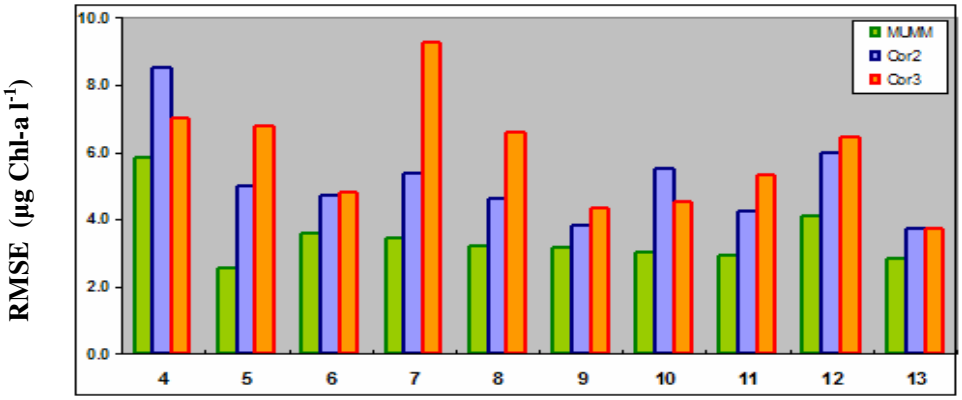

Figure 71 – RMSE distribution over the model boxes : 2000

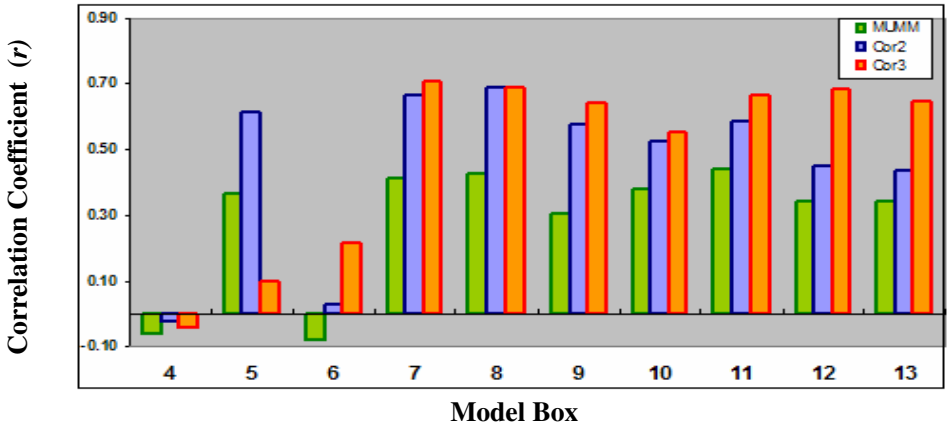

Figure 72 – Correlation distribution over the model boxes : 2001

ANNEX VII – QUALITY CONTROL MASKING

This annex presents the analysis performed to assess the quality control i.e. flag masking more adequate for chl-a retrieval. Comparisons were made at a box scale for the years 2000 and 2001. Once again, the OC3 algorithm was the reference data set. Both 2000 (Figure 5 & Figure 69) and 2001 (Figure 75 & Figure 76) years, exhibited low impact on the chl-a retrievals. Two trends are distinct, masking glint increases chl-a distributions and angle masking slightly decreases them. There is no apparent relationship between sensor and solar zenith angle and chl-a error, in both years (Figure 22). Some daily maps were presented in Figure 78 to exhibit the differences resulting from the correction procedure of possible straylight contaminated pixels.

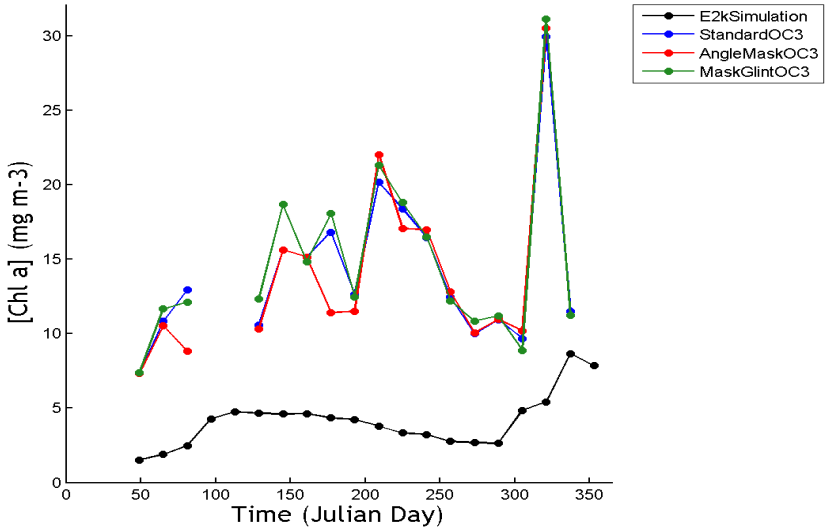

Figure 73 – Quality Control Options : Time series Box 7 - 2000

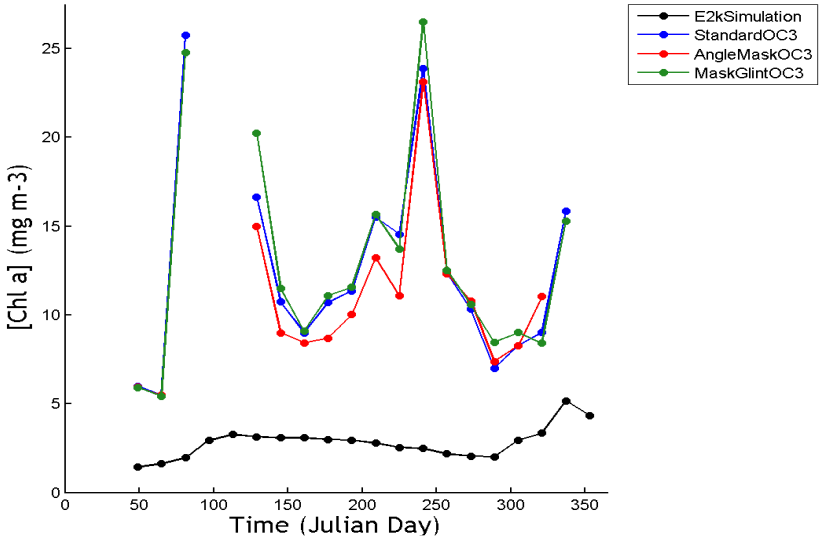

Figure 74 – Quality Control Options : Time series Box 11 - 2000

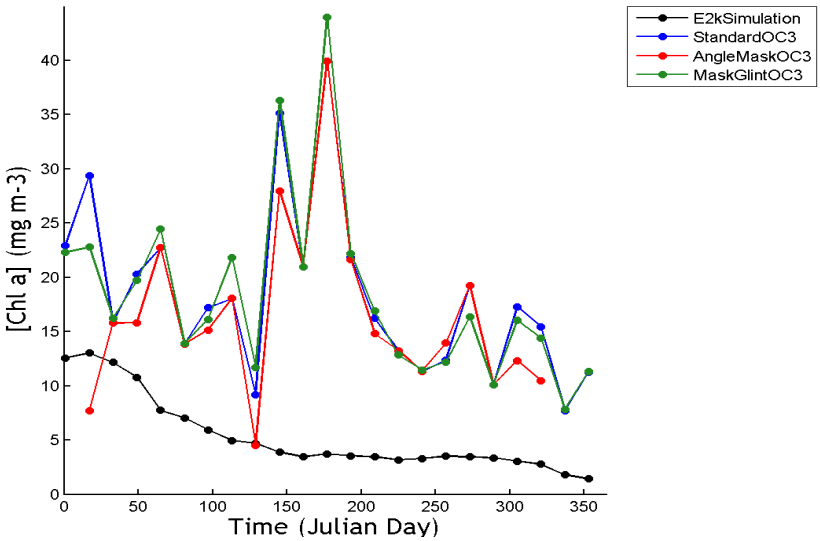

Figure 75 – Quality Control Options : Time series Box 08 - 2001

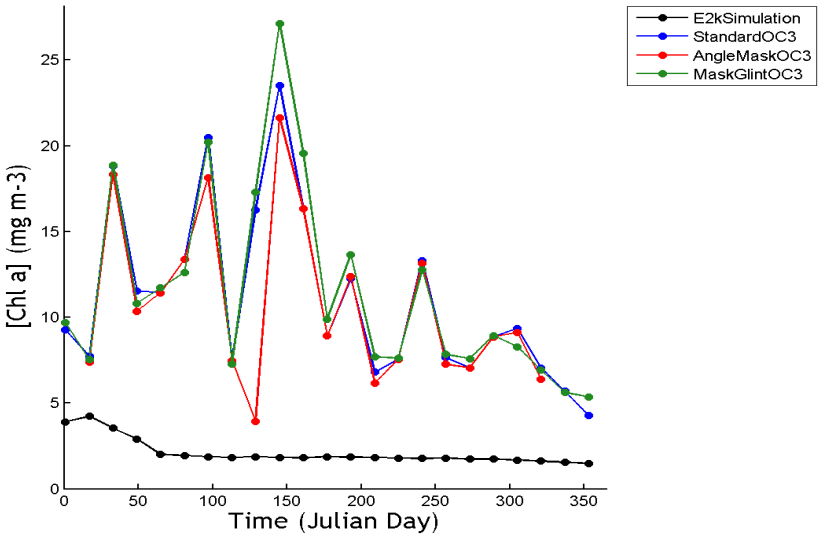

Figure 76 – Quality Control Options : Time series Box 13 - 2001

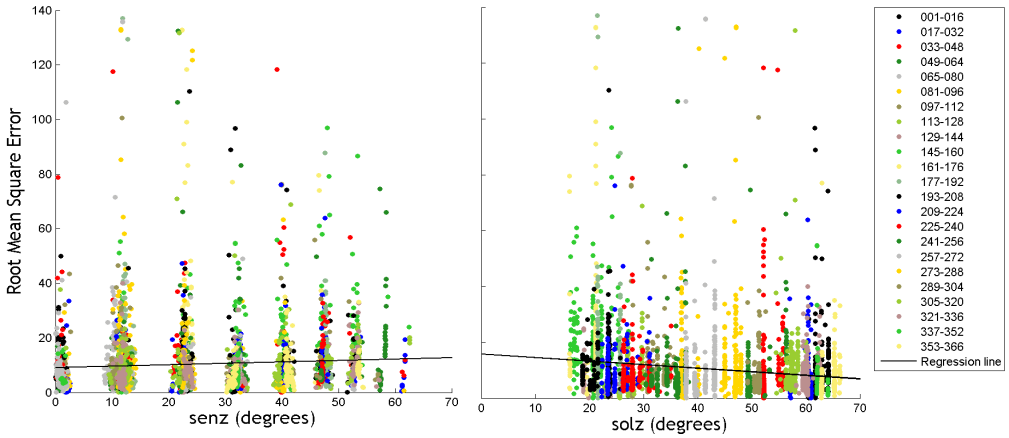

Figure 77 – Geometry (solar and sensor zenith angle) *vs.* RMSE : 2001
The legend indicates the compositing period i.e. the initial and final Julian day

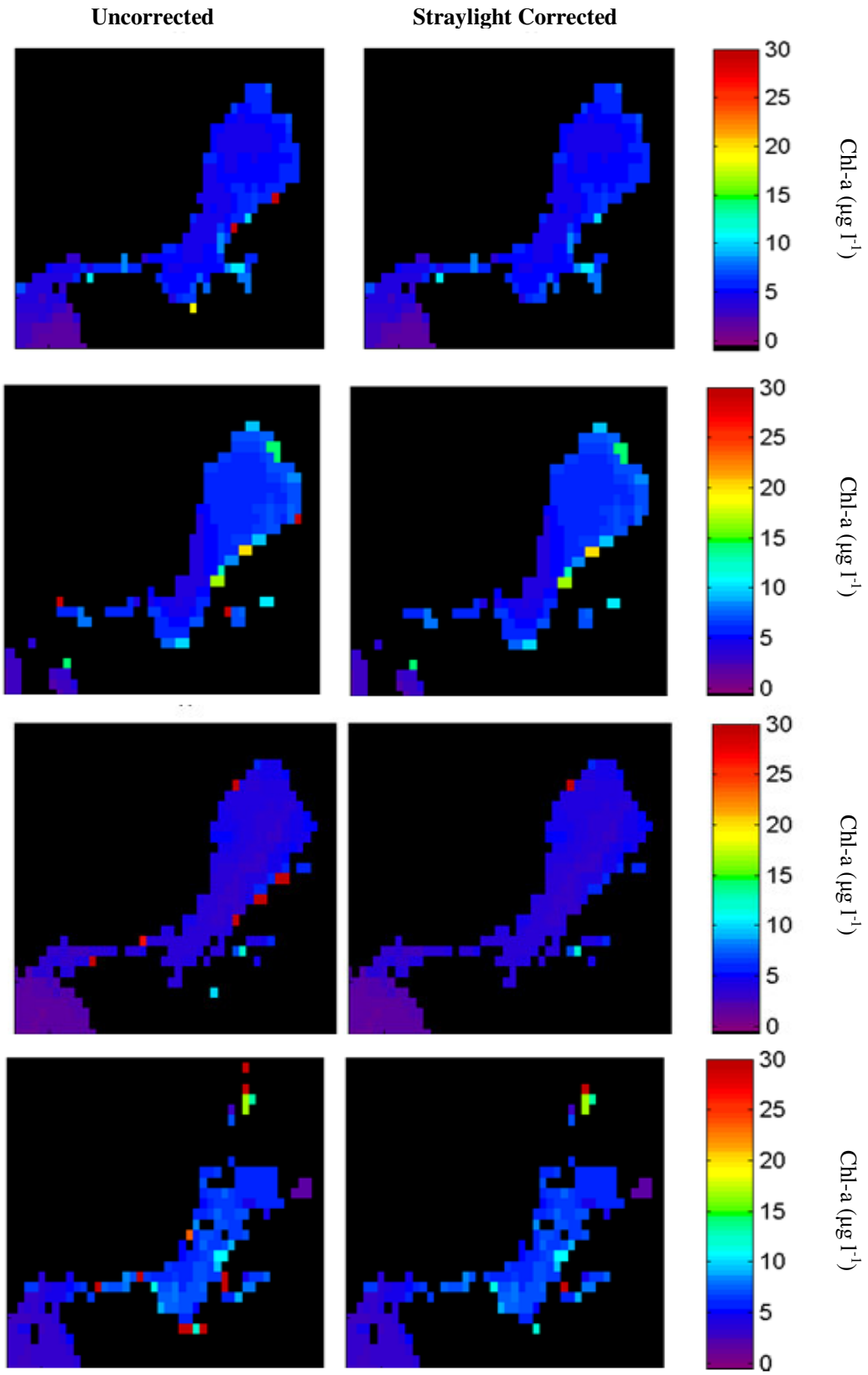

Figure 78 - Daily chl-a images before (left) and after (right) straylight correction

ANNEX VIII – TEMPORAL AND SPATIAL COMPOSITING

1) TEMPORAL COMPOSITING: 16day

Some hypothesis were tested to assess their impact on the 16day composited images (

Figure **79** & Figure 80):

a) Outliers were removed according to 1 and 2 standard deviation thresholds
b) Daily images were filtered according to tidal state both ebb\flood and high\lowtide
c) Minimum number of files in a composite

Note pixels were not spatially aggregated into boxes and the plots below show all pixels within the estuary. Besides the reference data set, these hypotheses were also tested using the MUMM atmospheric procedure with glint masking.

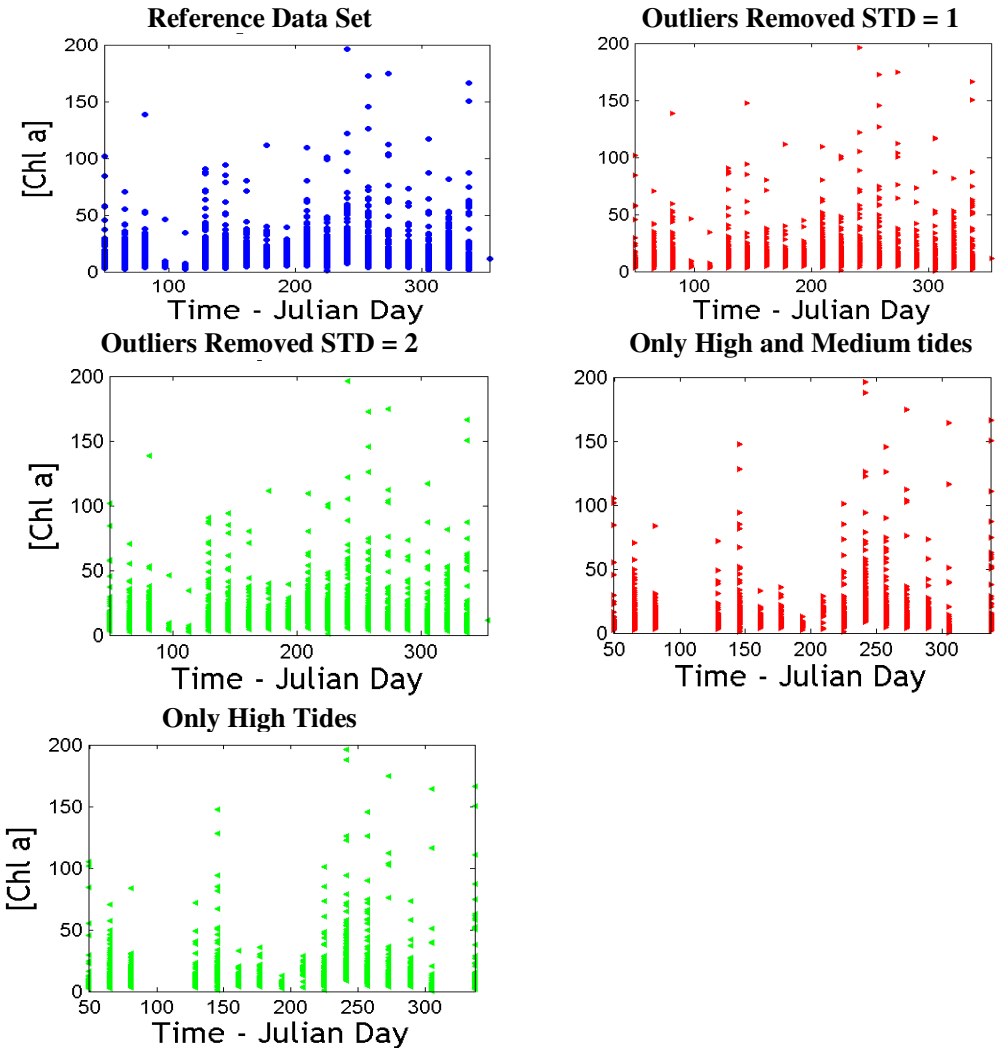

Figure 79 - Outlier and Tidal Height impact on 16day composites : 2000

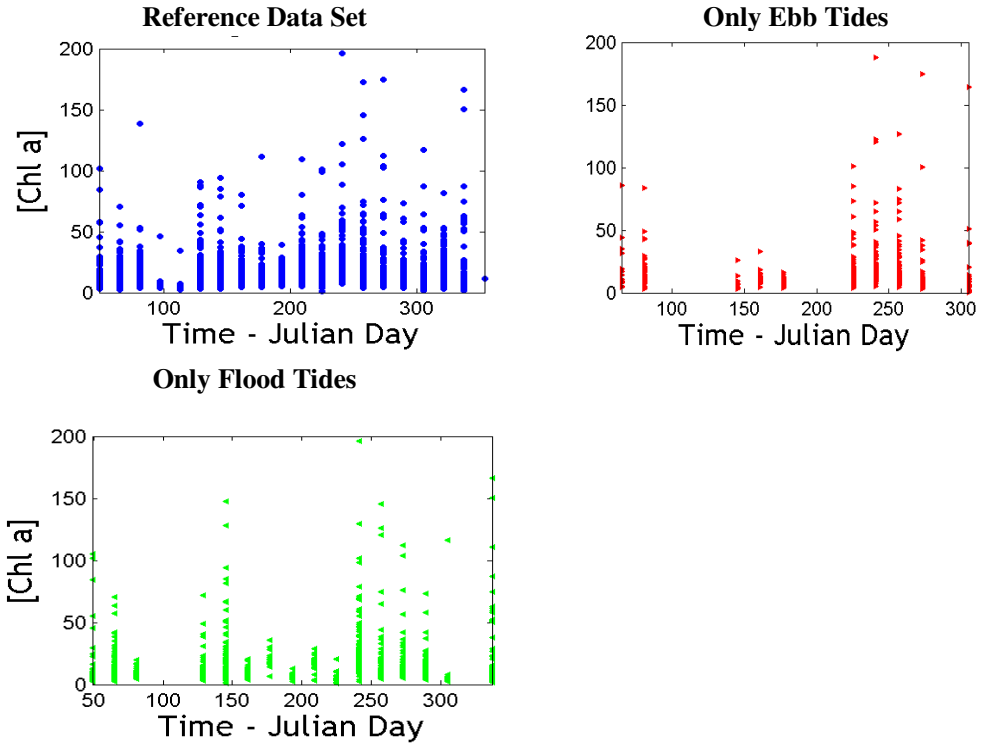

Figure 80 – Tidal state impact on 16day composites : 2000

Tidal state, height and outlier removal using STD thresholds showed no clear pattern concerning the anomalously high chl-a values. Flood tides, apparently, contribute to higher errors, however, the data set as scarce images acquired during ebb tides and therefore no robust inference could be made. The number of files in a composite can influence the 16day composite accuracy, particularly, if there are scarce daily images within and/or if their spatial coverage is limited. Atypically high chl-a values seemed to be linked to lower number of files in the compositing period. However, removing files with few files would result in a scarce data set.

2) SPATIAL COMPOSITING: 13 Model Boxes

In order to understand the chl-a distribution within each model box, spatial histograms were made for each box and for every compositing period. The majority were normal distributions but some exceptions occur (Figure 24; Figure 82; Figure 83; Figure 84). Frequently, the average is deviated from the gross distribution of chl-a values due to the presence of apparent outliers, Figure 24 is a good example. For boxes 4, 5 (not shown) and 12 the distributions are highly irregular probably due to their limited spatial coverage thus high sensitivity to resampling and land and bottom reflectance contamination.

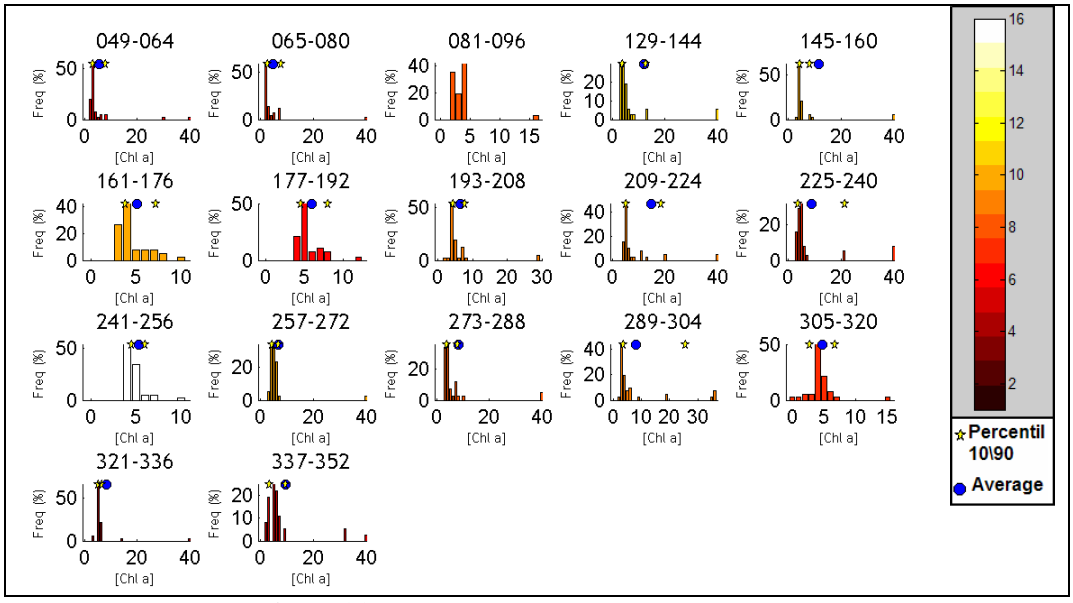

Figure 81 – Spatial histograms : Box 10 – 2000

The histograms have the value frequency (%) in y axis and chl-a concentration in the x axis
The scale bar represents the number of MODIS daily images in a composite

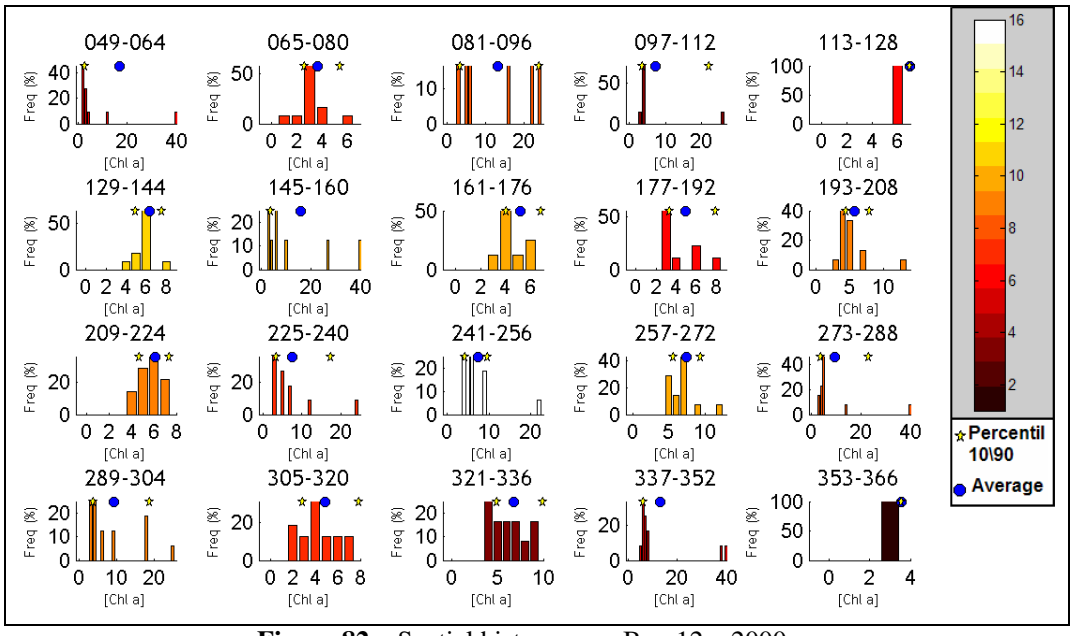

Figure 82 – Spatial histograms : Box 12 – 2000

The histograms have the value frequency (%) in y axis and chl-a concentration in the x axis
The scale bar represents the number of MODIS daily images in a composite

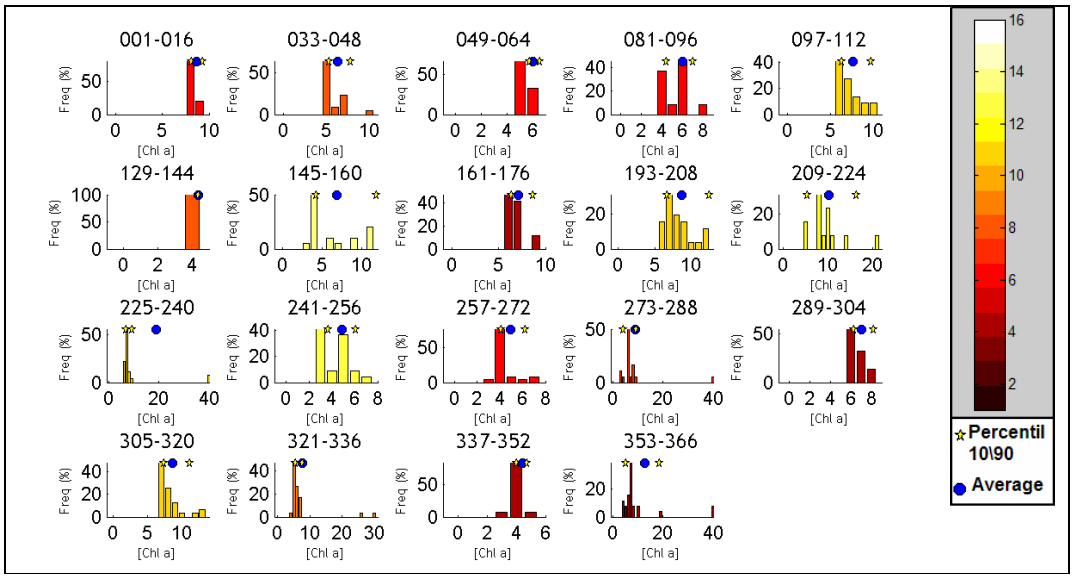

Figure 83 – Spatial histograms : Box 6 – 2001
The histograms have the value frequency (%) in y axis and chl-a concentration in the x axis
The scale bar represents the number of MODIS daily images in a composite

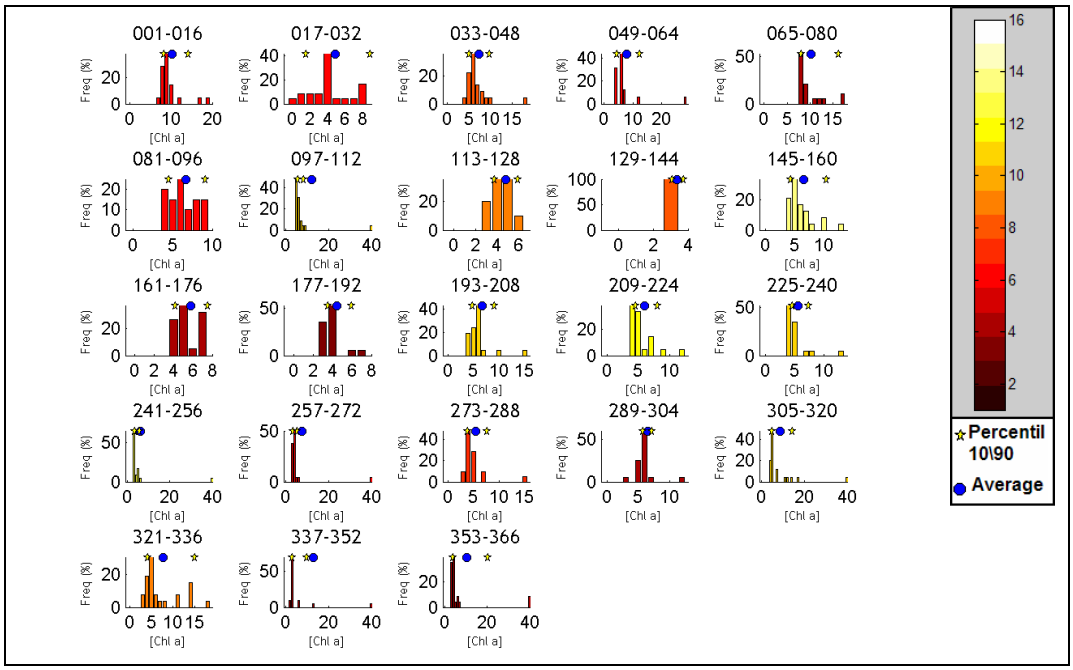

Figure 84 – Spatial histograms : Box 11 – 2001
The histograms have the value frequency (%) in y axis and chl-a concentration in the x axis
The scale bar represents the number of MODIS daily images in a composite

ANNEX IX – REGIONAL CALIBRATION OF CASE 2 ALGORITHMS

This annex exhibits the spectral analysis performed for the year 2000 (Figure 85) and 2001 (Figure 86). Calibration plots for regional Case 2 algorithms are exhibited in Figure 87, Figure 88. The comparison between the predictions using the ratio R_{678}/ R_{551} and E2K simulations, along with the temporal distribution of the latter, are exhibited in Figure 89.

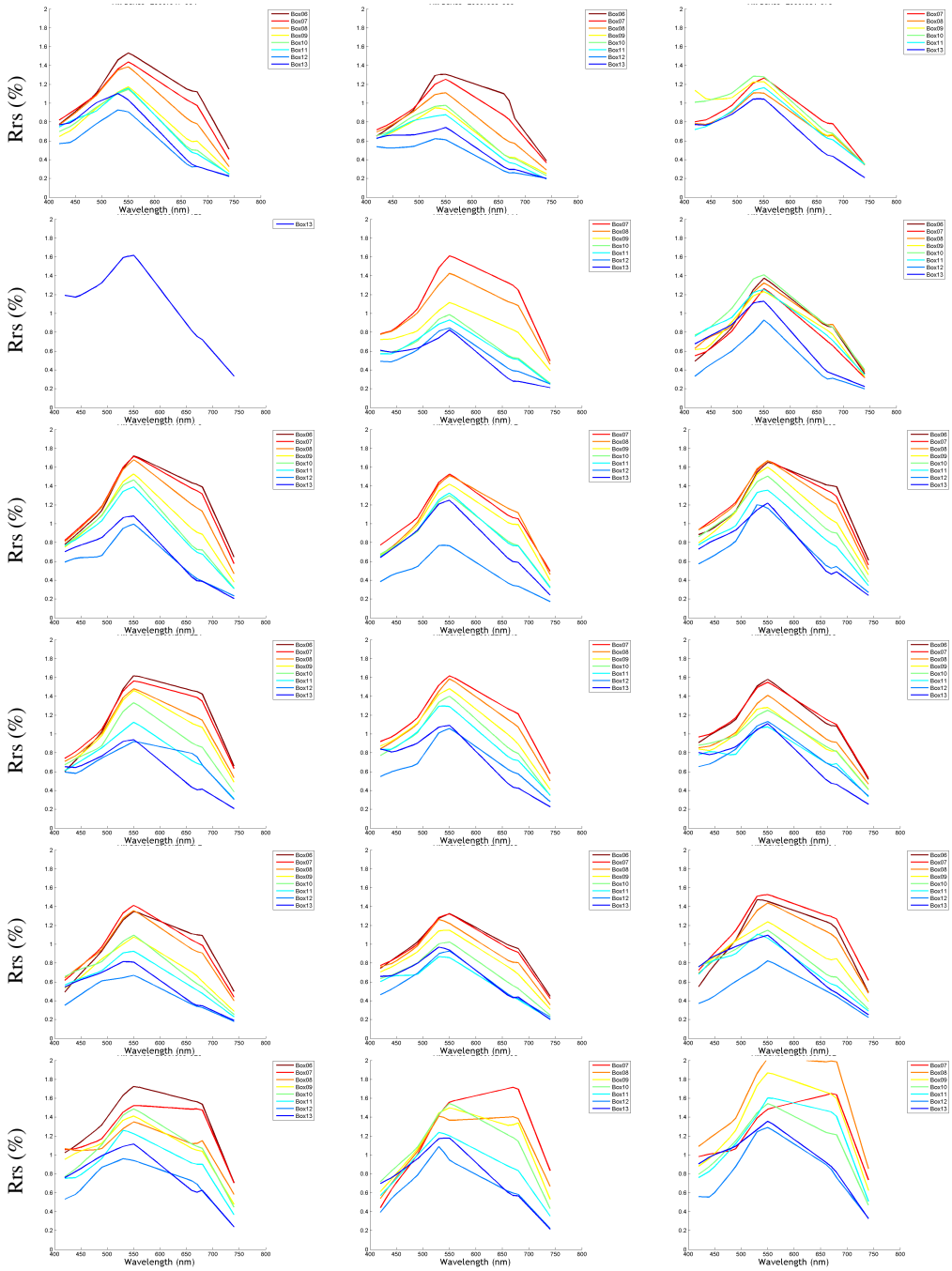

Figure 85 - Spectral Signatures for all boxes per compositing period : 2000

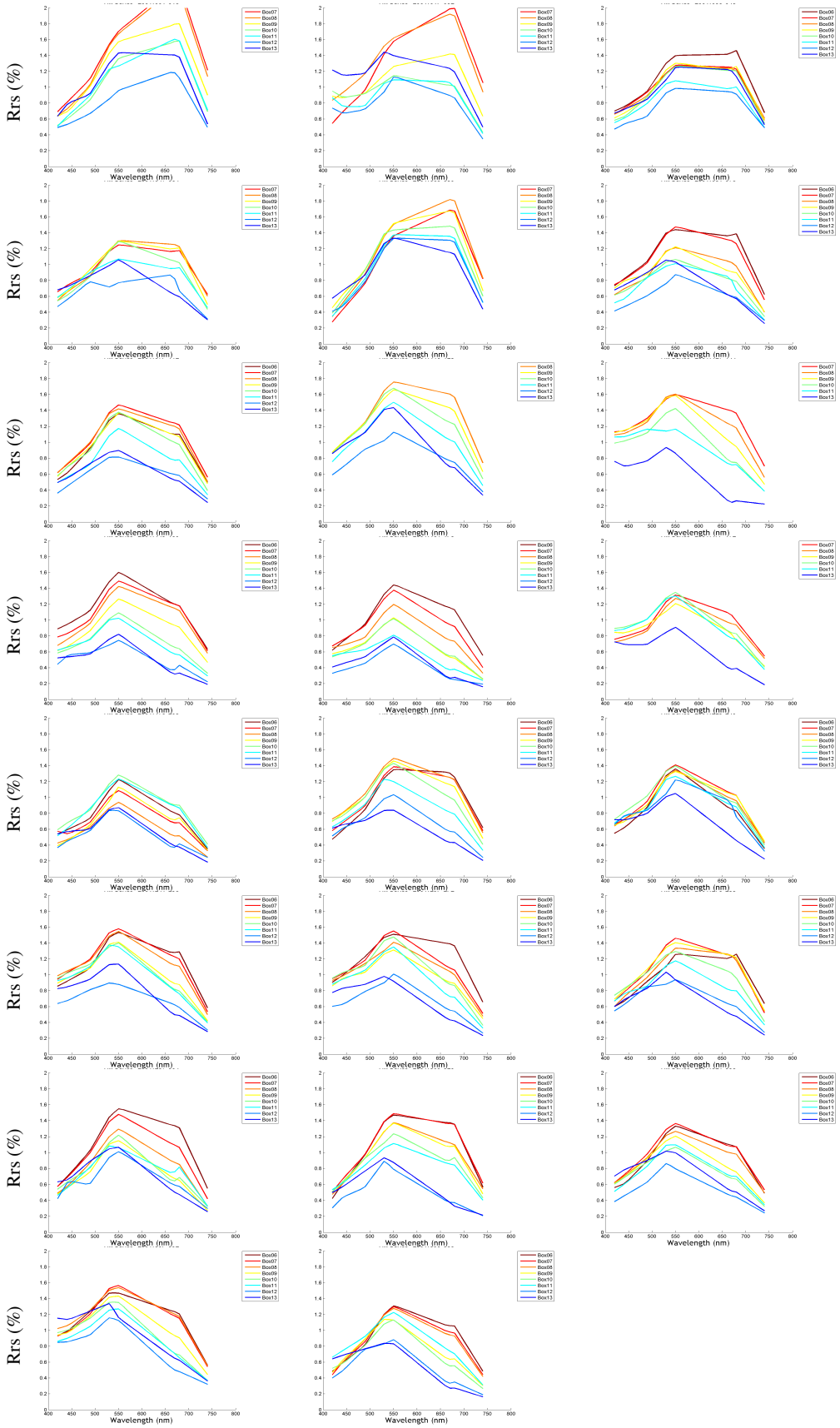

Figure 86 - Spectral Signatures all boxes per compositing period:2001

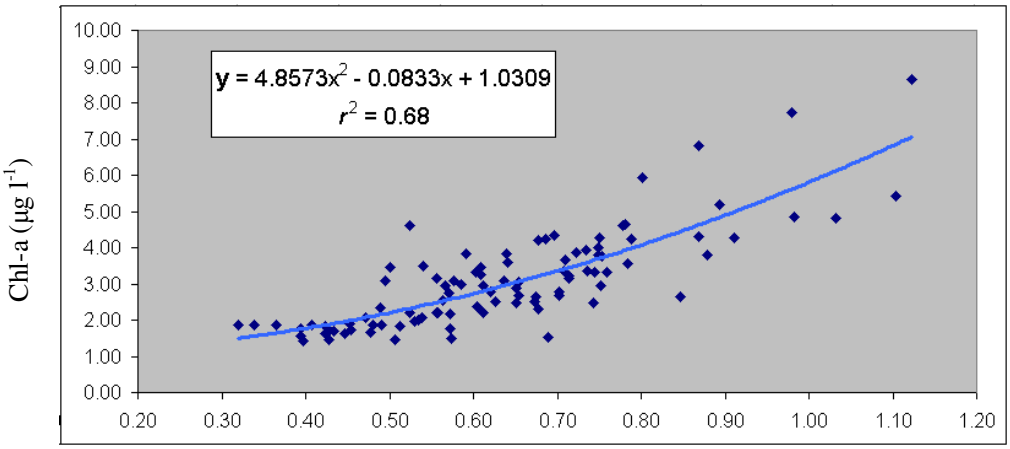

R_{678}/ R_{551}

Figure 87 – Calibration plot using the ratio R_{678}/ R_{551} : 2000

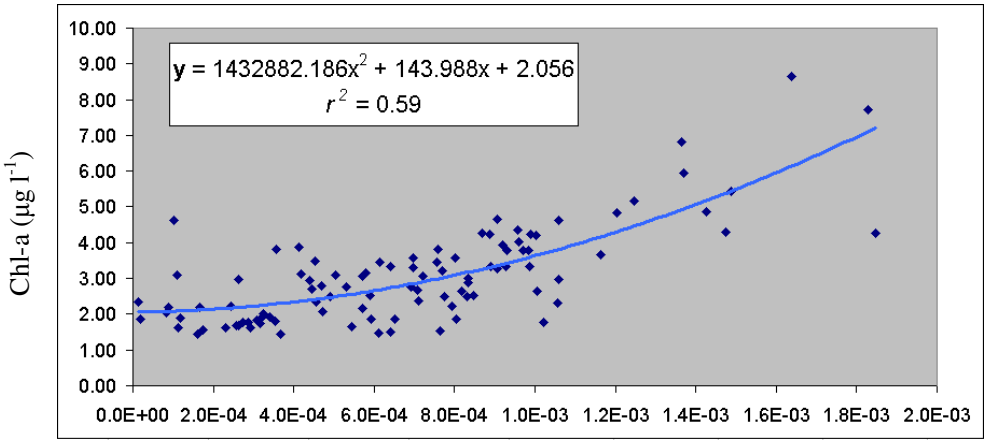

FLH

Figure 88 – Calibration plot using the Fluorescence Line Height : 2000

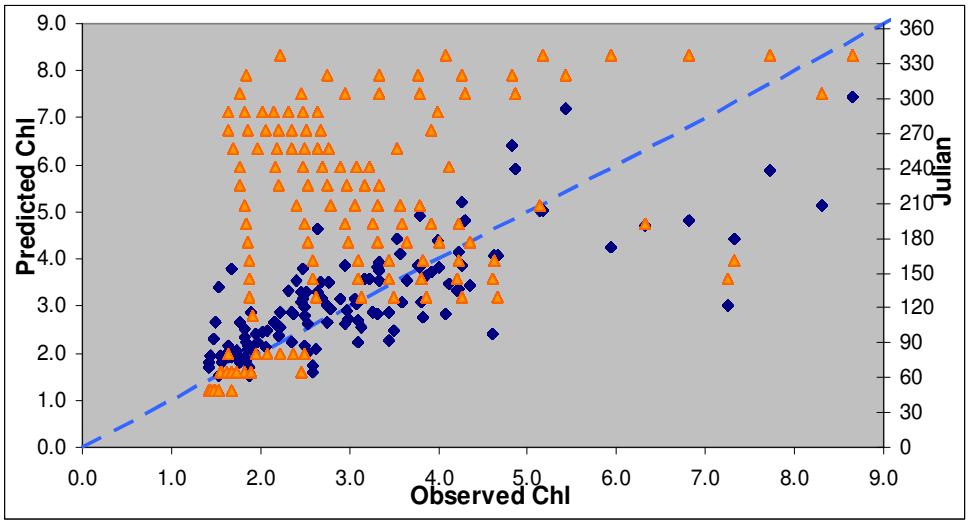

Figure 89 – Predictions vs. Observations using the ratio R_{678}/ R_{551} (blue); Chl-a temporal distribution (2000)

ANNEX X – PRELIMINARY ASSESSMENT CASE 1 CHL-A ALGORITHMS

This annex comprises some of the results obtained comparing the E2k 16day box chl-a simulations with the equivalent Case 1 remote sensing retrievals. Time series for all analyzed boxes is showed for 2000 (Figure 90) and 2001(Figure 92). The error analysis for both years is done in Figure 34, Figure 37, Figure 94 and Figure 93, and Table 41-Table 46). Spatial analysis is done using non-spatially aggregated 16day chl-a values plotted against the distance to ocean (Figure 96). River flow is also plotted against chl-a retrievals by the Carder algorithm (Figure 97). The performance of the OC3 algorithm using the AtmCor3 and MUMM atmospheric correction procedures is compared in Figure 98.

Table 41 – Case 1 algorithms performance for the year 2000 - MAE (%)

Box	OC3	Carder	Clark	GSM
6	58.0	56.6	36.0	43.4
7	68.2	65.7	28.5	31.3
8	66.8	68.3	25.5	27.5
9	54.7	56.5	25.6	20.7
10	67.1	53.9	19.5	21.8
11	78.3	68.2	15.7	22.6
12	139.5	125.9	52.0	27.8
13	93.4	88.1	16.8	31.8

Table 42 – Case 1 algorithms performance 2000 - RMSE (μg chl-al^{-1})

Box	OC3	Carder	Clark	GSM
6	2.35	2.35	2.65	3.99
7	2.48	2.33	1.98	2.02
8	2.04	2.13	1.54	1.39
9	1.65	1.70	1.20	1.01
10	1.82	1.56	0.87	0.88
11	2.00	1.88	0.56	0.81
12	3.30	3.13	1.68	0.79
13	1.71	1.67	0.35	0.64

Table 43 – Case 1 algorithms performance for the year 2000 - correlation (*r*)

Box	OC3	Carder	Clark	GSM
6	0.23	0.33	0.15	-0.34
7	-0.01	0.09	0.04	-0.17
8	0.45	0.33	0.35	0.29
9	0.68	0.60	0.57	0.59
10	0.67	0.80	0.77	0.49
11	0.81	0.82	0.82	0.41
12	0.31	0.41	0.04	0.62
13	0.62	0.83	0.58	0.63

Table 44 – Case 1 algorithms performance for the year 2001-MAE (%)

Box	OC3	Carder	Clark	GSM
6	52.9	62.1	42.7	45.6
7	68.9	62.7	38.7	34.5
8	69.8	63.0	37.6	35.6
9	64.5	60.3	35.5	32.6
10	69.0	62.0	33.5	28.8
11	78.6	72.7	31.4	27.2
12	146.0	133.8	496.0	>1000
13	111.7	105.7	47.3	34.7

Table 45 – Case 1 algorithms performance for the year 2001 - RMSE (μg chl-a l^{-1})

Box	OC3	Carder	Clark	GSM
6	3.54	3.76	4.50	5.22
7	3.41	3.85	4.25	4.23
8	3.21	3.11	3.87	4.07
9	3.11	2.85	3.68	3.69
10	3.04	2.72	3.29	3.38
11	2.79	2.45	2.77	2.88
12	4.07	3.49	46.72	>1000
13	2.36	2.37	1.79	0.83

Table 46 – Case 1 algorithms performance for 2001 - correlation (*r*)

Box	OC3	Carder	Clark	GSM
6	-0.06	0.03	-0.19	0.24
7	0.41	0.14	0.28	0.25
8	0.43	0.44	0.26	0.04
9	0.33	0.48	0.23	0.15
10	0.29	0.46	0.21	0.08
11	0.45	0.60	0.33	0.25
12	0.39	0.57	-0.10	-0.10
13	0.35	0.64	0.04	0.37

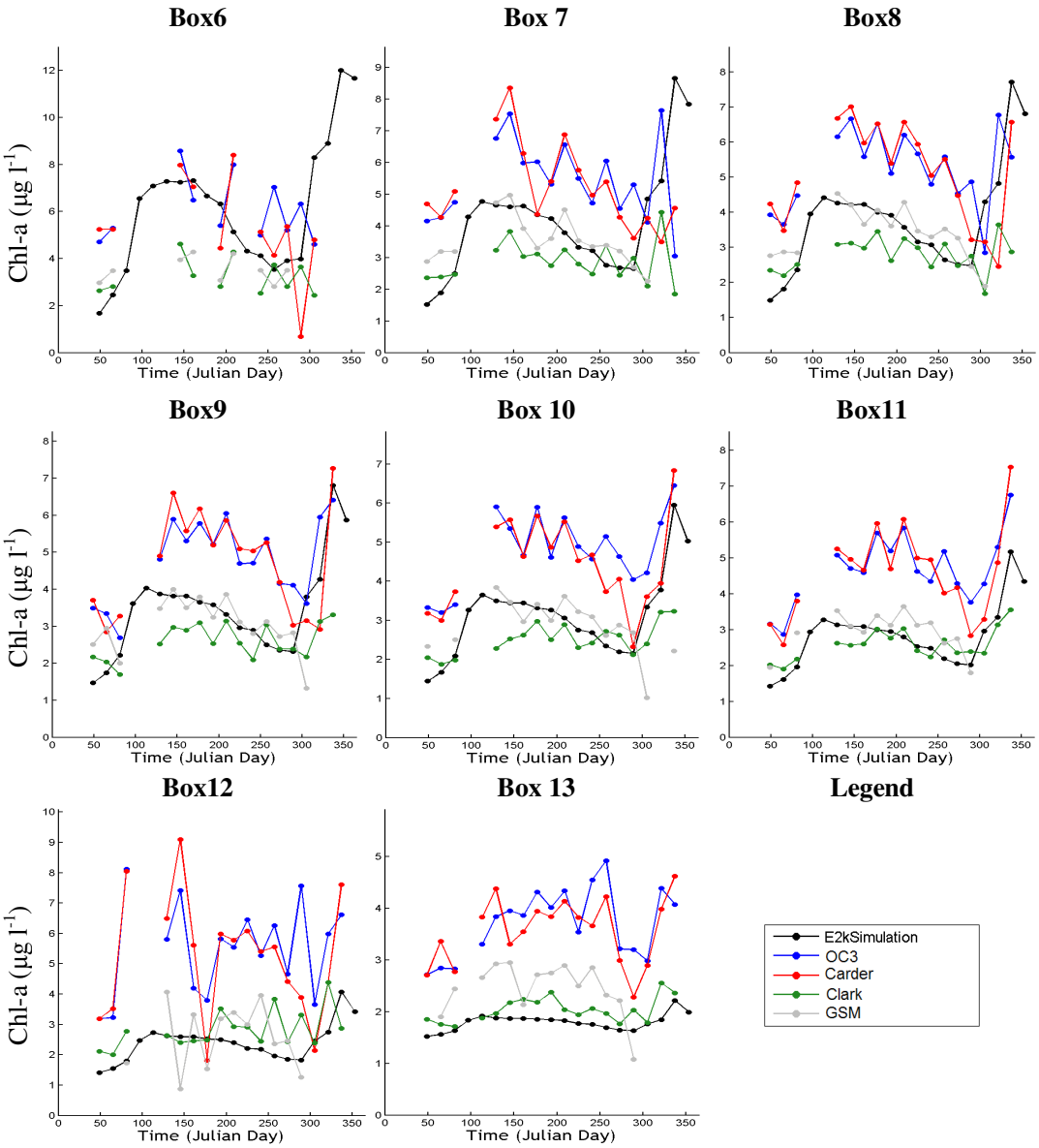

Figure 90 - Existing Algorithms Pre-Assessment : Time Series 2000

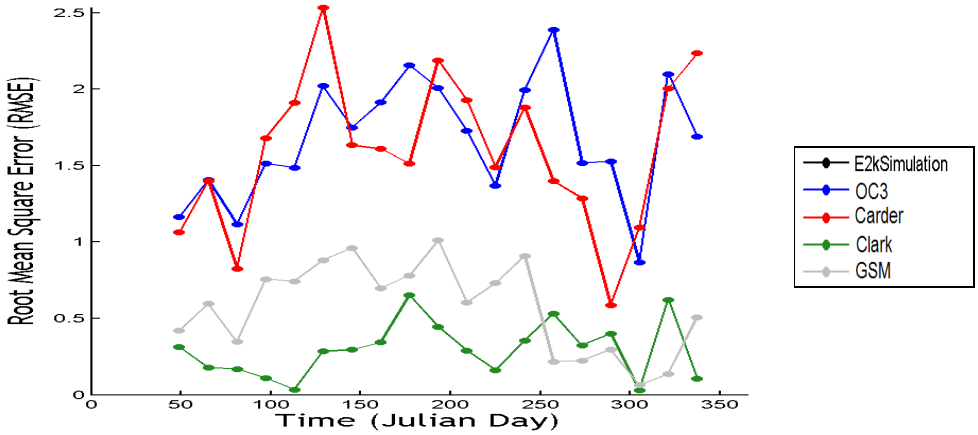

Figure 91 – Case 1 Algorithms RMSE distribution: box 13 2000

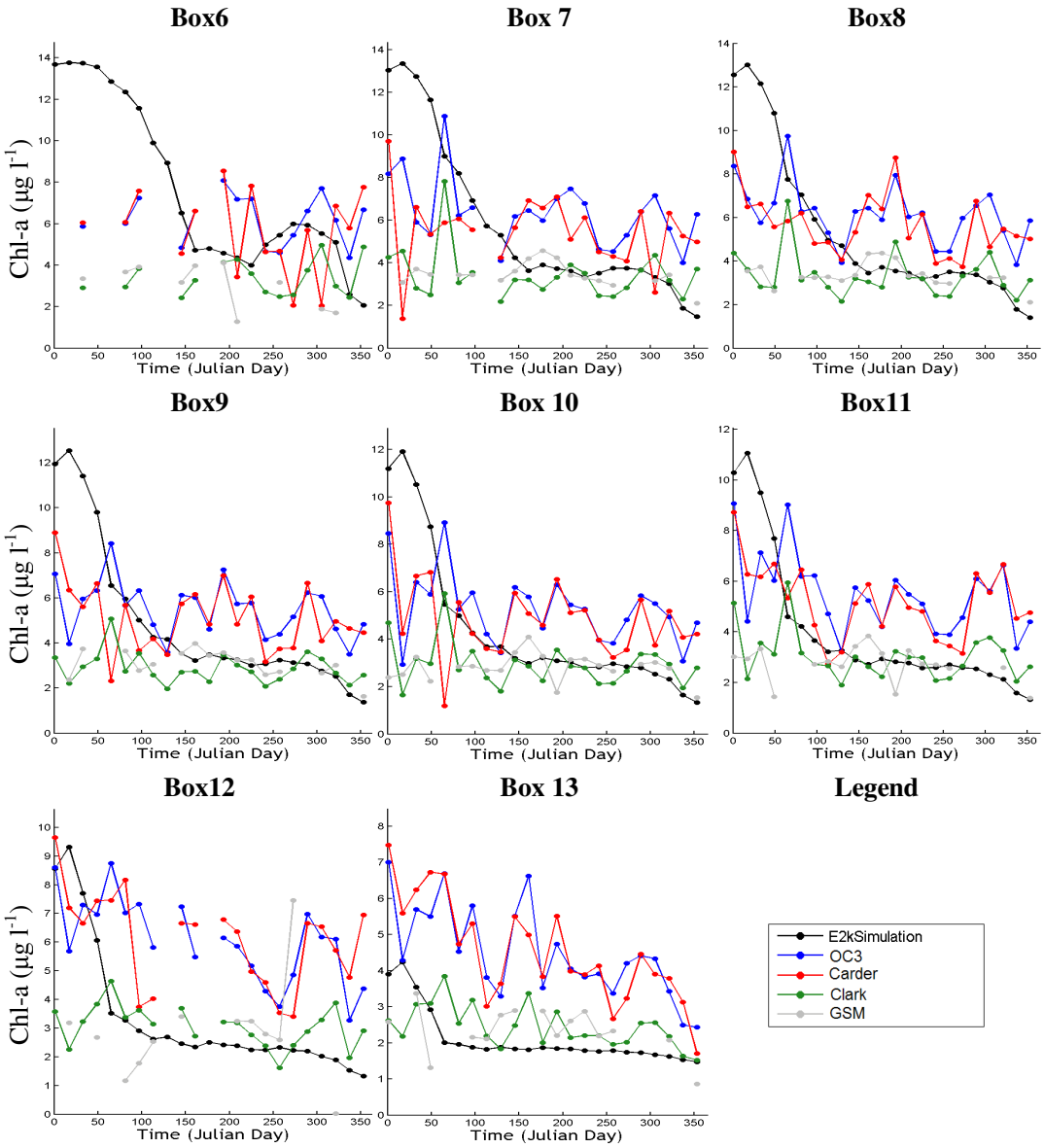

Figure 92 - Existing Algorithms Pre-Assessment : Time Series 2001

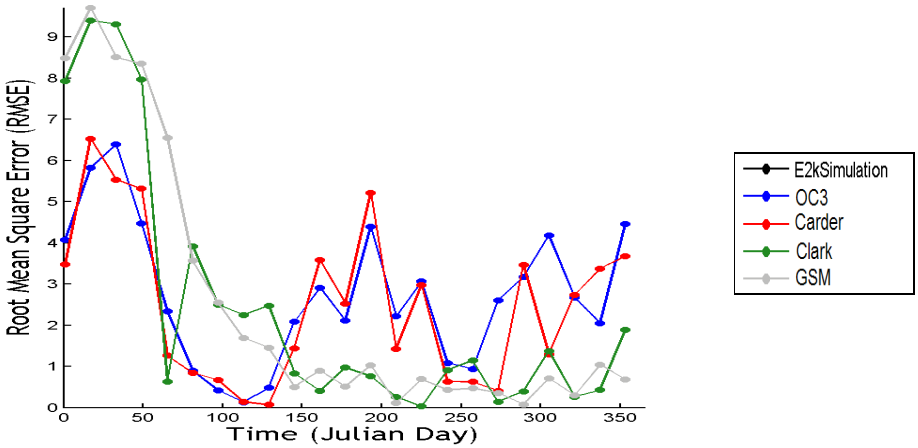

Figure 93 – Case 1 Algorithms RMSE distribution: box 8 2001

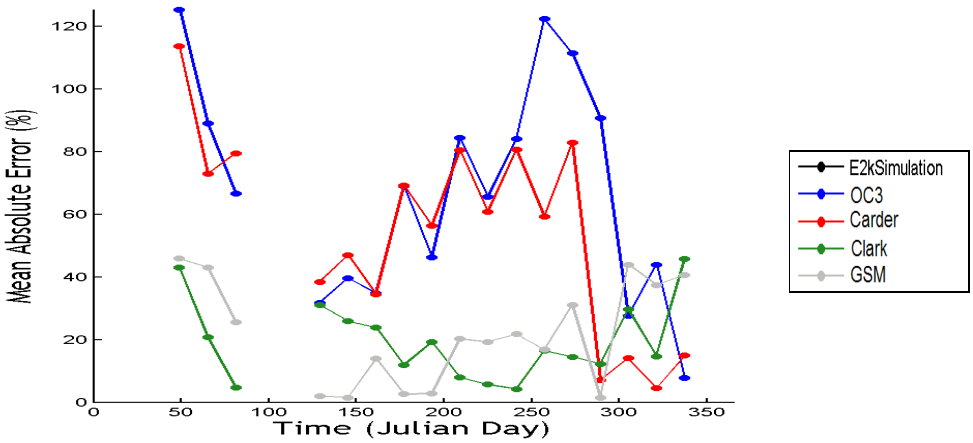

Figure 94 – Case 1 Algorithms MAE distribution: box 10 2001

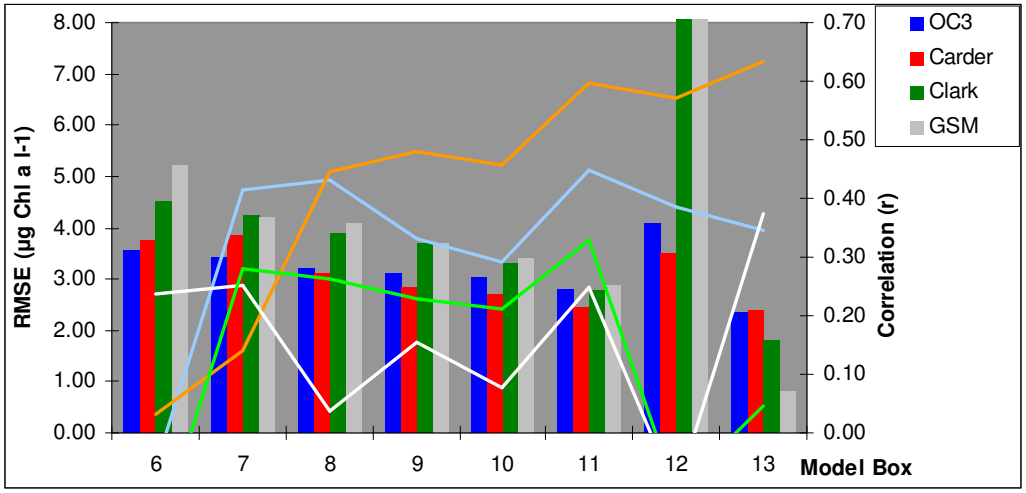

Figure 95 – Case 1 algorithms performance per box : 2001
Bars indicate RMSE and lines the correlation (*r*), per box

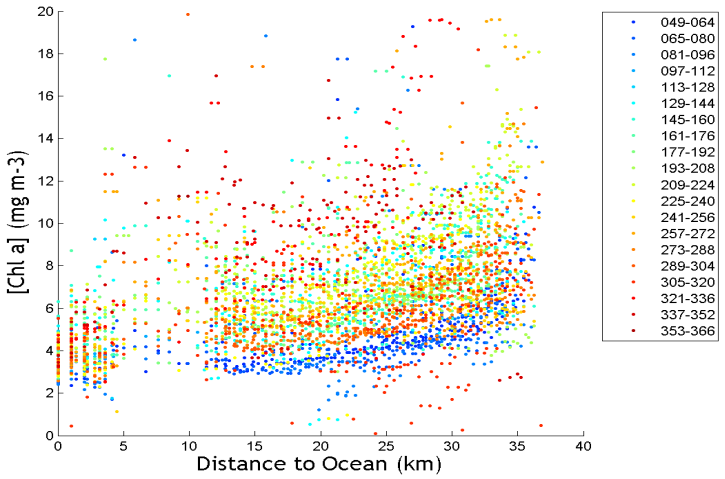

Figure 96 – Chl-a concentration vs. Distance to Ocean: GSM (2000)

The legend indicates the compositing period

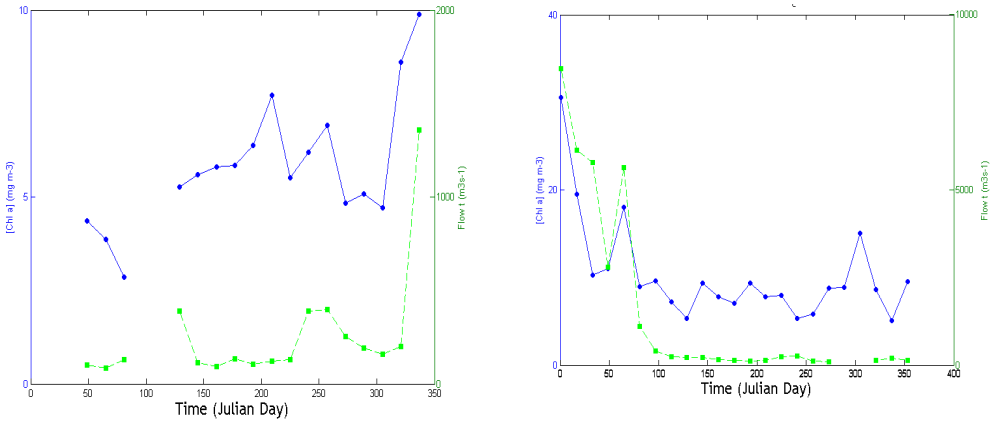

Figure 97 – Chl-a concentration vs. 16day Flow: Carder algorithm in 2000 for box 9, r=0.63 (on the left) and box 8, r=0.50 (on the right)

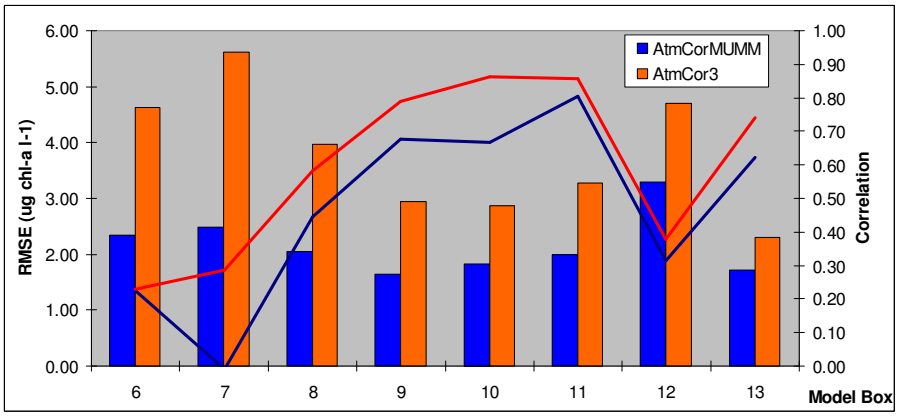

Figure 98 – Performance comparison Cor3 and MUMM atmospheric correction procedures, using the OC3 algorithm (2000)
Bars indicate RMSE and lines the correlation (*r*)

ANNEX XI – PRELIMINARY ASSESSMENT OF REGIONALLY TUNED ALGORITHMS

The temporal distribution of the tuned and original OC3 algorithm was exhibited in Figure 99 and its performance, in Figure 100. The most relevant regionally tuned Case 2 algorithms were exhibited in Figure 101 along with their performance per box, in Tables 1-3, for the year 2000.

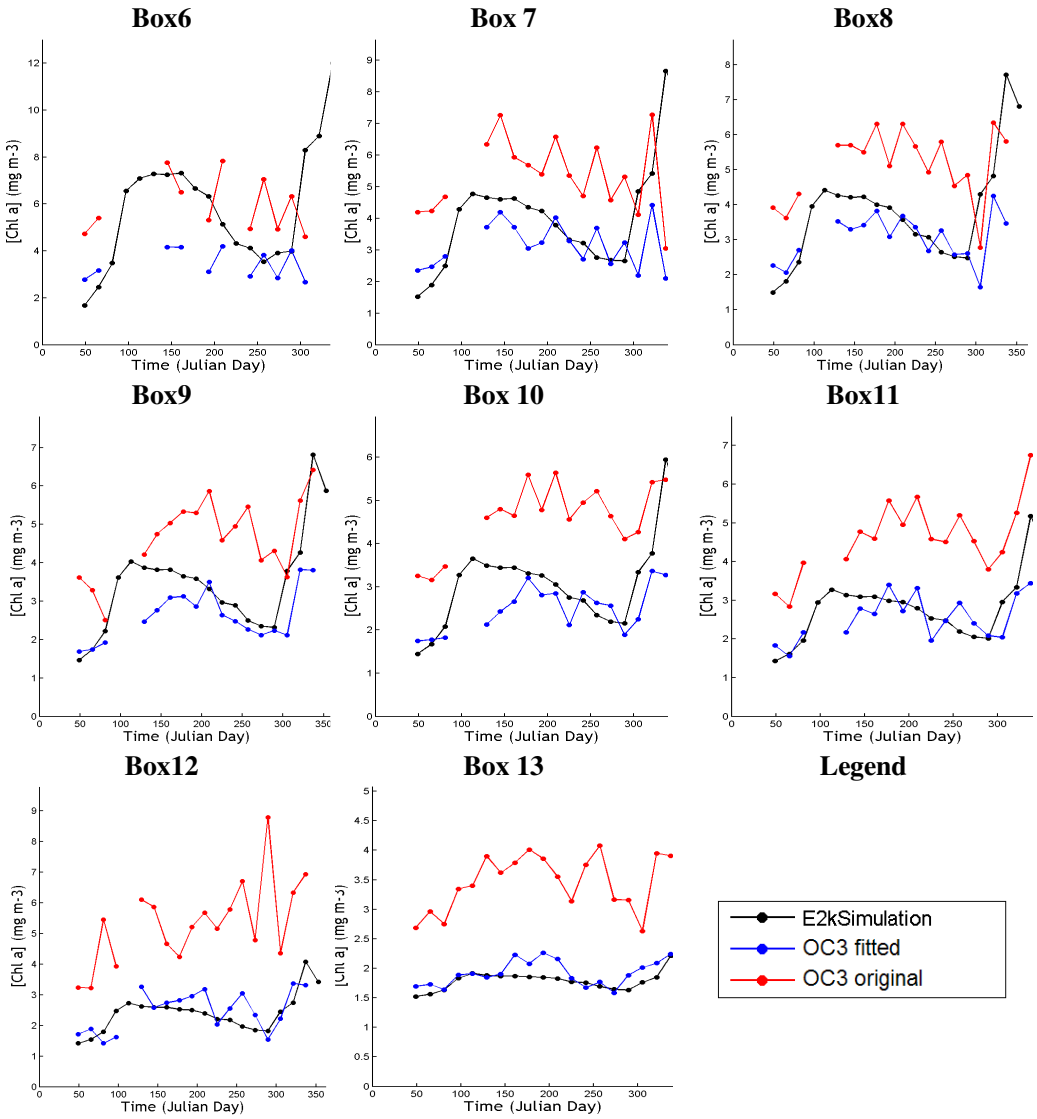

Figure 99 – Comparison of OC3 tuned vs. OC3 original: Time Series 2000

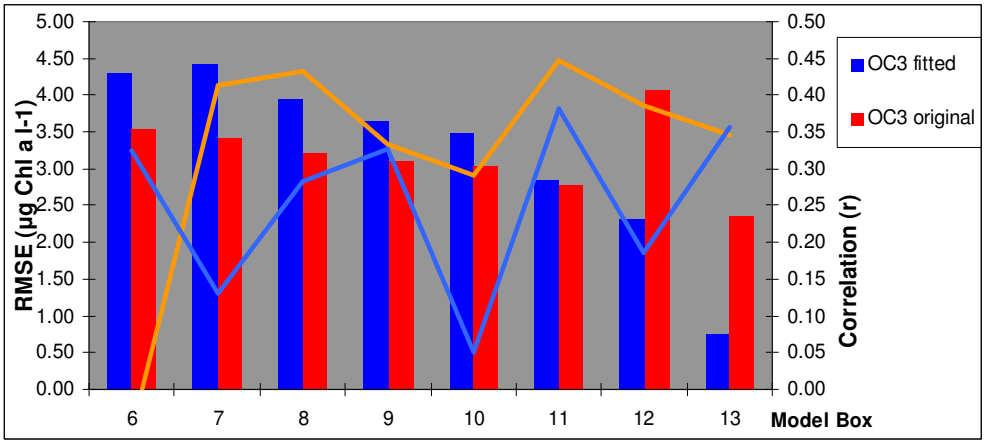

Figure 100 – Tuned OC3 performance : 2001
Bars indicate RMSE and lines the correlation (*r*), per box

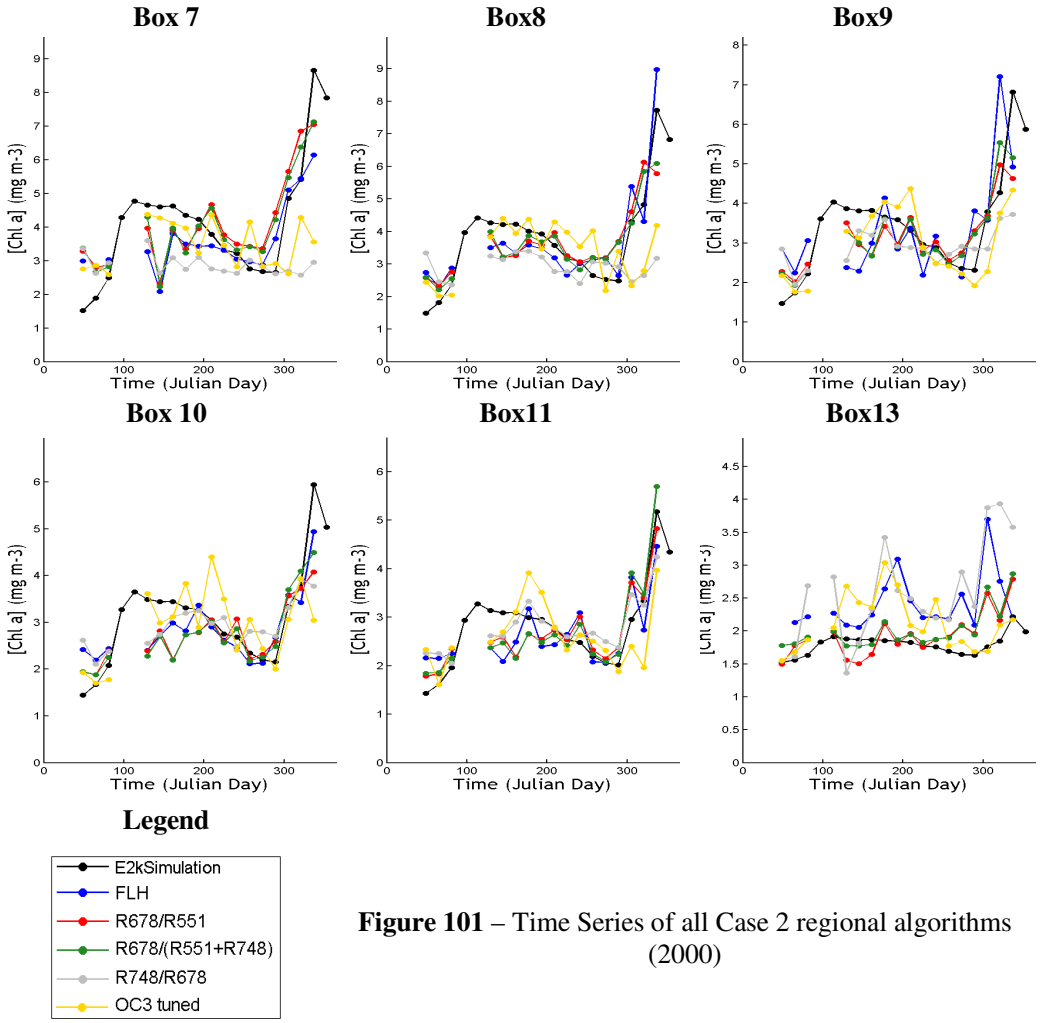

Figure 101 – Time Series of all Case 2 regional algorithms (2000)

Table 47 – Case 2 algorithms performance for the year 2000 - RMSE (μg chl-a l^{-1})

Box	OC3 tuned	FLH	R_{678}/R_{551}	$R_{678}/(R_{551}+R_{748})$	R_{748}/R_{678}
7	1.51	1.13	1.13	1.06	1.92
8	1.25	0.70	0.84	0.74	1.50
9	0.83	1.23	0.77	0.72	0.99
10	0.86	0.55	0.69	0.64	0.72
11	0.62	0.56	0.44	0.48	0.45
13	0.48	0.76	0.33	0.34	1.04

Table 48 – Case 2 algorithms performance for the year 2000 – MAE (%)

Box	OC3 tuned	FLH	R_{678}/R_{551}	$R_{678}/(R_{551}+R_{748})$	R_{748}/R_{678}
7	24.53	22.57	30.12	27.42	34.31
8	25.14	19.96	21.19	18.73	30.57
9	16.89	31.76	17.81	16.80	21.52
10	17.38	16.99	15.90	15.50	18.73
11	17.68	18.89	13.86	14.28	15.44
13	19.28	35.42	14.63	14.50	46.32

Table 49 – Case 2 algorithms performance for the year 2000 - Correlation

Box	OC3 tuned	FLH	R_{678}/R_{551}	$R_{678}/(R_{551}+R_{748})$	R_{748}/R_{678}
7	0.43	0.75	0.73	0.76	0.01
8	0.49	0.89	0.81	0.86	0.25
9	0.76	0.51	0.79	0.80	0.71
10	0.56	0.87	0.79	0.81	0.75
11	0.67	0.74	0.85	0.85	0.89
13	0.56	0.00	0.46	0.53	0.42

ANNEX XII – CASE 1 AND CASE 2 ALGORITHMS: INDEPENDENT ASSESSMENT (2002)

The comparison between E2k simulations and the remotely retrieved chl-a was exhibited using the Case 1 algorithms (Figure 99) and regionally tuned algorithms (Figure 103). The error and correlation comparison, between the performance of the OC3 original and tuned algorithms, was shown in Figure 100. Finally, the spectral signatures for 2002 concerning all boxes are shown in Figure 86 and Figure 106.

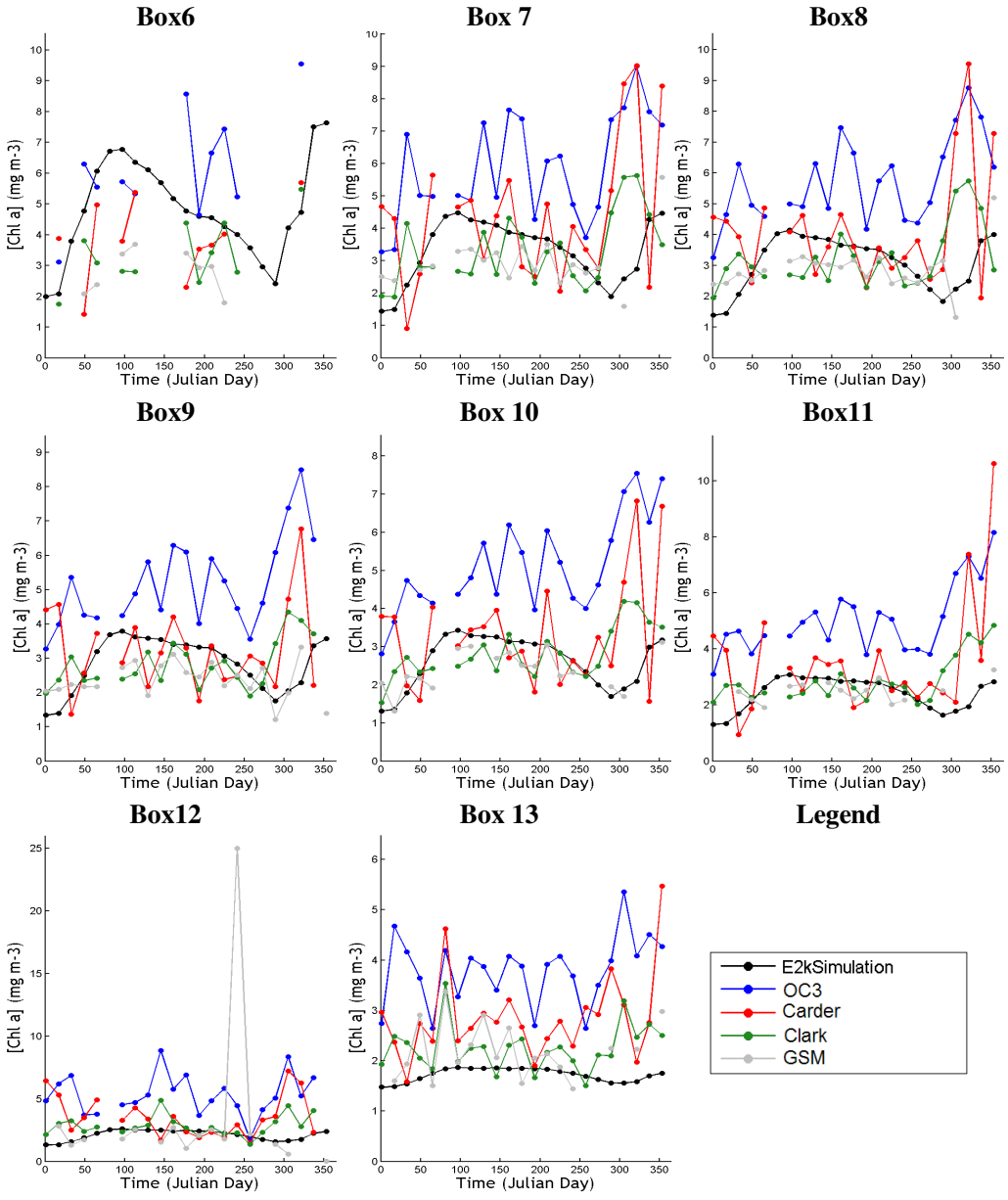

Figure 102 – Case 1 Algorithms Assessment : Time Series 2002

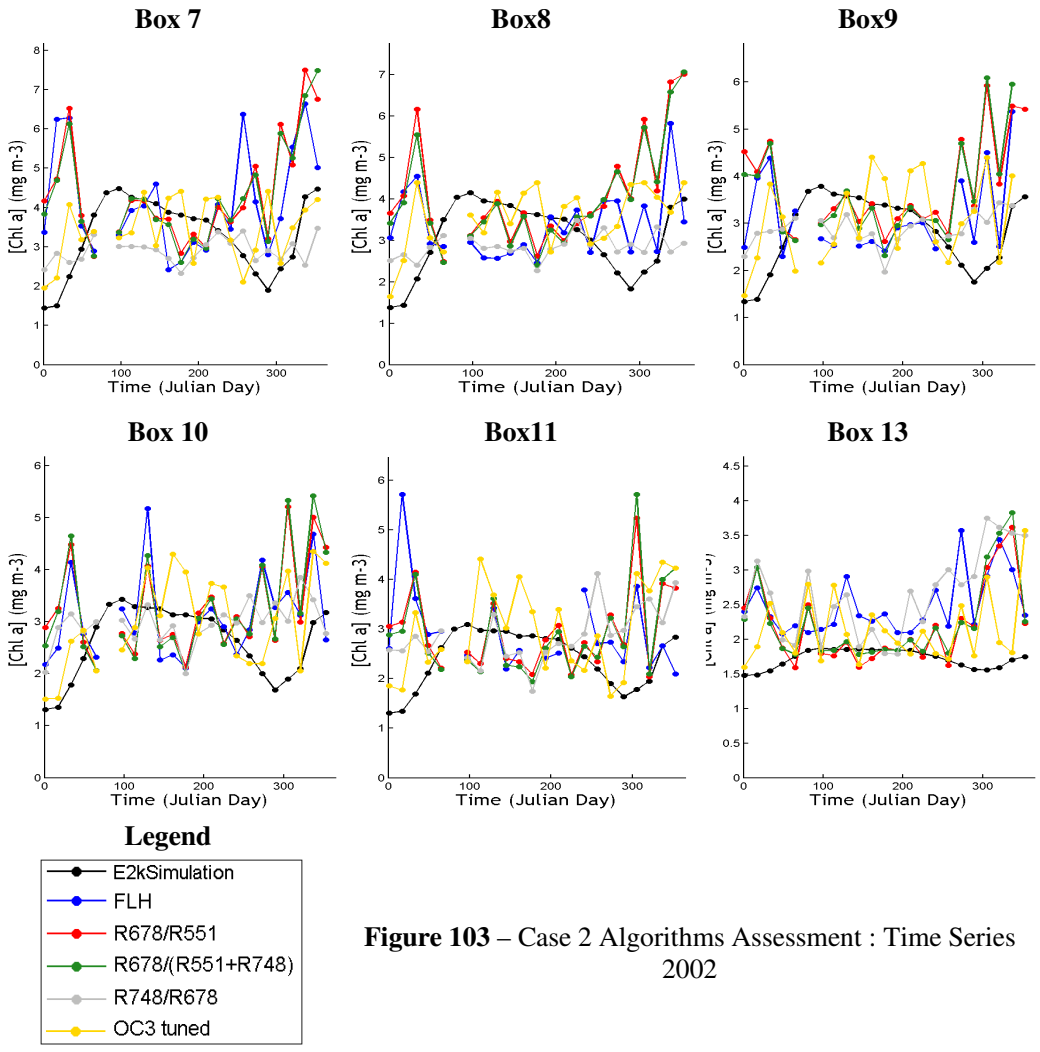

Figure 103 – Case 2 Algorithms Assessment : Time Series 2002

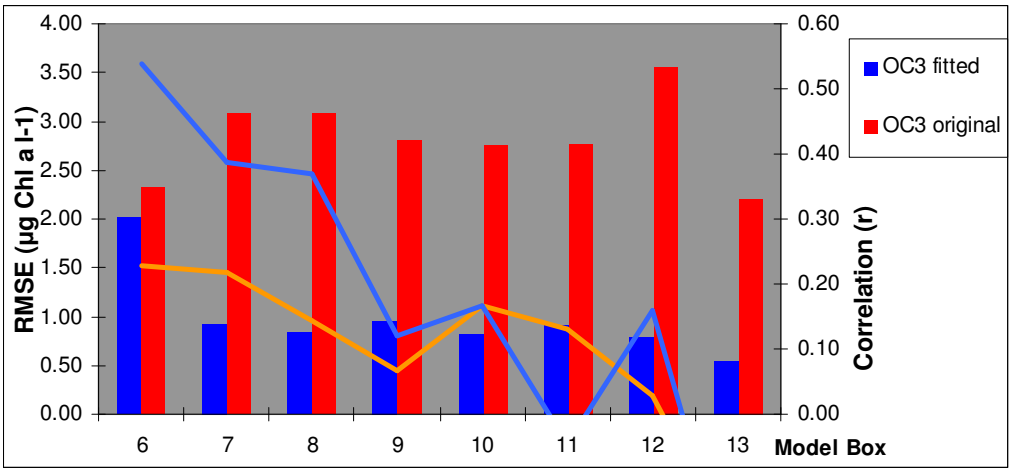

Figure 104 – Tuned OC3 performance : 2002
Bars indicate RMSE and lines the correlation (*r*), per box

Table 50 – Case 1 algorithms performance for 2002 - MAE (%)

Box	OC3	Carder	Clark	GSM
6	52.75	77.71	52.97	61.20
7	66.09	102.10	36.39	32.05
8	41.42	35.46	29.91	45.88
9	95.21	73.07	36.95	25.88
10	105.62	66.83	41.55	28.62
11	103.32	54.41	34.67	27.36
12	110.37	58.07	31.42	15.94
13	122.59	67.73	39.02	18.34

Table 51 – Case 1 algorithms performance for 2002 - RMSE (μg chl-a l^{-1})

Box	OC3	Carder	Clark	GSM
6	2.65	3.99	4.58	2.35
7	2.85	4.81	1.97	1.68
8	2.33	1.86	2.05	2.57
9	3.10	2.53	1.39	0.88
10	3.09	2.35	1.36	0.80
11	2.82	1.64	1.02	0.88
12	2.84	1.73	0.92	0.47
13	2.93	2.33	1.07	0.49

Table 52 – Case 1 algorithms performance for 2002 - correlation (*r*)

Box	OC3	Carder	Clark	GSM
6	0.11	0.13	0.16	0.31
7	0.13	0.22	0.17	0.43
8	0.23	0.23	0.15	0.51
9	0.25	0.01	0.05	0.58
10	0.12	-0.12	-0.08	0.51
11	0.06	-0.25	-0.02	0.32
12	0.22	-0.02	0.07	0.81
13	0.20	0.11	0.01	0.30

Table 53 – Case 2 algorithms performance for year 2002- RMSE (μg chl-a l^{-1})

Box	OC3 tuned	FLH	R_{678}/R_{551}	$R_{678}/(R_{551}+R_{748})$	R_{748}/R_{678}
7	0.92	1.94	1.99	1.92	0.96
8	1.08	1.32	1.93	1.83	0.87
9	1.07	1.33	1.69	1.70	0.83
10	0.85	1.16	1.36	1.42	0.89
11	1.02	1.36	1.23	1.30	0.99
13	0.65	0.90	0.80	0.84	1.13

Table 54 – Case 2 algorithms performance for the year 2002 – MAE (%)

Box	OC3 tuned	FLH	R_{678}/R_{551}	$R_{678}/(R_{551}+R_{748})$	R_{748}/R_{678}
7	26.72	60.70	62.43	60.88	27.54
8	34.47	45.29	63.76	61.67	28.87
9	36.07	47.81	59.37	59.69	30.70
10	27.99	42.92	51.42	52.33	34.92
11	36.48	53.04	47.57	49.21	41.28
13	27.00	45.34	33.99	33.12	55.45

Table 55 – Case 2 algorithms performance for the year 2000 - Correlation

Box	OC3 tuned	FLH	R_{678}/R_{551}	$R_{678}/(R_{551}+R_{748})$	R_{748}/R_{678}
7	0.46	-0.18	-0.08	-0.03	0.30
8	0.29	-0.21	-0.15	-0.12	0.19
9	0.22	-0.23	-0.34	-0.40	0.03
10	0.56	0.00	-0.17	-0.15	-0.07
11	0.44	-0.46	-0.31	-0.28	-0.20
13	0.05	-0.39	-0.58	-0.53	-0.48

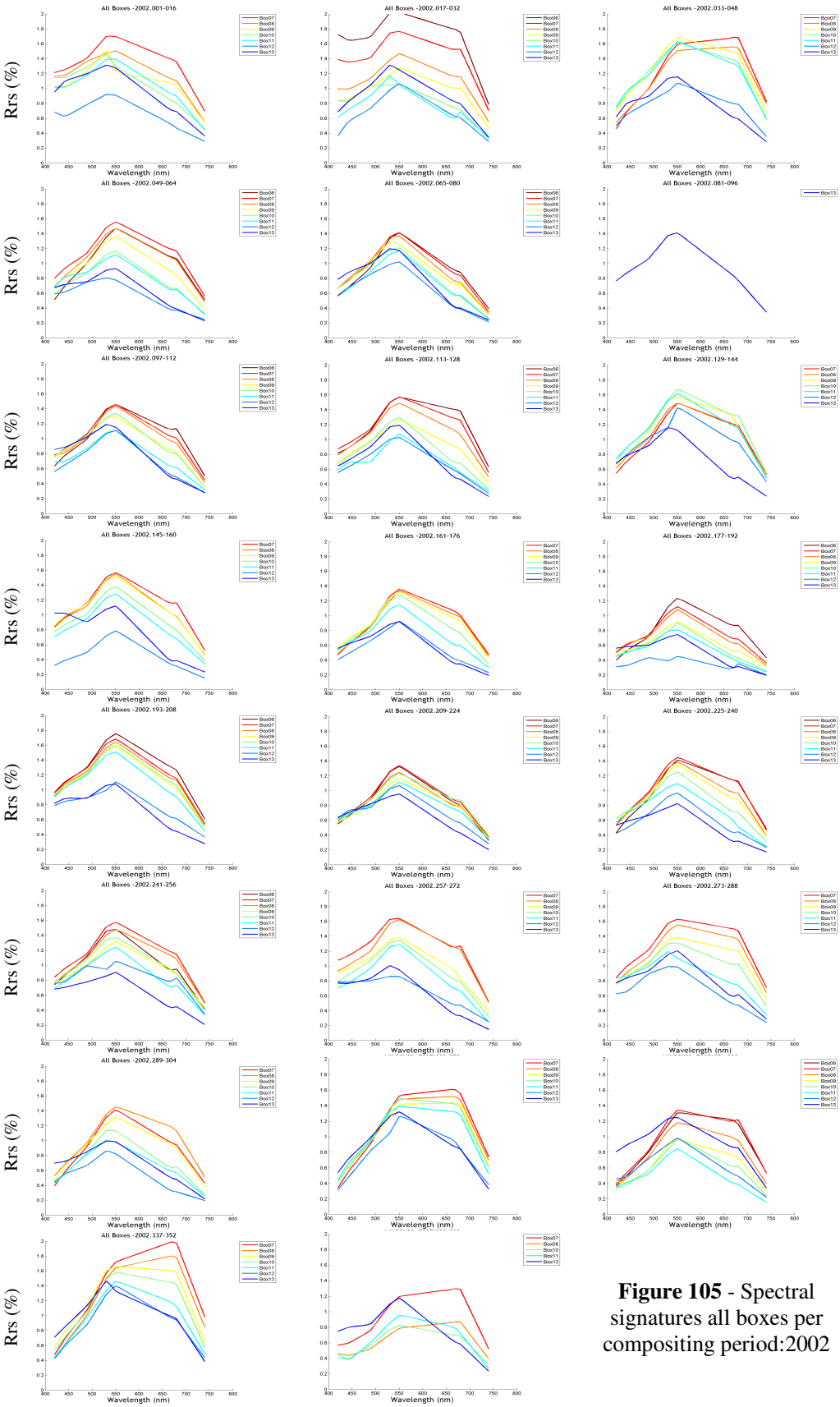

Figure 105 - Spectral signatures all boxes per compositing period:2002

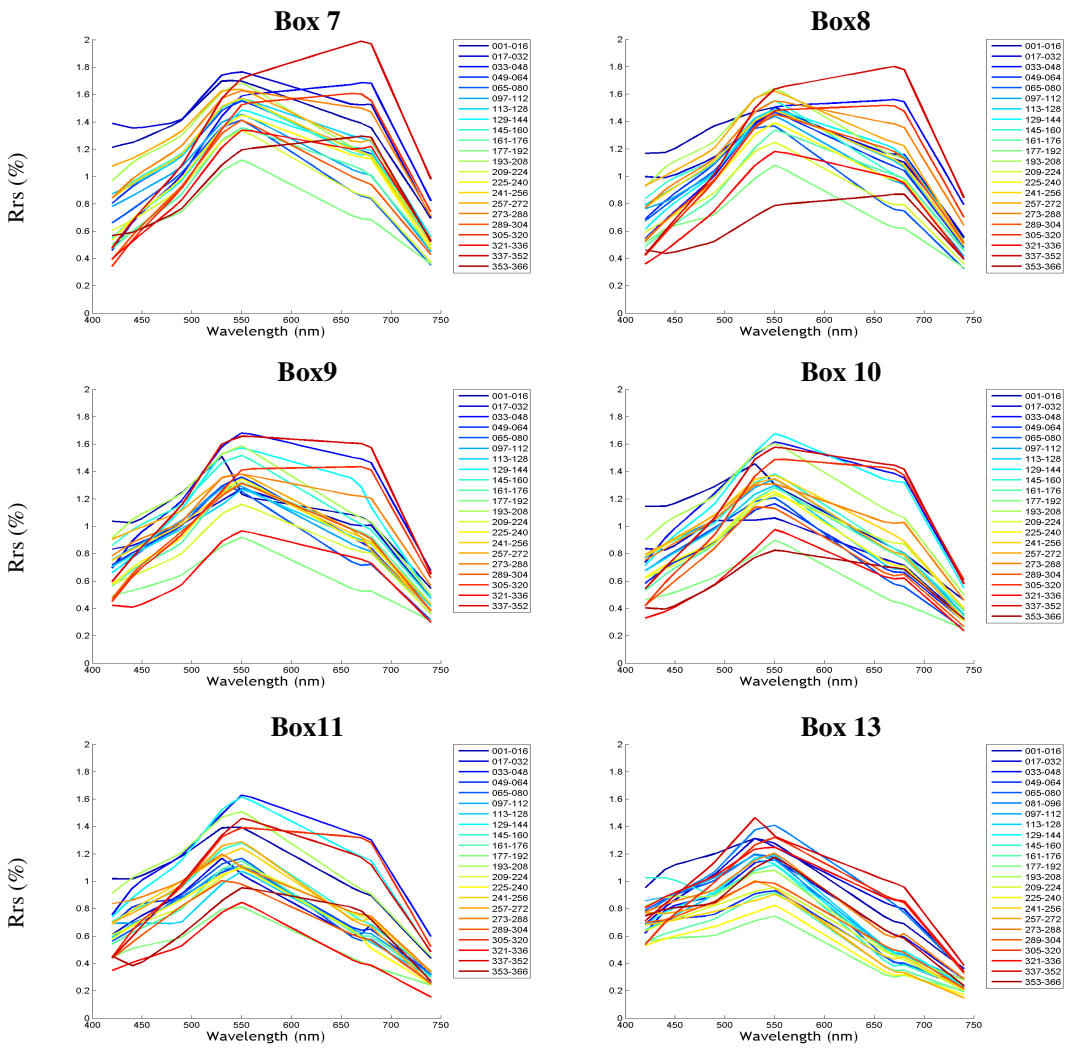

Figure 106 – Spectral signature distribution over time (2002)
The legend and associated line colours indicate the composites Julian day range